



HUNGARIAN UNIVERSITY OF AGRICULTURE AND LIFE SCIENCES

**CHARACTERISTICS, EFFECTS AND MITIGATION OF URBAN HEAT
ISLAND IN DEVELOPING URBAN REGIONS**

THE Ph.D. DISSERTATION

DOI: 10.54598/001070

LI HUAWEI

Budapest

2021

The PhD School

Name: **Hungarian University of Agriculture and Life Sciences**
Landscape Architecture and Landscape Ecology

Discipline: Agricultural Technology

Head: **Dr. László Bozó**
University professor, DSc, MHAS
MATE Institute of Horticultural Science
Department of Soil Science and Water Management

Supervisors: **Dr. Sándor Jombach**
Associate professor, PhD
MATE Institute of Landscape Architecture, Urban Planning and
Garden Art
Department of Landscape Planning and Regional Development

.....
Approval of the Head of Doctoral School

.....
Approval of the Supervisor

In the decision of the Doctoral and Habilitation Council of Hungarian University of Agriculture and Life Sciences from the 3rd of **June 2021** the following Review Committee was appointed to conduct the public defense:

REVIEW COMMITTEE

Head:

Dr. László Bozó, PhD, DHAS

Members:

Dr. Albert Fekete, PhD, DLA

Dr. Ákos Bede-Fazekas, PhD

Dr. Zsombor Boromisza, PhD

Dr. András Jung, PhD

Opponents:

Dr. Nóra Skarbit, PhD

Dr. Ildikó Réka Báthoryné Nagy, PhD

Secretary:

Dr. Krisztina Filep-Kovács, PhD

TABLE OF CONTENT

LIST OF ABBREVIATIONS	1
1. INTRODUCTION.....	3
1.1 Research background	3
1.2 Research questions.....	5
1.3 Research significance and goals	7
1.4 Framework of the dissertation.....	8
2. LITERATURE REVIEW	11
2.1 Urban heat island (UHI) concepts.....	11
2.1.1 The cause of UHI.....	12
2.1.2 Urban ground surface heat balance.....	15
2.1.3 Types of UHI	18
2.2 Review of the UHI measurement methods	20
2.2.1 Ground based measurement.....	20
2.2.2 Data from Remote sensing techniques	22
2.3 The impact of UHI.....	28
2.3.1 Increase urban energy consumption	28
2.3.2 Impact on climate	29
2.3.3 Impact on the atmospheric environment.....	29
2.3.4 Affect human health and thermal comfort	29
2.4 Urban heat island research review	29
2.4.1 The UHI research development analysis	32
2.4.2 Summary of urban heat island research.....	37
2.5 Research gap	38
3. METHODS AND MATERIALS.....	39
3.1 Study areas.....	39
3.1.1 Zhengzhou city	39
3.1.2 Budapest city	41
3.2 Data collection	43
3.2.1 Meteorological data	44

3.2.2 Geospatial GIS data and tools.....	45
3.2.3 Field survey data and equipment	48
3.2.4 Other additional -statistical data	50
3.3 Research methodology in each survey.....	51
3.3.1 Temporal and spatial UHI investigation	51
3.3.2 Park cooling intensity survey and analysis	55
3.3.3 Small scale green space cooling effect survey.....	58
3.3.4 Vertical factors of UHI survey.....	59
3.4 Summary of methods	61
4. RESULTS AND DISCUSSIONS.....	63
4.1 Spatio-temporal changes of UHI with the expanding city	63
4.1.1 Temporal atmospheric UHI intensity based on long-term meteorological data	63
4.1.2 Spatial surface UHI intensity variations based on geospatial data	69
4.1.3 Discussion and further research proposals.....	81
4.1.4 Summary and outlook of UHI in Zhengzhou	85
4.2. Mapping and analysing park cooling effect on SUHI based on satellite images	87
4.2.1 Relation between park types, LST and PCI.....	87
4.2.2 Relation between park LST and its impact factors	88
4.2.3 Relation between PCI and its impact factors	90
4.2.4 PCI changes with the distance measured from park edge	93
4.2.5 Discussion and further research proposals.....	95
4.2.6 Summary of park cooling effect survey.....	99
4.3. Analysis of cooling and humidification effects of different coverage types in Small Green Spaces (SGS).....	100
4.3.1 Statistical results of atmospheric conditions in the study plot.....	100
4.3.2 Changes in temperature and humidity of different vegetation coverage types.....	101
4.3.3 Comparison of influencing factors on green space cooling and humidification.....	104
4.3.4 Discussion and further research proposals.....	105
4.3.5 Summary of cooling and humidification effects of different vegetation coverage types	108
4.4. Characterize the vertical and green spaces factors on SUHI	110
4.4.1 Elevation and slope aspect influence on LST.	110
4.4.2 Vegetation height and building height effect on LST	113
4.4.3 Green space factor's effect on LST	115

4.4.4. Discussions and further research proposals	117
4.4.5 Summary of vertical factor effects.....	118
5. NEW SCIENTIFIC RESULTS	120
6. CONCLUSION AND USABILITY OF RESULTS.....	129
6.1 Summary of the dissertation	129
6.2 Implications for urban and landscape planning	131
REFERENCES.....	133
LIST OF FIGURES.....	149
LIST OF TABLES.....	152
ACKNOWLEDGEMENT.....	153
APPENDIX	154

LIST OF ABBREVIATIONS

AT - Air Temperature	NDWI - Normalized Different Water Index
CFD - Computational Fluid Dynamics	NIR - Near Infrared Band
CD – Canopy Density	PCI - Park Cooling Intensity
Frac_Dim - Fractal Dimension Index	PAR - Photosynthetically Active Radiation
FVC - Fractional Vegetation Cover	Paratio - Perimeter-Area Ratio
GCI - Green space Cooling Intensity	PET - Physiologically Equivalent Temperature
GIS - Geographic Information Systems	RH - Relative Humidity
ha - hectares	RTE - Radiative Transfer Equation
HAU - Henan Agricultural University	SCA - Single Channel Algorithm
IBM - Imaged-based Method	Shape_Idx - Landscape Shape Index
LAI - Leaf Area Index	SGS - Small Green Space
LCZ - Local Climate Zone	SUHI - Surface Urban Heat Island
LSE - Land Surface Emissivity	SVF - Sky View Factor
LST - Land Surface Temperature	SWIR - Shortwave Infrared Band
LULC - Land Use /Land Cover	TCD – Tree Cover Density
m - Meters	TIR - Thermal Infrared
m ² - Square Metres	TIRS - Thermal Infrared Sensor
MLA - Mean Leaf Angle	TOA - Top of Atmosphere
MNDWI - Modified Normalized Different Water Index	Tmrt - Average Radiant Temperature
MWA - Mono Window Algorithm	UCI - Urban Cool Island
NDBI - Normalized Different Build-up Index	UCR - Urban Compactness Ratio
NDISI - Normalized Different Impervious Surface Index	UHI - Urban Heat Island
NDVI - Normalized Different Vegetation Index	UHII - Urban Heat Island Intensity
	URI - Urban heat island Ratio Index
	USGS - United States Geological Survey

UTC - Coordinated Universal Time

UWG - Urban Weather Generator

WD - Wind Direction

WS - Wind Speed

ΔT - temperature difference

$^{\circ}\text{C}$ - Degree Celsius

1. INTRODUCTION

1.1 Research background

Urban heat island effect and urbanization, from the United Nations Convention on Climate Change in 1992 to the Kyoto Protocol in 1997, and from the "Bali Roadmap" to the Copenhagen World Climate Conference in 2007 (Christoff, 2008), the world's attention global warming and carbon emissions have been growing. The proportion of urban heat islands is increasing and the intensity of its impact is rising rapidly, which is closely related to the accelerating urbanization process in the world. Consequently, it leads to an increase in energy consumption, pollution, death or decline of human and living organisms, and other problems, which directly threaten the sustainable development of cities.

The **rapid development of urbanization** has led to the continuous expansion of the scale of the city, the rapid growth of the impervious area of the city, the original natural **urban surface layer** of the city has been changed, and human activities and industrial production have greatly changed the material and energy balance near the ground in the city. This has led to many environmental problems. As the most prominent feature of urban climate, the urban heat island effect has always attracted people's attention (Oke 1982). According to many research reports by scholars from the World (Deilami et al. 2018; Wu, Ren 2018), most cities on the earth, regardless of their size, latitude, coastal or inland location, topography or environment, all have an urban heat island effect. In Seoul, South Korea, the average heat island intensity increased by 1.3°C during 1962 to 2017 (Hong et al. 2019). From 1960 to 2000, Phoenix city experienced a minimum temperature rise of 0.47°C per decade (Golden 2004). In New York, a growth of the Central Park atmospheric UHI strength from 2.0°C in 1900 raised to 2.5°C by 2000 (Gaffin et al. 2008).

Urban heat islands have **resulted a series of problems** on the quality of life of urban residents, urban climate, urban ecological environment, etc., most of which are negative. The urban heat island effect causes the temperature in the city to rise rapidly during the day, but atmospheric UHI intensity at night even stronger (Grimmond, Oke 2002). At the same time, the heat island effect will aggravate air pollution. These factors may cause some urban residents to feel unwell, breathing difficulties, heat cramps, exhaustion, non-fatal heat stroke, etc. heat-related diseases, which affect the health and thermal comfort of urban residents (US EPA 2014a). In addition, the urban high temperature formed by urban heat islands will also increase energy consumption in summer, increase pollutants and greenhouse gas emissions seriously threaten the ecological environment and sustainable development of the city. With the global warming, the problem of the heat island effect will become more prominent and serious. Therefore, research on strategies and

measures that can slow down and reduce the urban heat island effect is of great significance for improving the urban thermal environment, improving the city's livability, and realizing the sustainable development of the city.

Urban green space and urban heat island effect

As the most important part of the urban ecosystem, **urban green space** plays a vitally important role in **regulating** the **urban climate** and assisting the city in coping with future climate changes by influencing atmospheric water and thermal cycles (Kong et al. 2014). Studies have confirmed that increasing vegetation greening is the most economical and effective strategy to alleviate the urban heat island effect (Doick et al. 2014; Du et al. 2017, Bartesaghi et al. 2018). Green vegetation can reduce the air temperature of the surrounding environment through shadow and evapotranspiration, thereby reducing the urban heat island effect on both micro and local scales. In hot climates, trees planted around buildings can change the energy balance of the building, and the energy consumption of air conditioning by blocking the solar radiation from the windows, walls, and roof of the building, even the reflected radiation from the surrounding environment (Lin et al. 2010; Armson et al. 2012; Chatterjee et al. 2019). At the same time, within the entire city, green area such as parks, community greens, and roof gardens can regulate the energy balance of the entire city by increasing the evaporation area, which can effectively reduce the air temperature in the urban area and increase the air humidity (Thani et al. 2013; Zhang et al. 2013, Antonini et al. 2020;). Urban parks and green spaces, as the most important component of urban green spaces. In recent years, the cooling effect of urban parks and green spaces has become a hot spot in the study of urban ecological environment, and has received extensive attention from researchers (Cao et al. 2010; Oliveira et al. 2011; Chen et al. 2012; Zhang et al. 2013). Numerous studies had confirmed that urban parks and green spaces have a significant cooling effect compared with surrounding urban environments. The average temperature of green spaces is 0.5-2°C lower than that of the surrounding environment (Jansson et al. 2007), some research showed the green cooling intensity reached 2-3.8°C (P. Cohen et al. 2012), even some parks have a cooling intensity of 6.9°C (Oliveira et al. 2011). The average cooling intensity of parks during the day can reach 0.94°C (Bowler et al. 2010). Therefore, under the movement of green cities, eco-cities, and low-carbon cities, increasing urban green area and vegetation coverage and optimizing the spatial pattern of urban green spaces are considered important strategies for human health issues to alleviate problems caused by climate change and urban heat island effects.

Ecological city development

Human beings are not only the creators of cities but also users and managers of cities and nature. In the past, extensive and rapid urbanization process in China, the scale and economic value of urban space created by humans have been increasing. At the same time, it has also brought about a large number of problems such as waste of resources and environmental pollution. Under the

constraints of resources and the environment, human harmony and sustainable development with nature face bottlenecks. Moreover, the continuous increase of the urban population and people's material living standards have also caused tremendous pressure on the originally fragile urban ecological environment. The existing ecological environment quality and natural environmental resources have been difficult to satisfy human beings in terms of physical health and spiritual pleasure demand. Therefore, how to create livable, comfortable and safe spaces for human living and production, protect the natural ecological environment and the living space of plants and animals, and ultimately achieve sustainable urban and rural development is a hot issue that many scholars urgently need to consider (Chao et al., 2012). China's urban development and transformation are imminent, and it has also become a key topic for many scholars. Howard's "**Garden City**"(Tizot 2018), Le Corbusier's "**Radiant city**" (Fitting 2002), Wright's "**Broad Acre City**" (Dougherty 1981) and Mumford's "**Organic City**" (Casillo 1992) have always been hot models for scholars to explore and learn from, and introduce compact cities and propose smart cities based on the problems in China's urban development and "**Sponge City**" (Chan et al. 2018) and other development models. As a whole, the urbanization model should be more smarter and ecological.

In 2018, the Chinese government put forward a national strategy - "**Park City**" to build a newly formed urban planning model to make cities more ecological. "The expectation of a city is like a grand park so that when people go outside the door, they feel they are in the park¹" (G. Wang et al., 2019). This is the vision of "**Park City**".

How to achieve this goal in the future development of the cities in modern civilization? Furthermore, how to avoid the problems with the next phase of urbanization in a developing country like China, which has a high population density and high urban agglomeration level? Quite a lot of urban issues should be draw attention, especially in urban planners, landscape architects, decision-makers and stakeholders. As a researcher in landscape architecture, in this dissertation I focused on the urban heat environment and how to mitigate this negative phenomenon.

1.2 Research questions

Despite there has been much research on the UHI from **different research directions**, most UHI studies relied on single countries, primarily the western countries and other high-income countries with limited variability in density resulting in an underestimation of potential effects. As for developing regions in China, for instance, the urban heat island characteristics in Zhengzhou city,

¹ Source: "Chengdu Consensus on Park City", 2018.

which has a rapid development and **still expanding**² in the near future, it is a gap to characterize the process at the local scale and micro scale.

At the city scale, the UHI is significantly influenced by the urbanization process, such as the land use/cover changes, the growth of the impervious surface, and the decrease of vegetation. To quantify the impact factors of UHI can give a guide to future planning, especially based on the long-term big data sources. On the other hand, urban development has many indicators, such as the growth rate of the urban population, built-up area, GDP, green coverage rate, which also have an impact on UHI. This dissertation aimed to quantify important planning and design variables that influence urban heat island and thus provide urban planning and design strategies that mitigate the UHI intensity at the local scale and micro scale stage by manipulating these variables. In terms of this problem, the general research questions come out:

Can the UHI effect be mitigated by manipulating planning variables³ of green space in a rapidly urbanized city like Zhengzhou?

To answer this question, first I need to analyze the UHI characteristic and features from the past to summarize the main factors contributing to the UHI. Thus I could give a solution to mitigate this phenomenon in the future, and the first question was presented:

Q1: In the past four decades (1989 - 2019) of Zhengzhou, what are the spatio-temporal characteristics of surface urban heat island (SUHI) of rapid urbanization based on the data of long-term weather station and remote sensing? What are the changes in the spatial characteristics of atmospheric UHIs by the new urbanization model⁴ compared to the past model? What are the main urban development indicators GDP, population density, urbanization rate, etc.) related to the urban heat island?

Since 2018, China has put forward the "Park City" strategy, which aimed to build a more livable city in the future, as green spaces like urban parks do not only contribute to the urban landscape, but play an important role in mitigating urban environmental problems. Concerning the UHI issue, here comes the second research question:

Q2: What are the cooling effect characteristics of urban parks in urban heat islands in Zhengzhou city? What kind of parks could be planned and designed in terms of mitigating surface UHI by modify park design parameters?

² Based on the new urban planning Zhengzhou central city will reach 15 million population in 2030, while the population was 10 million in 2018.

³ It simply means using data to quantitatively guide landscape planning and design.

⁴ The new urbanization model focuses on environmental protection and ecological design to solve urban environmental problems, unlike the model of the past.

As large green spaces such as urban parks in the city had been demonstrated as urban cool islands (UCIs) based on remote sensing techniques. However, considering the shortage of resolution on satellite images, as the maximal resolution is 30m, which could not illustrate the internal structure of green space, if we zoom into green space, what kind of vegetation structure should be designed from the point of mitigating the urban heat? Within this scale, the third question comes up:

Q3: What are the cooling and humidification characteristics of small-scale green spaces in summer time? What kind of vegetation structure should be designed to mitigate urban heat effects by regulating small green spaces design parameters?

Many cities are still in a rapid urbanization speed currently and will continue to expand in the future. What is the direction when the city is expanding as regarding the urban topographical factors and elevation? Apart from the horizontal factors of urban structures, what kind of impacts of vertical dimension factors of vegetation and buildings exists in the city area on urban heat island? Is it possible that vertical factors can be modified to mitigate the urban heat island?

Q4: What is the relation between the vertical factors such as elevation, slope aspect, building height, building orientation, vegetation height and LST? How do these vertical parameters influence SUHI effect and what could do to mitigate UHI in design?

Above are the general research questions focus on the urban heat island topic, this dissertation intends to do a comprehensive investigation from the urban local scale to micro-scale, in order to use the scientific results to put forward the proposal to urban planning and landscape design.

1.3 Research significance and goals

In the past year of 2020, the world experienced the "California wildfire," "Australian bushfire (Black Summer)," "Brazil wildfires," which caused forest destruction and serious consequences, the intensity of fire has been attributed in part to the extreme weather and global warming due to the climate change and human activities. According to statistics, more than 50% of the global population are urban; it is estimated that by 2050, the proportion of the urban population will exceed 66% (United Nations 2020). Therefore, we are facing the increasing climate issue now and in the future, as one of the widely demonstrated urban environmental problems. The research on urban heat island impacts is still consequential.

The dissertation focuses on the UHI characters and UHI related factors. Systematic research from urban scale to micro scale, from horizontal level to vertical level, is applied to investigate surface UHI to reduce surface UHI impacts and give the proposal in future urban planning and landscape design. The main goal of the dissertation can be divided into four parts below:

--**On urban scale**, in the context of extreme rapid urbanization (many megacities in China), with the assistance of long-term observation data and satellite images to explore the **spatial-temporal**

UHI change and its impact factors, coupling with remote sensing. Simultaneously, examining the different effects of the "urbanization" process under the new urban development context in recent years.

--**On local scale**, in the context of mitigation strategies by modifying green space planning and design, take urban parks as a research object to explore optimal **park type, size, shape and characters** regard to cool down the city.

--**On micro-scale**, the vegetation design of small green spaces such as gardens impacts on mitigating the urban heat environment. To investigate the impacts and mitigation of **vegetation coverage types** on urban thermal problems.

--**In vertical dimension**, to investigate the impacts of elevation and slope orientation on surface UHI, and explore the impact **vegetation height and buildings' height and types** on UHI.

With explicit and feasible plans and design strategies, planners and landscape architects could build a more comfortable and sustainable city.

1.4 Framework of the dissertation

This dissertation contains **six chapters** (*Figure 1.1*). Chapter 1 introduces the **research background**, research questions, and overview of research objectives on the urban heat island effect. The following is a brief overview of the content of the subsequent chapters.

The **second chapter** is a **literature review**, summarizing the history related to UHI research. UHI's definition, research methods and essential results are listed. Introduced and discussed UHI's international research. The current research questions of Zhengzhou were also determined.

The **third chapter** is about the research **methods and data sources** of this dissertation and introduces the general profiles of the research area. This chapter introduces the data sources, measurements, collections, and cycles used. The research questions and research framework of UHI research are summarized and elaborated.

The fourth chapter is the research results and analysis, which includes **four parts**.

The **first part** introduces the **temporal and spatial analysis of UHI in Zhengzhou city during the last four decades**. Based on long-term data from urban weather stations and satellite image data, two methods are used to graphically analyze the temporal and spatial characteristics of Zhengzhou's heat island response. At the same time, statistical regression models are also studied to assess the influence of factors in the urbanization process on UHI.

The **second part** of the fourth chapter analyzed the **cooling effect of urban parks**, with analyzing the impact of different factors such as park type, park size, park internal structural characteristics and park location on reducing UHI.

The *third part* of the fourth chapter was the **analysis of the impact of small-scale green space** on the thermal environment. Through the field survey in small-scale green space plot, the impact of different types of vegetation coverage on the environment's cooling and humidification effects is analyzed.

The *last part* of the fourth chapter is the **analysis of the vertical factor characteristics** on urban heat island effect. Taking Budapest as the main research area, the vertical dimension factors related to surface urban heat island were investigated.

The **fifth chapter** is the **new scientific results**, focusing on the results of this dissertation on UHI research. From the research results, it provides guidance and suggestions for future urban planning and design, landscape planning and design on mitigating the urban thermal environment.

The **sixth chapter** is the **conclusion, summarizing** the main research results. This chapter also explains the benefits of this research. Usability of results are proposed.

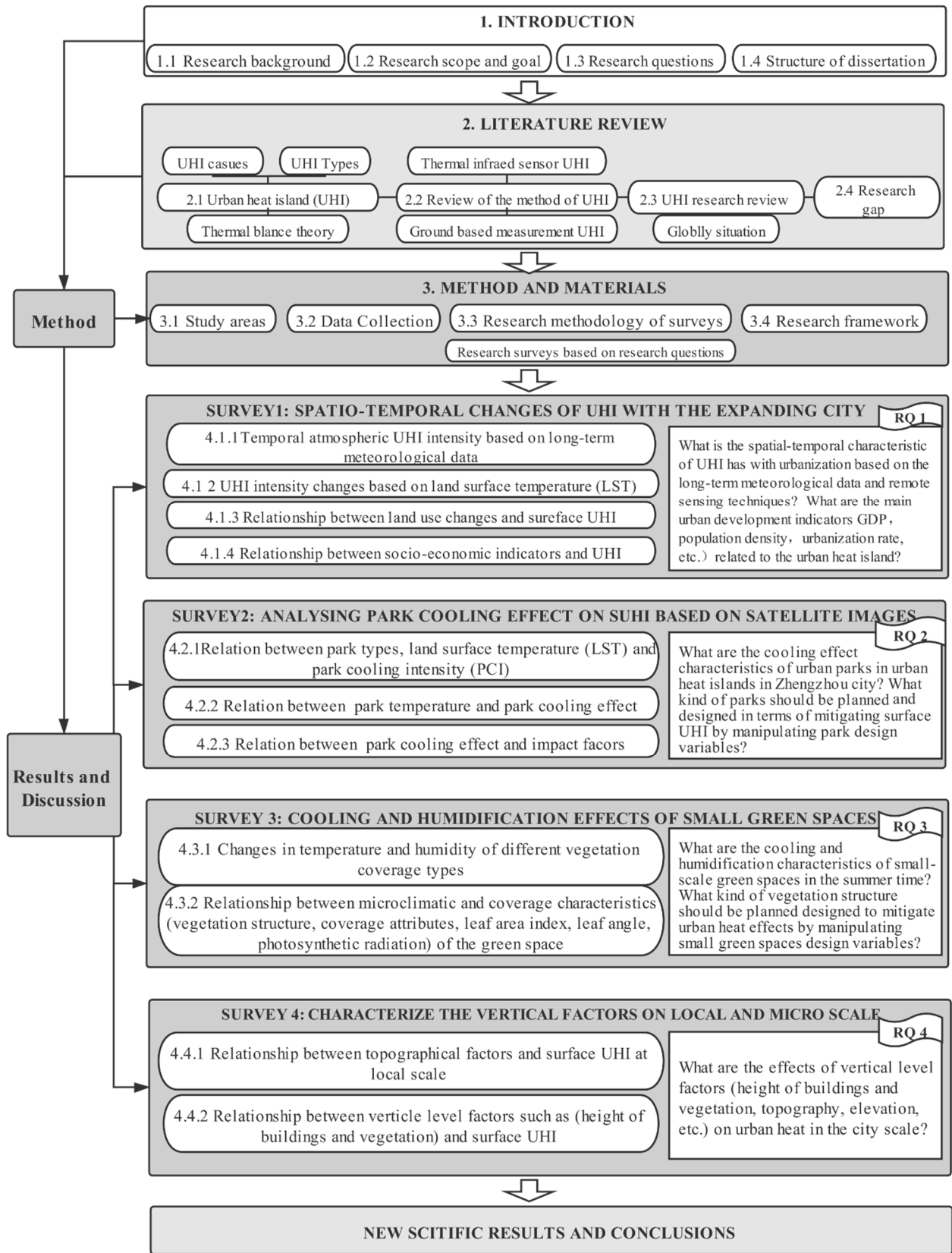


Figure 1.1: Structure of the dissertation

2. LITERATURE REVIEW

2.1 Urban heat island (UHI) concepts

In the **process of urbanization**, the natural vegetation has been replaced by a large number of buildings and impervious pavements, coupled with the discharge of various anthropogenic heat sources⁵, making the **temperature** in the **center** of the city **higher** than the temperature in the surrounding **suburbs or rural areas**. This phenomenon is called Urban Heat Island (UHI) effect (Oke 1982; Rizwan et al. 2008; Taha 1997). In short, the urban heat island is a kind of “man-made” space, much warmer than the surrounding countryside, especially at night (*Figure 2.1*). **In 1815**, Luke Howard conducted the first systematic urban climate study, and measured what is now called the UHI effect (Howard 1818) in London and nearby villages based on a thermometer. In this early study, Howard determined almost all the reasons that led to the development of atmospheric UHI. Subsequent research on urban climate replicated Howard's findings from urban-rural thermometer pairs about 2m high in many cities, and a large number of UHI maps generated by moving wires appeared in the literature in the 1930s. Afterwards, Helmut Landsberg published a comprehensive summary of UHI research (maps and statistics) conducted mainly in European and North American cities in his book entitled "Urban Climate" (Landsberg 1981). In the 1970s and 1980s (Oke 1973, 1982), the focus shifted from the early descriptive work to the many basic contributions made by Oke, exploring the process of urban impact, laying the foundation for the modern treatment of this subject.

After the basic concepts and methods of urban heat island effect were put forward, it had been attracted the attention and research of scholars all over the world. Subsequently, relevant research in this field was successively carried out in countries and cities of different latitudes, different climate zones, different scales, and geographical locations were studied successively. Almost all cities have different degrees of urban heat island effect. Especially with the advent of globalization and the rapid economic development, especially the continuous expansion and development of cities in developing countries, the rapid growth of urban populations, the emission of large amounts of man-made heat and pollution, and the increasing density of buildings have caused serious environmental problems. The natural landscape has been changed, and the phenomenon of urban heat island effect has become increasingly prominent, which has drawn attention and further research is still needed..

⁵ Mostly of heat-related problems originating in human activity, e.g. traffic, using of air conditioner, power plants etc

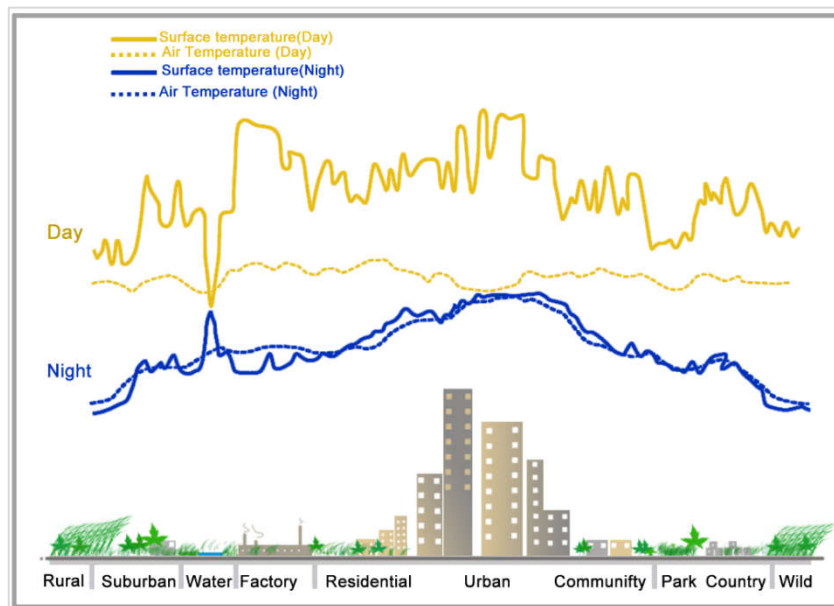


Figure 2.1: Day and night Surface temperature and Air temperature changes in different area (modified from EPA 2008)

2.1.1 The cause of UHI

The cause of the urban heat island effect is related to many factors. The most **fundamental reason** is the **replacement of the surface layer**⁶, as well as the impact of the urban form, the heat released by anthropogenic heat sources, air pollution, and the geographic location and weather conditions of the city. It can be summarized as natural factors and anthropogenic factors. The combination of these two factors forms the urban heat island effect (Kolokotroni, Giridharan 2008; Mohajerani et al. 2017; Oke, Cleugh 1987). Among the above factors, the change of the city's urban surface layer is the main reason for forming the urban heat island effect (Oke et al. 1992; Ooka et al. 2011).

The **urbanization process** has caused significant changes in the urban surface layer of the city. An impervious urban structure has replaced the previous water-permeable surface. The area of materials, such as concrete and asphalt, is continuously expanding. Areas are constantly being replaced in cities. The changes in urban surfaces have changed the local land surface's physical and chemical properties, affecting the heat exchange process between the soil and the atmosphere, affecting the local climate (Zhao et al. 2013).

Studies used spectral hybrid analysis technology to extract urban impervious surface and vegetation coverage information. They investigated the impact of urban impervious surface and vegetation cover changes on land surface temperature during urbanization. The results showed that impervious surface and land surface temperatures have a strong positive correlation. Specifically,

⁶ Replacement of the surface layer means: Urban land is transition from natural elements such as vegetation and agriculture land.

the impact of the change of the urban surface layer on the urban heat island effect is mainly manifested in the aspects listed in the following chapters.

2.1.1.1 Difference in thermal properties

The thermal properties of permeable and impervious surfaces are significantly different. **Asphalt, concrete, and other impervious surfaces absorb and store much heat**, conduct fast, and have higher thermal conductivity and heat capacity than permeable surfaces in suburban areas. Studies have shown that the temperature of asphalt pavements and roofs during the day is much higher than the air temperature (Bhattacharya et al. 2009). These thermal properties' differences result in significantly higher heat storage in urban areas' urban surface layer than suburban and rural areas. At night, this heat is transmitted to the atmosphere in the form of long-wave radiation. During the daytime, the urban surface layer in the suburbs stores less heat than the urban area. The temperature of the urban surface layer and the surface temperature decreases faster than in the urban area (Mirzaei et al 2010).

2.1.1.2 Impervious surface affects evaporation

During the **evaporation process**, soil moisture will absorb heat from the environment and reduce the surrounding area's temperature. However, the impervious surface of the city isolates the connection between the soil and the atmosphere. This connection includes both direct heat transfer and soil moisture (Bornstein 1968; Kotthaus, Grimmond 2014). Besides, during rainfall, rainwater can infiltrate into the soil, bringing part of the heat into the ground and providing moisture for soil evaporation (H. Zhang et al. 2013). However, due to cities' impervious surfaces, these processes can no longer be realized, and precipitation is quickly discharged into urban drainage pipes. The area of impervious surface in cities is much higher than that in the suburbs, which is one reason for the urban heat island effect.

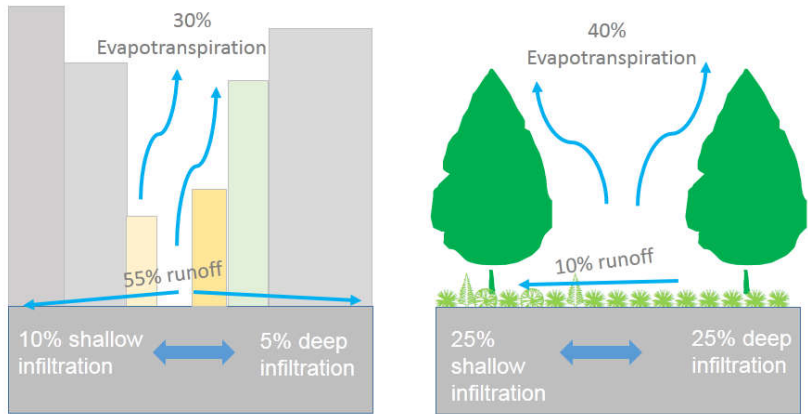


Figure 2.2: Comparison of evapotranspiration between urban areas and natural ground cover areas (modified from EPA, 2008)

Highly developed urban areas, which are characterized by 75%-100% impervious surfaces, have

less surface moisture available for evapotranspiration than natural ground cover, which has less than 10% impervious cover (*Figure 2.2* left). This characteristic contributes to higher surface and air temperatures in urban areas.

2.1.1.3 The physical characteristics of urban canopy layer

The **impermeable** concrete, asphalt has a strong absorbing effect from solar energy and can quickly increase the temperature (Hien et al. 2011). At the same time, some other high-albedo urban surfaces will reflect the light. In addition to the influence of urban building facades, the light reflects multiple times in the city, repeatedly heating the atmosphere, impervious to the building's surface and exterior. The facade also absorbs and reflects light repeatedly, increasing the temperature in the city (Miao et al. 2009). On the contrary, the surface's heat absorption capacity in the suburbs is not as good as that of the asphalt road. The suburbs do not have many urban surfaces with high albedo (Bhattacharya et al. 2009; Erell et al. 2014; Taha 1997), so the city's temperature is higher than in the suburbs.

2.1.1.4 Man-made heat sources

Anthropogenic heat mainly includes the heat generated by residents' production, transportation, and construction facilities (Adelia et al. 2019; Sailor, Lu 2004; Taha 1997). That is, waste heat generated by human activities, which contribute to the formation of urban heat islands. The industrial machines in the city and the daily life of humans consume much energy. Some cold regions consume many fossil fuels every winter (coal-fired heating is the primary method in cold climate regions), which is very important for local climate and air quality. At this time, human-made heat sources can reach or exceed the degree of heat radiated by the sun. Studies have shown that Anthropogenic heating can reach up to 60 W/m^2 in summer and winter, while anthropogenic heating is usually more extensive, up to 75 W/m^2 (Sailor, Lu 2004).

Plants take water from the ground through their roots and emit it through their leaves, a process known as transpiration. Water can also evaporate from tree surfaces, such as the stalk, or surrounding soil.

2.1.1.5 Other factors

There is a clear correlation between the size and geometry of the city and the heat island (Andreou 2014). The greater the density of urban buildings the greater the heat island's intensity (Verbai et al. 2014). Research suggests that different building structures and urban geometries are among the reasons for forming urban heat islands. The highest temperature areas in the city are often related to deepest urban canyon⁷ (Andreou 2014). Correspondingly, that is usually distributed in the city

⁷ An urban canyon (also known as a street canyon) is a place where the street is flanked by buildings on both sides creating a

center. Besides, the larger the city and population, the stronger the heat island effect (Oke 1973; H. Zhang et al. 2013). Studies have shown that different geographical locations of cities are also the main factors causing urban heat islands. In addition to the city's internal causes, the formation of urban heat islands also requires a combination of external weather conditions. Most urban heat islands appear under calm or breezy weather conditions, such as clear weather and little cloud or no cloud, because there is no automatic convection under such weather conditions. The pressure gradient is small, the atmosphere structure is stable, and the pressure field is stable. For example, **most parts of China** are controlled by the **subtropical high pressure** in summer, mainly downdraft, and there are many calm winds. The heat near the ground is not easy to dissipate, which further intensifies the urban heat island effect.

2.1.2 Urban ground surface heat balance

With the process of urbanization, changes in the **urban surface energy budget** have become an important factor affecting the urban climate. The surface energy balance is often presented as the basis for numerical **energy models** interested in quantifying **energetic processes** within a given area (T.-W. Lee et al. 2012; Oke et al. 1992; Ooka et al. 2011). Figure 2.3 shows the balance of the main energy components in a typical urban area. It has been confirmed that the heat difference caused by different coverage types (land use/land cover) between urban and rural areas is an important reason for the urban heat island effect (Bokaie et al. 2016; X.-L. Chen et al. 2006; J. Jiang, Tian 2010; Middel et al. 2012). The thermodynamic properties and dynamic characteristics of various urban surface layer types in cities are very different, such as heat capacity, albedo, roughness, surface resistance, etc., so that the mechanical turbulence generated by the city can transport momentum, heat and water vapor within the city. The difference is obvious. Therefore, the redistribution of solar radiant energy under the urban surface layer and the impact of urban surface characteristics on the heat budget are factors that cause changes in the urban thermal environment.

canyon-like environment. Urban canyons affect various local conditions, including temperature, wind, light, air quality, and radio reception, including satellite navigation signals.

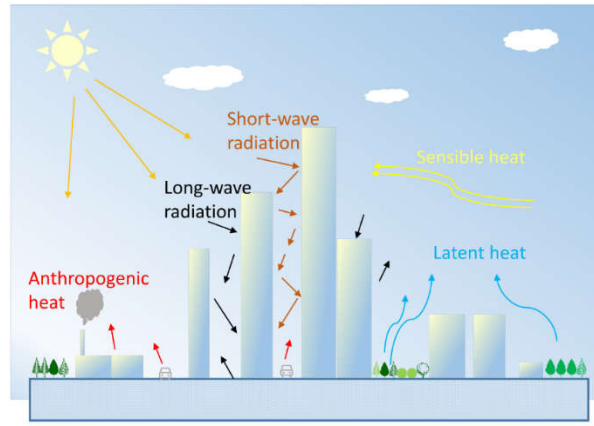


Figure 2.3: Concept of heat balance of urban surface layer (Ooka et al. 2011).

The local-scale urban meteorological parameterization scheme (LUMPS) is a parameterized scheme completed over many years by famous urban climatologists such as Oke and Grimmond. It is used to simulate the energy balance of urban space (Grimmond, Oke 2002). LUMPS has been verified in many cities in different regions and latitudes around the world, and compared with energy balance models of many different types of cities around the world (Andreou 2014; Chang et al. 2007; Oliveira et al. 2011; Skoulika et al. 2014; Yupeng Wang, Akbari 2016), which can better simulate the change characteristics of each component of the city's energy balance. Figure 2.4 illustrates the main **urban surface energy balance** components. Same as the main formulas (Nunez, Oke 1977; Oke, Cleugh 1987; Oke et al. 1992):

$$Q^* + Q_F = Q_E + Q_H + \Delta Q_S + \Delta Q_A \quad (1)$$

Where Q^* is Net radiation; Q_F is Anthropogenic heat flux; Q_E is the latent heat flux between the urban surface layer and the atmosphere; Q_H is the sensible heat flux between the urban surface layer and the atmosphere; ΔQ_S is the storage heat flux of the surface layer; ΔQ_A is the change of heat flux (Net horizontal advective heat flux).

$$\Delta Q_S = Q^* + Q_F - Q_H - Q_E \quad (2)$$

So the surface energy can be simplified as the difference between the all-wave radiation heat (Q^*) plus the anthropogenic heat flux (Q_F) minus the sensible heat flux (Q_H) and latent heat flux (Q_E), which shows in the Equation (2) given above.

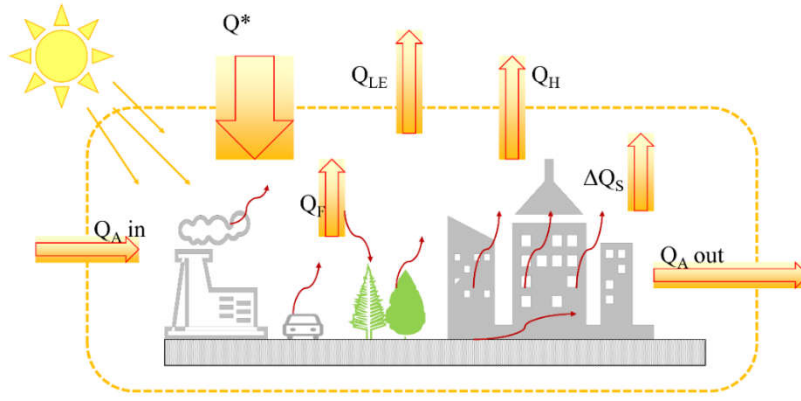


Figure 2.4: Depiction of the urban surface energy balance components in a typical urban area (Hrisiko et al. 2021; Soushi Kato, Yamaguchi 2007; Oke, Cleugh 1987).

The surface heat can use the above equation to calculate the heat storage in a certain area (Roberts et al. 2006). For the specific case of the energy model, **sensible heat flux** captures most of the anthropogenic effects in urban areas. **Heat flux** is also believed to capture many human influences in sensible heat measurement. Therefore, the prediction of ΔQ_S based on the angle of surface energy obtained by remote sensing is compared with the two heat storage approximations assuming that Q_F is considered to some extent.

Relationship between energy and temperature

In order to analyze the relationship between **energy and temperature**, an unrealistic ideal state is set. That is, regardless of the impedance of temperature transfer and transfer, the relationship between energy and temperature is simply expressed as:

$$Q = c \times m \times \Delta T \quad (3)$$

Where, Q is the energy received or absorbed by the object, the unit J, mainly from solar radiation; c is the specific heat capacity of the object, the unit J/(Kg.K); m is the mass in Kg; ΔT is the increase (or decrease of the object) temperature difference in K. Assuming that the energy is completely transferred instantaneously, the temperature difference between the impermeable layer and the vegetation layer can be simply expressed by the following formula:

$$\Delta T = \Delta T_{VE} - \Delta T_{IS} = \frac{Q_{VE}}{c_{VE} \times m_{VE}} - \frac{Q_{imp}}{c_{wg} \times m_{IS}} \quad (4)$$

where, the subscripts represent vegetation (VE) and impervious layer (IS) respectively; ΔT is the temperature difference between impervious layer and vegetation layer.

It can be assumed that all the heat consumed by surface evapotranspiration comes from the surrounding air, and the following equation can be derived from equation (5-6):

$$\Delta Q_e = \Delta Q_e(IS - VE) = c_{air} \times m_{air} \times \Delta T_{air}(IS - VE) \quad (5)$$

$$\Delta T_{air} = \Delta T_{air}(IS - VE) = \frac{\Delta Q_e}{c_{air} \times m_{air}} \quad (6)$$

Where, ΔQ_e is the difference in latent heat between the vegetation cover and the impermeable layer, in W/m^2 ; c_{air} is the specific heat capacity of the air; m_{air} is the air quality; ΔT_{air} is the difference in temperature between the vegetation layer and the impermeable layer.

After the **urban surface layer** is transformed into an artificial surface through the natural surface, it has a certain impact on the components of the radiation balance, but in general, the difference in the net radiation Q' between the suburbs is not large, and the maximum will not exceed 5% (Oke 1982, 1988). However, the **anthropogenic heat** release Q_F , **sensible heat** exchange Q_H , and **latent heat** exchange Q_E are obviously different between urban and rural areas. These are the reasons for the urban heat island effect, especially the change in the proportion of sensible heat and latent heat. The impact is the most important (Offerle et al. 2006; Oke 1988). The difference and distribution pattern of urban internal temperature are also mainly due to the **heterogeneous urban surface layer** having different **thermal properties** and energy balance, which in turn causes the difference in surface temperature and near-surface air temperature. The main reason for the cooling effect of urban green space is that most of the net radiation obtained by green space in the growing season of plants is used for **evapotranspiration**, which converts solar radiation energy into latent heat without increasing air temperature, increases air relative humidity, and effectively reduces air temperature (Taha 1997). Most of the net radiation obtained by the green space is used for the evapotranspiration of the vegetation during the vegetation growing season, and the latent heat is significantly greater than the sensible heat, which makes the park green space to have obvious ecological effects of cooling and humidification during the growing season.

2.1.3 Types of UHI

Generally speaking, UHI can be measured by two methods: one of them is **surface UHI** (SUHI); the other one is **atmospheric UHI** (*Table 2.1*). Atmospheric UHI is defined into two different types: canopy layer UHI and boundary layer UHI.

Table 2.1: General characteristics difference between Surface and Atmospheric Urban Heat Islands (UHI) modified from (EPA, 2014)

Characteristics	Surface UHI	Atmospheric UHI
Temporal	Present at all times of the day and night	May be small or non-existent during the day;
Development	Most intense during the day and in the summer	Most intense at night or predawn and in the winter
Peak Intensity (Most intense UHI conditions)	More spatial and temporal variation: Day: 10 to 15°C Night: 5 to 10°C	Less variation: Day: -1 to 3°C Night: 7 to 12°C
Typical Identification Method	Indirect measurement: Remote sensing Thermal camera	Direct measurement: Fixed weather stations Mobile traverses
Typical Depiction	Thermal image. LST map	Isotherm map Temperature graph

2.1.3.1 Surface UHI

The surface UHI is always defined by the surface temperature, **which is measured on the surface of the landscape elements**. The calculation method of land surface temperature mainly relies on remote sensing technology, such as the thermal band to extract the temperature, band 6 of Landsat TM and Landsat ETM+, band 10 of Landsat 8 OLI, and other measuring tools such as thermal sensors, thermal imaging cameras. By applying those thermal sensors, different scales and types of surface temperature can be obtained, such as urban street scale, micro scale.

2.1.3.2 Atmospheric UHI

According to the definition of urban heat island, the heat island is the difference between the temperature of the city and the temperature of the surrounding rural areas. The early response of the heat island was measured by **fixed weather stations** in urban and rural areas. This process calculation uses **air temperature** and can be calculated according to the vertical elevation of the city. The city is divided into the urban boundary layer and urban canopy layer (**Figure 2.5**): 1) **Urban boundary layer (UBL)**: It is the area between the top of the building or the top of the tree and the area extending to the place where the urban landscape no longer affects the atmosphere. This area is usually less than 1.5 kilometers from the ground (Oke, T.R. 1982). 2) **Urban canopy layer (UCL)**: It is the part of the air layer where humans live, from the ground to the top of the trees and the roof. The thermal environment changes in this layer are heterogeneous and are affected by human activities strong influence.

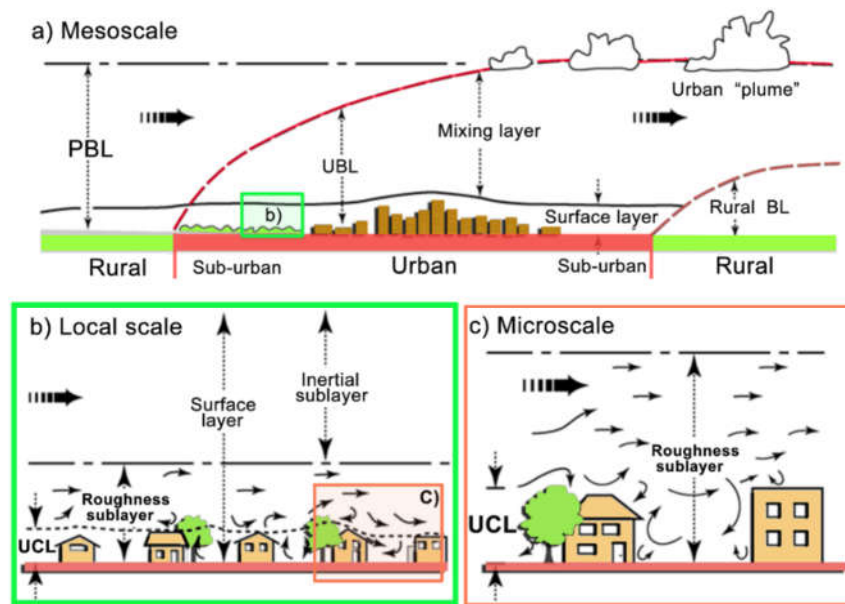


Figure 2.5: Three scales to distinguish urban area and atmosphere for climatic study (Oke, 1997, Piringger et al., 2002), Climatic scales and vertical layers found in urban areas. Planetary Boundary Layer (PBL) and Urban Boundary Layer (UBL) at mesoscale (a); Urban Canopy Layer (UCL) at local scale (b) and micro scale (c).

2.2 Review of the UHI measurement methods

UHI research method mainly contain two approaches to obtain the data: ground based measurement and remote sensing techniques.

2.2.1 Ground based measurement

Urban heat island is the temperature difference between a city and its surrounding rural sites. It can be seen from the definition that the data for studying the phenomenon of heat island mainly comes from meteorological sites and observations. **Before the 1970s**, there was no remote sensing technology support, and fixed weather stations were used as the only data source for heat island effect research. In 1815, Howard first conducted UHI research based on ten years of meteorological data, and discovered UHI in London's climate research (Howard 1818).

However, because the weather station cannot fully **represent the temperature of the city**, there are some deviations from the UHI research results. With the development of weather technology and the increase in the number of weather stations, the coverage network of fixed weather stations has been expanded, and weather data can better represent urban areas. In the extensive network of fixed weather stations in urban and rural areas, long-term coverage of meteorological data has become a common method for long-term analysis and dynamic model research (Karl et al. 1988; Kłysik, Fortuniak 1999; Kim, Baik 2005; Chow, Roth 2006; S.-H. Lee, Baik 2010). Until today, in the UHI time dynamic changes and analysis, weather station data is also the source of data.

Compared with the instantaneous data of satellite imagery, the weather data can cover the time and seasons well, and can show the short-term dynamic changes and temporal and spatial characteristics.

The latest data on heat island research is still to quantify the urban heat island phenomenon through the data difference between the city's fixed weather station and its surrounding weather stations. Describe the impact of UHI in the city (Hong et al. 2019). With the development of urban heat islands, different views and methods have emerged in the research of urban heat islands. Stewart and Oke (2012) developed a general local climate zone (LCZ) landscape classification system, which describes the physical conditions of field stations or weather stations and their local environment through classification, thereby defining temperature differences in different climate zones to compare the intensity of heat islands Distribution and classification (Siu, Hart 2013; Stevan et al. 2013).

With the development of sensors, **mobile sensors** have become more and more tools for meteorological research. They have the characteristics of **portability, mobility, automatic recording** and long-term use. Therefore, mobile measurement methods are ground measurement methods. The survey instrument is installed on a moving vehicle, and then moves along the study area for a specific period of time while measuring. Practice has proved that this is an effective method to evaluate the small and medium-scale thermal environment changes in cities (Oke 1973; Unger et al. 2000, 2010, 2001; Rodríguez et al. 2020). The earliest mobile measurement was to use cars to measure temperature changes and meteorological data at different locations in the city (Oke, East 1971; Oke, Fuggle 1972; Oke 2009;).

This method was subsequently confirmed by many studies (Fung et al. 2009; Hart, Sailor 2009; Unger et al. 2001) were also carried out in Szeged, Hungary, Singapore, Oregon, and Hong Kong respectively. The study examined the super radiation intensity). The current UHI research based on meteorological data mostly uses portable weather stations and mobile sensors, mainly focusing on the community and street level research UHI (Chang et al. 2007; Bencheikh, Rchid 2012; Skoulika et al. 2014; Park et al. 2017).

Meteorological data can be generated not only by measurement, but also by software **simulation**. On a large scale, WRF is often used to simulate wind, temperature, and humidity on a mesoscale (Göndöcs et al. 2017; Huidong Li et al. 2019). Many scholars use software to predict and quantify the urban heat island effect. Dada expanded the methods and data sources of heat island research. On a small scale, UMEP (Lindberg et al. 2018), ENVI-met software (Katsoulas et al. 2017; Yilmaz et al. 2018) and RayMan (Gulyás et al. 2006; Thorsson et al. 2007; H. Lee, Mayer 2016; Taleghani et al. 2015;) also commonly use street-scale and courtyard thermal environment simulations to guide urban and planning and landscape design.

2.2.2 Data from Remote sensing techniques

There are **shortcomings for weather station data**, in spite of traditional atmospheric UHI researches uses observations from two or several stations in city area and surrounding rural areas. However, the city has a complicated surface structure and has changes, which produces great heterogeneity inside. Therefore, using one site or multiple sites to represent the city temperature is usually not enough. In addition, the surrounding areas of the city can have different topographical and environmental characteristics. For different types of land cover, rural sites around cities may not accurately represent the surrounding rural temperature. To sum up, the accuracy of using meteorological sites as the research urban heat island effect is closely related to the site coverage density and there are deviations.

Land Surface Temperature Retrieval Algorithms:

Land surface temperature (LST) represents the temperature of the earth's surface and is one of the most important data recorded by **satellites** in recent decades. It is widely used in fields including urban climate and **surface heat island** (Giannini et al. 2015; J. Jiang, Tian 2010; Liu, Weng 2008; K. Mao et al. 2005; Qin et al. 2001; Sinha et al. 2014; Weng et al. 2004), surface evapotranspiration (Bhattacharya et al. 2009; Erell et al. 2014; Litvak et al. 2017), hydrological cycle measurement, vegetation monitoring, environmental monitoring, global climate change and other fields. Many studies have focused on the importance and influence of LST on various topics (Ndossi, Avdan 2016; Weng et al. 2004; Yuan, Bauer 2007). In addition, LST has been approved as one of the high priority parameters of the International Geosphere and Biosphere Program (IGBP) (Townshend et al. 1994). LST can be estimated based on radiation measurements from weather stations. However, because this method is based on point measurement, temperature-based measurement often does not allow large-scale monitoring. Therefore, the TIR data of thermal remote sensing makes up for the gaps in large-scale research. Large-scale spatiotemporal LST analysis.

To extract LST from satellite images, many **methods** have been developed in current research. The main algorithms include splitting, **Radiative Transfer Equation** (RTE) (Barsi, Barker, et al. 2003; Li et al. 2013; Price 1983; Sekertekin 2019; Susskind et al. 1984), **Single Channel Algorithm** (SCA)(F. Chen et al. 2015; J. C. Jimenez-Munoz et al. 2009; Jiménez - Muñoz, Sobrino 2003, 2004; Juan C. Jimenez-Munoz, Sobrino 2010; Qin et al. 2001), **Mono-Window algorithm** (MWA)(Qin et al. 2001; F. Wang et al. 2015) and **Split Window Algorithm** (SWA) (Becker, LI 1990; COLL et al. 1994; Jiménez-Muñoz et al. 2014; Mao et al. 2005; Price 1984; SOBRINO et al. 1996; Wan, Dozier 1996; Yu et al. 2014). While the first three methods (RTE, SCA, MWA) can be applied to Landsat 5 TM, 7 ETM+ and 8 OLI/TIRS data, the SWA is only suitable to Landsat 8 OLI/TIRS data, since it requires at least two TIR bands. Additionally to the two thermal bands, MWA also needs near-surface air temperature for the effective mean atmospheric temperature computation.

In addition to the emissivity and atmospheric transmittance common to all methods, MWA also requires other methods to obtain an effective average atmospheric temperature, so the air temperature near the surface is also required; on the contrary, RTE and SCA require upward and downward atmospheric emissivity to perform LST retrieval. The essential difference between these methods lies in the mathematical formulas and input parameters. In order to obtain an accurate land surface temperature reversal from space, emissivity and other atmospheric parameters need to be used to correct the brightness temperature. The following section summarizes the key steps and differences of the five methods.

2.2.2.1 Planck function

The Planck function is used to calculate the intensity of thermal radiation. This function shows the amount of thermal electromagnetic radiation that a black body can emit under thermal equilibrium conditions at a known temperature. Using the LSE of the known area, the LST of the area can be estimated by the inverse calculation of the Planck function. Under the assumption that the land surface is a black body (that is, an object with an emissivity of 1), calculate the brightness and temperature recorded by the sensor in space. The Planck function can realize the emissivity correction of brightness temperature, and the land surface temperature after emissivity correction is shown in formula (7).

$$T_s = \frac{BT}{1 + \left[\frac{\lambda \cdot BT}{\rho} \right] \cdot \ln \varepsilon} \quad (7)$$

where T_s is the land surface temperature (K); BT is the at-sensor brightness temperature (K), λ is the wavelength of the emitted radiance; ρ is the $(h \cdot c / o) = 1.438 \cdot 10^{-2}$ mK and ε is the spectral emissivity.

2.2.2.2 Mono Window Algorithm (MWA)

The **brightness temperature** obtained should be corrected for LSE and atmospheric parameters, which may affect the data obtained by the sensor in the space due to the absorption and scattering of electromagnetic radiation. In order to obtain reasonably high-quality LST, the study found the method of MWA (Qin et al., 2001; Wang et al., 2015). The algorithm needs to use LSE, atmospheric transmittance and effective average atmospheric temperature. Sensitivity analysis of MWA shows that the difficult-to-estimate ground emissivity error has relatively little effect on the possible LST estimation error, and the latter is more sensitive to the possible error of transmittance and average atmospheric temperature (Qin et al., 2001). The verification of simulation data under various conditions of seven typical atmospheres indicates that the algorithm can provide accurate LST retrieval from Landsat 5 TM and Landsat 7 ETM+ data. In most cases, the difference between the retrieved value and the simulated value is less than 0.4°C (Qin et al., 2001), the Equation (8) is below:

$$T_s = \frac{a_i(1-C_i-D_i)+[b_i(1-C_i-D_i)+C_i+D_i]T_i-D_iT_a}{C_i} \quad (8)$$

Where T_s is the Land Surface Temperature (LST), T_i is the brightness temperature from Equation (4), T_a is the effective mean atmospheric temperature, $a_i = 67.355351$ and $b_i = 0.458606$. The values of C_i and D_i can be calculated using the Equations (9) and (10), respectively (Qin et al., 2001).

$$C_i = \varepsilon_i \tau_i \quad (9)$$

$$D_i = (1 - \tau_i)[1 + (1 - \varepsilon_i)\tau_i] \quad (10)$$

Where ε_i is the ground surface emissivity and τ_i is the atmospheric transmittance. T_a , ε_i and τ_i are the three parameters needed to convert the brightness temperature to LST. In order to acquire the effective mean atmospheric temperature of an area, Qin et al. introduced linear relations for the approximation depending on the location of the atmosphere of an area of study.

2.2.2.3 Single Channel Algorithm (SCA)

The definition of the Single Channel Algorithm (SCA) is to use the remote sensing radiation value of a thermal infrared channel of the satellite to realize the temperature inversion algorithm (J. C. Jimenez-Munoz et al. 2009; Jiménez - Muñoz, Sobrino 2003; Juan C. Jimenez-Munoz, Sobrino 2010). Since both TM data and ETM+ data have only one thermal infrared band, the single-window algorithm is mainly used for terrestrial temperature inversion of TM and ETM+ data. Compared with the multi-channel NOAA and MODIS data, the thermal bands of TM and ETM+ data have the highest spatial resolution of 120 meters and 60 meters, so the inversion of regional surface temperature has more extensive applications.

The inversion of land temperature with this algorithm generally goes through three steps: converting the image brightness value to the radiance value; performing precise atmospheric correction; and extracting the emissivity information. Due to the complexity of the inversion process, some scholars later improved the SCA for TM images into an SCA suitable for the ASTER remote sensor (Juan C. Jimenez-Munoz, Sobrino 2010; Ndossi, Avdan 2016). First, the 13th band (10.25-10.95um) and 14th band (10.95-11.65um) Planck equation is linearly simplified, and then the single-window algorithm is used to establish equations for the 13th and 14th bands of ASTER respectively, thus forming a single-window algorithm for the ASTER remote sensor, and briefly describes the acquisition of parameters Introduction. Jimenez-Munoz et al. proposed a single-window algorithm that only needs to know the atmospheric water vapor content to retrieve the surface temperature (J. C. Jimenez-Munoz et al. 2009; Jiménez - Muñoz, Sobrino 2003). The algorithm shown in the Equations (11-13) below:

$$T_s = \gamma[\varepsilon^{-1}(\psi_1 L_{\text{sensor}} + \psi_2) + \psi_3] + \delta \quad (11)$$

$$\gamma = \left\{ \frac{C_2 L_{\text{sensor}}}{T_{\text{sensor}}^2} \left[\frac{\lambda^4}{C_1} L_{\text{sensor}} + \lambda^{-1} \right] \right\}^{-1} \quad (12)$$

$$\delta = -\gamma L_{\text{sensor}} + T_{\text{sensor}} \quad (13)$$

Where T_s stands for LST, T_{sensor} is the at sensor brightness temperature in Kelvin, λ is the effective wavelength of a thermal infrared band in use, $C_1 = 1.19104 * 10^8 \text{ W} \cdot \text{m}^{-2} \cdot \text{sr}^{-1} \mu\text{m}^4$ and $C_2 = 14387.7 \mu\text{m} \cdot \text{K}$. The ψ_1, ψ_2 , and ψ_3 atmospheric parameters can be estimated from Equations (14-16), respectively.

$$\psi_1 = 0.14714w^2 - 0.15583w + 1.1234 \quad (14)$$

$$\psi_2 = -1.1836w^2 - 0.3760w - 0.52894 \quad (15)$$

$$\psi_3 = -0.04554w^2 + 1.8719w - 0.39071 \quad (16)$$

The advantage of this method is a high accuracy, but the calculation is complicated, and the amount of work input required when the research area is large.

2.2.2.4 Radiative Transfer Equation (RTE).

The radiative transfer equation method is also called the atmospheric correction method. Atmospheric correction software compiled mainly according to the radiative transfer equation, and then estimate the atmospheric up and down radiation and the total atmospheric transmittance, and then combine the specific emissivity of the surface objects, and then use the Planck radiation function to find the final, the equation uses the infrared channel extracts the land surface temperature. This algorithm has been successfully used in several studies on LST retrieval (Giannini et al. 2015). RTE is shown in formula (17).

$$L_\lambda = [\varepsilon_\lambda L_\lambda(T_s) + (1 - \varepsilon_\lambda)L_{\text{down}}]\tau + L_{\lambda\text{up}} \quad (17)$$

where L_λ is the thermal infrared radiance received by satellite a sensor which is mainly comprised of surface radiance, down-welling radiance from the atmosphere and up-welling radiance to the atmosphere (Barsi, Schott, et al. 2003); τ is the atmospheric transmittance; ε is the land surface emissivity; $L_\lambda(T_s)$ is the radiance of a blackbody target of kinetic temperature T_s ; L_λ up is the upwelling or atmospheric path radiance; and L_λ down is the down-welling or sky radiance.

In this step the meteorological data of study areas during the satellite overpass time is usually not easy to obtained, therefore, another approach was employed to calculate the atmospheric conditions, studies had demonstrated NASA's Atmospheric Correction Parameter Calculator (Barsi, Barker, et al. 2003) could simulate the atmospheric conditions. Then the land surface radiance, $L_\lambda(T_s)$ of kinetic temperature T_s can be calculated by Equation (18)

$$L_{\lambda}(T_s) = \frac{L_{\lambda} - L_{\lambda up}}{\tau \varepsilon_{\lambda}} - \frac{1 - \varepsilon_{\lambda}}{\varepsilon_{\lambda}} L_{\lambda down} \quad (18)$$

With the radiance calculated, the radiances are converted to LST using the relationship which is similar to the Planck equation with two prelaunch calibration constants of K1 and K2. To do this, Equation (19) has been used in the study (Sinha et al. 2014; Srivastava et al. 2009).

$$T_s = \frac{K_2}{\ln\left(\frac{K_1}{L_{\lambda}(T_s)} + 1\right)} \quad (19)$$

Where T_s is the LST in Kelvin which is changed to degree Celsius ($^{\circ}\text{C}$) by subtracting 273.15; and K_1 and K_2 are thermal constants whose values are obtained from the metadata file.

2.2.2.5 Imaged-based Method (IBM)

The four methods above have a common problem when used to extract the LST; they need to check or calculate the near-real-time atmospheric profile data. However, it is difficult to acquire the history of near-real-time atmospheric profile data (air temperature, relative humidity) when the satellites pass over the study area, which is necessary when utilizing these methods. Therefore, an imaged-based method (IBM) which only uses the Top of Atmosphere (TOA) spectral radiance and the NDVI was proved in many studies (Li et al. 2009; Y. Li et al. 2012; Shen et al. 2016; Weng 2003). The TOA spectral radiance and reflectance can be found from the profile of the Landsat TM/ETM and Landsat-8 OLI/TIRS data (Department of the Interior, U.S. Geological Survey 2019; Shen et al. 2016; USGS, 2019).

For this method the Planck function also used to realize the emissivity correction of brightness temperature, and the land surface temperature after emissivity correction is shown in formula (20).

$$T_s = \frac{BT}{1 + \left[\frac{\lambda \cdot BT}{\rho}\right] \cdot \ln \varepsilon} \quad (20)$$

where T_s is the land surface temperature (K); BT is the at-sensor brightness temperature (K), λ is the wavelength of the emitted radiance; ρ is the $(h \cdot c / o) = 1.438 \cdot 10^{-2}$ mK and ε is the spectral emissivity. The algorithm is based on the NDVI image (Zhang et al. 2006) in **table 2.2**,

Table 2.2: Algorithm based on the NDVI image (Zhang et al. 2006).

NDVI	Land surface emissivity(LSE)
NDVI < -0.185	0.995
-0.185 <= NDVI < 0.157	0.985
0.157 <= NDVI < 0.727	$1.009 + 0.047 * \ln(\text{NDVI})$
NDVI > 0.727	0.990

For land surface emissivity, another approach can be from different land use types: water (NDVI < 0) was assigned a value of 0.9925, urban impervious areas and bare soil ($0 \leq \text{NDVI} < 0.15$)

were assigned a value of 0.923 (Isaya Ndossi, Avdan 2016; Nichol 2005; Shen et al. 2016; F. Wang et al. 2015), and vegetation ($NDVI > 0.727$) was assigned a value of 0.986 (Valor, Caselles 1996). Otherwise, there was a modeling relationship with the NDVI values through the following equation 21 (GRIEND, OWE 1993):

$$1.009 + 0.047 * \ln(NDVI) \quad (21)$$

This imaged-based method was not repaid on the atmospheric profile data, however, the selected satellite images should be the high quality with **clean (cloudless), calm (windless), and sunny weather conditions**, where the influence of atmospheric factors are minimal.

2.2.2.6 Summary of the LST retrieval methods

Remote sensing is an important source of Earth observation using satellite imagery, which is applied to large-scale studies with convenience, cheapness, accuracy (depending on the research design), and faster results than traditional observation methods. The main methods for surface temperature (LST) are listed in the above section. As a major source of data for heat island studies, surface temperature (LST) is also an important parameter for many scientific disciplines because it affects the interaction between the land and the atmosphere. So far, many LST retrieval algorithms based on remotely sensed images have been introduced, where the land surface emissivity (LSE) is one of the main factors affecting the accuracy of LST estimation. In *table 2.3*, I summarized and assessed the advantages and disadvantages of LST retrieval methods using different LSE models and current Landsat mission data.

Table 2.3: Summary of the main LST retrieval methods

Method	Features	Disadvantages	Reference
Plank function	Convert from spectral radiance (thermal band) and wavelength to temperature, Easy data acquisition	The low accuracy of the results caused by treating the Earth as an ideal blackbody radiation	(Planck 2013; Z. M. Zhang, Lee 2009)
Radiative Transfer Equation (RTE)	Suitable for all satellite products in the Landsat series with infrared band	1. The calculation process is complicated 2. Since atmospheric parameters and near-surface temperature (historical data) are not easily available for satellite imaging.	(Barsi, Schott, et al. 2003; Price 1983; Sekertekin 2019; Srivastava et al. 2009; Zhaoliang et al. 2013)
Mono-Window algorithm (MWA)	1. Considering the influence of land surface emissivity and atmospheric radiation , the surface temperature is more accurate 2. Required near-surface air temperature and atmospheric humidity	Atmospheric Correction Parameter data need to be used for substitution, which has an impact on	(Qin et al. 2001; Tsou et al. 2017; F. Wang et al. 2015)

Single Channel Algorithm (SCA)	1. Considering the influence of land surface emissivity and atmospheric radiation, the surface temperature is more accurate 2. Required atmospheric humidity	the accuracy of inversion results	(J. C. Jimenez-Munoz et al. 2009; Jiménez - Muñoz, Sobrino 2003; Jiménez-Muñoz et al. 2014; Juan C. Jimenez-Munoz, Sobrino 2010)
Imaged-based Method (IBM)	1. the calculation process is relatively simple and easy to operate 2. No atmospheric parameter correction is required 3. Using land surface emissivity to improve the accuracy	Neglecting the influence of atmospheric radiation factors on the surface temperature inversion	(Li et al. 2009; Y. Li et al. 2012; Shen et al. 2016; Weng 2003)

2.3 The impact of UHI

The urban heat island effect is one of the most obvious characteristics of urban climate and one of the important elements reflecting the quality of urban ecological environment. Due to the high temperature near the surface in the center of the heat island, the atmosphere moves upwards, forming a pressure difference with the surrounding area, and the near-surface atmosphere in the surrounding area converges to the central area, thus forming a low-pressure vortex in the center of the city, which is bound to cause people's life, industrial production, and Atmospheric pollutants formed by burning fossil fuels in the operation of vehicles accumulate in the central area of the heat island, endangering people's health and even lives.

2.3.1 Increase urban energy consumption

The urban heat island effect in summer has exacerbated the appearance of extremely high temperatures, which will inevitably lead to the use of cooling appliances such as **air conditioners** and electric fans. In the case of household appliances, the peak heating demand increases the pressure on the grid. Studies have shown that every time the temperature rises by 0.6°C in summer, the city's peak **electricity consumption** will increase by 1.5% to 2%. In the United States, the continuous rise in temperature in the city center means that 5% to 10% of the entire community's electricity demand is used to compensate for the Energy Saving Potentials and Air Quality Benefits of Urban Heat Island Mitigation. In extreme thermal events, the urban heat island will exacerbate this situation, and the energy consumed by cooling will cause the system to overload the urban power supply. Greenhouse gases, especially carbon dioxide (CO₂), emitted by electricity generated by fossil fuels, will exacerbate global climate change.

2.3.2 Impact on climate

The urban heat island effect has a significant impact on urban weather. It will bring many kinds of abnormal weather and extreme disaster weather, such as **heavy rains and hurricanes** (Demanuele et al. 2011). The urban heat island effect can also change urban wind fields, clouds, fog, precipitation, lightning, etc. (Morris et al. 2001; M. S. Alonso et al. 2007; Memon, Leung 2010). Urban heat island effect can increase precipitation in cities, but the urban heat island effect only increases precipitation without causing rain, but it does not increase rainfall frequency (Terray, Cassou 2000; Bodri et al. 2005).

2.3.3 Impact on the atmospheric environment

The urban heat island effect is related to the quality of the atmospheric environment. In high-temperature weather, the airflow containing a large amount of smoke and dust rises due to the heat island, which seriously pollutes the near-surface air. At the same time, urban exhaust pollutants include sulfur dioxide (SO₂), Nitrogen oxides (NO_x), particulate matter (PM), carbon monoxide (CO) and mercury (Hg) form secondary pollutants through photochemical reactions, which will cause more significant harm to the environment (Akbari 2005). The continuous high temperature in cities can accelerate specific atmospheric chemical cycles, leading to an increase in surface ozone. In addition, the evaporation of biological hydrocarbons will be affected by the high-temperature environment, and which could be related to the formation of ozone in the troposphere (Fallmann et al. 2016).

2.3.4 Affect human health and thermal comfort

Under the influence of the heat island effect, severe air pollution will occur over the city, posing a hazard to human health. Many human diseases are caused by the heat island effect (Tomlinson et al. 2011b). Related studies have found that the human body's physiological activities have a very close relationship with the environmental temperature. In excessively high temperatures, the human body will feel uncomfortable. Even cause-related diseases such as the respiratory system, cerebrovascular, and heart, and the mortality rate will also increase significantly (EPA 2014a).

2.4 Urban heat island research review

Urban areas are the center of human activities, energy consumption, and greenhouse gas emissions, which contribute to global climate change. Most of the cities are located in plains at lower elevations (United Nations. 2019). Due to the composition of the **urban canopy layer** of the city (urban roughness) such as impervious surfaces, buildings, municipal facilities, etc., (Bottema 1997), have led to a change in the local climate that has, resulted in problems such as

urban heat island (Rodler, Leduc 2019). Local climate change is caused by two different but related reasons. One of them includes surface cover, building materials and forms (Alexander et al. 2016). The other one is anthropogenic activities, such as industrialization, transportation, solid waste generation, and excess waste water generation have also been reported to influence the natural structure of cities (Reichle 2020). Urban form also has an impact on urban heat island, as many researchers have demonstrated this (Ng et al. 2011; Thani et al. 2013). Due to the lack of considering the relations between urban forms and urban ventilation in city planning, the urban ventilation environment is getting worse and worse, hence, increasing the intensity of the heat island effect. This drawback forms the backbone of enormous research interest in the adjustment of urban form and urban function, especially adjusting the microclimate to mitigate the heat island effect. Urban heat island is related to many other factors such as meteorological parameters, material properties and those kinds of impact factors (*Table 2.4*) has been demonstrated in many research and publications.

a) Urban heat island models

Most studies analyze the **urban heat island effect by using satellites** (Jenerette et al. 2007; Jiang, Tian 2010; Tomlinson et al. 2011a; Jiménez-Muñoz et al. 2014; Bokaie et al. 2016; Azhdari et al. 2018). The surface temperature obtained from the image needs to be calibrated. Although there is a certain relationship between the surface temperature and the air temperature, this relationship becomes extremely uncertain due to the heterogeneity of the surface. Furthermore, human thermal comfort is related to air temperature, mean radiant temperature, wind speed and relative humidity (Antoniadis et al. 2018; Galagoda et al. 2018), thus, studying the characteristics of microclimate at the city scale is more conducive to interfacing with urban planning. From the thermal conduction studies, the simulation method was commonly used to investigate in a different scale. For example, Urban Weather Generator (UWG) model was mainly applied to simulate the local microclimatic phenomena in the city scale (J. Mao et al. 2017). In mesoscale weather simulation, the Computational Fluid Dynamics (CFD) model was widely used to estimate the thermal conduction and heat flux in city areas such as buildings and street levels (Adelia et al. 2019; Salvati et al. 2020).

b) Urban heat island and mitigation studies

Urban cool island (UCI) usually refers to that the areas that have a lower temperature compared with its surroundings such as vegetation areas and water bodies in cities (W. Lin et al. 2015; Zardo et al. 2017). **Vegetation** changes the three-dimensional space of the city seasonally and also changes the incident and reflected energy of the sun. Vegetation cools down the air and surfaces through evapotranspiration and shadows. Soil and water use their own absorption and high heat capacity to achieve the cooling effect (Kotthaus, Grimmond 2014). In addition to the physical properties of the above mentioned and other urban constituent materials, the impact of green space

layout is also proven (Andreou 2014; Skelhorn et al. 2014). At present, there are two main scales for studying the cooling effect of **urban green space**. The first one is large-scale research based on satellite imagery and meteorological data (Du et al. 2016; Hamada et al. 2013; Huawei Li, Wang, Tian, et al. 2020). These studies applied indicators such as **Park Cooling Intensity (PCI)** and **Green space Cooling Intensity (GCI)** to quantify the cooling effect of UGS (Cao et al. 2010; Du et al. 2017; W. Lin et al. 2015). The other one is small scale research through field observation and application of models (Bencheikh, Rchid 2012; Yafei Wang et al. 2015; Antoniadis et al. 2018). Field observation data can more directly and accurately characterize the dynamic relationship between urban green space and atmospheric temperature than other spatial datasets derived from satellite imagery. This approach at this scale, has an important practical guiding significance for the rational planning and layout of urban green space. Compared with the large-scale landscape design, the small-scale design is easier to manage. The small green spaces (SGSs) like cells in the city, play an important role in regulating the microclimate (Park et al. 2017). Specifically, they play a significant role in improving the environmental quality of local microclimate. However, the role played by SGSs have often been neglected in research.

Table 2.4: A summary of the main factors related to UHI trends. Sources: Based on (Arnfield 2003)

Impact factors	UHI trend	Reference research
Cloud	With Cloud cover ↑ UHI ↓	(Alonso et al. 2007; Eliasson 1996; Hong et al. 2019; Memon, Leung 2010; Morris et al. 2001)
Wind	With Wind speed ↑ UHI ↓	(Hong et al. 2019; Memon, Leung 2010; Morris et al. 2001; Unger et al. 2001)
Precipitation	With Precipitation ↑ UHI ↓	(Hong et al. 2019; Terray, Cassou 2000)
Humidity	With humidity ↑ UHI ↓	(Fan et al. 2019; Masterton, Richardson 1979; Unger 1999; Yahia et al. 2018; Z. Zhang et al. 2013)
Snow	With Snow cover ↑ UHI ↓	(Giridharan, Kolokotroni 2009; Huawei Li, Wang, Jombach 2020; Yin, Zhang 2014)
Sky view factor (SVF)⁸	With SVF ↑ UHI ↑	(Gál et al. 2009; Hämmerle et al. 2011; Unger 2009)
Latitude /Location	With latitude ↑ UHI ↓	(Unger et al. 2018; Upmanis et al. 1998; Yang et al. 2020)
Albedo	With Albedo ↑ UHI ↓	(Bhattacharya et al. 2009; Erell et al. 2014; Taha 1997; US EPA 2014b)
Surface emissivity	With emissivity ↑ UHI ↓	(Griend, Owe 1993; Huang et al. 2012; Mohamed et al. 2017; Sekertekin, Bonafoni 2020; Sobrino et al. 2001; Sobrino, Jiménez-Muñoz 2014; Valor, Caselles 1996)

⁸ A Sky View Factor (SVFs) represents the ratio at a point in space between the visible sky and a hemisphere centered over the analyzed location (Oke 1981).

In the studies of Urban Cold Island (UCI) effects and UHI mitigation (Ng et al. 2012; Rasul et al. 2017), two methods were widely used to quantify the cooling effect of green space and park areas. These are called Green space Cooling Intensity (GCI) and Park Cooling Intensity (PCI) (Oliveira et al. 2011; Du et al. 2017). GCI is defined as the temperature difference between green space and the average temperature of the whole study area. While the PCI usually determined as the temperature difference between the inside park area and its outside within a 500m buffer area (Cao et al. 2010; W. Lin et al. 2015). These two methods are used to describe the cooling effect of green spaces and parks. Studies also show that vegetation coverage has a significant effect on the reduction of UHI (Kawashima 1990; Weng et al. 2004; Yuan, Bauer 2007).

On top of this, the **impervious surface area** is positively correlated with LST and contributes the most to UHI (Chen et al. 2006; Yuan, Bauer 2007; Gartland 2008). Some studies use landscape factors to analyze the UCI and GCI on mitigating the UHI effect (Liu, Weng 2008; J. Li et al. 2009; Estoque et al. 2017). The parameters include shape index (Shape_idx), fractal dimension (Frac_Dim) and landscape connectivity. One research study focused on the role of green space in reducing the UHI effect. This research looked at the distance changes of the green space cooling effect in relation to the characteristics of green space bodies with regards to **green area features** (size, shape, etc.) and UHI. The results of these studies showed that the cooling effect of green space is complex (Cao et al. 2010; Du et al. 2017; Oliveira et al. 2011). PCI related studies mostly used remote sensing imagery as base data. According to a study based partly on surrounding vegetation, water body and impervious surface (Du et al. 2017), the cooling effect of parks is also depending on types of outside the park spaces.

The **air temperature** is also employed to examine the cooling effect of parks on UHI (Kolokotroni, Giridharan 2008; Shinsuke Kato, Hiyama 2012). It is also noted that the **patch and pattern** of a park has a relationship to the cooling effects that it has on the UHI it forms part of. Some researches employ the **thermal conduct theory**, a physical science methodology, to investigate the heat balance (between park and its surrounding area) when studying the urban thermal environment (Kanda, Moriizumi 2009; Monteith, Unsworth 2013; Kotthaus, Grimmond 2014), this method can assist in providing a methodical approach to understanding the cooling effect of park.

2.4.1 The UHI research development analysis

Bibliometrics review is a common research tool for comprehensive analysis (Eck, Waltman 2007; Waltman et al. 2010; Alonso et al. 2018). The early stages of research can extract important information, such as the development process, research trends, research status, hot issues, important research articles, and major contributors to the research field (Jinguang Zhang et al. 2020). To provide a basis for mastering the research field and formulating research plans in a short time. Studies showed that the Web of science (WoS) database focuses on the natural science area,

although it contains fewer categories than Scopus (Falagas et al. 2008; Mongeon, Paul-Hus 2016). Urban heat island is a topic that mainly belongs to environmental science and atmospheric science.

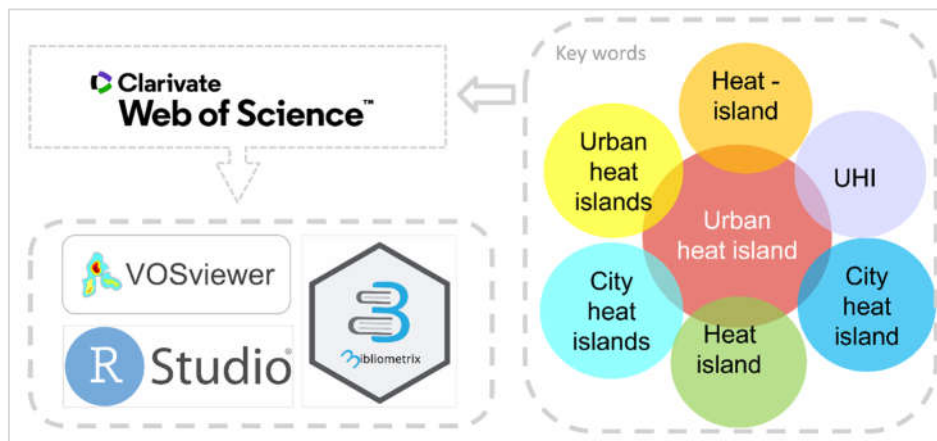


Figure 2.6: The workflow of the bibliometrics methods and the keywords used in searching UHI scientific publications in WoS database.

On this basis, followed the rule of search engine of WoS database, by search the keywords "**urban heat island**" or "**Heat island** "or "**urban heat islands***" "**city heat island***" "**city heat islands**" or "**UHI***" as the conditional base (*Figure 2.6*), the period was selected from 1975-2020. After that, I exclude the publications, which are not the research areas from the recordings. For example, the publication subjects belong to the cell, toxicology, industrial, business, psychology, etc. After refined data and the content control was carried out, I finally obtained 7808 useful recordings (*Figure 2.7*). It was found that the UHI researches had a slow growth period between 1975 and 1990, only 65 related UHI publications, while after the 21st century, it became a rapid increase and published 1157 UHI researched with ten years in 2001-2010. In the past ten years from 2011-2020, the UHI related researches had an **explosive growth**, with a 5982 related scientific product published only 10 years and still increasing. We can see from the statistics that the heat related environmental degradation are widely expanding with globalization.

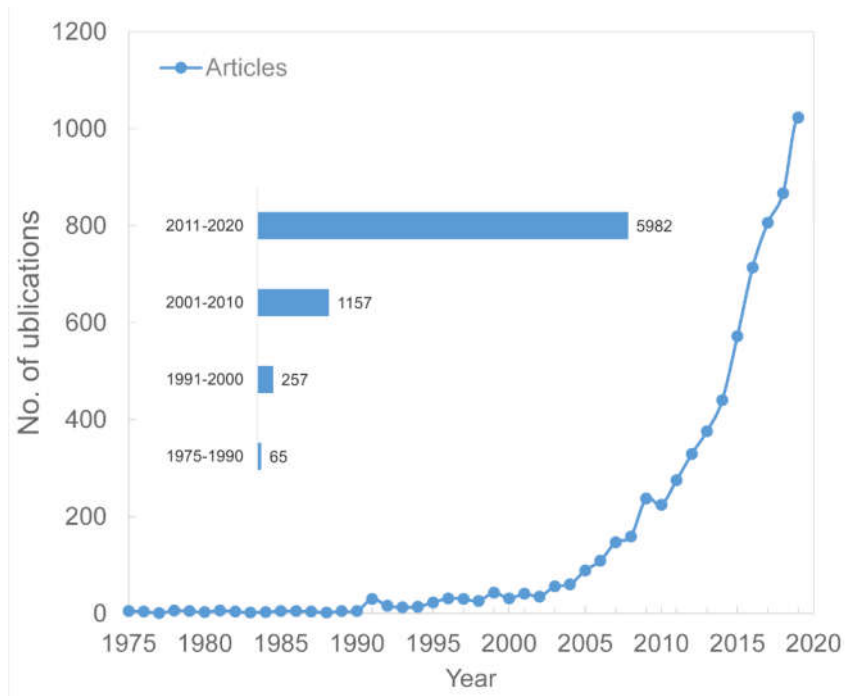


Figure 2.7: Scientific productions during 1975-2020 from Web of Science (WoS).

From the 7808 publications, it could be classified into four types: articles (76.74%), proceeding papers (14.7%), reviews (3.4%), and others (5.1%) see Figure 2.8. Articles are the main form on UHI researches, while conference related UHI topics are also frequent focused in the past academic symposium both internationally and locally.

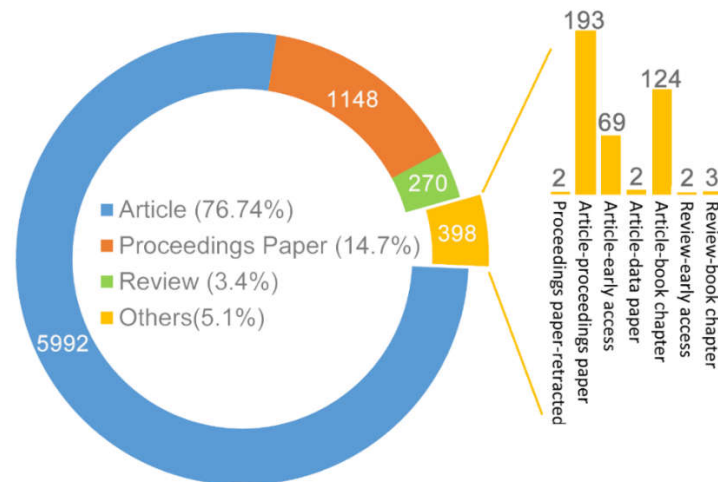


Figure 2.8: Types and percentage of the publications from 1975-2020 from WoS database (search date: Nov.14, 2020).

The year 1975-2020 by using the statistic software. Most frequent key words: heat island effect, urbanization, Land surface temperature; relationship, landscape pattern. etc. I summarized the keywords which appeared more than 50 times in 7808 articles from 1975-2020 see Figure 2.9. UHI and UHI intensity are measured by the temperature difference between urban and rural areas.

The research indicators in the literature include temperature, surface temperature, land surface temperature and air temperature. The statistical results show that the surface temperature is the most commonly used temperature indicator, with 407 occurrences and 348 occurrences above air temperature (*Appendix 1*). **These two indicators represent two types of UHI: atmosphere UHI and surface UHI.** The former (usually 1.5-2 m) is determined by field measurements, while the latter is derived directly from satellite data inversion of ground thermal radiation. With the widespread application of remote sensing technology in UHI research, remote sensing satellite land surface temperature is expected to continue to popularize in UHI research (2010-2020). However, as a well-known basic indicator, despite the difference between surface temperature and temperature, the two usage levels have remained stable in the past ten years. Since the surface temperature usually cannot reflect the defense on the time scale, the air temperature data still cannot be replaced. With the development of computer technology, numerical simulation technology has also been widely used in the study of urban climate and heat islands. Therefore, "simulation" increased from 70 times in 2000-2009 to 397 times in 2010-2020 (*Appendix 1*). Therefore, it can be seen from the data source that UHI research data sources are divided into three types: meteorological measurement, remote sensing technology, Numerical Simulation (*Table 2.5*).

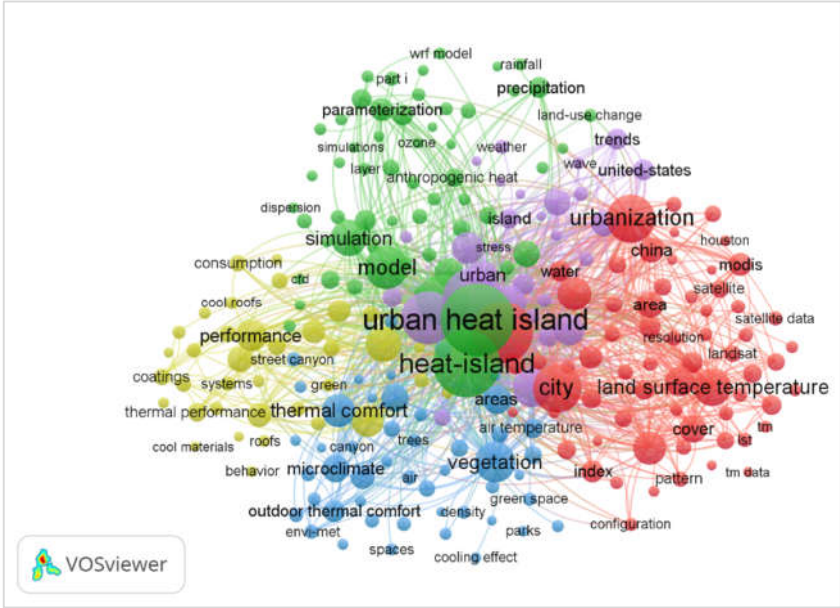


Figure 2.9: Keywords word cloud from the UHI publications from 1975-2020.

Factors of the UHI: The scientometric analysis on keywords such as urbanization, land use, surface, energy, solar reflectance, vegetation, albedo, and man-made heat, have high frequencies. Urbanization and vegetation are the core themes for the period 2000-2020 (*Appendix 1*). In fact, urbanization and the resulting land use and surface changes are the main cause of UHI. These results can be explained from previous literature reviews.

1) Urbanization has resulted in the lower albedo of impermeable surfaces (such as asphalt,

concrete, brick, and rebar), and higher thermal conductivity and heat storage capacity than permeable surfaces in rural areas (Bhattacharya et al. 2009, 2009; Taha 1997), which leads to radiation conditions in urban areas more solar radiation is absorbed and stored underneath than in rural areas; therefore, albedo is considered to be one of the main reasons for UHI.

- 2) The reduction of vegetation and the increase of impervious surfaces reduce the loss of latent heat from vegetation and soil (Weng et al. 2004; Yuan, Bauer 2007). It is the gradual accumulation of thermal energy in urban areas, and the latent heat cannot offset the sensible heat (Bowen 1926; Oke, Cleugh 1987; Ooka et al. 2011).
- 3) High buildings and high-density buildings reduce the sky view factors (geometric shapes of street canyons), thereby reducing long-wave radiation loss and turbulent heat transfer, which is another main reason for the high temperature in urban built-up areas (János Unger 2004).
- 4) The burning of fuel will release a large amount of waste heat from factories, automobiles, air conditioners, and other sources. On the other hand, emissions from urban industries and activities generate greenhouse gases, which contribute to more long-wave absorption, while exacerbating global warming. Pollutants from industrial and automobile exhaust, especially aerosols, can induce air, water and soil pollution (US EPA 2014a).

Table 2.5: Summary of reviews of UHI publications from 1997

Year	Focus	Publications
1997	Review of impacts of surface albedo, evapotranspiration, and anthropogenic heating	(Taha et al.1997)
2003	Review of the application of thermal remote sensing with particular emphasis on the UHI <i>effect</i>	(Voogt, Oke 2003)
2003	Review of turbulence, exchanges of energy and water , and the urban heat island	(Arnfield 2003)
2004	Review of the intra-urban sky view factor -temperature relationship	(Unger et al. 2004)
2005	Satellite Remote Sensing of Urban Heat Islands	(Weng et al.2005)
2007	Use of Satellite Remote Sensing in Urban Heat Island Studies	(Stathopoulou, Cartalis 2007)
2008	Review on the generation, determination and mitigation of Urban Heat Island	(Rizwan et al. 2008)
2009	Thermal infrared remote sensing for urban climate and environmental studies: Review of Methods, applications, and trends	(Weng et al. 2009)
2011	Review of the techniques used to study UHI	(Mirzaei, et al.2010)
2011	Remote sensing land surface temperature for meteorology and climatology review	(Tomlinson et al. 2011a)
2013	Review of strategies to mitigate adverse UHI effects	(Gago et al. 2013)
2015	Review of urban heat island intensity	(Tzavali et al. 2015)
2015	Review on the impact of urban heat island and global warming on the power	(Santamouris et al.

	demand and electricity consumption of buildings	2015)
2015	Review of the compatibility of each type of model suitable for various objectives and scales of UHI studies	(Mirzaei 2015)
2016	Review on the impact of urban geometry and pedestrian level greening on outdoor thermal comfort	(Jamei et al. 2016)
2017	Review on remote sensing of urban heat and cool islands	(Rasul et al. 2017)
2017	Review on land surface temperature and emissivity estimation for urban heat island assessment	(Mohamed et al. 2017)
2017	Review on the impact of urbanization and climate change on urban temperatures	(Chapman et al. 2017)
2018	Review of spatio-temporal factors, data, methods, and mitigation measures	(Deilami et al. 2018)
2020	Review development of urban heat island evaluation methodology	(Sangiorgio et al. 2020)
2021	Review on urban heat island impact on buildings energy demand and mitigation strategies	(Tian et al. 2021)

2.4.2 Summary of urban heat island research

From the bibliometrics method review on UHI related publications, it was found that:

1) There are **7808** publications from 1975 to 2020, which belongs to **57 types** of subjects; from **1620** sources (Journals, Books, conferences paper, etc.), the **references** number is **147,611**, totally **15,824 authors** published their work.

2) The most relevant top three **journals** are **Energy and Buildings; Building and Environment** and **Urban climate**. **Chinese Academic of Science** (561, 5.63%) and **Arizona State University** (222, 2.12%) were the top two research institutions (*Appendix 2*). China (19.95%), the U.S.A. (15.86%), and Italy (5.01%) were the top 3 countries that have the most publications in UHI (*Appendix 3, 4*). Weng QH and Santamouris M were the two most prolific authors (*Appendix 5*).

3) The top 9 disciplines include **environmental science** (2150; 27.54%), **atmospheric science** (2061; 26.40%), building science (1181; 15.13%), remote sensing (973; 12.46%), energy and fuel (948; 12.40%), Civil engineering (948; 12.14%); Green sustainable science technology (682; 8.73%), engineering environment (584; 7.48%), earth science (525; 6.72%) see *Figure 2.9*.

4) **Oke T.R.** (5989 times) and **Santamouris M** (3089 times) were the most-cited authors in the citation aspect (*Appendix 6*). The most cited top 3 sources are Energy and buildings; Building and Environment; Atmospheric environment (*Appendix 7*). The most cited top 3 institutions were the Chinese academy of science, Arizona state university, and Nanjing University (*Appendix 8*).

5) **Research trends** from the keywords clusters: from 1975-2012; the main topic is vegetation and UHI; UHI model; temperature measurement; from 2013-2020; the main topics were: Urban heat island and its impact, mitigation; impacts (*Appendix 9*). In the future, the main trend is the adaptation to the urban heat environment

2.5 Research gap

Concerning Zhengzhou city, which experienced a rapid urbanization process during the past 40 years, with the increased awareness of the environmental problems, new-built towns and districts were guided by the ecological city planning and design principles, such as Zhengzhou green network planning and implementation, Zhengzhou water system planning, Spongy city plot, etc. New term urbanization and urban renewal present a different vision compare with past planning way.

In this situation, how is this new term urbanization process impact the urban environment and urban problems? Is it reacting to past urban problems such as urban heat island? Previous research (Unger et al. 2001; Chen et al. 2006; H. Zhang et al. 2013; Bokaie et al. 2016; Mohajerani et al. 2017) only focus on the relationship between the UHI and urbanization process, the factors of urban land use /land cover, and did not compare the past to recent. Besides, urban heat island mitigation strategies should put into practice in various scales such as urban scale, local scale, and micro-scale. Systemic research on urban heat islands in Zhengzhou city is requisite from the perspective of an expanding city. This is also a research gap.

The research on urban heat island characteristics research in high-density and high-speed expanding city is still not sufficient detailed (Li et al. 2019a; Min et al. 2018; Z. Wang et al. 2018; Zhao et al. 2018) from the landscape architect point of view, especially in the Zhengzhou region, China

---Sub direction: Surface UHI related factors in rapid developing city such as the urban Land Use /Land Cover (LULC), the character of built-up area, vegetation, parks, urban expansion direction, coupling with long-term meteorological data, other socio-economic factors such as urbanization rate, population density, etc.

The research related to urban heat and the cooling effect of green spaces **is not always universality** to guide urban planning and **urban landscape design with respect to different region and city.**

--- the microclimate level related factors on urban thermal environment in small green spaces, such as vegetation types, the height of plants, leaf angle, etc

The research related to surface urban heat island characteristics on vertical factors **are less and not sufficient research findings** to guide urban planning and **urban landscape design.**

--- the vertical variables such as the topographical factors, building height, vegetation height etc. in terms of mitigating UHI by manipulating urban landscape planning and design variables.

3. METHODS AND MATERIALS

In this chapter, the study areas and samples are introduced, at the same time, all the methods and materials which are used in this dissertation also being presented. Subchapter 3.1 is the study area background information, Subchapter 3.2 is the materials are employed for all the investigation, Subchapter 3.3 is the methodology and workflow for the entire dissertation. Apart from that, some details of the methods and materials will be presented in each survey in the following chapters.

3.1 Study areas

In the dissertation, two cities are used as the study area, which are Zhengzhou city, China and Budapest city, Hungary.

3.1.1 Zhengzhou city

Zhengzhou is the capital and largest city of Henan Province in the central part of the People's Republic of China. It is one of the National Central Cities in China (**Figure 3.1**), the center of central plains area and serves as the political, economic, technological, and educational center of the province, as well as a major transportation hub in China (highway, railway, aviation, communication). The Zhengzhou metropolitan area is the core area of the Central Plains Economic Zone. Greater Zhengzhou was named as one of the 13 emerging mega-cities in China in a July 2012 report by the Economist Intelligence Unit, and officially named as the eighth National Central City in 2017 by the central government in Beijing. As a center of China's national transportation network, there are railways connecting Zhengzhou and Europe, and a bustling international airport (Asia, Europe, Africa, America, Oceania).

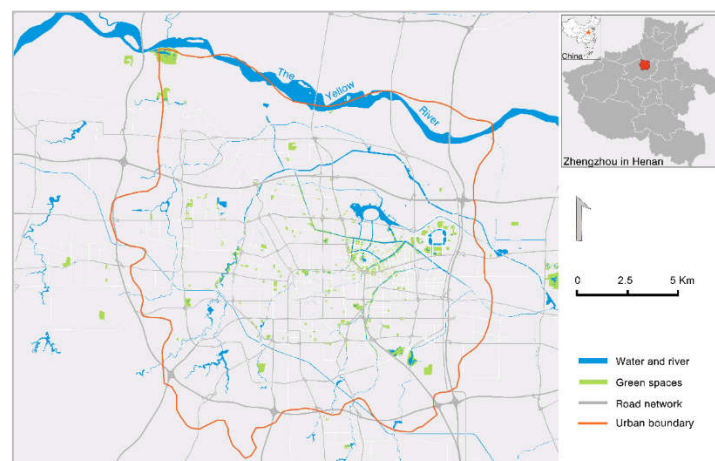


Figure 3.1: Location of the study area Zhengzhou in Henan province, Henan province in China.

3.1.1.1 Geography of Zhengzhou

Zhengzhou is located north of the province's central and south bank of the Yellow River, the topography of Zhengzhou region is high in the west and low in the east. The altitude difference is obvious. Plain areas (6-135.2m above sea level), hilly areas (135.2-315.4m above sea level), low mountain areas (315.4-495.6m above sea level) and middle-high mountainous areas (495.6 above sea level) respectively account for 50%, 24%, 19%, and 7% of the entire area (**Figure 3.2**).

The section of the Yellow River flowing through the prefecture extends 150.4 km (93.5 mi). Mountains loom over the western counties of Gongyi and Dengfeng while the easternmost county of Zhongmu is a vast, fertile floodplain, with the counties in between being hilly transitions.

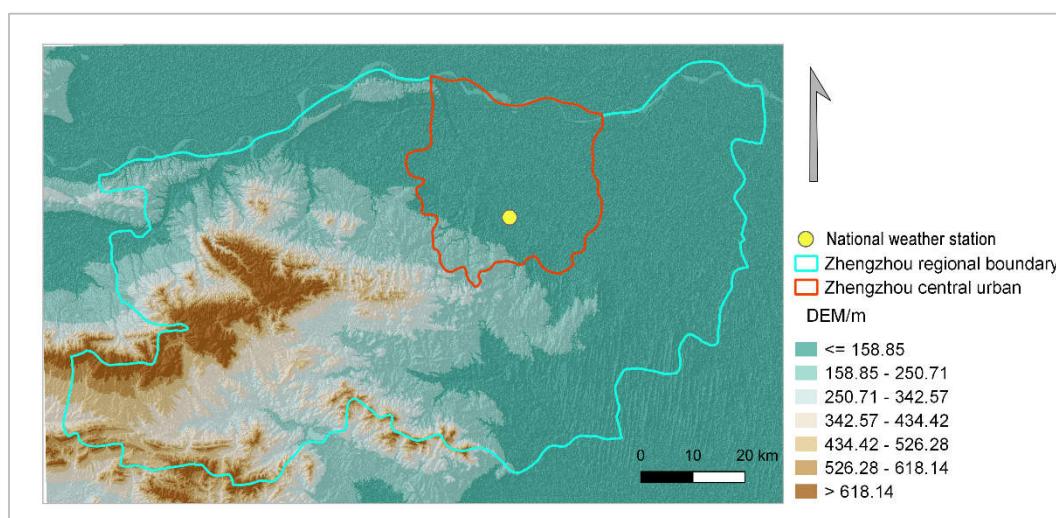


Figure 3.2: Topographic elevation map of Zhengzhou city

3.1.1.2 Climate of Zhengzhou

Zhengzhou lies in a dry-winter humid subtropical climate zone according to the Köppen climate classification system (Beck et al. 2018). According to Zhengzhou **national weather station** (**Figure 3.2**) and meteorological record (**Figure 3.3**), the annual average temperature was 15.6 °C; August was the hottest, with a monthly average temperature of 25.96 °C; January was the coldest, with a monthly average temperature of 2.156 °C. The annual average rainfall was 542.15 mm. The annual average sunshine hours is 2341.25 hours, which is the highest in the suburbs of Zhengzhou, with an accumulated temperature of 467.32°C above 10°C, which is very suitable for the growth and reproduction of crops. The annual average wind speed is 2.0 m/s (the largest on the top of Songshan Mountain), and the maximum wind force is 9 levels. It is the largest in spring in March and April and winter in December and January, and the smallest in August, September and October. The wind direction is mostly northwesterly. The average total surface radiation was 278.03 Wh/m², and the average global Horizon radiation was 291.23 Wh/m². The yearly average wind direction was SSE (157.54 degree). Average relative humidity was 65.98%.

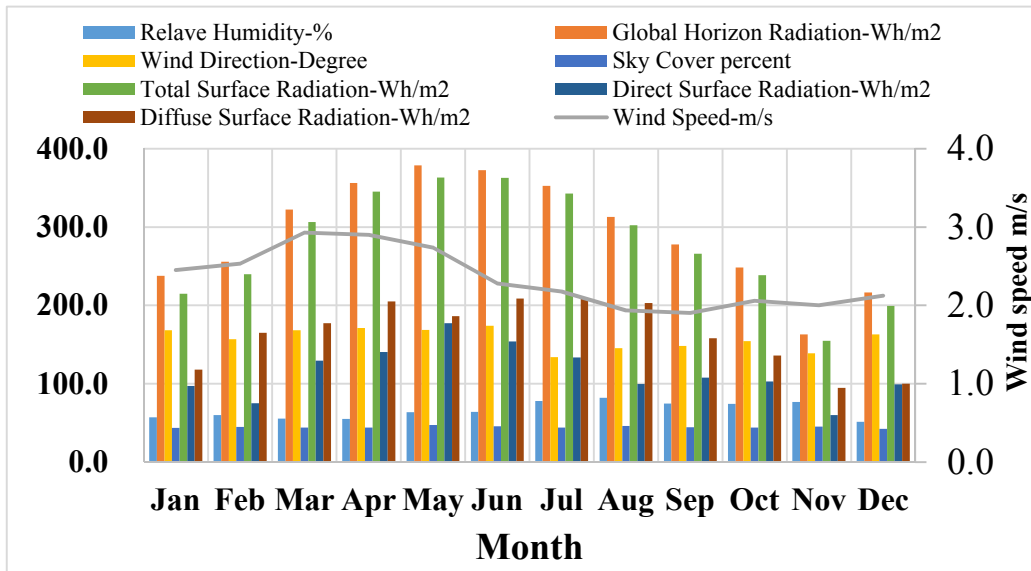


Figure 3.3: Monthly average weather data summary based on the Zhengzhou national weather station (No.570830, Elevation 110m).

3.1.2 Budapest city

Budapest is the capital city of Hungary, located in the central part of the country (*Figure 3.4*). The city had an estimated population of 1.75 M inhabitants and has a land area of about 525 km². Budapest's climate is humid continental climate (Dfb) based on Köppen-Geiger climate classification (Dfb), which has relatively cold winters and warm summers (Beck et al. 2018). According to the long-term observation data record from 1991-2019 (OMSZ, 2020), the mean temperature in Budapest is 11.30°C.

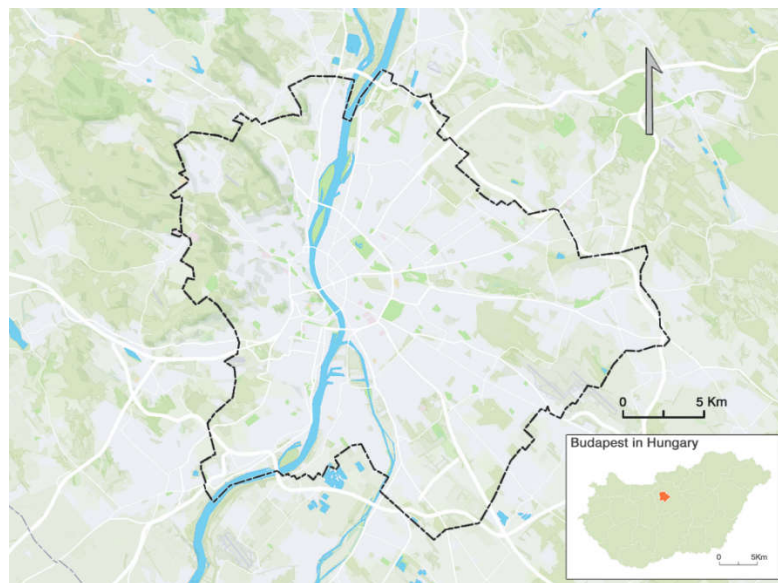


Figure 3.4: The location and green spaces of Budapest (source: OSM)

3.1.2.1 Geography of Budapest

Budapest, spatially placed at the center of the Carpathian Basin, lies on an ancient route linking the hills of Transdanubia with the Great Plain. Budapest lies in Central Hungary, surrounded by settlements of the agglomeration in Pest county. The capital extends 25 and 29 km (16 and 18 mi) in the north-south, east-west direction respectively. The Danube enters the city from the north; later it encircles two islands, Óbuda Island and Margaret Island. The third island Csepel Island is the largest of the Budapest Danube islands, however only its northernmost tip is within city limits. The river that separates the two parts of the city at its narrowest point in Budapest. Pest lies on the flat terrain of the Great Plain while Buda is rather hilly.

The wide Danube was always fordable at this point because of a small number of islands in the middle of the river. The city has marked topographical contrasts: Buda is built on the higher river terraces and hills of the western side, while the considerably larger Pest spreads out on a flat and featureless sand plain on the river's opposite bank (<https://www.britannica.com/place/Budapest>). Pest's terrain rises with a slight eastward gradient, so the easternmost parts of the city lie at the same altitude as Buda's smallest hills, notably Gellért Hill and Castle Hill.

The Buda hills consist mainly of limestone and dolomite, the water created speleothems, the most famous ones being the Pálvölgyi cave (total length 7,200 m or 23,600 ft) and the Szemlőhegyi cave (total length 2,200 m or 7,200 ft). The hills were formed in the Triassic Period. The highest point of the hills and of Budapest is János Hill, at 527 metres (1,729 feet) above sea level. The lowest point is the line of the Danube which is 96 metres (315 feet) above sea level. Budapest is also rich in green areas. Of the 525 square kilometres (203 square miles) occupied by the city, 83 square kilometres (32 square miles) is green area, park and forest⁹. The forests of Buda hills are environmentally protected¹⁰.

3.1.2.2 Climate of Budapest

Budapest has a humid continental climate (Dfb) according to the Köppen climate classification (Beck et al. 2018), with relatively cold winters (near of a humid continental climate when the 0 °C isotherms are used) and warm summers (near of an oceanic climate) according to the 1971-2000 climatological norm (OMSZ, 2020). Considering the average monthly average temperatures of Budapest for many years, it can be said that the coldest month is January, while the warmest is July. The average annual temperature fluctuation is 21.9 °C (**Figure 3.5**). The warmest month (with the highest average high temperature) is July (26.7°C). The month with the lowest average high temperature is January (2.9°C). The month with the highest average low temperature is July

⁹ Source: https://www.budapest.com/city_guide/general_information/geography_of_budapest.en.html

¹⁰ Source: <https://www.dunaipoly.hu/en/places/protected-areas/protected-areas-1/protected-landscape-area-of-buda>

(16.8°C). The coldest month (with the lowest average low temperature) is January (-1.6°C).

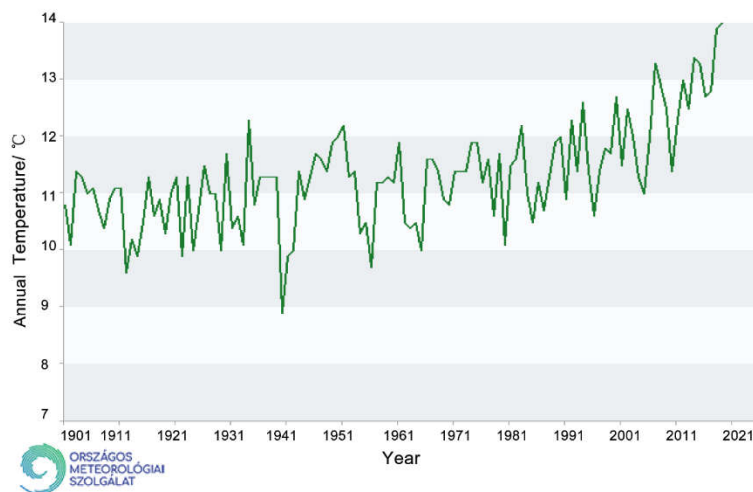


Figure 3.5: The annual mean temperature of Budapest from 1901-2020

The average annual rainfall in Budapest is 516 mm (*Appendix 10*), with two rainier periods (early summer and late autumn) and two drier periods (mid-winter-early spring and early autumn). The least rainfall falls in February-March, and the wettest months - in roughly twice the amount - are May-June. The wettest month (with the highest rainfall) is June (63mm). The driest month (with the lowest rainfall) is February (29mm). Months with the highest number of rainy days are May and June (8 days). Months with the lowest number of rainy days are September and October (5 days).

The average number of hours of sunshine in Budapest is 2010 hours on average (*Appendix 11*), but it shows great variability from year to year. A typical annual course of sunshine duration can be observed, with a maximum in the summer months (250-280 hours per month) and a minimum in the November-January period (60-70 hours per month). The month with the most sunshine is July (Average sunshine: 8.7h). The month with the least sunshine is December (Average sunshine: 1.7h).

3.2 Data collection

In this dissertation, several types data and materials are used for different scales and dimensions purpose, those database are categorized into four sets: **1) Meteorological data; 2) Geospatial GIS data; 3) Field survey data; 4) other additional-statistical data.**

3.2.1 Meteorological data

In order to analyze the long-term **atmospheric urban heat island (UHI)**, the **fixed weather station observation data** were applied to illustrate and analyze the temporal changes of the UHI base on air temperature. In Zhengzhou region, there are three observatories which have more than 40 year history to record the weather data. The urban station is located in the south part of Zhengzhou central area (34.72, 113.65; elevation, 110.4m), which can represent the temperature in urban area, Around the urban weather station, the environment had been changed dramatically due to the rapid urbanization during the study period: According to the Local Climate Zones(LCZs) classification (Stewart and Oke, 2012), the urban station was **LCZ D** (before 2000), after 2001, the LCZ changes from LCZ 6, LCZ 4, LCZ 1 respectively (*Appendix 12*). Another station located the rural part which represents the rural temperature. Xinzheng (34.38, 113.72; elevation, 116.6m) station, which has a 35km distance to urban station. Local Climate Zones classification for Xinzheng station also changed with the development, the Xinzheng station type was **LCZ D** before 2009, and after that, the LCZ changes from **LCZ 6** to **LCZ 4**, respectively (*Appendix 13*) . those two observatories are also China’s national station with the international standard (*Figure 3.6*).The data were provided by the Henan Provincial Climate Centre and Zhengzhou Meteorological Bureau, the historical temperature data from 1981 to 2019, in total 38 years.

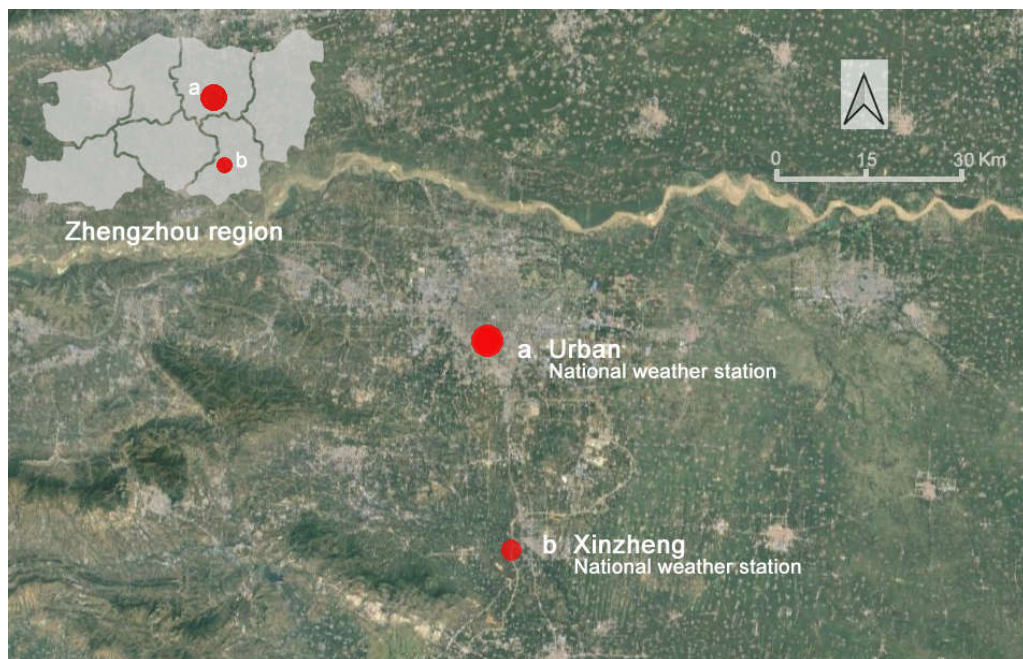


Figure 3.6: Location of surface stations in Zhengzhou city and its surrounding rural weather station: a) urban area; b) Rural station:Xinzheng; (modified from ©2019 Google earth maps)

Based on the location of the weather station, the urban station represents as “urban” temperature, and the stations at Xinzheng represent as “rural” temperature.

3.2.2 Geospatial GIS data and tools

In this research, the geospatial data such as **satellite images** (Landsat 5 TM, Landsat7 ETM+ and Landsat 8 OLI-TIRS) was used to analyze the **SUHI** temporal and spatial characteristics as well as other factors contribute the UHI effects. Besides, **Google Earth Maps** were also applied as the base map to define the land use and supervised land use classification, and the related tools such as ENVI 5.2, QGIS 3.14 and ArcGIS 10.2 software were used to extract the geospatial data from Landsat images by using remote sensing. As this research has four surveys in different sites, I categorized the data by different study city.

3.2.2.1 Geospatial data of Zhengzhou city

To explore the city expanding and **surface UHI** spatial distribution, a total of 16 Landsat images from USGS (earthexplorer.usgs.gov; *Appendix 14*) were used to classify **land use and land cover (LULC)** in Zhengzhou city. Those 16 satellite images were selected with cloud-free and high radiometric conditions. As the thermal infrared and sensors are different between Landsat 5 TM, Landsat7 ETM+ and Landsat 8 OLI-TIRS, they have different spatial resolution and band number, which are spatial resolution of 120 m for Landsat 5 TM, 60 m for Landsat 7 ETM+ (band 6 in both sensors), and 100 m for Landsat 8 OLI-TIRS images (band 10), but all three optical-bands sensors have a spatial resolution of 30 m.

Apart from the satellite images data, the other related data such as **Digital Elevation Model (DEM)**, **Digital Surface Model (DSM)** and **Google Earth maps** of Zhengzhou city as the base maps to assist the analysis, the summary of the data used are in the *Table 3.1*. Other digital GIS data such as the location and information of stations from the Henan Provincial Climate Centre and Zhengzhou Meteorological Bureau. However, some primary data were not permitted to public.

Table 3.1: Geospatial database used in research of Zhengzhou

Name	Description	Resolutions/Date	Sources
DEM	Topographic study of elevation profile	30m/2000	USGS, STRM
DSM	The natural and built/artificial features of the environment	4m /2016	Commercial UAV
Google Earth Maps	Urban Surface information and changes profile	Different years with different resolution,	Google
OSM	Digital urban structure data can be transformed into GIS files.	Different years with different resolution,	OSM website

3.2.2.2 Geospatial data of Budapest

Satellite images, **thermal camera images**, and **DEM** were used. Those materials were used to

extract LST with a combination of field surveys, GIS analysis, and statistical analysis. The measured temperature data is mainly LST from satellite imagery. Additionally, the DEM also used to analyze the slopes and aspects to explore different temperature characteristics based on topography. GIS software (QGIS 2.18&3.14 and ArcGIS 10.2) were used to retrieve the surface temperature from Landsat 8 satellites. The sample sites of different land-use types were selected based on Google's very high resolution (VHR) satellite image and field survey experience.

Satellite data source

In this survey, Budapest's five Landsat 8 satellite images were used (**Table 3.2**). These were chosen and downloaded from the USGS (<https://earthexplorer.usgs.gov/>). The images focus on the peak winter from November to March. Budapest's heating season is mostly from mid of October to mid of April, and this period is represented by leafless landscape scenery. The images were prepared on sunny days around 10:33 (Central European Time) and these have almost no cloud coverage, which means that the results will show the typical situation of bright, sunny days. In order to get more accurate LST map, I applied **average land surface temperature (LST)** (the near period in the same season same year) method to calculate **the Budapest LST**.

Table 3.2 Landsat images used to estimate land surface temperature

Date	Satellite types	Scale
27.11.2013	Landsat 8 OLI-TIRS	Full Budapest coverage
23.06.2014*	Landsat 8 OLI-TIRS	Full Budapest coverage
15.02.2014*	Landsat 8 OLI-TIRS	Full Budapest coverage
18.02.2015*	Landsat 8 OLI-TIRS	Full Budapest coverage
12.07.2015*	Landsat 8 OLI-TIRS	Full Budapest coverage
13.08.2015*	Landsat 8 OLI-TIRS	Full Budapest coverage
27.05.2016*	Landsat 8 OLI-TIRS	Full Budapest coverage
31.08.2016*	Landsat 8 OLI-TIRS	Full Budapest coverage
25.01.2018	Landsat 8 OLI-TIRS	Full Budapest coverage

**this same period images used to calculated the average LST map*

Data from Pan-European High Resolution Layers (Copernicus)

To analyze topographic characteristics and define the significant southern and northern slopes, DEM, which was downloaded from the **Copernicus** website¹¹ and Lechner Institution was used.

¹¹ Copernicus is the European Union's Earth observation programme, looking at our planet and its environment to benefit all European citizens. It offers information services that draw from satellite Earth Observation and in-situ (non-space) data. <https://www.copernicus.eu/en>

The geospatial GIS data used were summarized in **Table 3.3**.

Table 3.3: High resolution layers used in this research from Copernicus

Data	Year	Resolution	Source
Tree Cover Density (TCD)	2015	20m	Copernicus
Building Height (BH)	2012	10m	Copernicus
Street tree layer (STL)	2015	10m	Copernicus
Forest Type (FTY)	2015	20m	Copernicus
Dominant Leaf Type(DLT)	2015	20m	Copernicus
Small Woody Feature(SWF)	2015	5m	Copernicus
Grassland	2015	20m	Copernicus
DEM	2000	30m	USGS (STRM)
nDSM of Budapest	2015	20m	Lechner Institution.

Copernicus: <https://land.copernicus.eu/pan-european/high-resolution-layers>

USGS: <https://earthexplorer.usgs.gov/>

Thermal camera imaging of Budapest

This research also used thermal imaging to illustrate surface temperature in the city and the instrument was the "Seek thermal Pro" camera¹² with a 320 x 240 resolution thermal sensor. It is portable, lightweight, and easy-to-use, based on the Seek application on a smartphone. The method included a parallel use of real photography in the field. An illustration is shown by comparing thermal and real images (**Figure 3.7**).

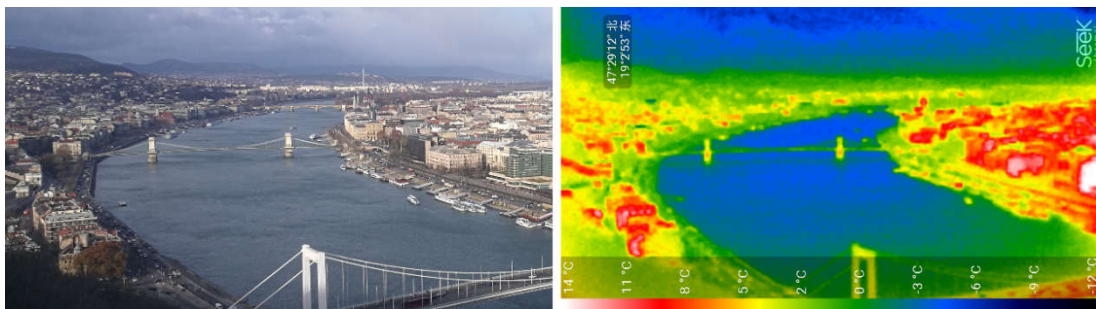


Figure 3.7: The real image and the thermal image showing the Budapest city center's surface temperature measured by the Seek Pro heat camera from Gellért hill (at 12:50 on 28. 12. 2018).

The thermal image and the real image were prepared parallel simultaneously so that the areas of different temperatures could be recognized. The thermal image includes the legend of temperature in Celsius degree. A diverse color scale can be set with the software. The analysis of thermal images in the survey was assisted by the combined use of real photo contours.

¹² A thermal imaging tool can connect with a smartphone or tablet and take thermal images. <https://www.thermal.com/compact-series.html>

3.2.3 Field survey data and equipment

For **small scale and micro scale** survey, the on-site measurement is necessary to collect the local **meteorological data** (temperature, relative humidity, wind direction, wind speed, photosynthetic radiation) and other relevant information. Several measurement tools and instruments are used to survey those data. All the information on measurement instruments and tools used in this survey can be found in *Appendix 15*.

3.2.3.1 Small-scale green spaces measurement samples selection

The study plot was selected on the campus of Henan Agricultural University (HAU) in Jinshui district, within Zhengzhou city. The entire campus is about 23 ha. The area is located on the east side of the campus, next to the east gate (*Appendix 16*). Garden A, B, C and D are 0.21 ha; 0.26 ha; 0.23 ha and 0.25 ha, respectively (*Figure 3.8*). These gardens are surrounded by teaching and learning buildings. The average height of the surrounding buildings is about 18 meters, so the energy exchange with the surrounding was relatively weak compared with the area with no surrounding by buildings.

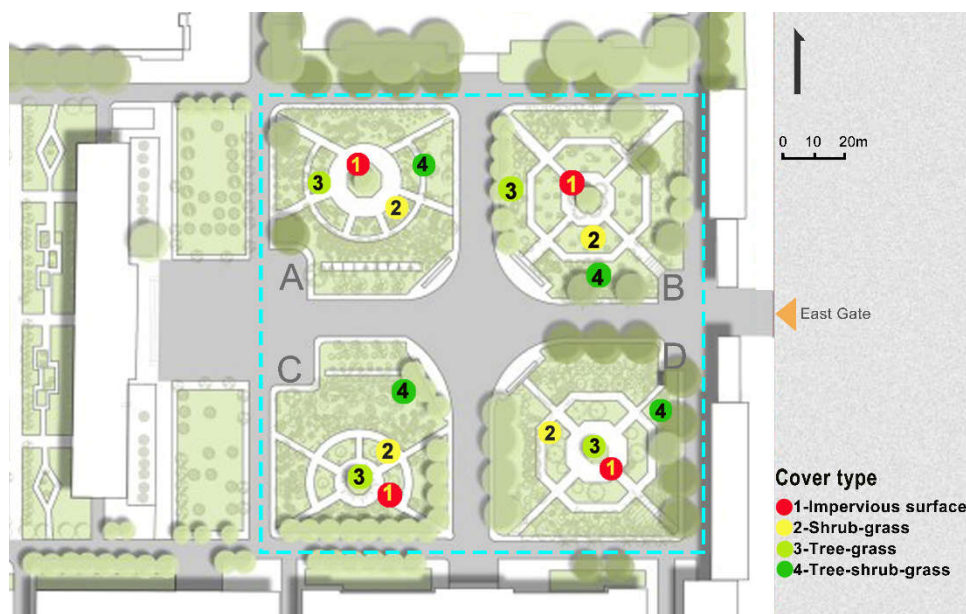


Figure 3.8: Location of study area and the 16 measurement sites, four coverage types of each garden (A, B, C, D) in HAU old campus

3.2.3.2 Field survey and on-site measurement

This survey chose four coverage types (1-impervious surface, 2-shrub-grass, 3- tree-grass, 4-tree-shrub-grass) in each garden (A, B, C, D), 16 measurement points in total (*Figure 3.8, Appendix 17, Appendix 18*). It should be emphasized that different colors are selected according to the four types of features in the illustration. Red represents the impervious surface, yellow represents the Shrub-grass type, light green represents the Tree-grass-type, and the dark green represents the Tree

-shrub-grass multilayer (≥ 3) community. It can be seen from the color that the richer the vegetation cover the more green it was.

1) Measurement of air temperature and humidity by using iButton tools

In view of the need for continuous synchronized observations at different points, 16 iButton sensors¹³ were used in the study to set the same observation time and frequency. The iButton was invented and exclusively produced by Dallas Semiconductor, and can be installed almost anywhere. In each site, iButton sensor was placed inside a homemade radiation shield (paper cup) at 1.5 m above the ground, the iButtons were fixed in a tripod in case of coverage type 1 and 2 (no tree cover), while the iButton in type 3 and 4 (with tree cover) were fixed in the tree directly (**Figure 3.9**).



Figure 3.9: 16 measurement points in garden A, B, C, D; Plant canopy imager and weather station used in measurement.

The measurement time was conducted between August 7-9, 2019 with sunny and calm days in summer. The air temperature (AT) and relative humidity (RH) data were automatically recorded every 5 minutes. Considering the wind speed and direction impact on the AT and RH, the study refers to the local wind speed and wind direction (**Figure 3.9**) recorded by a long-term fixed small weather station on the campus, in order to correct and analyze the results.

Measurement of plant canopy parameters

¹³ iButton is a widely used temperature and relative humidity data logger.

In addition to temperature and humidity, we used CI-110 Plant Canopy Imager. The CI-110's digital platform was enabled to simultaneously capture wide-angle plant canopy images and estimate Leaf Area Index (LAI) (Vanderbilt 1985) and Photosynthetically Active Radiation¹⁴ (PAR) (Norman, Jarvis 1974) levels from a single canopy scan. In order to analyze the influence of these factors on temperature and humidity, the canopy analyzer was applied to measure PAR, CD, LAI, Mean leaf angle (MLA), and other data in each sample point (*Appendix 19*). The units for PAR is $\mu\text{mol}/\text{m}^2\text{s}$ and this metric is commonly referred to as the Photosynthetic Photon Flux Density or the number of photons in the 400-700 nm range received by a specified area over a given period of time. This value will range from 1 to 2000 $\mu\text{mol}/\text{m}^2\text{s}$. LAI is used to characterize plant and forest canopies (Carlson, Ripley 1997). In this study the LAI is calculated based on the measured gap fraction of the image. This part uses the Otsu method (Otsu 1979; Sezgin, Sankur 2004) to calculate the LAI value of each site.

The leaf angle distribution of a plant canopy is the angular orientation of the leaves in the canopy¹⁵. In LAI calculations, this is described mathematically as a statistical distribution of leaf angles on different planes. Plant canopies can range from having more erectophile **leaf area distributions**¹⁶, such as onions which have very vertical orientation of their leaves, to more planophile, such as strawberries or oak trees that have more horizontal orientation of their leaves.

3.2.4 Other additional -statistical data

In order to analyze the atmospheric UHI related factors such as urbanization indices: urban population, urbanization rate, GDP, Area of built-up area, green spaces rate, those kinds of socioeconomic data were applied from the urban Bureau of Statistics department. For the study area of Zhengzhou city, the socio-economic census included each year's indicators: Urbanization rate; Park area per person; city population, Population density; GDP; Built-up area, and the time scale is from 1981 to 2019. These data (*Appendix 20*) were obtained from the Zhengzhou Bureau of Statistics¹⁷ and a statistical report on the national economy and social development of Zhengzhou.

¹⁴ Photosynthetically active radiation (PAR) sensors is installed in the arm of Plant Canopy Imager CI-110, its value can be measured directly by this instrument.

¹⁵ The leaf angle distribution refers to the orientation of the leaves within the canopy (CI-110 Manual, <https://cid-felix.gitbooks.io/ci-110-operation-manual/content/>).

¹⁶ One type interpretation of leaf angle distributions.

¹⁷ Zhengzhou official annual data statistics: <http://tjj.zhengzhou.gov.cn/>

3.3 Research methodology in each survey

This research aims to investigate the dynamic changes of UHI characteristics with city development and the relationship between surface UHI and green spaces, for the green space cooling effect, urban parks as the sample to represent the green space, and the small green space effect on urban thermal environment in micro scale also analyzed. Meanwhile, the surface UHI feature at geography level also explored in terms of the vertical indicators such as elevation, slope aspect and tree height. Based on the research questions, the methodology and approaches are divided into four parts.

3.3.1 Temporal and spatial UHI investigation

This survey aims to investigate **research question1 (section1.2)**. To explore the questions, two approaches were used, for the **temporal changes** of urban heat island, long-term meteorological data (section 3.2.1) instead of remote sensing could be used for analysis. As for the spatial characteristics of surface UHI, the satellite images (section 3.2.2) were applied to characterize the **distribution of surface UHI**, those two methods are the main approach to study the UHI. Four terms (1989; 2000; 2009; 2019) of satellite images were employed to analyze spatial expanding and land use/land cover changes, more specifically, investigate the relationship between **urbanization process and the UHI**. By studying the UHI characteristics with different data. It is of significance for the understanding of the temporal dynamics of UHI for an expanding megacity, in terms of sustainable urban planning to mitigate the local level climate change and environmental problems as well.

As for the indicators to quantify the UHI and urbanization process, the LST retrieval method and land use classification method and other indices were used below.

3.3.1.1 Method of atmospheric urban heat island intensity

The atmospheric UHI intensity can be calculated based on the formula (22) below:

$$UHII = T_u - T_r \quad (22)$$

Where the T_u is urban station (a) temperature, T_r is the rural temperature, and in this chapter the T_r is the value of the rural station (Xinzheng station, b).

By using the long-term data, the yearly atmospheric UHI was analyzed based on the yearly mean temperature, the seasonal atmospheric UHI was also illustrated from mean temperature in each season, the four seasons are: spring (March to May); summer (June to August); autumn (October to November); winter (December to February). Apart from the seasonal atmospheric UHI study, the atmospheric UHI of different time also examined by choosing mean hour temperature. The four different hour data (2 am; 8 am; 2 pm; 8 pm;) were selected to represent the different time

periods regard of day and night atmospheric UHI, which used to compare the atmospheric UHI variables in different seasons.

3.3.1.2 Land surface temperature retrieval

The LST method were applied based on the satellite data I obtained in the section 3.2.2.1, and according to the method form the section 2.2.2, imaged-based methods(IBM) chose as the method in this research.

3.3.1.3 Calculation of urban heat island ratio index and Surface UHI intensity

In the present study, spatio-temporal variation of surface UHI was calculated using LST data obtained from 16 satellite images in four different years. For this purpose, the retrieved LST images were normalized using Eq. (23) (Qiao et al. 2014):

$$LST_i = \frac{LST - LST_{min}}{LST_{max} - LST_{min}} \quad (23)$$

Where LST_i is the normalized value of pixel i ; T_{max} is the maximum LST value and T_{min} is the minimum LST value in study area.

Thus, the **mean standard deviation** method was applied to classify the different LST pattern (Shirani-bidabadi et al. 2019), from the above, the LST_i were categorized into five thermal classes (**Table 3.4**): low-temperature area, secondary low temperature area, medium- temperature, secondary high-temperature area and high-temperature area.

Table 3.4: Temperature classification by using mean standard deviation method.

Intervals	Temperature Classification
$T \leq T_{mean} - 1.5 \text{ std}$	low temperature area
$T_{mean} - 1.5 \text{ std} < T < T_{mean} - \text{std}$	secondary low temperature area
$T_{mean} - \text{std} < T \leq T_{mean} + \text{std}$	medium temperature
$T_{mean} + \text{std} < T \leq T_{mean} + 1.5 \text{ std}$	secondary high temperature area
$T > T_{mean} + 1.5 \text{ std}$	high temperature area

Therefore, LST level distribution in Zhengzhou was established and the area of each level was calculated. Finally, the contribution rate of urban land to SUHI was quantified using **urban heat island ratio index**¹⁸ (URI) through Eq. (24) (Qiao et al. 2014; Xiong et al. 2012 p. 2; Xu 2010):

$$URI = \frac{1}{100m} \sum_{i=1}^n w_i \cdot p_i \quad (24)$$

where m is the number of normalized temperature levels; i is the level value of temperatures higher

¹⁸ An index used to quantify the urban heat island strength with in different period land surface temperature maps (Xu, 2010).

than rural areas; n is the number of temperature levels higher than medium level, mainly depicting SUHI; w_i denotes weighted values using the values of secondary high and high temperature; and p is the area percentage of level i .

Surface urban heat island intensity

According to the definition of the UHI, The intensity of the UHI effect is measured as the difference between the urban temperature and the rural temperature, traditionally, the temperature is from the weather station, but as for the surface temperature, the UHI intensity can be defined mean intensity of the surface UHI intensity (SUHII) to analyze the phenomenon of SUHI of the four terms((1989; 2000; 2009; 2019)), as in Equation (25), similar to the study method on UHI based on meteorological data.

$$\text{SUHII} = T_u - T_r \quad (25)$$

Where SUHII is the mean intensity of surface UHI in the study area, T_u is the mean LST in the urban area or the built-up land, and T_r is the mean LST of non-built-up land.

Urban expansion measurement

The compactness ratio of urban area is an important concept reflecting the urban form (Y. Chen 2011; Haggett et al. 1977; Xiong et al. 2012), and its calculation equation (26) is as below:

$$\text{UCR} = 2 \frac{\sqrt{\pi A}}{P} \quad (26)$$

Where UCR is the **urban compactness ratio**, A is the area of urban build-up land, and P is the perimeter of urban boundary contour. UCR ranges from 0 to 1; a higher value indicates a more compacted shape and a value closer to 1 indicates that the urban built-up land has a higher occupation, and vice versa. In general, if urban land expansion changes in the infilling way, the concavity of urban edges will decrease because the urban internal gaps are gradually filled up, and as a result, the urban form tends to be more compact.

3.3.1.4 Spectral indices calculation

Spectral indices have been used to quantify the land surface information in many studies,

This research also used five indices to classify the satellite image of the study area (**Table 3.5**), which have been successfully proven by other researchers. The six indicators are Normalized Difference Water Index (NDWI) (Gao 1996), Normalized Different Build-up Index (NDBI) (Pla et al. 2017), Normalize Difference Vegetation Index (NDVI), Fractional Vegetation Cover (FVC) (Kikon et al. 2016), Modified Normalize Difference Water Index (MNDWI) (Han-qiu 2005) and Normalized Difference Impervious Surface Index (NDISI) (Xu 2010). These indices can represent the surface coverage information of the study area.

Table 3.5: Spectral indexes of Landsat image used in study.

Name	Equation	Description
NDWI	$\frac{NIR - SWIR}{NIR + SWIR}$	Normalize Difference Water Index (NDWI) is a remote sensing based indicator sensitive to the open water surface and water content of leaves.
NDBI	$\frac{SWIR - NIR}{SWIR + NIR}$	Normalized Different Build-up Index (NDBI) is a remote sensing based indicator sensitive to build-up areas
NDVI	$\frac{NIR - R}{NIR + R}$	Normalize Difference Vegetation Index (NDVI) is used to determine the density of green on a patch of land.
FVC*	$\frac{NDVI_i - NDVI_{min}}{NDVI_{max} - NDVI_{min}}$	The Fractional Vegetation Cover (FVC) mainly depicts the vegetation abundance of ground surface.
MNDWI	$\frac{G - SWIR}{G + SWIR}$	Modified Normalize Difference Water Index (MNDWI) is an indicator used to determine the open water area.
NDISI	$\frac{TIR - [(MNDWI + NIR + SWIR)/3]}{TIR + [(MNDWI + NIR + SWIR)/3]}$	Normalize Difference Impervious Surface Index (NDISI) indicator is used to estimate impervious surface.

*Notes: * Where NDVI_i is ndvi value of a pixel i; NDVI_{min} is minimum value; NDVI_{max} is maximum value. R, G, NIR, SWIR, TIR are the bands of Landsat images.*

3.3.1.5 Land use classification

To analyze the urbanization process and SUHI, land use classification was used to map land use types. Studies showed that **vegetated season** is the optimum period for the supervised classification (Hütt et al. 2016; Karila et al. 2019), therefore, four Landsat satellite images (1989, 2000, 2009, 2019 see *Appendix 14*) in summer were chosen to conduct the land use classification. In the image interpretation process, Google Maps were used to assist the interpretation of remote sensing images, and all images use the world 1984_UTM_49N coordinate system. Use ENVI5.3 software first to perform a Radiometric Correction on the image, and then use the FLAASH tool to perform Atmospheric Correction on the image. This step uses a combination of maximum likelihood supervised classification and visual interpretation in supervision classification. After classification, Majority/Minority Analysis, Clump Classes and Several modules of Combine Classes post-process the classification results. Finally, based on the high-resolution Google earth maps to verify the classification accuracy of the classification results through the confusion matrix. The LULC classification had **five categories**: Water (including rivers, reservoirs and ponds); Built-up (buildings, urban roads, industrial areas, commercial areas, construction land and construction site), green space (including urban green space, woodland and grassland, etc.), agricultural land (including arable land, orchards and vegetable gardens) and bare land (wasteland, rivercoast land

and bare land). The Change Detection statistics module in ENVI5.3 is used to calculate the change and transfer matrix of land use to quantify the dynamic evolution of land use and analyze the relationship with the heat island effect.

3.3.1.6 Analysis methods and related tools

Temporal atmospheric UHI analysis were conducted by the materials and indices mentioned above. **Firstly**, atmospheric UHI changes based on long-term meteorological data (1981-2019) were analyzed and illustrated by Excel and SPSS 25; **Secondly**, based on the remote sensing data from the Landsat images, the relationship between LULC changes and SUHI were explored and illustrated by ArcGIS10.2 and QGIS 3.14 as well, urban heat island ratio index (URI) was employed to quantify and compare the atmospheric UHI intensity in the different seasons and years (1989; 2000; 2009; 2019). At the same time, the role of green spaces and impervious surfaces played on SUHI were analyzed by using the spectral indices in section 3.3.1.3 to determine the green space mitigation in SUHI. **Thirdly**, the socio-economic indicators in section 3.2.4 were used to explore the indirect factors of urbanization and atmospheric UHI effect.

3.3.2 Park cooling intensity survey and analysis

This survey aims to investigate **research question 2** (section 1.2). To explore the question, the Landsat 8 image of July 2019 (section 3.2.2.1, *Appendix 14*) was selected from Landsat collection to obtain Land Surface Temperature (LST) by using Radiative Transfer Equation (RTE) method (section 2.2.2.4), and present land cover information by using spectral indices (section 3.3.1.3). Additionally, high-resolution Google Earth images were used to select 123 parks (*Figure 3.10, table 3.6*) in Zhengzhou city (section 3.1.1), grouped in five categories, to explore the impact factors on park cooling effect. **Park Cooling Intensity (PCI)** has been chosen as an **indicator** of the park cooling effect which will quantify its relation to park patch metrics.

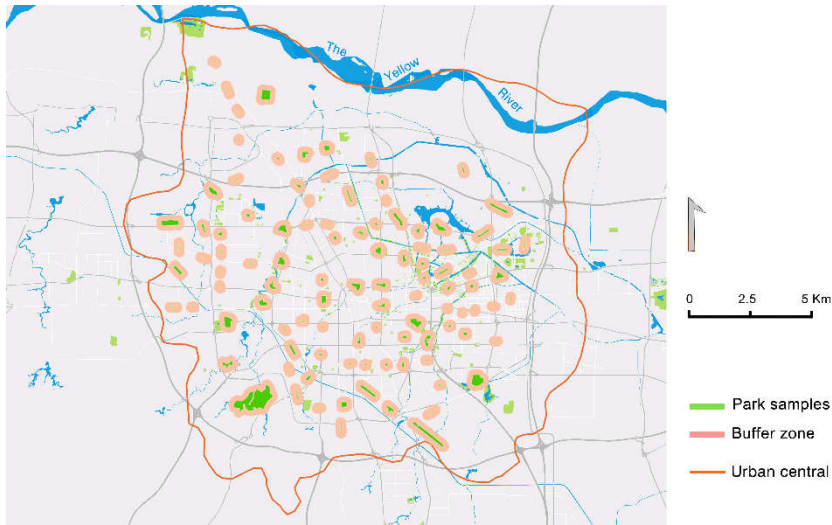


Figure 3.10: The 123 sample parks in Zhengzhou

3.3.2.1 Sample park selection in Zhengzhou

Based on the classification applied in Chinese urban planning regulations and the distribution of parks in Zhengzhou city, this chapter selected five park types¹⁹ (**Table 3.6**), 123 (one hundred and twenty three) parks in total as study sites. The parks boundaries were determined based on high-resolution Google Earth images and low-altitude UAV (drone) images. As the original spatial resolution of the Landsat thermal infrared band is 100m, we selected sample parks larger than 2 hectares.

Table 3.6: Statistics and details of 123 sample parks by types

Category	No.	Percent	Max.(ha)	Min.(ha)	Main example
Urban park	59	48%	87.16	3.12	City park, District park
Theme park	10	8%	108.53	10.61	Botanical garden, Zoo
Street park	28	23%	25.26	1.23	Pocket park, community park.
Linear park	19	15%	62.02	2.13	Riverside park, roadside park
Urban square	7	6%	6.64	2.15	Square

3.3.2.2 Determination of the Park Cooling Intensity (PCI)

Park Cooling Intensity (PCI) usually calculates the temperature difference between the inside and outside of the park (Spronken-Smith, Oke 1998; Chang et al. 2007; Cao et al. 2010). It can be air temperature or land surface temperature. In this chapter, the PCI (units in °C) was defined as the mean LST difference. Eq. (27):

$$PCI = \Delta T = T_u - T_p \quad (27)$$

Where T_u is the mean LST of an urban area of the **500m buffer zone** outside of the park, and T_p is the mean LST inside the park. The buffer zone includes the area around the park, which contains different land cover types: buildings, roads, impervious surfaces, trees, and green spaces.

3.3.2.3 Patch descriptors of the park

In this survey, several indicators were applied to characterize the impact factors on PCI (**Table 3.7**). By using the ArcGIS 10.2 tools, we calculated fractal dimension (Frac_Dim), perimeter-area ratio (Patario) and shape index (Shape_idx) in patch level. From the previous studies, those three indicators were used as the main patch metrics, and had been widely employed to analyze landscape patterns, both in class level and patch level (Estoque et al. 2017; Li et al. 2009; Liu et

¹⁹ Five park types: urban park, theme park, street park, linear park, urban square, which based on 《Standard for Classification of Urban Green Space》 CJdJ/T85-2017.

al. 2008). These initial base studies were successful in demonstrating the characteristics of landscape patterns both in regional and local scale (Y. Li et al. 2012). This survey investigated the relation of these indicators to park cooling effect in sample areas of Zhengzhou city. Low fractal dimension are described as simple, non-waving, straight boundaries, high fractal dimension means waving edges of park and surroundings.

Table 3.7: Park metrics

Name	Equation	Description
Perimeter-Area Ratio*	$Paratio = \frac{P_i}{A_i}$	P_i = perimeter (m) of patch i. A_i = area (m^2) of patch i. Paratio equals the ratio of the patch perimeter (m) to area (m^2) (Lei et al. 2012).
Landscape Shape Index*	$Shape_Idx = \frac{0.25P_i}{\sqrt{A_i}}$	Landscape shape index provides a standardized measure of total edge or edge density that adjusts for the size of the landscape (Lei et al. 2012).
Fractal Dimension Index*	$Frac_Dim = \frac{2\ln(0.25P_i)}{\ln A_i}$	Fractal Dimension Index reflects the extent of shape complexity across a range of spatial scales (Lei et al. 2012).

* Source: https://www.umass.edu/landeco/research/fragstats/documents/fragstats_documents.html

In addition to the three metrics, this survey used three indices (NDWI, FVC, NDISI) to classify the satellite image of the study area (section 3.3.1.3 **Table 3.5**). These indices can represent the surface coverage condition inside of the park.

3.3.2.4 Analysis methods for sample park analysis in Zhengzhou

Statistical analysis was performed by SPSS 25.0 and Microsoft Excel. After retrieval of the LST, FVC, NDWI, NDISI values from the satellite image, QGIS was used to obtain summarized values of each sample area. Then SPSS was applied to conduct the linear regression analysis to quantify the relationship among LST, FVC, NDWI, NDISI, and PCI. For the park patch metrics calculation, we used the ArcGIS spatial analysis method to obtain the following parameters of each sample park: area, paratio, shape index and fractal dimension. The same linear regression analysis was made to PCI and LST. Additionally, the related coefficient was also utilized to detect and verify the result.

For the regression analyses, first, Pearson correlation tool was used to obtain the main significant impact factors, and then analyze the regression relationship between the two factors in a targeted manner to find the optimal curve fitting model. The final presented fitting model is the best explanation of the relationship between specific factors within the selected sample park. The framework of this survey could be found in Figure 3.11.

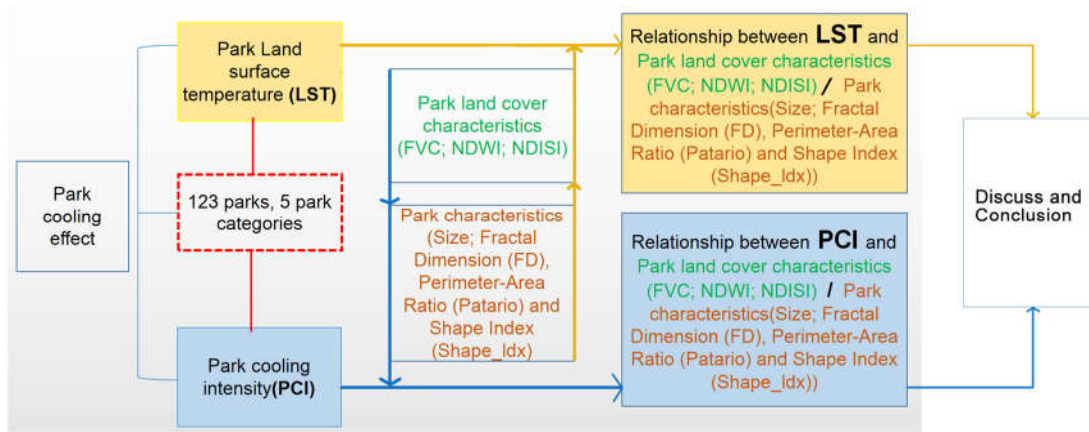


Figure 3.11: The research framework of park cooling effect survey

3.3.3 Small scale green space cooling effect survey

This survey aims to investigate **Research Question3: What is the relation between the microclimate and the vegetation structure and surface cover type characteristics in small-scale green spaces (SGSs)? What plants community should be designed in terms of mitigating urban thermal environment by manipulating vegetation design variables?**

To explore and investigate the questions, This survey carried out the measurement of the weather parameters (temperature, relative humidity, wind direction, wind speed, photosynthetic radiation) of the 16 sites in four types of coverage (Impervious surface; Shrub-grass; Tree-grass; Tree-shrub-grass) in a university campus (section 3.2.3). At the same time, the coverage characteristic parameters, such as Canopy Density (CD), Leaf Area Index (LAI), Photosynthetically Active Radiation (PAR), Mean Leaf Angle (MLA), of each plot were analyzed and compared.

Data analysis

In small green spaes survey, data analysis was conducted mainly from the following aspects:

- 1) Summarize the overall changes of the research subjects during the measurement period, comparing the effects of four types of coverage during the day and night on temperature and humidity
- 2) Using the measured data of different dates, analyze the spatiotemporal changes of temperature and humidity between the four types of coverage, especially the comparative analysis of the measured values of the four types of coverage, and obtain the effect of the type of coverage on the temperature and humidity changes
- 3) By comparing the four factors (PAR, CD, MLA and LAI) to different degrees of impact on temperature and humidity.

In the data analysis, SPSS version 25 was used to analyze and illustrate the spatiotemporal changes of temperature and humidity. At the same time, in order to compare the human comfort of different

green space types, the Rayman software was used to quantify the thermal index at different points (Oh et al. 2020; Sharmin et al. 2019). Specifically, **Physiologically Equivalent Temperature (PET)** was used as an indicator to measure human comfort. Its principle is based on human energy balance, mainly calculated from meteorological factors such as radiation intensity, air temperature, air humidity, and wind speed. The medium dressing index and human activity selection software aggregate high standard values. It should be noted that here mean radiant temperature was applied before calculating the PET (*Appendix 21*), and the average radiant temperature (Tmrt) was calculated based on the method described in one article (Jendritzky, Nübler 1981), and other studies have also used this method (S. Cohen et al. 2020; H. Lee, Mayer 2016; Thorsson et al. 2007). Tmrt can be regarded as the synthesis of all radiant fluxes, and it is an indicator to calculate the comprehensive influence of the surface temperature in a given area. Therefore, it is an important factor that determines human comfort, and has better response ability in low wind and hot weather. However, the change in Tmrt depends largely on the microclimate and local factors (such as the type of surface material and coverage type), which are comprehensive factors.

This survey selected the noon time (11:30am-01:30pm) when the radiation and the air temperature were the highest, this largely reflects the difference of vegetation types. Given the changes in weather conditions during the observation period, the median values were used in this analysis because they were a better way to generalize when outliers are present. The median value shows the midpoint of the observed value, so it is less affected by the extreme value than the average value.

3.3.4 Vertical factors of UHI survey

This survey aims to investigate **Question 4: What is the relation between the vertical level variable such as elevation, slope aspect, building height, building orientation, and tree height and surface UHI? What should be designed in terms of mitigating surface UHI by manipulating vertical variables?**

To explore and investigate the questions, Budapest was taken as the study area (as Budapest owns a significant terrain in the urban area). On this basis, this survey was carried out by applying remote sensing data (Section 3.2.2.2; *Table 3.1, 3.2, 3.3*), field survey, and measurement (thermal camera). More specifically, the vertical data was extracted from the DEM and DSM using GIS analysis, besides the buildings' height from the particular products made by Copernicus institution. Tree height data extracted from the DSM map and tree layer was based on vegetation layer (Street tree layer; Forest type layer, Dominant Leaf Type, Small Woody Feature, Grassland in *Table 3.3*). Those data could achieve the analysis of the vertical factors on UHI impacts. It included two main parts in terms of the research questions. Firstly, this survey analyzed the relationship between vertical elements such as tree height, building height, elevation, slope aspect, and LST. Secondly,

this survey analyzed the green space factors such as tree cover density, vegetation types (grass, small woody, tree leaf types), and their correlation to LST.

Elevation and aspect influence on LST

The elevation map was generated from DEM data (STRM) in section 3.2.2.2 table 3.4, first Budapest was classified into two elevation classes (above 300 m asl²⁰ and below 120 m asl) and two slope aspects (northern and southern). And the winter average LST map was generated from the satellite images (**Table 3.3**) by using the method in section 3.3.1.2. Subsequently, by using the LST map, the elevation classes and slope classes were compared and illustrated in the following results part.

Tree height and building height on LST

Based on the geospatial data in section 3.2.2.2, **Table 3.3**, vegetation layer was based on the data from high resolution layers products from Copernicus website. Then, the height data was extracted from the nDSM (normalized Digital Surface Model 2015) Lechner Institution. Building height data could be obtained directly from the products of Building height (BH) in **Table 3.3**. The LST map was generated from the relative year in summer in 2015 (**Table 3.2**). And the method used to extract the LST also the same as in section 3.3.1.2.

Green spaces types on LST

The green spaces types in this survey LST mainly refer to the vegetation coverage types in Budapest urban area, such as grassland, small woody and tree. The tree type includes the dominant leaf types (DLT): broadleaves types and coniferous types. Those data could be directly obtained from the Copernicus website in **Table 3.3**. The LST map was generated from the relative year in summer in 2015 (**Table 3.2**). And the method used to extract the LST also the same as in section 3.3.1.2.

Statistical analysis

The zonal statistical (QGIS 2.18) analysis was applied to get the mean LST values from the map (**all the coordinate reference system is converted EPSG: 32634 - WGS 84 / UTM zone 34N - Projected**). By using this tool, a mean LST was extracted from all corresponding pixels. According to a previous study (Woodcock, Strahler 1987), the optimal spatial resolution to capture spatial patterns using remotely sensed imagery was approximately half to three-quarters of the object dimension's size in the scene. The 60×60 m spatial resolution is approximately the optimal spatial resolution in analyzing the scale effect on monitoring SUHI (X.-L. Chen et al. 2006). Therefore, we performed analyses at the finest spatial scale as the data allowed, which was appropriate to capture UHI's spatial features and relevant land-use types. The sample sites we

²⁰ Land surface elevation in metres above sea level (asl)

selected were all bigger than 5 hectares; this means that they were much higher above the limit that previous research. The relationship analysis method was applied by SPSS 25 software and Micro office excel 2013, and the figure illustration was generated by using Photoshop CS6 software.

3.4 Summary of methods

In this research, several methods were applied. The data in this dissertation (section 3) was generated with changing of the research scale and research questions. *Figure 3.12* illustrates the research framework and its components.

This dissertation contains four main parts and could be divided into **four scale**, urban scale, local scale, micro-scale and vertical dimension. The remote sensing data was applied to investigate the UHI temporal and spatial characteristics at the **urban scale**, including the long-term changes from climate, and the relationship between SUHI and urban green space was determined in general. Furthermore, to investigate the **green space cooling effect**, urban parks were chosen as the typical green space in urban areas to investigate urban parks' cooling mechanism, such as park form, park type, size, shape, and other related factors. Subsequently, I continued the research on a **micro-scale** to investigate the impact factors at the garden level—the plant design variables in terms of the mitigation of urban thermal environment on a micro-scale. Finally, the vertical factors correlated with SUHI were investigated to fulfill UHI research's dimension. Those vertical factors include the elevation degree, tree height, building height, slope aspect. Besides, the green space factors such as tree cover density, plant community types (grass, small woody, vegetation leaf types) were also analyzed. Those factors could give guidance to future urban landscape planning and design regarding UHI mitigation.

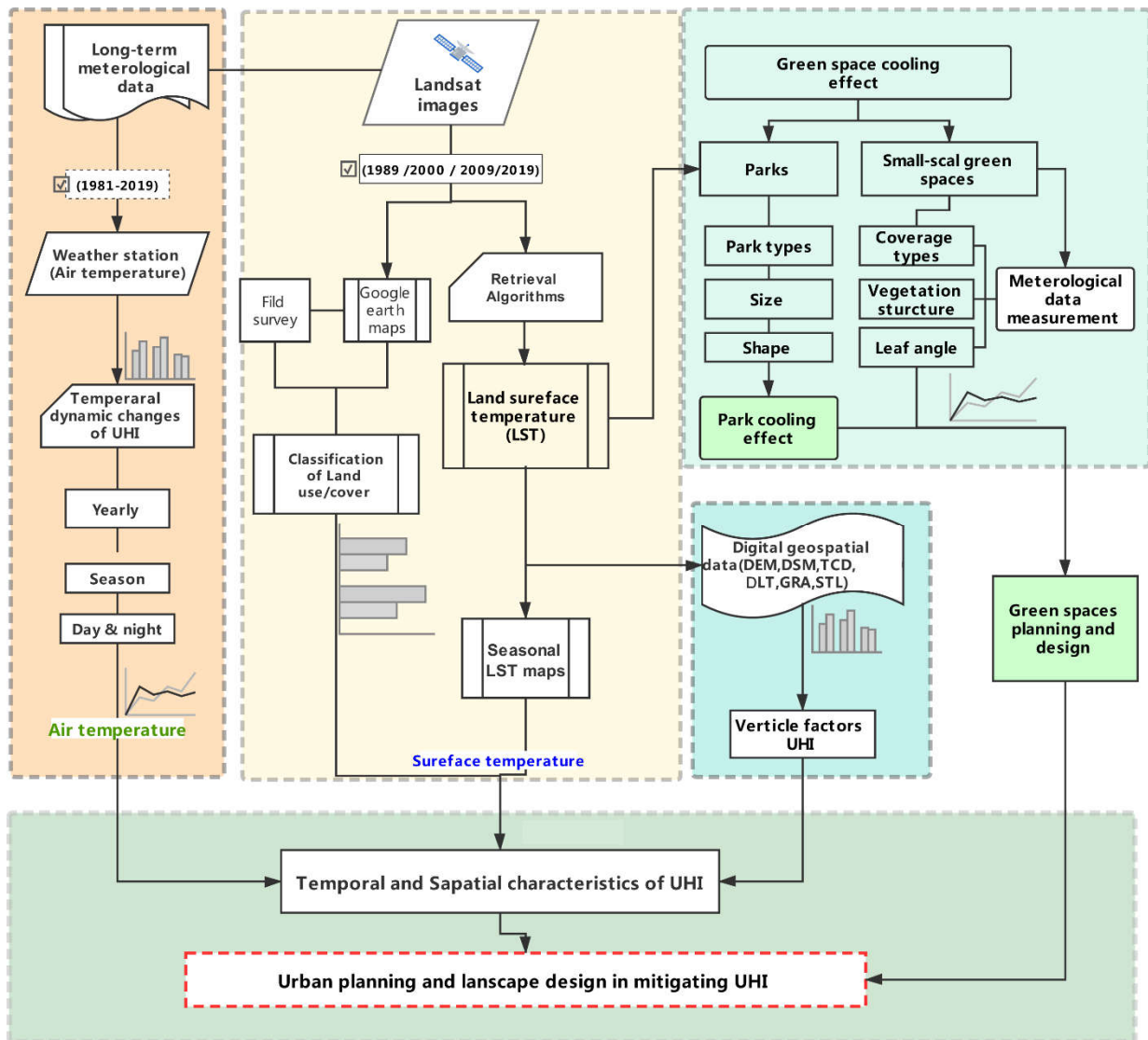


Figure 3.12: Summary of workflow and method components in the research framework

4. RESULTS AND DISCUSSIONS

In this chapter, the results and discussion based on the four research questions (section 1.3) and four surveys (section 3.3), which were divided into four parts (4.1; 4.2; 4.3; 4.4) are interpreted. Each subchapter formulated with a research question. For each survey, the explanation contains two main parts, results and discussions, respectively.

4.1 Spatio-temporal changes of UHI with the expanding city

In this part, I answer **Research Question 1: what are the spatio-temporal characteristics of surface urban heat island (SUHI) of rapid urbanization based on the data of long-term weather station and remote sensing? What are the changes in the spatial characteristics of atmospheric UHIs by the new urbanization model compared to the past model? What are the main urban development indicators GDP, population density, urbanization rate, etc.) related to the urban heat island?**

To explore and investigate the questions, two methods were used, for the temporal changes of urban heat island, long-term meteorological data instead of remote sensing could be used for analysis. As for the spatial characteristic of SUHI, the satellite images (Landsat series) were applied to characterize the distribution of SUHI, those two methods are the main approach to study the UHI.

In Zhengzhou city, over the last 40 years (1981-2019) long-term weather station data used to characterize the atmospheric UHI changes with different urbanization phases. At the same time, four terms (1989; 2000; 2009; 2019) of satellite images were employed to analyze spatial expanding and land use/land cover changes, with aim of investigating the relationship between urbanization and the SUHI process. By studying the UHI characteristics with different data, it is of high significance for the understanding of the temporal dynamics of UHI for an expanding megacity, in terms of sustainable urban planning to mitigate the local level climate change and environmental problems as well.

4.1.1 Temporal atmospheric UHI intensity based on long-term meteorological data

In the following sections, the interpretation is divided into four parts: the first part is the long-term trends of air temperature; the second part is temporal dynamics of atmospheric UHI intensity; the third part is diurnal and nocturnal atmospheric UHI intensity variation in four seasons; the last part is atmospheric UHI intensity changes with socio-economic development indicators.

4.1.1.1 Long-term trends of air temperature

Based on the air temperature data collected in section 3.2.1 from the three weather stations (*Figure 4.1*), the air temperature changes was analyzed over time (1981-2019).The figure shows that the temperature both in urban and rural raised in amplitude and speediness, but the magnitude ($R^2 = 0.82$)²¹ increase of urban temperature was more significant than in rural areas. During the last four decades, the average urban temperature (Zhengzhou station) raised up by 0.67 °C per decade, while the rural temperature (Xinzheng station) raised with 0.43 °C per decade. This result was consistent with the prior research (Ren et al. 2008), the increased temperature value is close to 1.96°C with four decades. The warming rate of Zhengzhou is 2.2 times bigger than the global warming trend over land of about +0.9°C (Hansen et al. 2010) during 1981-2019.

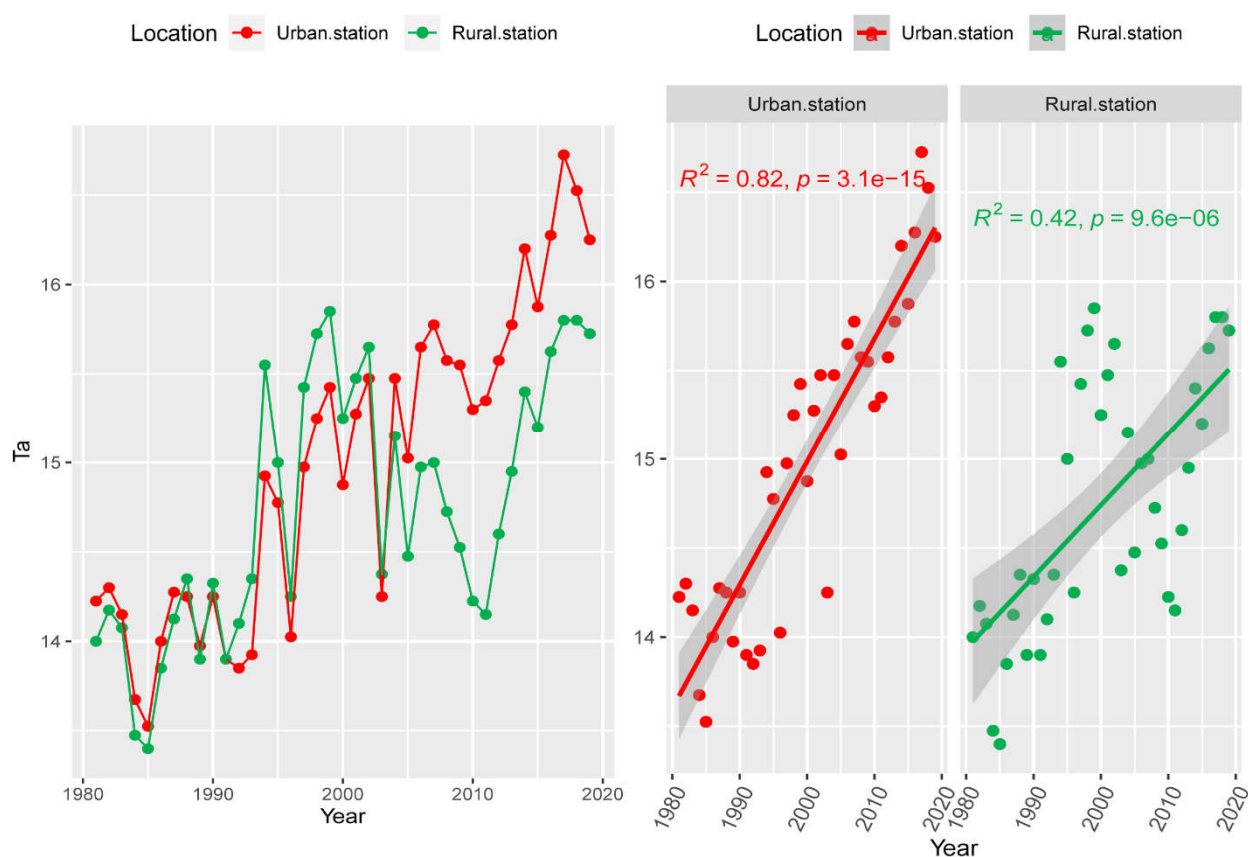


Figure 4.1: The annual average temperature of three weather stations (urban station: Zhengzhou; rural station: Xinzheng) from 1981 to 2019.

When I look into the time scale on temperature changes, before the 2000, the difference of the temperature between urban station and rural station was not predominant, as shown from the vertical offset between the two lines in *Figure 4.1*. However, after the year 2000, especially after

²¹ The linear trends show the line regression between temperature and each year, and R^2 is the correlation coefficient.

2005, the red curve had a shape increase compared to the other green curve, which suggested that the atmospheric UHI intensity was stronger. The reason is that before 2000, both of the urban and the rural station were with the same type of LCZ D (low plants in land cover types), after 2000, the environment of the urban station was changed (also in LCZ types) due to the rapid urbanization (*Appendix 12 and 13*), the urban station LCZ type changed from LCZ D to LCZ 1 (*Appendix 12*) with the urban development, this results in the urban temperature was much higher than rural area station (*Figure 4.1*). In addition, with regard to the urbanization process (*Appendix 22*) and policy implications reasons determined by the prior study (Mu et al. 2016). Urbanization is the key driver that contribute to the urban temperature raise.

4.1.1.2 Temporal dynamics of atmospheric UHI intensity based on seasonal data

The annual mean temperatures of urban and rural areas provide a computationally straightforward atmospheric UHI signal for Zhengzhou city. Following the method based on the urban and rural weather station defined in section 3.3.1.1, the atmospheric UHII based on air temperature was estimated in *Figure 4.2*. Besides, the seasonal atmospheric UHII was performed in terms of the four phases of the year. *Figure 4.2* reveals that the apparent atmospheric UHI phenomena after the turn-of-century (2000), the highest atmospheric UHII is up to 1.2 °C (2017), and the second highest is 1.15 °C (2011). However, before the year 2000, the atmospheric UHII value was mainly negative numbers, which indicated that the annual average temperature in rural areas is higher than that of in urban region, with no atmospheric UHI signal during this period (1981-1999).



Figure 4.2: Annual and seasonal mean of atmospheric UHI intensity (UHII) in Zhengzhou over the past decades (1981-2019).

Concerning the seasonal strength of the city’s atmospheric UHI, during 1981-2019, the summer (average atmospheric UHII is 0.64°C) and spring (average atmospheric UHII is 0.51°C) seasons are generally the strongest atmospheric UHI times of the year and winter the weakest (average atmospheric UHII is -0.11°C). Autumn is in the middle (average atmospheric UHII is 0.1°C). When inspecting the details of the four seasons, summer atmospheric UHII stands out of the four seasons, and the highest atmospheric UHII is 1.7°C (appeared in 2010&2011), it is consistent with the average annual UHI in the passage above. Moreover, the seasonal atmospheric UHII after 2000 are almost above zero even in winter season. The summer season performs the substantial atmospheric UHII of the year.

4.1.1.3 Diurnal and nocturnal atmospheric UHI intensity variation in four seasons

To obtain a better spatial and time characterization of Zhengzhou city’s atmospheric UHI, hourly calculations were performed. Due to the more intensive data requirements for this, only four nodes time data were selected to represent the diurnal (8 am and 2 pm) and nocturnal (2 am and 8 pm). The annual (*Figure 4.3*) and seasonal (*Figure 4.4*) changes based on four-time points are used to analyze the atmospheric UHII effect during the day and night.

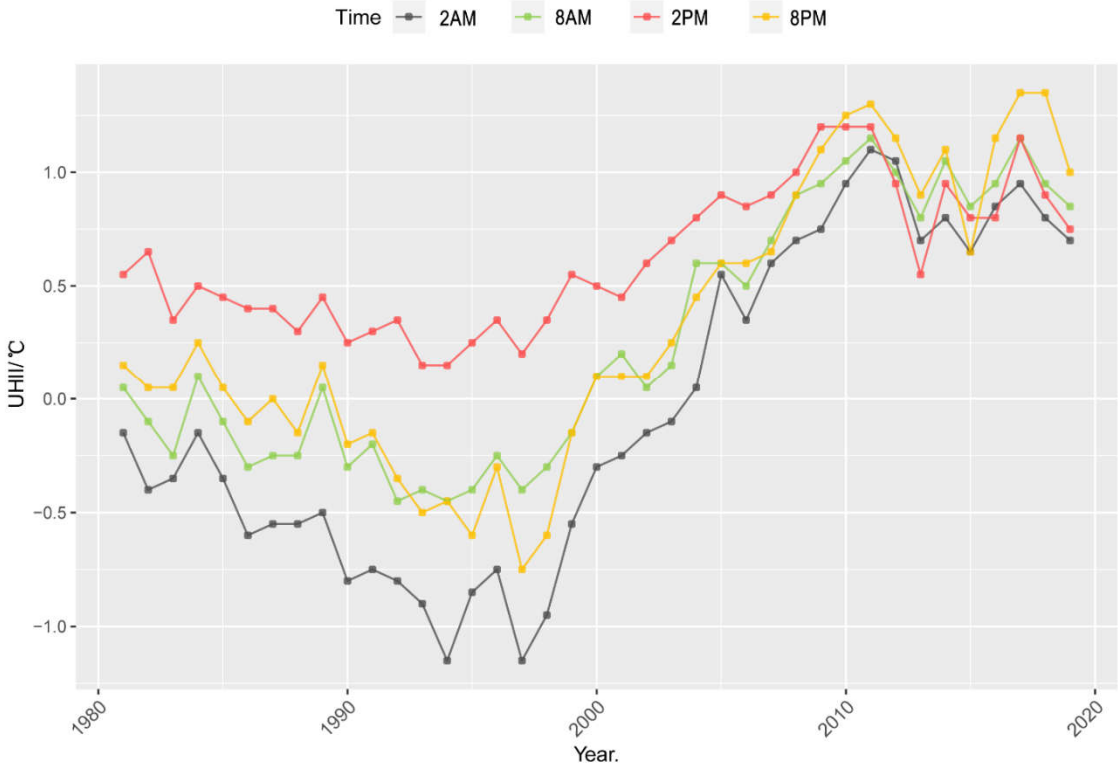


Figure 4.3: Mean of atmospheric UHI intensity (UHII) of each year at different daytime and nighttime hours in Zhengzhou over the past years (1981-2019).

From the annual results of the *Figure 4.3*, it can be seen that the atmospheric UHII during the day and night shows a time change. Before the year 2000, the atmospheric UHII during the day was

significant only, and it was negative at night. After the turn of the century, atmospheric UHII during the day and night showed a significant increase. Among them, atmospheric UHII at night (8 pm) is the strongest after 2010.

In terms of the seasonality of the heat island (**Figure 4.4**), during 1981-2019, there was a heat island effect during the day and night in the four seasons. In the four selected hours, the heat island was relatively stronger at 2pm (average value 0.616°C) and 8pm (average value 0.318°C), and the heat island at 2am (average value -0.036°C) is the weakest.

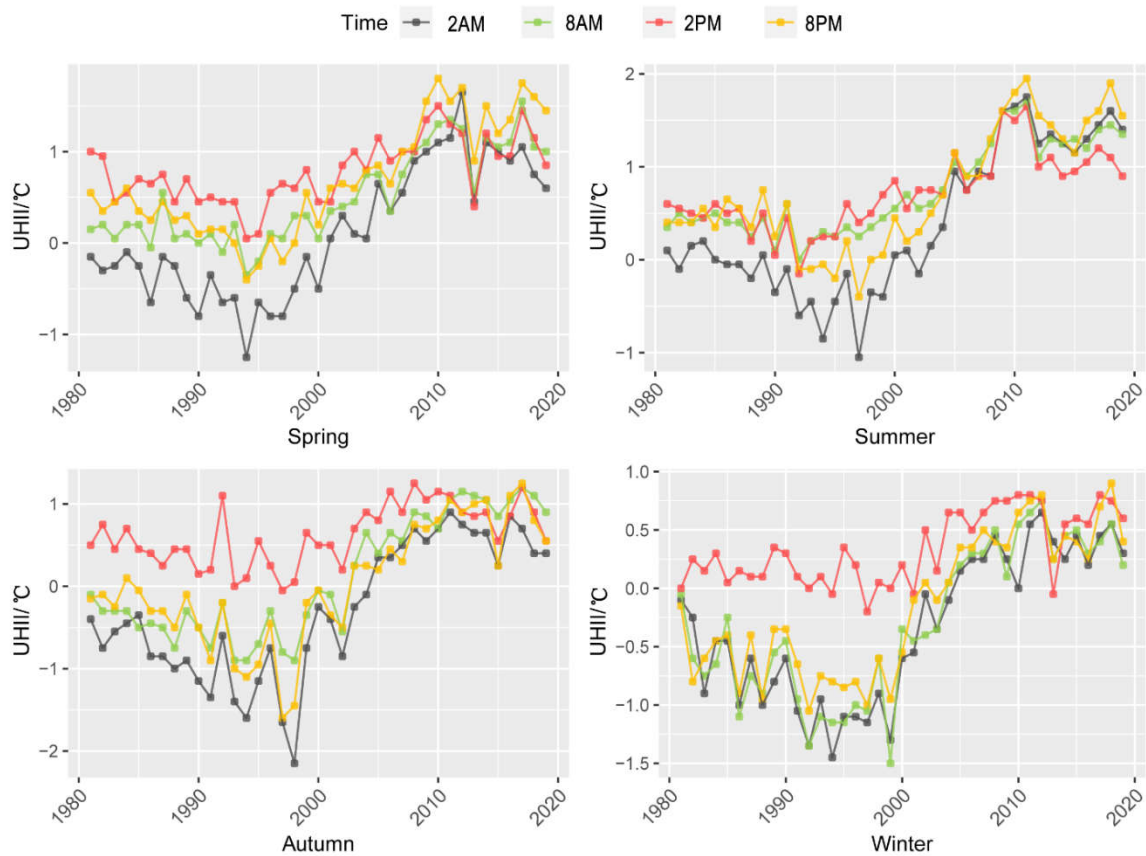


Figure 4.4: Four hourly mean of atmospheric UHI intensity (UHII) of four seasons in Zhengzhou over the past years (1981-2019).

In summer, except for the early morning (2 am), the heat island effect exists in the other three times. The atmospheric UHII at 2 pm is the most obvious. The atmospheric UHII at the selected time node shows an upward trend over time and all are positive after 2000. The average of the four periods in summer is the maximum of 0.65°C in the four seasons, and the atmospheric UHII peak is 1.95°C (2011). Generally, the heat island response during the day is lower than the heat island effect at night. There is also an obvious heat island effect in spring. The maximum atmospheric UHII in spring is 1.8°C (2010), and the average atmospheric UHII in the four hours (2 am, 8 am, 2 pm and 8 pm) is 0.10°C; 0.49°C; 0.79°C, 0.68°C, respectively. The average values of the four

periods in autumn and winter are 0.11 °C and -0.1 °C. The heat island effect in the daytime is greater than at night, and 2pm is the time when the heat island is mildest.

4.1.1.4 Atmospheric UHI intensity changes with socio-economic development indicators

Based on the urbanization database of Zhengzhou from section 3.2.4, the relationship between socio-economic development indicators and atmospheric UHII was analyzed, the five year-end independent variables (*Table 4.1*) and atmospheric UHII Pearson correlation were first examined from 1981-2019, the result showed that there was a predominant correlation as present in *Table 4.1*. The correlation coefficients were all larger than 0.78 ($P < 0.01$).

Table 4.1 Pearson correlation analysis between the socio-economic development indicators and atmospheric UHII

	Built-up	Population	UR	PD	GDP
Pearson correlation	0.824**	0.857**	0.824**	0.788**	0.788**
UHII Sig. (2-tailed)	.000	.000	.000	.000	.000
N/year (1981-2019)	39	39	39	39	39

PD is population density; UR is urbanization rate; ** Correlation is significant at the 0.01 level.

The linear regression (*Appendix 23*), subsequently, was examined between the UHII and year-end data: Built-up area, Population, Urbanization rate, Population density, GDP. The results showed that there was a positive linear correlation between UHII and urbanization indicators (*Table 4.2*). As the Pearson correlation (CC*) values are all above 0.78 and with a significant level ($P < 0.01$) of interpretation. It can be concluded that all socio-economic development indicators are significant factors contributing to the UHI effect.

Table 4.2: Correlation analysis between the atmospheric UHII and socio-economic driving factors in Zhengzhou

Indicators	Regression model*	R ²	P value	CC*
Built-up area (km ²)	y=0.0031x-0.3505	0.68	0.01	0.82
Population(ten thousands)	y=0.0036x-0.7464	0.73	0.01	0.86
Urbanization rate (%)	y=0.0362x-1.673	0.63	0.01	0.82
Population density(km ²)	y=0.0019x-1.4726	0.67	0.01	0.79
GDP	y=0.0001x-0.0358	0.62	0.01	0.78

y stands for UHII. CC is correlation coefficient, R² value tells you how much variation is explained by the model, the greater R² the better the model. If the p-value is less than the significance level (usually 0.05) then the model fits the data well.

From *Table 4.2*, we can see that in the past 40 years, **100 km²** growth in the **built-up area** result in 0.31 °C increase, and **1 million** growth in the population result in 0.19 °C increase. The same

trend can be estimated regard of the other driving factors. According to the model of population growth and UHI intensity, the atmospheric UHI intensity may increase 0.95 °C by 2030 (5 million population increase is estimated by then).

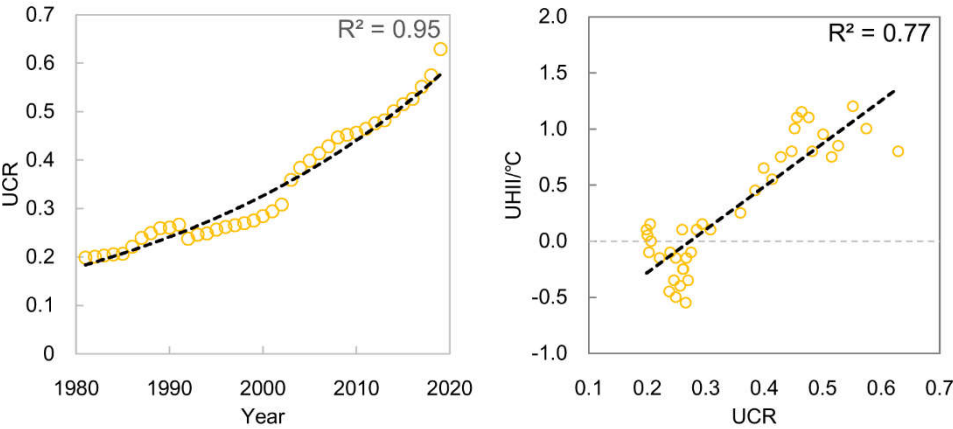


Figure 4.5: Regression analysis between the urban compactness ratio (UCR) and time (left), linear regression between UCR and atmospheric UHI (right) from 1981-2019.

The urban expansion can be quantified by the UCR²² index based on the method in section 3.3.1.3, by used the built-up area annual statistics (*Appendix 20*) from the section 3.2.4, the relationship between urban growth and atmospheric UHI was studied, and the result in *Figure 4.5*, it was shown that the UCR value growth was obvious with the years from 1981-2019. Before 2000, the ratio of urban growth was relatively slow. After 2000, the UCR had a rapid increase which indicated that the urban area was sharply filled up. When analyzed the relationship between atmospheric UHI and UCR during the past 4 decades, it was discovered that the URC had a significant positive effect on atmospheric UHI.

4.1.2 Spatial surface UHI intensity variations based on geospatial data

The following interpretation is divided into six parts to analyze the results based on the method used in section 3.3.1, which gives a comprehensive analysis of surface UHI characteristics on Zhengzhou city.

4.1.2.1 LULC classification and changes

The **LULC classification** of Zhengzhou (method in **section 3.3.1.4**) for the past four decades was evaluated using the **Kappa coefficient**, and the classification accuracy for 1989, 2000, 2009, 2019 was 91.2%, 90.4%, 88.9%, and 87.3%, respectively. The overall accuracy is higher than 87%. It

²² UCR is the urban compactness ratio, UCR ranges from 0 to 1; a higher value indicates a more compacted shape and a value closer to 1 indicates that the urban built-up land has a higher occupation, and vice versa. In general, if urban land expansion changes in the infilling way, the concavity of urban edges will decrease because the urban internal gaps are gradually filled up, and as a result, the urban form tends to be more compact.

revealed that the LULC classification results were of quite a high quality. The results were shown in the **Figure 4.6**. It was found that built-up land and agricultural land were the two main land-use types of Zhengzhou, and the main type of land transition was between the two classes as well (**Figure 4.6**). Green spaces and water areas also played an important role in land coverage type. It was discovered that the water area class was increased, especially, from 2010 to 2019.

Green spaces experienced a reduction (20.07 % - 10.04%) from the year 1989-2000 (**Figure 4.7**), due to the urbanization took place and caused the replacement of green space to built-up area. However, with the urban expansion from 2000-2019 (**Figure 4.7**), the green space, on the contrary, subsequent appeared modest growth (10.04% -16.46%).

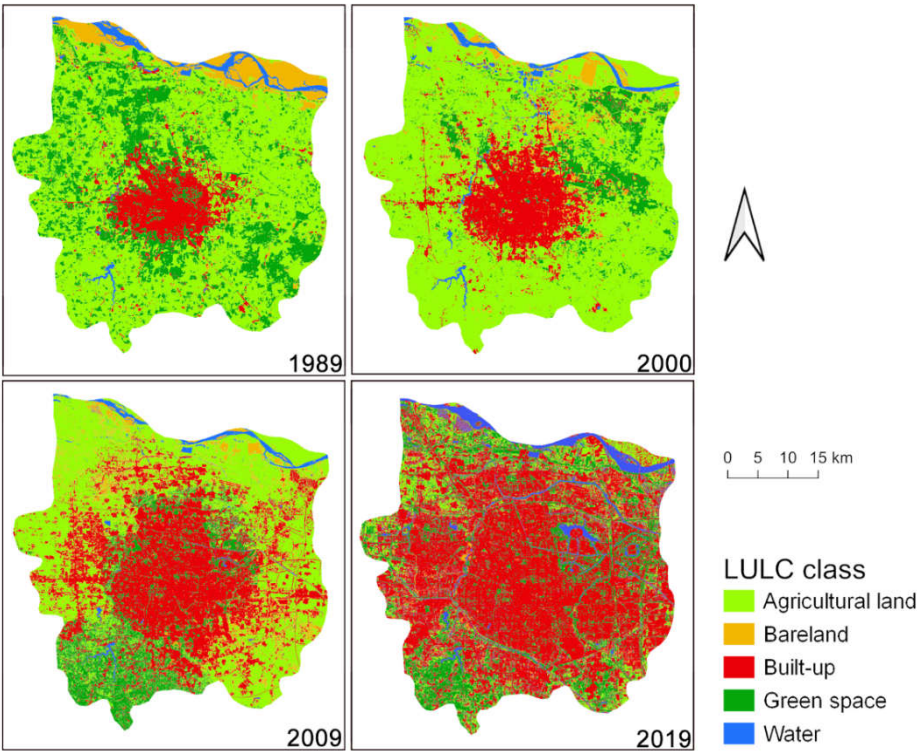


Figure 4.6: Maps of LULC (land use land cover) classification of Zhengzhou central city on Jun. 2, 1989; Aug.27, 2000; Aug.12, 2009; Jul.7, 2019.

From the year 1989-2019, the LULC in the study area had substantial changes, the dominant trend of LULC was the increase of Built-up land (10.1%-58.3%) and the decrease of agricultural land (69.6% to 25.1%). The predominant reason was the urbanization and industrialization process in China in the past 40 years.

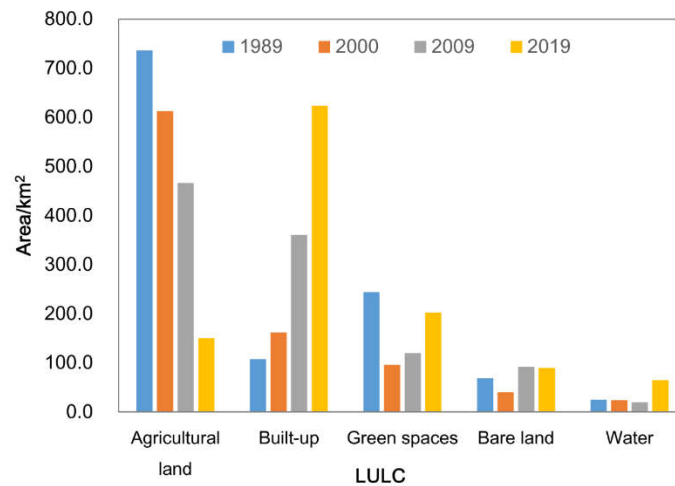


Figure. 4.7 Changes of LULC based on the five classes from the 1989-2019 of Zhengzhou central urban.

4.1.2.2 Spatial distribution surface UHI

The LST distribution performance can be illustrated by using the LST_i^{23} classes of the four years of summer LST maps from 1989-2019. Based on the method in section 3.3.1.2, the surface UHI pattern was categorized into five classes: low-temperature area, secondary low-temperature area, medium- temperature, secondary high-temperature area and high-temperature area see **Figure 4.8**. The high-temperature zone (red color) is mainly distributed on the built-up area (buildings, urban roads, industrial areas, commercial areas, construction land and construction site) and harvested land areas (especially on the year of 1989 and 2000), while the relatively low-temperature areas are located in the agricultural land and green space (blue and yellow). The lowest temperature zone is the places where water covered surface areas (dark blue). The LST pattern is strongly correlated with the LULC distribution and types in **Figure 4.6**, also shown in the integrated map in **Appendix 24**. The dominant heat island zone is in the central urbanized area, but this is also a small proportion of high-temperature areas located in the suburban area where mostly the harvested land and main road, relatively there are some low-temperature patches in the urban central area where the water surface and high vegetated areas are located.

²³ LST_i is the normalized value of land surface temperature.

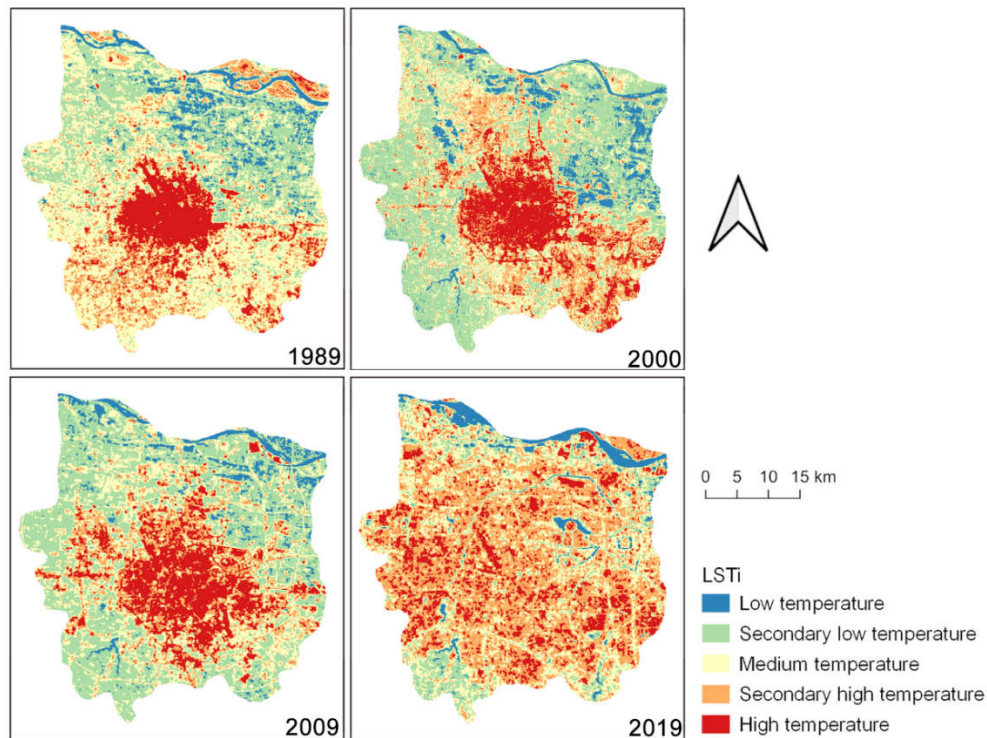


Figure 4.8: Maps of LST pattern based on the LSTi²⁴ classes approach of Zhengzhou central city on Jun. 2, 1989; Aug.27, 2000; Aug.12, 2009; Jul.7, 2019.

In terms of the yearly comparison of LST distribution, it was discovered that the classes in high-temperature zones (dark red color) was less dense with the year changes, as we can see the medium temperature (yellow color) and secondary high-temperature class (orange color) were inset into high-temperature zones. It can be explained by the urban green spaces also increased with the rapid urbanization, especially in newly built districts and urban renewal areas in Zhengzhou city if we compare the LULC map and LST map in 2019 (*Figure 4.6 and 4.8*).

In order to illustrate the spatial distribution of LST, Zhengzhou central city area was divided into eight zones by different directions (N, NE, E, ES, etc.) zone (*Figure 4.9*). In addition, the mean LST of each zone was extracted to represent the temperature degree, it was found that the heat expanding direction is correlated with the urban expanding direction, and the high LST zone is consistent with the **development direction of urbanization**. On one hand, the urban sprawl form is outward, which is from the central to outside non-urbanized area (*Figure 4.6, 4.8*). On the other hand, the main thermal expansion direction is concentrated on S-E and E (2000, 2019 in *Figure 4.6 and 4.9*), which is because of the new districts and urban planning in this two directions under the policy movement in Zhengzhou. The LST distribution was significantly related to the

²⁴ LSTi is the normalized value of land surface temperature.

LULC patterns (*Figure 4-6, 11, 12*).

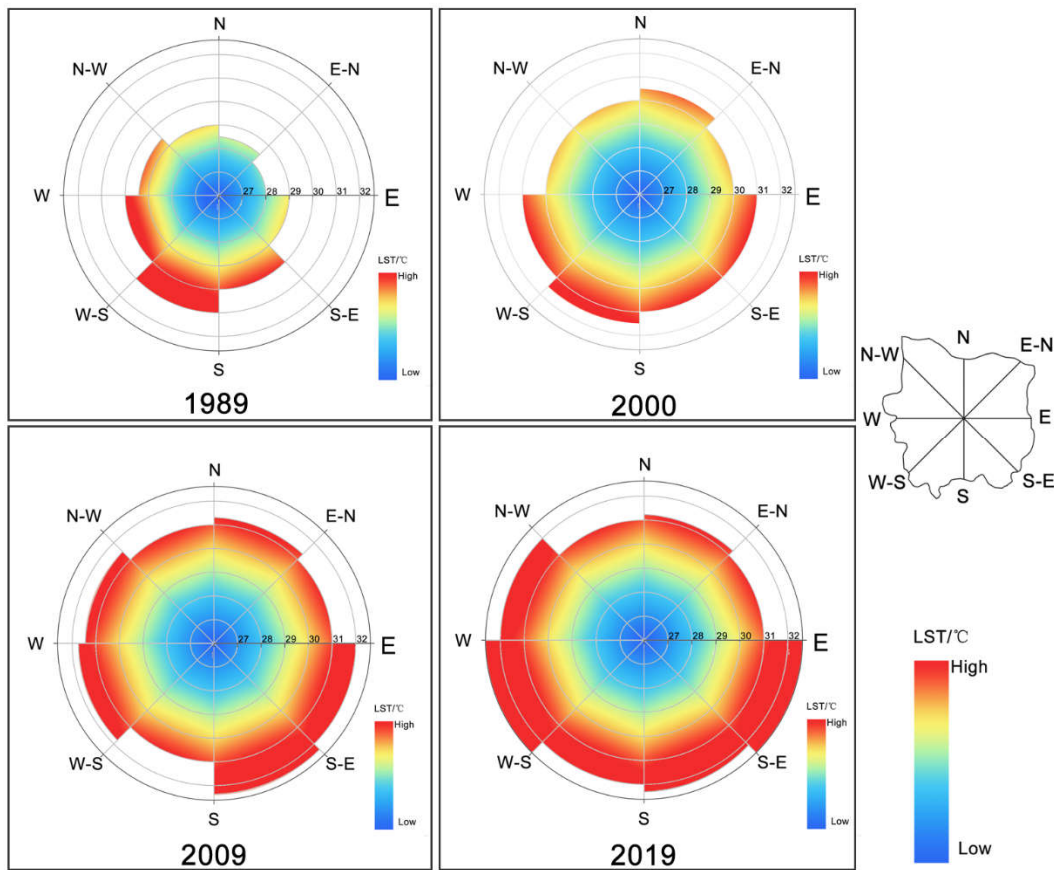


Figure 4.9: Mean LST degree of eight slices of Zhengzhou central urban, the angle of each zone is 45 degree, all the temperature range is from 27 °C- 32 °C, each grid is 1 °C.

When I looked at the spatial LST pattern with traverse approach by E-W and S-W profile of the four directions, the relationship between the location and LST value was applied to examine the LST distribution. In this analysis, Summer time satellite images were used to calculate and examine the LST distribution profile, and the “terrain profile” plugin was employed to portray the polyline data on summer of the year 1989, 2000, 2009, 2019. The results in *Figure 4.10* revealed that the LST in the urban central area was higher than the suburban both along the E-W and S-N direction on four selected dates. More specifically, there was a relatively obvious trend of LST difference between urban and suburban with the changes in the past 4 decades, which means the difference of the temperature is relatively getting smaller from 1989 to 2019. We can see from the trend line (red dotted line) in *Figure 4.10* that, the waviness trend line was becoming flat as the more urbanized area was growing. As a result, the temperature difference declined between the central city and suburban, geographically. Due to the spatial heterogeneity (with a complex assemblage of impervious surface and permeable surfaces) of the urbanized area, the LST changes along the two lines displayed various.

Among the selected four terms LST maps investigation, the profile on Aug.27, 2000, had the predominant LST difference between the **urban center** and its surrounding **suburban area**, it was found the highest mean LST (35.01°C) on that day (*Appendix 25*), which also revealed extreme LST (maximal LST 46.54°C). While the secondary significant LST difference appeared on Jun. 2, 1989 (E-W), it also increased when it comes to the edge of urban. The **harvested arable land** mostly causes this phenomenon with the bare surface. Compared to the other two curves in 2009 and 2019, the urban expansion made the low LST difference between intra-city and outward.

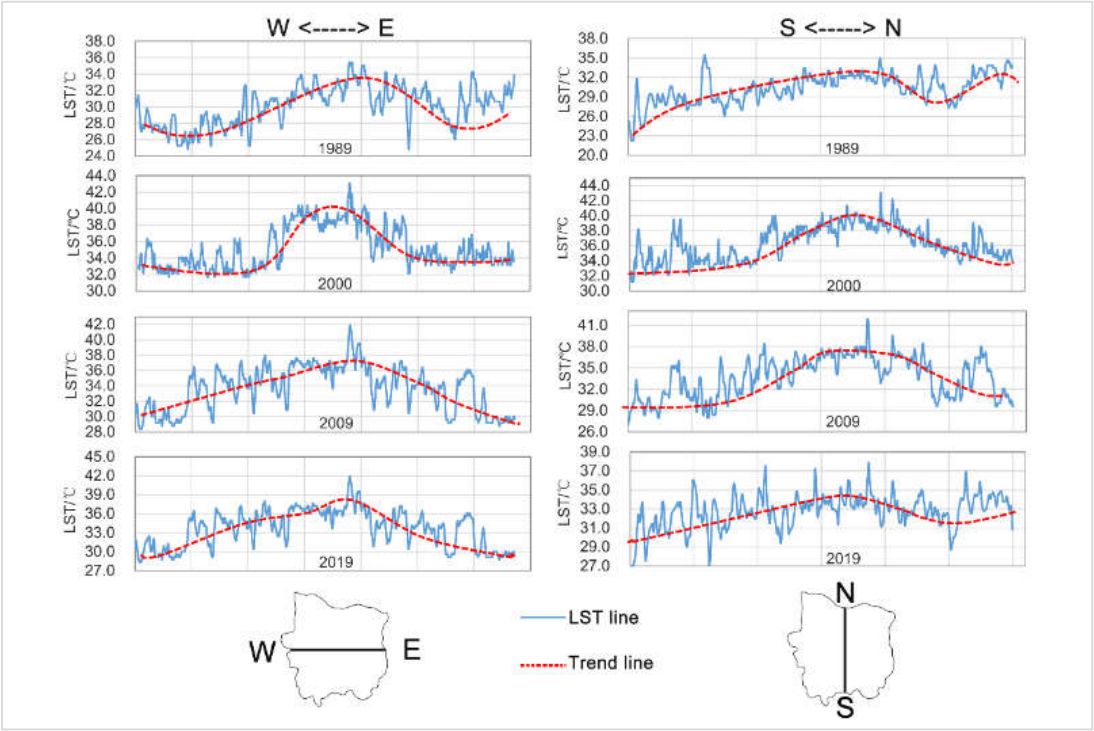


Figure 4.10: The LST change based on E-W and S-N profile on Jun. 2, 1989; Aug.27, 2000; Aug.12, 2009; Jul.7, 2019, respectively.

LST pattern distribution was also investigated using the city three urban rings of the city based on the ring road of Zhengzhou central city area (*Figure 4.11*). In this analysis, the mean LST showed that the first ring, which is located in the central part, has the highest LST in all the four selected maps, the figure displayed a significant LST decrease from the first ring to the third ring. This shows up with gradual change in red color from dark to light (*Figure 4.11*). In this histogram, the highest LST appeared in the year 2000, consistent with the result presented in the above paragraph. It is worth to mention that due to the harvested land (June is the time for the wheat harvest in the study area), the third ring was higher than in the second ring in 1989. We can see from the *Table 4.3* that the first ring was 1.61°C higher than the second ring and 3.43 °C higher than the third ring in average of the four terms. In addition, the mean LST difference between the first ring and the third ring could reach to 5.37 °C(2000) in maximal.

Table. 4.3 Mean LST (°C) of the three rings form 1989 of Zhengzhou central urban

Ring	1989/06/02	2000/08/27	2009/08/12	2019/07/07	Mean LST
First	31.06	37.88	35.59	33.06	34.40
Second	30.23	34.30	35.00	31.63	32.79
Third	30.52	32.51	30.63	30.23	30.97
T1	0.83	3.58	0.59	1.43	1.61
T2	0.54	5.37	4.96	2.83	3.43

T1 is the LST difference between the first ring and the second ring, and T2 is the LST difference between the first ring and the third ring.

In conclusion, firstly, the spatial difference of LST distribution is correlated with the LULC classification layout, Built-up area expansion is the dominant factor that contributes to the SUHI in Zhengzhou central city area. The SUHI phenomenon was significantly related to both the decrease of agricultural land and the growth of the built-up land.

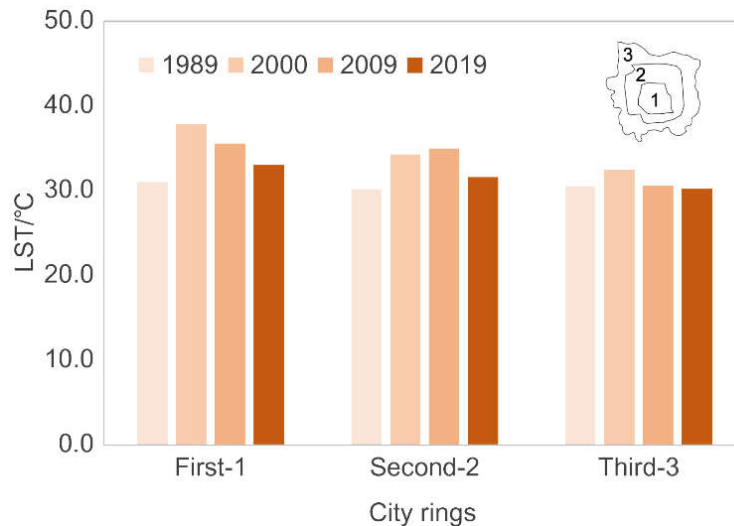


Figure 4.11: Comparison of mean LST of three rings based on the distance from the urban center, the three rings were defined by the city main road system of Zhengzhou central urban area. The four dates are on Jun. 2, 1989; Aug.27, 2000; Aug.12, 2009; Jul.7, 2019.

Secondly, the **LST pattern** is significantly associated with the **distribution of the urban expansion**, it was discovered that the high-temperature zone was driven by the form of the sprawl of the built-up area and the direction dominated by the urban development. Nevertheless, the LST pattern displayed as central area was higher than in suburban areas, and with the urbanization process, the temperature difference between the intra-city and outward became lower. From the map of LULC (**Figure 4.6**), it can be seen that the direction of urban expansion in Zhengzhou spreads from the first ring to the periphery. The first ring is the center of the city, which is not only a high-density building area and commercial area, but also a dense area of human activities, so the

temperature is the highest. With the intensity of urbanization, the green spaces and farmland in the third ring gradually become urban areas covered by impervious surface, and the temperature difference between the three rings of the city became smaller.

4.1.2.3 Spatial distribution of SUHI and LULC²⁵ types

The surface temperature pattern is related to the thermal characteristics of the **LULC type**. To study the impact of urbanization on the local thermal environment, it is necessary to study temperature changes through LULC. Therefore, we used GIS statistical tools to obtain the average LST for each land use/cover type. The results are shown in *Appendix 26, 27, 28, 29*. During the study period from 1989 to 2019, the **built-up area (BU)** showed the **highest average surface temperature**, **green spaces (GS)** had the second-highest average surface temperature among all LULC types in 1990, 2005, and 2009, and the average surface temperature of water surface type (WS) was the lowest in all years. The agricultural land (AL) type shows the variability caused by whether the **crop is harvested or not**. For the bare soil and the crop after harvest in the summer (1989), the newly planted crops (2000, 2009, 2019) show a significant difference. The surface temperature of the bare soil after harvest is higher than that of the period with crop coverage. It is worth noting that the proportion of the area of bare land (BL) is relatively small because the main urban area of Zhengzhou is located in the central plains and the land utilization rate is relatively high. Except for the bare land of the Yellow River banks, all land has been fully utilized and developed. Therefore, bare land temperature shows a lower temperature value due to its proximity to the water. Besides, bare land also includes land under construction in spectral identification.

In terms of **seasons**, the temperature of different coverage types presents different characteristics. According to the different seasons represented by the satellite images of different months selected in this study, although they cannot represent the characteristics of the entire season, they can reflect the differences in the area's seasons. In terms of different coverage types, the seasonal difference is **summer > spring > autumn > winter**. In addition, due to the complexity of the internal surface coverage of different coverage types, the Built-up (BU) type usually has the highest range value, indicating that the internal temperature difference was large, and the structural heterogeneity is large. It can also be seen from the standard deviation (*Appendix 26, 27, 28, 29*) that winter has the lowest standard deviation among the influences of seasons on different coverage types. The standard deviation of water surface (WS) and green space cover (GS) types is small.

A detailed analysis of land-use/change (LULC) and LST in Zhengzhou city center showed that non-evaporative surfaces (such as asphalt and concrete) replaced natural vegetation was the reason that increased urban land surface temperature. Therefore, the way of optimizing land development

²⁵ LULC is the abbreviation for land use/land cover.

and land use planning could be applied to mitigate the LST distribution, such as increasing green space and water area to alleviate SUHI effects.

4.1.2.4 SUHI intensity based on LST

In this survey, the SUHI intensity was calculated by two methods in section 3.3.1.2. URI²⁶ was used to quantify and compare the SUHI intensity of images in different periods (references) based on remote sensing image data. At the same time, the surface UHI intensity was calculated according to the land classification results and the LST image (*Figure 4.12*). The purpose is to detect and compare the relative intensity of UHI through both methods.

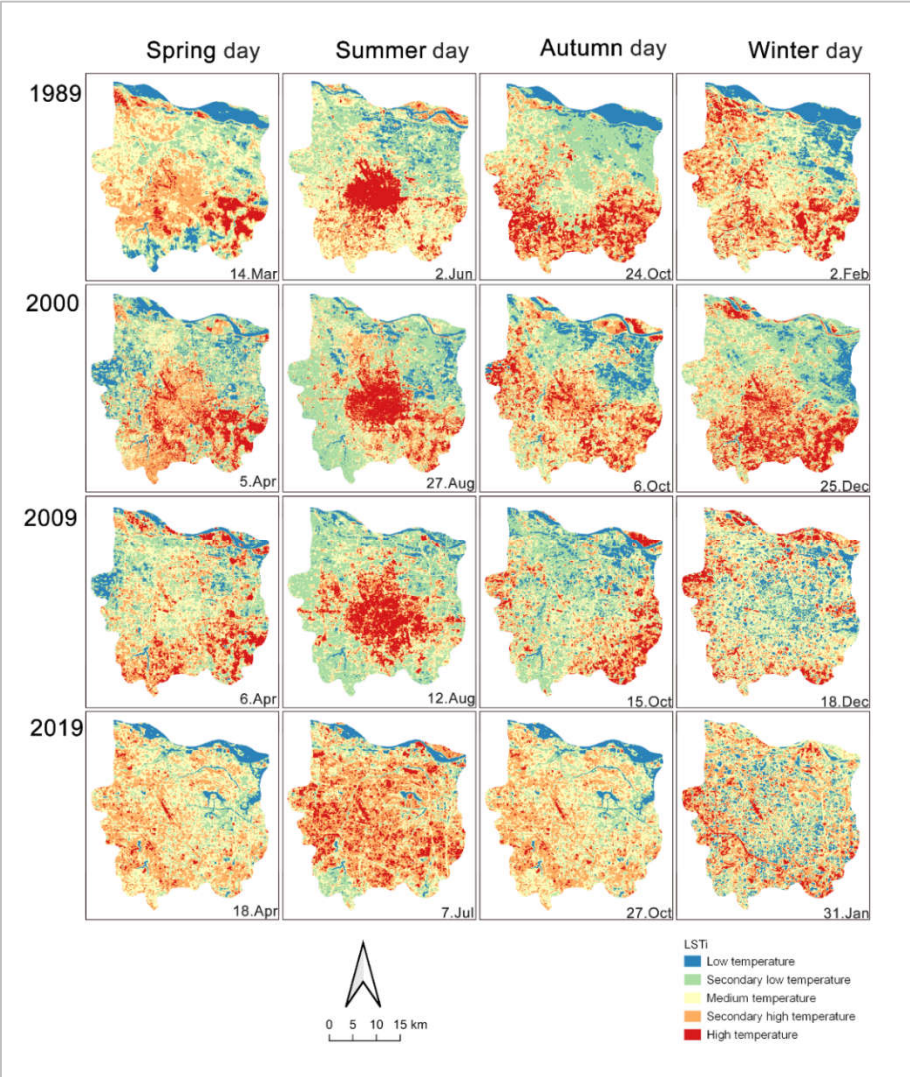


Figure 4.12: LST class distribution in different seasons from 1989 to 2019 of Zhengzhou central urban area.

Compared with the traditional method (weather station air temperature data) to calculate the SUHI

²⁶ URI is urban heat island ratio index, which used to quantify the urban heat island intensity of a city by a kind of high-temperature areas percentage, the detail could be found in section 3.3.1.3.

intensity, the data based on remote sensing is easy to obtain, besides, under the same weather conditions, the mapping of SUHI distribution density was larger illustrated by use of LST than by use of air temperature.

According to the calculation method of URI (section 3.3.1.3), from the time scale, the intensity of the heat island in Zhengzhou city had shown an upward trend year by year (**Figure 4.13**), and the heat island had shown a rising result in all seasons. The minimum value of URI was 0.18 (Feb. 2, 1989), and the maximum value that appears in the summer of 2019 is 0.35 (Jul. 7, 2019), indicating that the area of the heat island area was expanding with the process of urbanization. As the ratio of heat islands increases, the result of URI was also increasing.

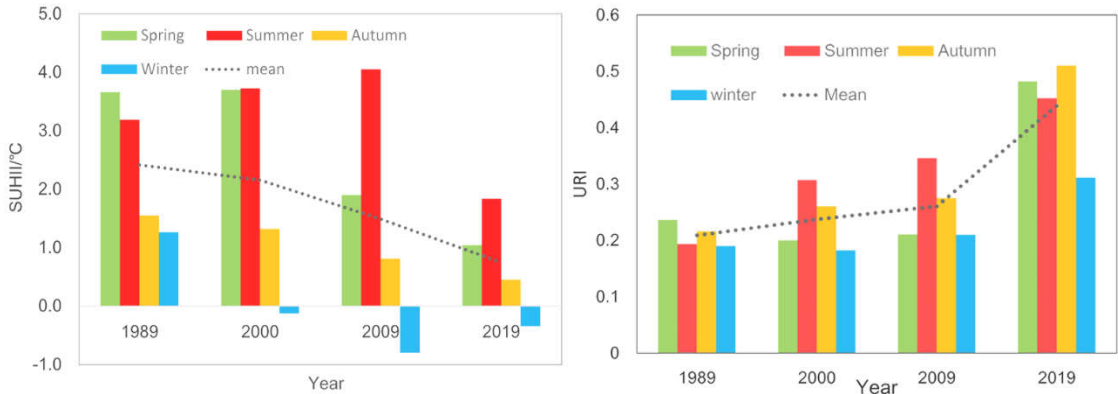


Figure 4.13: Surface UHII (left) and URI (right) values of the selected dates from 1989-2019 of Zhengzhou central urban.

This result is consistent with the spatial distribution of LULC in the previous chapter, as well as the spatial distribution of the LST patterns. In terms of seasons, the order of URI result was summer>spring>autumn>winter and the value was 0.35, 0.34, 0.25, and 0.22 respectively. The summer URI was the highest among the four seasons and the URI in winter was the lowest, but there was still a phenomenon that the temperature of urban built-up areas was higher than other areas.

I used the **SUHII method** to calculate the **heat island intensity** in different years and seasons. The SUHII result was the difference between the mean LST of the urban built-up area (BU) and the average mean LST of other four land-use types (AL, WS, BL, GS), which could be understood by the **relative heat island intensity**. The calculation result was shown in **Figure 4.13**. Unlike the result of URI, the value of SUHII showed a trend of increasing first and then decreasing from 2009 to 2019. From the LULC change (**Figure 4.6**) and the spatio-temporal change of LSTi²⁷(**Figure 4.12**), we could see that although Built-up (BU) has increased significantly by 33%, the green

²⁷ LSTi is the normalized value of land surface temperature.

space ratio in the central city area of the city has also increased. The green area in the new urban and old urban areas of Zhengzhou city has been improved, and the built-up (BU) area ratio in the study area has reached 48.3 %. The **high heterogeneity of the built-up area** (including commercial areas, residential areas, industrial areas, roads, etc., and green spaces attached to each area), resulting in a **smaller temperature difference** between the built-up area type and other types. Therefore, the SUHII method also **provides a new perspective** to explain the urban heat island effect changes.

4.1.2.5 Green space (NDVI, parks) and LST

NDVI is a very **significant indicator of green space**, and the different range of values represent land cover classes (*Appendix 30*). From the NDVI maps in *Figure 4.14*. I found that the distribution of vegetation coverage was consistent with land-use changes, which was due to the green space was replaced by built-up area with urban expansion from the LULC maps (*Figure 4.6*). It also could be recognized that the higher NDVI zones presented lower LST when compared the LST maps with NDVI maps (*Appendix 24*).

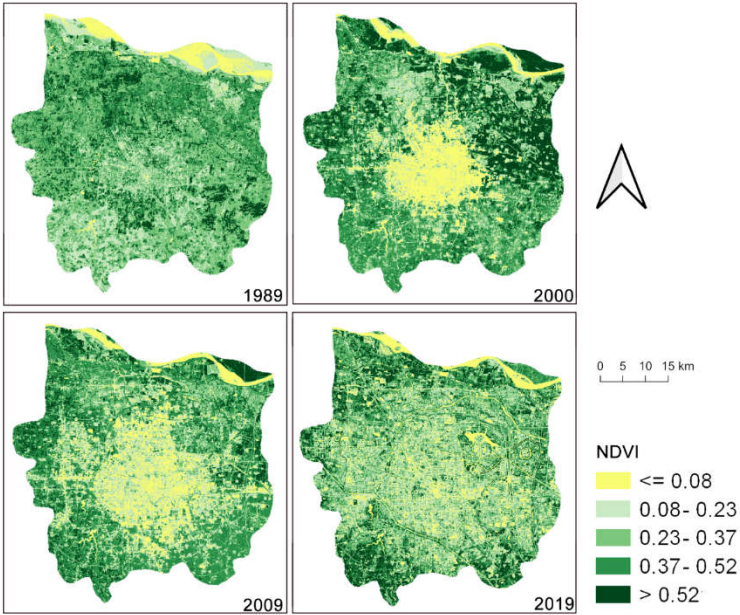


Figure 4.14: NDVI maps of Zhengzhou central city on Jun. 2, 1989; Aug.27, 2000; Aug.12, 2009; Jul.7, 2019

To analyze the relationship between the NDVI and LSTi relationship, a linear regression analysis was conducted based on the four direction profile in the *Figure 4.15*, according the NDVI research, the valid value for green spaces should be larger than zero, the **test the outlier** value also was applied to get the optimal result. From the results displayed in *Figure 4.15*, the coefficient in 1989, 2000 and 2019 were distributed around 0.30, however, the result of 2009 has a quite higher coefficient above the four dates, it indicated that the higher NDVI contributes to the **lower temperature zone** in an urban area. Therefore, the **higher vegetation coverage** could reduce the

surface temperature, and the urban green space can mitigate the SUHI phenomenon.

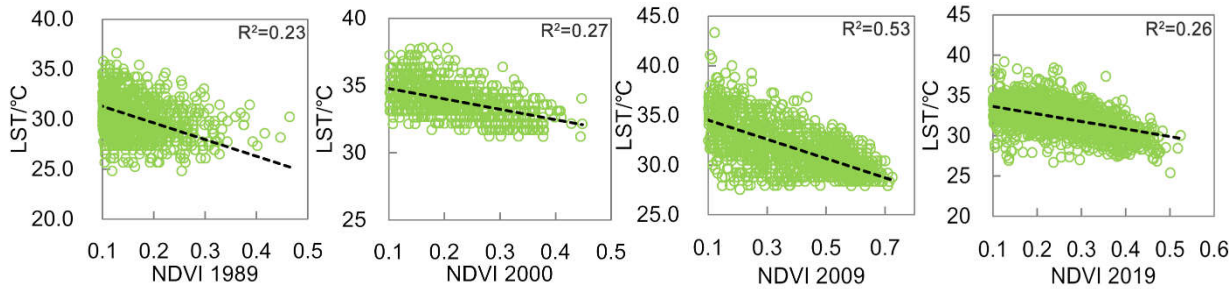


Figure 4.15: Linear regression between NDVI and LST on Jun. 2, 1989; Aug.27, 2000; Aug.12, 2009; Jul.7, 2019, respectively.

To better understand the detailed relationship between the green space and LST, nine regular urban green space samples were selected to quantify the temperature difference between green spaces and urban average temperature.

Table 4.4 Statistical parameters in the total urban area and the green space samples

	Urban	Green spaces samples
Mean LST (°C)	32.49	29.54
Stand Deviation (SD) (°C)	1.22	0.89
Range (°C)	12.21	5
Difference between mean values (°C)		2.95

The sample areas of green spaces also proved that higher vegetation coverage reflects lower LST, from *Appendix 31*, it was shown that the mean LST of city parks (Renmin Park, Zijingshan Park. *Table 4.4, Appendix 32*) about 2.95°C lower than the whole Mean LST in the urban area due to their water surface and vegetation rate in parks. Especially, the Jiangang reservoir area has the lowest LST among all the samples (*Appendix 31*), for its water area percentage almost over 90%. The second-lowest one is the nursery part for its 100% vegetation coverage. Therefore, green space can significantly reduce the SUHI effect.

4.1.2.6 Impervious surface indicator (NDISI), and Water surface indicator (MNDWI) and LST

In general, the urban area is composed of impervious surfaces (buildings, roads, squares, roofs, concrete structure) and permeable surfaces (vegetated area, water, soil). By using the spectral indices, these urban surface types could be extracted from the satellite imagery. Thus, following the method presented in section 3.3.1.4, 2000 random points samples were applied to explore the relationship between the impervious surface (NDISI) and LST. The result was shown in *Figure 4.16*, it was found that NDISI has a predominant positive influence on LST and the regression coefficient were 0.65 (Jun. 2, 1989); 0.57 (Aug.27, 2000); 0.81 (Aug.12, 2009); 0.84 (July.7,

2019) , respectively. This indicated that the impervious surface had a dominant influence on urban heat islands in Zhengzhou central city.

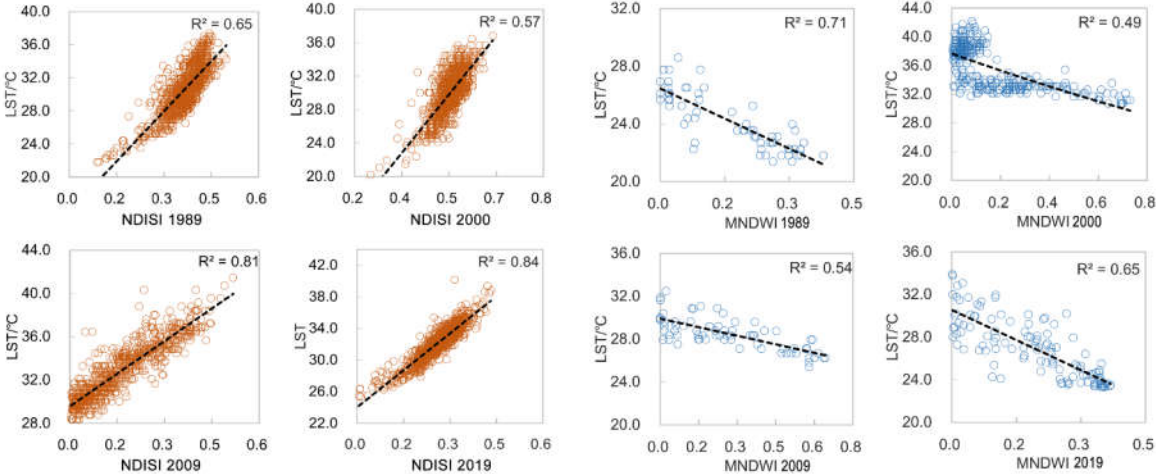


Figure 4.16: Linear regression analysis between NDISI (left), MNDWI (right) and LST from the random point samples (exclude the outliers and values of NDISI <0).

As MNDWI could also represent the moisture magnitude of vegetation and other urban coverage. The same approach used as above, the correlation of MNDWI with LST was also investigated. The correlation analysis in section 4.1.2.3 shows that the water area performed the lowest LST above all the LULC types. This analysis could further examine this negative correlation when we look at the linear regression between MNDWI and LST. A significant, highly negative correlation could be found in **Figure 4.16**, the linear regression coefficient was 0.71; 0.49; 0.54; 0.65, respectively. This finding is consistent with the result in section 4.1.2.3.

4.1.3 Discussion and further research proposals

In this survey, based on the meteorological data from 1981 to 2019, **long-term observation data was used to analyze atmospheric UHI temporal changes**. The traditional approach to quantify the UHI effect shows a straightforward way to portray the temporal local climate change (**Figure 4.1**). The temperature of Zhengzhou city has a gradual growth both in urban and rural areas, but the urban areas has a substantially higher increase compared with the rural areas (**Figure 4.1**). This result and urban climate change trends are consistent with many other researches (Chow, Roth 2006; Hansen et al. 2010; Lee et al. 2012). On the one hand, under the global warming context, the climate, especially in an urban area, experienced noticeable warming. Studies have determined that **urbanization** and **human activities** that result in energy consumption and carbon emission (Hansen et al. 2010; Reichle 2020), as a consequence, contribute to the greenhouse effect (US EPA 2014a). On the other hand, the urbanization process replaced the natural area's surface, changing the thermal capacity changed in an urban area; the urban area absorbs more heat than its surroundings. Those are the main reasons that can explain the increase of the urban climate change

in Zhengzhou city.

When we look at the result in section 4.1.1, the study area's atmospheric UHI effect has a watershed on turn-of-century (**Figure 4.2**). Because of the low rate of urbanization from 1989-2000, there are fewer differences in temperature between the urban and rural areas. But after 2000, the atmospheric UHI became significant and continually increasing. From the analysis between the atmospheric UHI and urban expansion indicators in section 4.1.1.4, atmospheric UHI change was associated with the socio-economic data such as Population, Urbanization rate, Population density, and GDP (**Table 4.1**).

Urban heat island and land use changes. Land use change in the region is the result of a combination of urbanization and economic development. These changes are characterized by a reduction in farmland area, a decline in forests and water bodies, and an expansion of urban areas (**Figure 4.6, 4.7**), which have become important factors affecting land surface characteristics. The urban thermal environment is also affected by changes in urban surface characteristics. The cause of land use land cover (LULC) changes had been studied by scholars (Chen et al. 2006; Jiang, Tian 2010; Bokaie et al. 2016; Mu et al. 2016; Fu et al. 2019), the land surface structure changes due to the process of urbanization, the conversion of non-urban into urban, the cropland, forest, arable land and other coverage types transform into build-up land, at finally made the changes of permeable surface conversion into impervious surface material. From 1981 to 2000, the built-up area in Zhengzhou increased with 68.2 km² (**Appendix 20**), and the number of increase is 518.15km² from 2000-2019, the built-up size in 2019 is 10 times larger than in 1981. In addition, the urbanization rate was from 35% in 1981 to 74.6% in 2019(**Appendix 20**). Urban expansion is a predominant factor that results in the SUHI effect in Zhengzhou city. Which all together result in the land surface temperature (**Figure 4.8, 4.9**)and air temperature (**Figure 4.1**) increase in the urban area, as a consequence, I found higher temperature in urban built-up areas and lower temperature in green spaces even in the urban center(**Table 4.3, Figure 4.11**). As regards the SUHI of Zhengzhou city, prior studies have shown different approaches to investigate that UHI, such as heat source-sink landscape patterns on SUHI (Zhao et al. 2018); landscape metrics and LST (Li et al. 2020); those studies provided a different view to clarify the important role of green space in mitigating the UHI effect.

In the central city of Zhengzhou, the **shadows of high-density buildings**, especially high-rise buildings, affect the surface temperature and the radiation. I selected 10 sample sites (**Appendix 33**) to analyze the temperature effects of shadows, and the results showed that the surface temperature in the non-shaded area is 0.74 °C higher than that in the shaded area (**Figure 4.17**). I selected typically the same coverage types: mostly wide roads next to high buildings (shaded) and far away from high buildings (non-shaded) within the city. This analysis proves the interference effect of shadows. However, since the study of LST analysis in Zhengzhou focused

on analyzing large-scale land-use types, the results of the analysis used the average temperature, so the modification effect of shading reduced.

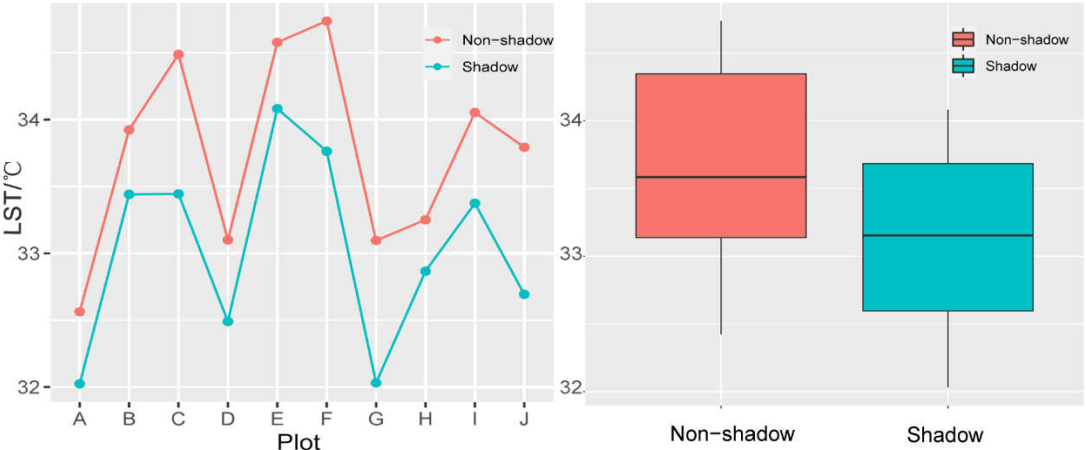


Figure 4.17: The land surface temperature (LST) of shadow and non-shadow from 10 plot with the same environment in Zhengzhou city.

Regarding UHI and urban growth, applying the UCR²⁸ indicator (Figure 4.6) to quantify the urban expansion had a consistent result as LULC illustration and mapping (Figure 4.6), which proved that the urbanization process contributes to the UHI and they had a significant correlation. Urban growth is the process of LULC changes and transition, especially the replacement of permeable land (agricultural land and green spaces, etc.) by impervious surface, in terms of the LST maps and LULC maps comparison. I conclude that **the increased high-temperature zones were generally located in the increased built-up area**. However, the **cool islands were generally in the type of green spaces and water areas**. This also can be recognized from analysis of urban expansion (Figure 4.6) and LST maps. The urbanization form in Zhengzhou was **from the center to outside**, which results in urban heat island sprawl from the center to the urban edge (Figure 4.9). By analyze Zhengzhou's profile map, it found that the SUHI in the center was higher than the external part in each direction of urban (Figure 4.10). Besides, the same results also were shown in the urban rings analysis in Figures 4.11.

I used **two methods** to examine the **SUHI intensity** in Zhengzhou city. Those two methods provided different perspectives to quantify the urban heat islands' development and change of SUHI. URI²⁹ reflected the percent of the urban high-temperature zones in urban built-up areas,

²⁸ UCR is the Urban Compactness Ratio, a higher value indicates a more compacted shape and a value closer to 1 indicates that the urban built-up land has a higher occupation, and vice versa. In general, if urban land expansion changes in the infilling way, the concavity of urban edges will decrease because the urban internal gaps are gradually filled up, and as a result, the urban form tends to be more compact.

²⁹ URI is urban heat island ratio index, which used to quantify the urban heat island intensity of a city by a kind of high-temperature areas percentage, the detail could be found in section 3.3.1.3

which is a relatively dynamic change with urban development. URI results indicated that the urban heat islands increase with the urbanization process during the past decades. However, the **SUHI intensity** method shows a different trend. In 2019, the SUHI experienced a decrease. Why did this happen? As SUHI intensity is the mean temperature difference between green spaces and other land-use types(section 3.3.1.3), in this regard, revealed that the green space and other land-use types had smaller temperature difference, others land-use became greener than before due to the green strategies in urban renewal and construction in Zhengzhou recent years. **For instance, “Park city”, “Ecological garden city”, “Spongy city”, “Urban double-repair; those urban development strategies** made a change for the urban landscape. With a high-increase of the urban blue and green infrastructure in new town areas (**Figure 4.18**), the average LST in new town samples(**Figure 4.18 c, d**) were 2.32°C lower than old town samples(**Figure 4.18 a, b**), while the green ratio in samples (**Figure 4.18**) were 11.98% (a); 16.65% (b); 38.60% (c) and 50.38% (d). Data showed that **in 2019, Zhengzhou increased green spaces by 12.1 km²**, and the green space rate, green coverage rate, and per capita park green space in built-up areas reached 36.2%, 41.2%, and 12.3 square meters, respectively. **Green development strategies** has been applied in modern Zhengzhou city in recent years and obviously, mitigate the UHI effect.

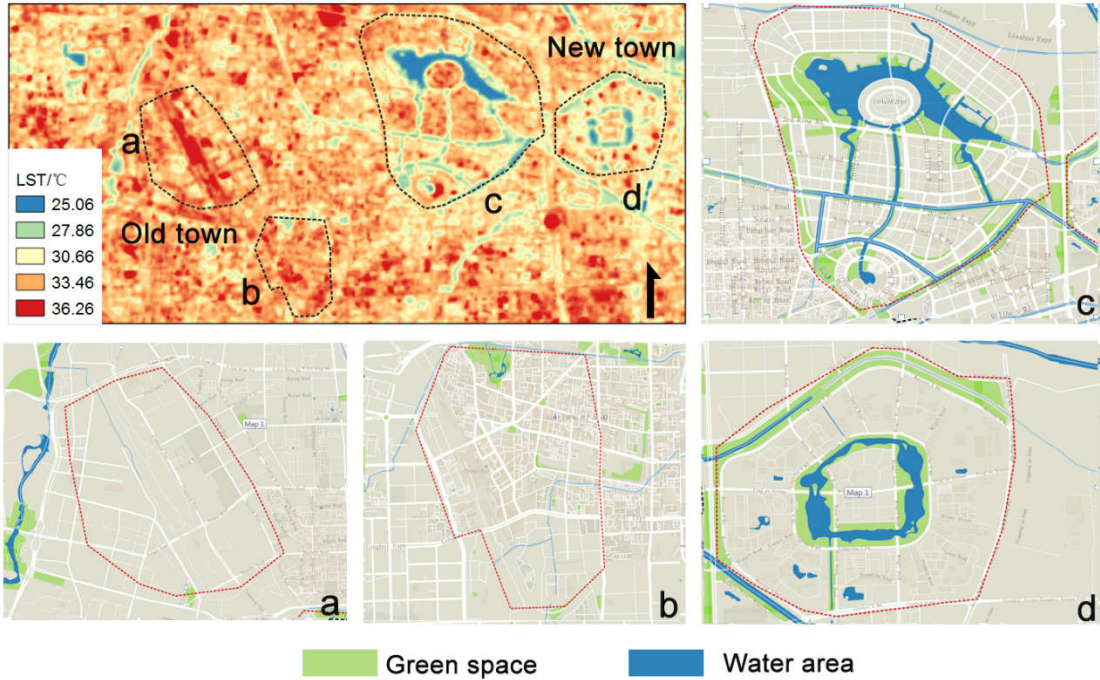


Figure 4.18: Comparison of LST between new town areas and old town areas of Zhengzhou in 2019. Old town samples: a). Zhengzhou south station; b). Zhengzhou railway station. New town samples: c). CBD; d). Longzihu zone.

Using green space (green network) to mitigate land surface temperatures

From the LST pattern maps of **Figure 4.8**, it can be found that the **green space and water areas**

are relatively **cool areas** (*Appendix 34a, b*; yellow and blue zones), while the urban densely built-up areas (*Appendix 34c*, red zones) were expanding as SUHI may not be avoided. With the development of the urban areas from 1989-2019, although the high-temperature zones area expansion, there was still some difference in LSTi distribution (*Appendix 24*). When we look at the summer LSTi maps in 1989 and 2000, the high-temperature clusters were dense. Not so many medium-temperature patches (yellow) and low-temperature patches (blue) color inside the high-temperature zone. But in the summer LSTi map of 2019, it can be found that lower temperature zones surround the high-temperature zones. If we compared the LULC maps in 2019, it could be easily recognized that the green space and water surface were increased, and the built-up areas were filled in vegetation and green. In Zhengzhou city, the **new districts** have higher green coverage than the **old town**, that because of the proper urban planning and design in urban structure and percentage of green rate. Thus, we can apply a more appropriate urban development model to mitigate the SUHI effect. The newly built-up districts in the future can be with a reasonable layout to optimize reduce the SUHI.

In 2018, China had put forward the “**Park city**” urban development strategy across the state (G. Wang et al. 2019). The important indicator of park city strategy is to build more parks, as well as green spaces and water surface **in new town** (*Figure 4.18*). From the analysis in *Figure 4.15 and Appendix 24*, the green space, especially the parks as the cool island to the SUHI, should take into account to be a solution. This is widely determined by many researches (Armson et al. 2012; X. Chen et al. 2012; Hamada et al. 2013; B.-S. Lin, Lin 2010; Zardo et al. 2017). In addition, the urban water area was also the cool island in terms of the SUHI effect. *Figure 4.16* had indicated the significant impact of water area on temperature. Previous studies (Du et al. 2016; Han-qiu 2005; Steeneveld et al. 2014; Xu 2006) had also proved the role of water on UHI. Recently research also established the blue-green synergy strategy (Gunawardena et al. 2017; Shi et al. 2020) to optimize the cooling effect regarding UHI.

4.1.4 Summary and outlook of UHI in Zhengzhou

This survey first used **long-term urban and rural weather station** data to analyze the air temperature changes and heat island intensity in Zhengzhou urban areas in the past 40 years (1981-2019). During the study period, the urbanization process raised the average annual temperature of Zhengzhou city to 0.67 °C per decade. This warming rate is 0.43 °C per decade, compared to neighboring rural areas. The analysis of the urban compactness ratio (UCR) showed that urbanization had an important **contribution** to the warming trend of Zhengzhou.

The **intensity** of urban heat island showed a clear watershed at the **turn of the century**. This is related to Zhengzhou's urbanization process and the **driving factors** of China's national development policy. The intensity of heat island during the day was smaller than that at night.

Socio-economic indicators also proved significantly correlated to the urban heat island.

Secondly, the study on the urban heat island effect of Zhengzhou based on the surface temperature of 16 satellite images showed that the heat island effect was closely related to the changes of LULC in the past 40 years (1989-2019). From 1981-2000, the built-up area increased 68.2 km², and the number of increase is 518.15km² from 2000-2019, the built-up size in 2019 was **10 times larger** than in 1981. Increased heat island area and increased built-up area was consistent in spatial distribution. The temporal and spatial distribution of heat islands showed the characteristics of high LST in center and low LST in suburbs. The increasing direction of heat islands was consistent with the **direction of urban sprawl**. Among the different types of urban land, construction land was the area with higher temperature among all types (except in winter). Green space and water were the cold islands of the city in summer. The spatial combination of different types of urban land use impacted the intensity of the heat island. The planning model (2019) of coupling green space and impervious surface reduces the density of the heat island.

The Urban heat island Ratio Index (URI) shows that heat islands have increased significantly with urbanization development. In contrast, the relative surface urban heat island intensity (SUHII) based on the difference between construction land and other land use shows that **in recent years, Zhengzhou's urban renewal and new city construction have achieved certain ecological effects**, which balanced the distribution of urban gray and green infrastructure, **increasing urban green space ratio in the built-up areas**. Hence, the impervious area and green space were closely coupled, which reducing local urban heat islands. However, the overall urban heat island area still increases due to the rapid urbanization in Zhengzhou. The regression analysis based on the vegetation index (NDVI) and water index (MNDWI) verifies the green space's cooling effect. The impervious surface (NDISI) had a positive effect on SUHI. This survey reveals that establishing the **blue-green synergy strategy** could optimize the cooling effect regarding the SUHI effect.

4.2. Mapping and analysing park cooling effect on SUHI based on satellite images

In the Park cooling effect survey, I intend to answer **Research Question2: What are the cooling effect characteristics of urban parks in urban heat islands in Zhengzhou city? What parks should be planned designed in terms of mitigating SUHI by modifying park design parameters?**

To explore and investigate the questions, the Landsat 8 image of July 2019 was selected from Landsat collection to obtain Land Surface Temperature (LST) by using Radiative Transfer Equation (RTE) method, and present land cover information by using spectral indices. Additionally, high-resolution Google Earth images were used to select 123 parks, grouped in five categories³⁰, to explore the impact factors on **Park Cooling Intensity (PCI)**³¹. The results show that: (1) Among the five studied park types, the theme park category has the largest cooling effect while the linear park category has the lowest cooling effect; (2) The mean park LST and PCI of the samples are positively correlated with the Fractional Vegetation Cover (FVC) and with Normalized Difference Water Index (NDWI), but these are negatively correlated with the Normalized Difference Impervious Surface Index (NDISI). We can suppose that the increase of vegetation cover rate within water areas as well as the decrease of impervious surface in landscape planning and design will make future parks colder. (3) There is a correlation between the PCI and the park characteristics. The SUHI effect could be mitigated by increasing of park size and reducing park fractal dimension (Frac_Dim) and perimeter-area ratio (Patario). (4) The PCI is influenced by the park itself and its surrounding area. These results provide an important reference for future urban planning and urban park design to mitigate the urban heat island effect.

4.2.1 Relation between park types, LST and PCI

Using land surface temperature analysis (method section (3.3.1.2.)), the LST map based on the 07/07/2019 satellite image was derived (**Figure 4.19 a**). The **mean park LST** was lower than the **mean LST of Zhengzhou city**. I analyzed the PCI of all the selected samples by comparing the five park types (**Table 4.5**), and results showed that the PCI of the five park types were different (**Table 4.5**): The average temperature of the **theme park** category is 30.01 °C; which is 2.14°C lower than the average temperature of Zhengzhou city. Its **cooling effect** is the strongest, where the average PCI reached 2.76 °C. The urban squares had the highest temperature, with an average LST of 32.13°C, which is still 0.02 °C lower than the average LST in Zhengzhou.

³⁰ Five park types: urban park, theme park, street park, linear park, urban square, which based on 《Standard for Classification of Urban Green Space》 CJdJ/T85-2017.

³¹ Park Cooling Intensity (PCI) calculates the temperature difference between the inside and outside of the park.

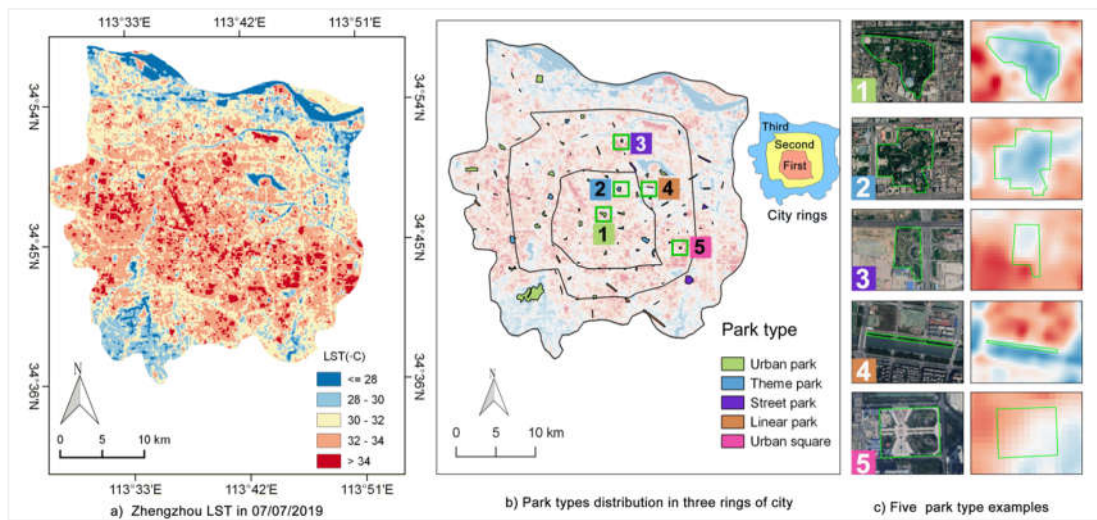


Figure 4.19: a) LST map of Zhengzhou city in 07/07/2019; b) Distribution of 123 parks samples; c) Five park type examples: 1-Urban park; 2-Theme park; 3-Street park; 4-Linear park; 5-Urban square

The result (*Table 4.5*) showed that PCI of the **theme park category** was the strongest, this is related to the content of the theme park. Linear parks had the lowest cooling effect; the PCI value was only 0.64 °C . Meanwhile, the cooling effect of the street park category is also at a comparatively low level, with its PCI only 0.16°C higher than the PCI of the street park group. The PCI of the urban square category was in the middle, it reached 1.44°C , but its average LST was the hottest among the five types. So based on the results, we can conclude that theme parks have the most substantial cooling effect in Zhengzhou city, while the linear park category contributes with a less cooling effect.

Table 4.5. Statistics of LST and average park cooling intensity (PCI) in different park types

Code	Type	No	Mean LST(°C)	Max (°C)	Min(°C)	Average PCI(°C)
1	Urban park	59	30.43	33.63	27.63	1.71
2	Theme park	10	30.01	34.62	25.97	2.76
3	Street park	28	31.32	37.80	25.34	0.8
4	Linear park	19	31.47	35.42	28.56	0.64
5	Urban square	7	32.13	33.90	31.10	1.44
6	Zhengzhou city	-	32.15	46.09	20.11	-

4.2.2 Relation between park LST and its impact factors

First, we analyzed the relation between park LST and the spectral indices inside the park. The

results showed that the mean park LST was significantly related to the FVC³², the NDISI³³, and the NDWI³⁴ (**Figure 4.20 c**). The cooling effect of the park is directly proportional to the park's vegetation percentage ($R^2 = 0.489$), indicating that more vegetation cover makes parks cooler (**Figure 4.20c**). For example, Xiongerhe park's FVC has one of the highest values (R^2 is 0.408), while the mean temperature is the lowest (28.06°C). Moreover, the average PCI of Xiongerhe shows it is much colder (2.18°C) than its surrounding area. The results showed that the water index (NDWI) plays a negative role in park LST (**Figure 4.20 b**), indicating that the NDWI value strengthens the cooling effect of the park. On the contrary, the impervious surface (NDISI) has a relatively positive effect on park LST. From the regression model between LST and NDISI, the coefficient of determination (R^2) reached 0.926 (**Figure 4.20 c**), revealing that the impervious surfaces have a significant impact on park temperature. The impervious surface is the main contributor to warm conditions of parks. We can conclude that water and vegetation have a positive impact on park cooling roles in Zhengzhou while the impervious surface increases the park warmth.

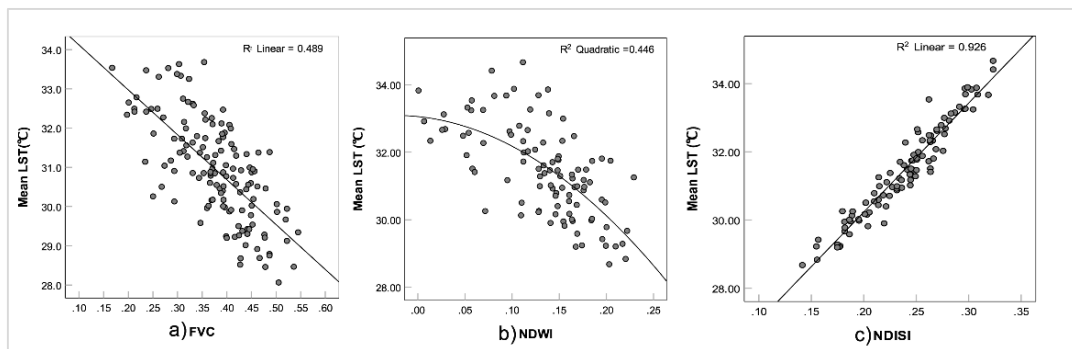


Figure 4.20: Regression analysis among mean park LST and, a) FVC, b) NDWI, c) NDISI.

Secondly, we analyzed the relation between park LST and **park characteristics** (patch metrics). The result of the analysis shows that patch metrics have relations to park LST. From **Figure 4.21**, **park size** is negatively correlated with the mean park LST (**Figure 4.21a**, $R^2 = 0.308$), which means the park size is one of the main factors of LST. We can see from the **Figure 4.21a**, if the park size was larger than 40 ha, the average LST was below 31°C, and the average LST appeared in a wide temperature range among the parks with the size below 20ha. Fractal dimension (Frac_Dim) and perimeter area ratio (Paratio) show a positive correlation with the park LST, and the coefficient of determination R^2 is 0.191, 0.280. This indicates that these two factors also have an impact on LST. The shape index (Shape_Idx) has no significant correlation with park LST

³² Fractional Vegetation Cover (FVC) is an index that depicts the vegetation abundance of ground surface.

³³ Normalize Difference Impervious Surface Index (NDISI) indicator is used to estimate impervious surface.

³⁴ Normalize Difference Water Index (NDWI) is a remote sensing based indicator sensitive to the open water surface and water content of leaves.

(*Figure 4.21d*). For example, the park with a maximum shape index (2.13) has the same LST (28.80°C) as parks with the lowest shape index (1.21) (*Figure 4.21 e*). From the results, we can conclude that the **park size** and **perimeter-area ratio** play a more critical role than other patch metrics in the sample parks of Zhengzhou city.

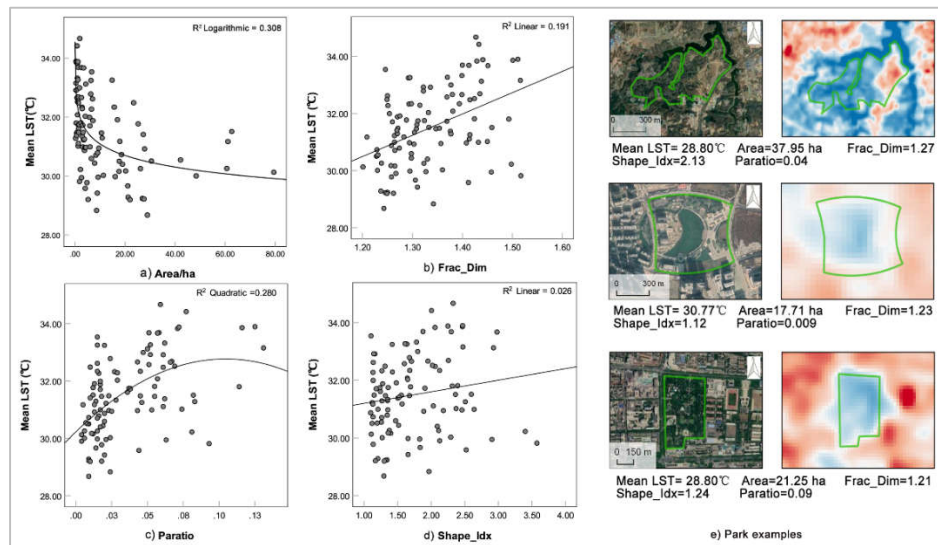


Figure 4.21: Regression analysis among mean park LST and park characteristics: a) Area; b) Frac_Dim; c) Paratio; d) Shape_Idx; e) Three park examples.

4.2.3 Relation between PCI and its impact factors

I analyzed the correlation between **park cooling intensity** and the characteristic **indicators** of sample parks: Fractional Vegetation Cover (FVC), Normalize Difference Impervious Surface Index (NDISI), Normalize Difference Water Index (NDWI). First, I analyzed the relation between PCI and the spectral indices inside the park. The results of correlation with PCI³⁵ are shown in *Figure 4.22*. I found that FVC has a positive effect on PCI: the more FVC we have, the higher PCI appears. However, the coefficient of determination R^2 is only 0.237. This means that PCI only partly depends on vegetation cover (FVC). *Figure 4.22b* indicates that higher NDWI contributes to higher PCI, this quadratic regression analysis coefficient of determination (R^2) is 0.433. Among the three factors, the NDISI has the strongest relationship with PCI (*Figure 4.22c*), the coefficient (R^2) is 0.618, which means the impervious surface has a significant influence on PCI. So from the park spectral indices results, we can recognize the park vegetation and water percentage play a decisive role in PCI, while the high impervious surface reduces the cooling effect of parks.

³⁵ Park Cooling Intensity (PCI) calculates the mean surface temperature difference between the inside and outside of the park.

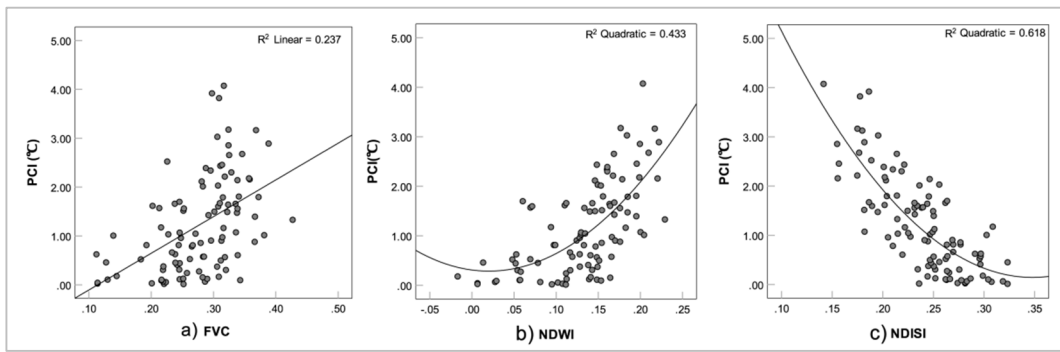


Figure 4.22: Regression analysis of park PCI and a) mean FVC; b) mean NDWI; c) mean NDISI.

Secondly, I analyzed the relation between **PCI and park characteristics** (patch metrics). PCI has a complex correlation with park patch metrics (*Figure 4.23*). Among the four analysis results, the size, fractal dimension (Frac_Dim), and perimeter area ratio (Paratio) regression coefficient of determination R^2 is 0.321, 0.355, 0.439, respectively (*Figure 4.23 a; b; c*) which means those three factors contribute to the PCI in general. While the shape index showed no significant correlation, as its linear model R^2 is 0.089 (*Figure 4.23d*). Park shape index does not contribute to PCI among the selected sample parks of Zhengzhou. It is found that parks with a size larger than 15 hectares(*Figure 4.23 e*) have significant cooling intensity (average PCI 2.23°C).

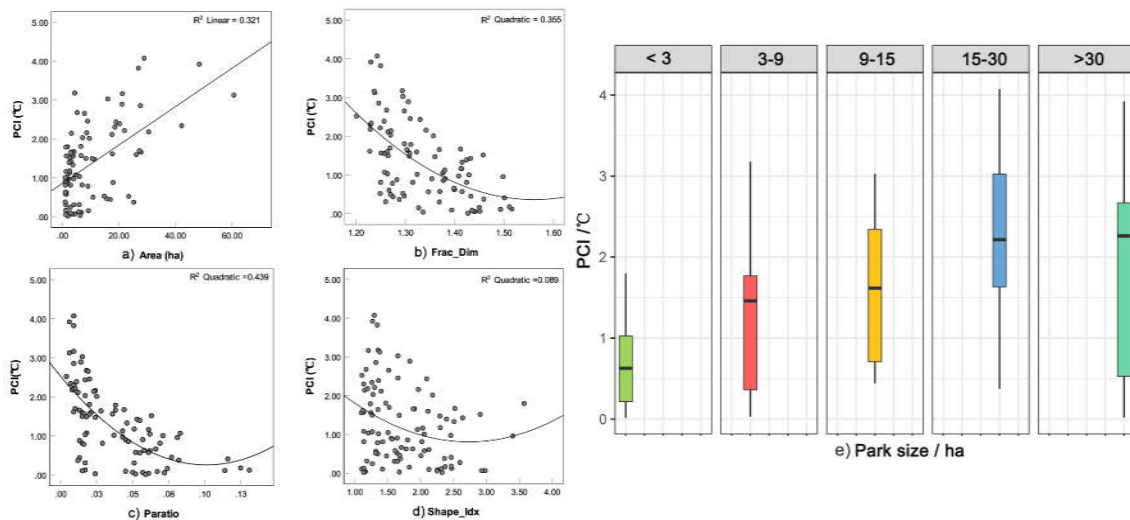


Figure 4.23: Regression analysis among PCI and mean park characteristics: a)Area; b) Frac_Dim; c) Paratio; d) Shape_Index; e) Boxplot of park size classes and PCI

Thirdly, I investigated the relationship between **PCI and the impact factor** of the park **surrounding** area. In order to analyze the impact of PCI and the type of land cover around the parks, I selected 43 parks with similar mean LST (within the range of 29.0°C-30.0°C) from the 123 samples (*Figure 4.24*). For external land cover types, I used spectral indicators: NDVI, NDWI, NDISI to measure vegetation, water coverage and impervious surfaces of the surroundings.

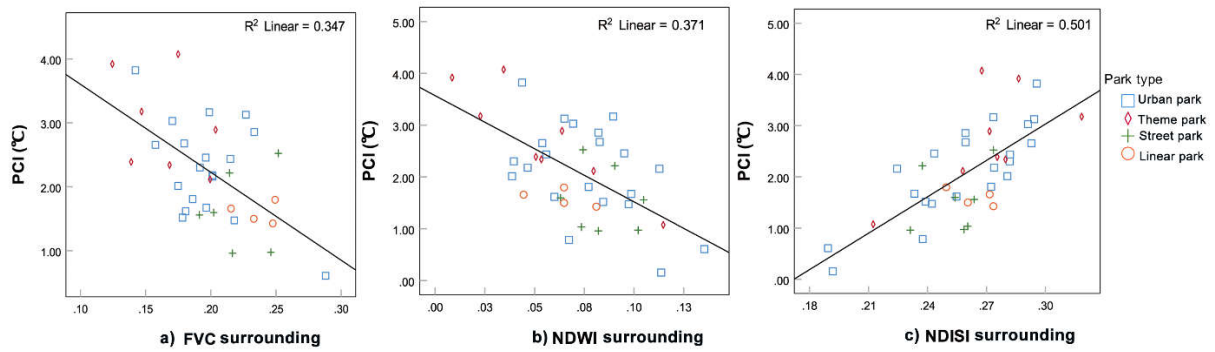


Figure 4.24: Regression analysis between the PCI and the impact factor of park surrounding area (500m buffer).

The linear regression analysis was used to analyze the PCI relationship with the three factors outside the parks. The results show (*Figure 4.24*) that in the case of parks within the LST range of 29-30 °C the type of land cover around the park has a significant impact on PCI. PCI has a negative correlation with surrounding vegetation and water bodies, and a positive correlation with surrounding impervious surfaces in cases I analyzed from elements within the same LST range (29-30°C). This shows that PCI is not only affected by the internal factors of the park but also related to the surrounding environment.

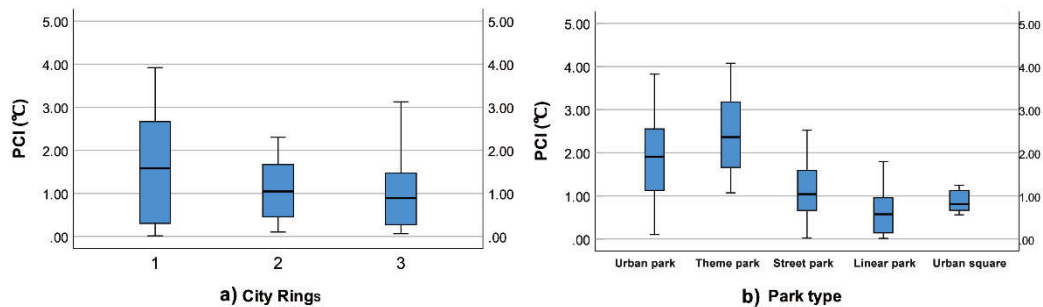


Figure 4.25: Analysis between PCI, location factor and park types (all 123 samples).

In addition, I analyzed the location factor on PCI based on the **city rings**. Zhengzhou city has three rings defined by the urban ring road (*Figure 4.25 a*), the first ring is the urban center area, which is more dense than the other two. The parks in the **first ring** have the **highest average PCI** (*Figure 4.25 b*), as the land cover types in the urban center are mostly commercial areas and built-up areas with tall buildings and impervious surfaces, which are warmer than other areas of the city. The third ring is low-density urban area and is covered with more green spaces and mostly low-rise buildings. I recognized that PCI is also influenced by the **location factor**, which is partly in relation to the different land cover types of park surroundings.

The park type can be defined based on different surrounding types, for example, linear park is mostly **located beside the road or river**. The urban square is usually located in the high-density

area. Due to this reason, the linear park and urban square show low PCI (*Figure 4.25b*). These results are mainly attributed to the different surrounding environments and land cover of different park types. So I concluded that PCI is also related to the surrounding land cover types.

4.2.4 PCI changes with the distance measured from park edge

In this survey, the method to calculate the PCI³⁶ is the difference between the average temperature inside the park and the average temperature within various distances (measured by using buffer zones) outside of the parks (*Figure 4.26*). This **algorithm** followed the previous studies (Cao et al. 2010; Chang et al. 2007; Spronken-Smith, Oke 1998) found that the threshold of the cooling effect of cooling is around 500m.

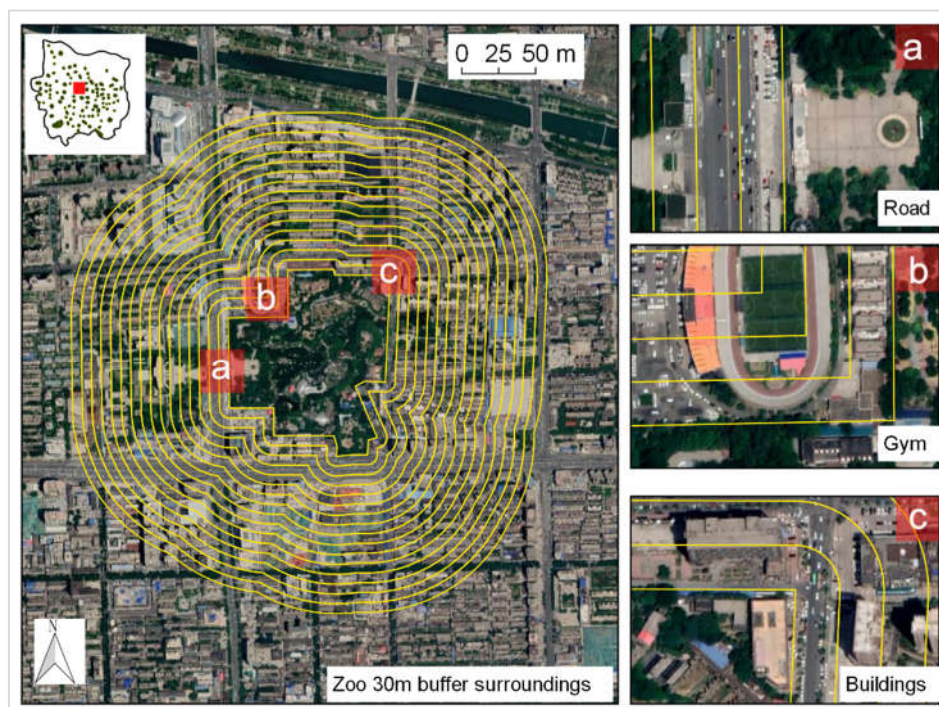


Figure 4.26: Buffer zones near the Zoo and the land surface cover condition detail in the first 3 buffers: a) Urban road; b) Gym, c) Buildings and road

In the urban land use planning, taking into account of the distribution pattern and service radius of the park, the **surrounding areas of the park** are generally impervious surface (Min et al. 2018; Mu et al. 2016), such as roads, residential areas, commercial areas, and industrial sites. Generally speaking, there is no connection to another green space within a certain range. So the 500m buffer zone may contain multiple types of land, which affects the results of the PCI.

³⁶ Park Cooling Intensity (PCI) calculates the mean surface temperature difference between the inside and outside of the park.

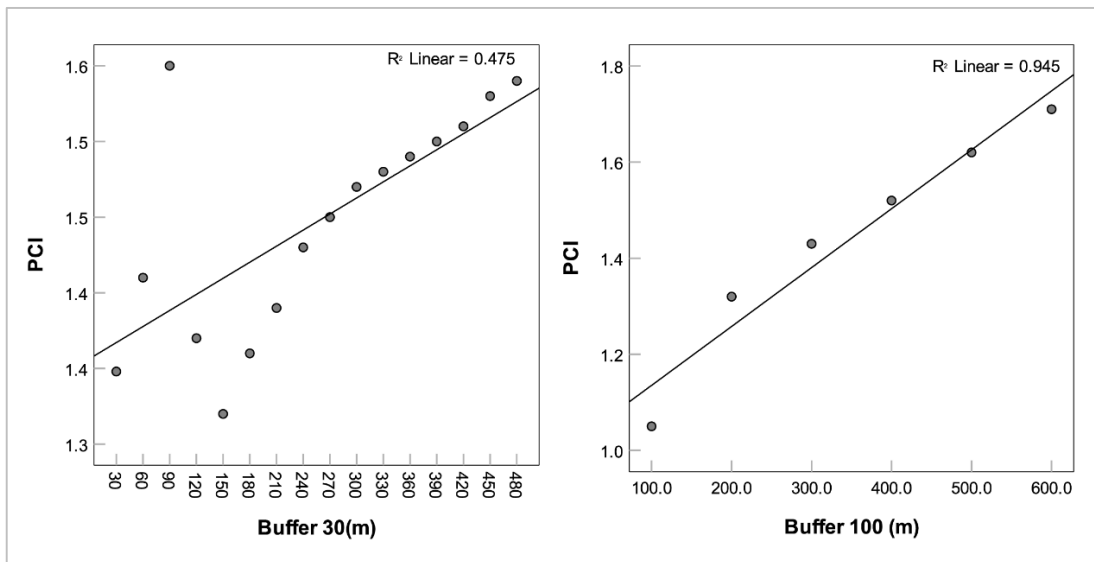


Figure 4.27: Regression analysis between average PCI and different buffer size based on the all the sample parks.

To explore the effects of different buffer sizes, I compared the **temperature variation** of the 30m and 100m buffer zone (**Figure 4.26**), 103 sample parks were employed to analyze the PCI changes with the distance. The results show that PCI appeared a sharp increase in 30m-90m by 0.15, which means that there was a significant difference between the buffer rings. Then, PCI experienced a sharp decrease from 90m to 150m, but from 150m to 480m, the park cooling effect became stronger, the reasons for those change may related to the **surroundings factors**, such as impervious surfaces, other green spaces, shaded areas and other land cover types that had effect on ground temperature. So this is the possible reason that with the distance increasing, the effect of the park on the nearby area were less obvious.

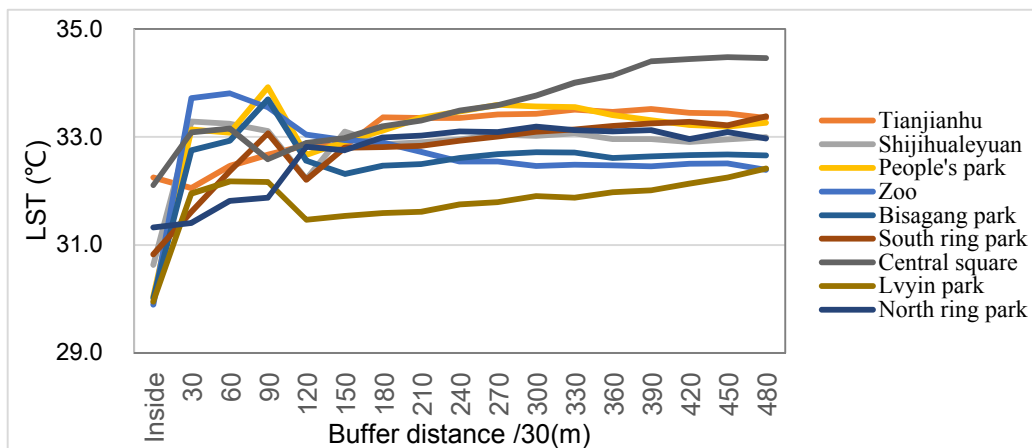


Figure 4.28: 9 Parks LST changes with buffer distance grows

For further analysis, I selected 9 parks as detailed study to analyze the average LST changes of different buffer zones, and the results were consistent with the overall **Figure 4.28**. The values in 30m buffers sharply increased, and the 60-120 meters range was complicated, while the LST of

the outer buffer rings from 150 m to 480m gradually rises to be stable (*Figure 4.28*). Taking a further analysis of the zoo as an example, from the Google satellite map, most of the surface type at the **edge of the park** is **roads**, buildings and other impervious surfaces (*Figure 4.26*). The surface coverage of the buffer zone in the range of 30m-90m is usually an **impervious surface** and is a typical area of the heat island in the city (Deng et al. 2012; Yuan, Bauer 2007).

However, the analysis in the buffer size of 100m showed broader results (*Figure 4.27*). As the distance increased, the strength of PCI increased as well. The analysis shows that linear regression model coefficient R^2 is 0.95, which is a significant positive correlation. So the results indicated that we need to investigate more possible factors related to PCI in a smaller buffer size, as it can reveal more details which might have an effect on PCI.

Overall, it can be clearly stated that the strength of PCI increases with the distance measured from the park boundary, based on the previous studies (Cao et al. 2010; Spronken-Smith, Oke 1998 p. 19), where the buffer size was regularly defined as 500m. But I recognized this definition need to be discussed based on my results. In case of my result, we need to investigate the **indicators** of the **surrounding environment** of the parks, and how those factors impact PCI, we can hypothesize those factors like building density, building shade, building height, land use and land cover, even the distance to other cool island, etc. which should be considered in the future.

4.2.5 Discussion and further research proposals

In this chapter, analyzing SUHI characteristics through 123 park samples in Zhengzhou is discussed. The correlation of LST and PCI has been argued through similar study results. The Park Cooling Intensity (PCI) was proved to be impacted by internal and external factors. Internal parameters (Area, Fractal dimension, Paratio, Shape index) were analyzed within the parks, and external parameters (NDVI and NDISI of surroundings) were analyzed in the neighborhood of the parks. The results were also summed to the zonal rings of the city. In this chapter, these results were discussed with similar results to other previous studies.

4.2.5.1 Impact factors of PCI

The results of section 4.2.1 show that park types can have a different impact on PCI. Among the five park types, the “**Theme park**” category has the highest PCI, which reaches 2.76°C. The reason is that the theme park has higher vegetation cover and higher water surface coverage than other types. For instance, Zhengzhou Botanical Garden, where the mean FVC, NDWI, NDISI is 0.40, 0.16, 0.19, respectively. More specifically, the vegetation coverage is higher than 50%, and the diversity of species is high as well, as its primary function is science education for citizens. The “**linear park**” category has the weakest PCI. This may be because the linear parks (*Figure 4.19c*, 4-linear park) are mostly riverside green spaces, or very close to the water surface (e.g.

Riverside Park). In case of linear parks in Zhengzhou, there is small LST difference between the park and its neighboring water surfaces³⁷. Therefore, the linear park type's average PCI of is the lowest.

For the results of PCI and its impact factors, I have similar conclusions. The FVC, NDWI, NDISI regression coefficient of determination (R^2) are 0.237, 0.433, 0.618, respectively. This means that the complex correlation between PCI and park characteristics cannot be represented only by those three factors. The park patch metrics (size, fractal dimension, perimeter-area ratio, and shape index) also could not determine alone the PCI variance. As we can recognize from section 4.2.3 PCI is also related to the types of the surrounding areas (*Figure 4.23, 24, 25*). High FVC and NDWI in surrounding areas make the buffer LST closer to the park internal LST, which results in low PCI. There is a positive effect between PCI and surrounding NDISI, related to the surrounding land cover types. As the result shown in *Figure 4.25*, the location factor and park type factor has also effect on PCI.

The cooling effect of the park can be explained from the perspective of **thermal balance** (Monteith, Unsworth 2013). We can use the heat transfer theory (Bowen ratio) as an analogy to explain some of the results of this survey. The **Bowen ratio** is the ratio of sensible heat flux to latent heat flux (Bowen 1926). The surrounding areas are heat sources because the heat capacity of these is significantly smaller than the heat capacity of the parks. In heat conduction, the thermal power (**sensible heat flux**) absorbed by the parks from the surroundings should be equal to the excess energy resistance by photosynthesis and transpiration (**latent heat flux**), thus the heat conduction reaches balance. A larger green space means more energy is dissipated which results in more conducted thermal energy. Therefore, parks with large sizes, high vegetation coverage, and high water surface rate have greater energy resistance, which reduces Bowen ratio, and finally, result in higher PCI.

Furthermore, the heat conduction can also explain why parks with high perimeter-area ratio (Paratio) and fractal dimension (Frac_Dim) have lower PCI. High Paratio and fractal dimension mean that the park boundary is in a large contact surface (complex edges) with the **surrounding heat sources**, which is conducive to heat conduction and heat exchange. This causes temperature difference decreases, resulting in lower PCI. At the same time, this can also explain the relationship between PCI and surrounding land cover. The ambient temperature also affects the heat transfer. As a whole, to increase the cooling effect of the park, it is recommended to consider the factors of the park itself, improve the resistance to the thermal environment, and increase latent heat³⁸, so as

³⁷ In Chinese cities, the linear park types are most located beside the river, however, the neighbouring areas are key factors in PCI (Park Cooling Intensity) calculations.

³⁸ Latent heat flux is the flux of energy from the Earth's surface to the atmosphere that is associated with evaporation or transpiration of water at the surface. In urban area, the vegetation play an important role in latent heat flux, and as a whole contribute

to reduce the heat island.

4.2.5.2 Impact factors of park LST

The results of section 4.2.2 reveal that high FVC, high NDWI will contribute to low park LST. Those findings are consistent with the results of the previous studies at the city level (Han-qiu 2005; Z. Jiang et al. 2006; Xu 2010). This is because the high rate of vegetation cover stores less solar energy and thus solar heat gain. The plants photosynthesis and transpiration absorbs the heat during those processes (US EPA 2014a). Those altogether lead to lowering the park LST. In remote sensing technology, NDWI mostly represents the water body and the vegetation surface. This result also coincides with the findings in another study (Xu 2006). A recommendation for planning purposes would be to increase the vegetation and water body ratio to decrease the park LST. As NDISI had been used successfully in previous studies (Sun et al. 2017; Xu 2010), we have used it to analyze the relationship of impervious surface to mean park LST. The results show that NDISI has a strong correlation with mean park LST. The reason is that the impervious surfaces have high thermal conductivity and low heat capacity, which lead to high LST. However, the impervious surface is an important part of park design, but we should optimize the surface rate during design. In terms of the results of park characteristics like the size, fractal dimension (Frac_Dim), perimeter-area ratio (Paratio), and shape index (Shape_idx) in patch level have an impact on park LST, and those independent factors reflect the park morphology. From the results, we can recognize that large size, low Perimeter-Area ratio, and low fractal dimension³⁹ decreases park LST.

Despite the practical findings in this survey, I have some limitations to some extent. First, the data of satellite images have its limitation to interpret the surface thermal environment; because the temperature also relates to the microclimate factors such as wind speed, wind direction and humidity. The results in this chapter can also be explained that park LST impact factors are the main reasons. Nevertheless, from the impact factors of park LST and PCI, the coefficient of determination (R^2) is not high. For instance, the FVC and NDWI regression value to mean park LST are 0.489 and 0.446, and it can only reveal that vegetation cover and water surface can explain only less 50% of the mean park LST variance. But the NDISI indicators have a significant relation to park LST, as its regression coefficient is 0.926, which means the impervious surface is the most crucial factor that brings higher LST in Zhengzhou. The analysis results of park patch metrics (size,

to mitigate the heat.

³⁹ Fractal dimension index is appealing because it reflects shape complexity across a range of spatial scales (patch sizes). A fractal dimension greater than 1 for a 2-dimensional patch indicates a departure from Euclidean geometry (i.e., an increase in shape complexity). Fractal dimension approaches 1 for shapes with very simple perimeters such as squares, and approaches 2 for shapes with highly convoluted, plane-filling perimeters.(FRAGSTATS Metrics)

fractal dimension, perimeter-area ratio, and shape index) and their relationship to park LST is even more complicated. Moreover, previous studies showed that even the meteorological factors (wind speed, wind direction, humidity) could influence the PCI value when we use air temperature to evaluate park cooling effect (Antoniadis et al. 2018; Lindén et al. 2016; Yafei Wang et al. 2015). In terms of future study on the park cooling effect, we should put those aspects into consideration.

4.2.5.3 Implications for urban planning and landscape design

According to the results I listed the possible proposal to urban planning and landscape design in the future. The planner and designer can follow the recommendation:

1) Increase the number of theme park types, increase the urban park size.

2) In landscape design and renewal: plan more vegetation and water area in parks, as well as reduce the impervious surface. At the same time, in case we follow PCI aspect of decreasing SUHI we could make the park shape less complex in site design with less curving boundaries and less waving edges (based on Frac_Dim), we can consider the options of lowering the perimeter area ratio of the park by designing compact layout (*Figure 4.29*). However this needs to be discussed from many other aspects (visual and ecological effects).

3) Add more parks (green spaces) in the area within high impervious surface ratio, in central city area, represented by tall buildings and impervious surfaces of commercial and built-up areas.

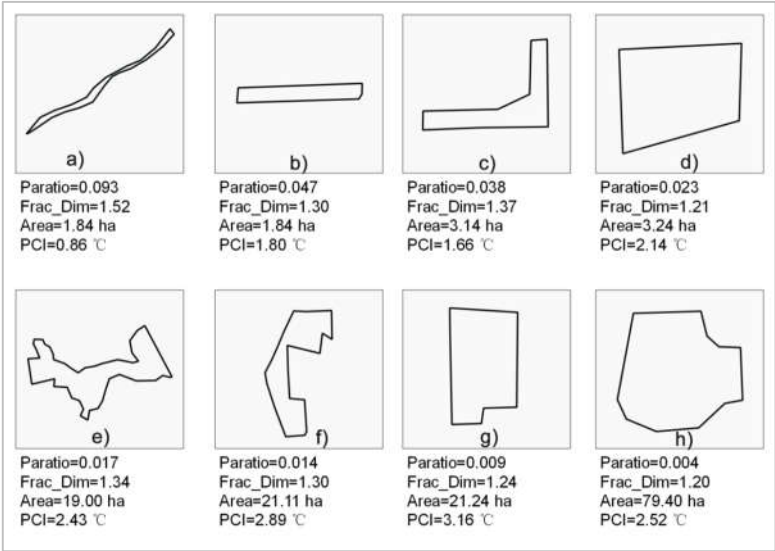


Figure 4.29: Comparison of PCI with different fractal dimensions (Frac_Dim) and perimeter area ratios (Paratio). Typical park shapes with higher Frac_Dim and Paratio values (a, b, e, f,) and typical shapes with lower Frac_Dim and Paratio values (c, d, g, h)

4.2.6 Summary of park cooling effect survey

This study used a comprehensive method to investigate the urban heat island phenomenon of Zhengzhou city in China. Using the radiative transfer equation (RTE) method to retrieve the LST, I analyzed the relation of particular factors to park LST and park cooling effect. The results of this chapter give a reference to characterize the complex correlation between SUHI and other factors in the expanding capital city of Henan province in China. The practical results can imply urban planners and stakeholders by providing scientific guidance for future urbanization and urban management. First, the results showed that parks have a cooling effect in the city, the mean LST of the park is 0.79°C lower than in the city. Different park types have different cooling intensity. The theme park category in Zhengzhou has the highest cooling intensity with the PCI reaching 2.76°C . The cooling intensity of the street park and linear parks is lower; with the PCI only reaching 0.8°C and 0.64°C . From the results of the park cooling effect analysis and its internal characteristics, we can recognize that the park LST depends mainly on the vegetation cover, water body and impervious surfaces in the park. Vegetation and water surface are the main factors of the park's cooling effect in Zhengzhou, but the impervious surface increases park LST. The study also shows a different linear correlation between the park LST and park patch metrics of Zhengzhou city. Park size and fractal dimension, perimeter area ratio affect park LST, while other geometric indicators such as shape index have no significant relation to the LST. Thus I recommend for planners to maximize park size and minimize perimeter area ratio to reduce the SUHI effect.

The PCI is influenced by the park itself and its surrounding area:

- 1) The characteristics of the park defined by its size, perimeter area ratio and fractal dimensions all affect the PCI directly. Because of these defining factors, there seems to be a positive correlation with FVC and NDWI, while NDISI has a negative impact on the PCI.
- 2) The PCI is influenced by the surrounding land cover types coupled with the type of vegetation cover and water coverage. Because of these surrounding influences, the PCI has a directly proportional relationship to the surrounding impervious surface cover. A park's PCI has many factors to consider its mitigating effects on the SUHI. By first considering the factors that influence a park's temperature, we can modify the park factors (park size, shape index, location, etc.) which help to mitigate the SUHI effects seen throughout cities.

I recommend additional planning consideration and construction of more parks in built-up urban areas especially around tall buildings and within large areas of impervious surfaces. Park types, such as theme parks and larger urban parks, should be considered with higher priority than above other park types.

4.3. Analysis of cooling and humidification effects of different coverage types in Small Green Spaces (SGS)

In this survey, I answer Research **Question3: What are the cooling and humidification characteristics of small-scale green spaces in the summer time? What kind of vegetation structure should be designed to mitigate urban heat effects by regulating small green spaces design parameters?**

To explore and investigate the questions, this chapter carried out measurement of **weather parameters** (temperature, relative humidity, wind direction, wind speed, photosynthetic radiation) of **16 sites in four types of coverage** (1-Impervious surface; 2-Shrub-grass; 3-Tree-grass; 4-Tree-shrub-grass) (**Figure 3.8** in section 3.2.3.1) in a university campus. At the same time, the coverage characteristic parameters, such as Canopy Density (CD), Leaf Area Index (LAI), Photosynthetically Active Radiation (PAR), Mean Leaf Angle (MLA), of each plot were analyzed and compared.

The results showed that there were obvious differences in temperature among different coverage types in SGS. The biggest difference was concentrated in the noon period when the solar radiation is the strongest during the day. The difference between the four types at night was small. The maximum air temperature difference among the four types could reach 8.9 °C and the maximum relative humidity difference was 28.5 %. The change trend of the four coverage types in four gardens basically showed the same trend within a day. The cooling effect of the multi-layer vegetation-covered (Tree-shrub-grass) area was the largest compared to impervious surface, indicating that tree cover was the core factor affecting the temperature. Temperature and relative humidity had a close correlation with surface coverage types and the vegetation coverage characteristics (such as CD and LAI). CD and LAI had a positive effect on cooling and increased relative humidity. The cooling and humidifying effects of plants were also related to PAR and leaf angle. Based on the results I assume that increasing the LAI and CD but reducing the leaf angle can improve the cooling effect of SGS. The results of this paper can provide suggestions for green space management and future landscape design to enhance the ecological benefits of urban green spaces.

4.3.1 Statistical results of atmospheric conditions in the study plot

As can be seen from **Table 4.6**, the highest temperature appears in the afternoon of 8th August 2019 (13:15 pm), with a temperature of 40.2 °C (point A1, impervious surface). The low-temperature zone appears at midnight (23:50 pm), before dawn (04:15 am, 05:35 am), the minimum temperature reaches 24.2 °C. Compared with the historical data of the same period, the value of the maximum temperature was higher than the highest value of extremely high

temperatures in history. This shows that the area I studied was hotter in 2019 than the history records of August in Zhengzhou shows. During the measurement period the mean PET value were all above the threshold 41 °C (*Appendix 21*), and thermal Perception was “very hot”, indicating that the weather was not comfortable for human activities. People could feel extreme heat stress (Sharmin et al. 2019).

Table. 4.6 Meteorological data statistics from the study period

Date	AT (°C)			RH (%)			WS (m/s)			PET(°C)
	Max	Min	Mean	Max	Min	Mean	Max	Min	Mean	Mean
7/8/2019	39.9 (15:30)	25.8 (23:50)	32.1	89.5	36.7	61.8	0.42	0.9	0.05	43.9
8/8/2019	40.2 (13:25)	24.2 (04:15)	30.7	97.7	39.5	70.2	0.17	0	0.02	45.7
9/8/2019	38.8 (10:20)	25.9 (05:35)	30.4	91.4	44.7	75.4	1.1	0	0.11	42.3

The median wind speed measured on the campus weather station for the 3 days was less than 0.1 m/s (*Table 4.7*), while the wind direction changed frequently. The wind direction was concentrated between WSW and S for the first day (07/08/2019), was quite various during the second day (08/08/2019), and was SW on the third day (09/08/2019) (*Figure 4.30*). However, considering the low wind speed (the average was less than 0.1m/s), the impact of wind on air temperature and humidity was negligible.

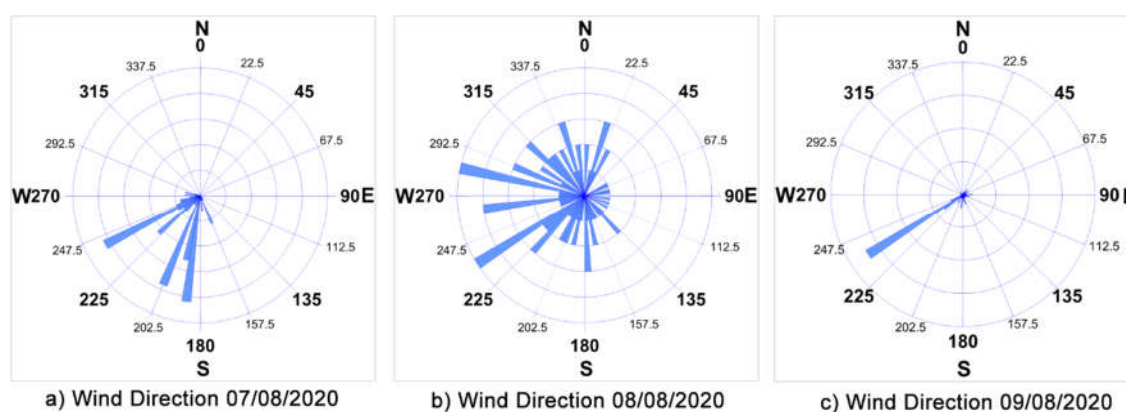


Figure 4.30: The wind direction of each days in August 7-9, 2019

4.3.2 Changes in temperature and humidity of different vegetation coverage types

From the data (*Figure 3.9*: Garden-A, B, C and D; Cover type 1, 2, 3 and 4), the following results can be obtained:

- a) The temperature shows as $AT1 > AT2 > AT3 > AT4$ ⁴⁰, but the humidity was opposite $RH4 >$

⁴⁰ AT1, AT2, AT3, AT4 is the air temperature of four coverage types: 1-Impervious surface; 2-Shrub-grass; 3-Tree-grass; 4-Tree-shrub-grass.

RH3 > RH2 > RH1⁴¹, indicating that **more vegetation coverage** makes the **temperature lower** and makes the surrounding **more humid**.

- b) The difference among the four coverage types in temperature and humidity was experienced. Additionally, the difference between day and night was also detectable. The difference (6:00 am - 18:00 pm), in the morning (around 6:00 am) and evening (18:00 pm) was smaller than that of around noon. The four types differ significantly in temperature and humidity values. At night (18:00 pm - 6:00 am), the temperature and humidity values of four types were relatively close. It is worth noting that the humidity of the impervious surface was greater at night than daytime. Sometimes it was higher than the humidity of the other three vegetation coverage types, but with relatively close temperature values.
- c) The four coverage types (1, 2, 3 and 4) basically showed the same temporal change trends ('W' & 'M' shape) in air temperature (AT) and relative humidity (RH) (*Figure 4.31*). The type 1 (impervious surface) has the highest temperature and the lowest relative humidity, while the type 4 (tree-shrub-grass) multilayer vegetation structure has the lowest temperature. The biggest temperature difference can reach 8.9 °C (between 1-impervious and 4-tree-shrub-grass cover types). The maximum relative humidity difference is 28.5% (Garden B: B1 and B4). Even the lowest temperature difference reached 5.2 °C (Garden C, C1 and C4, 08/08/2019, 11:34 am), and the humidity difference was 14.4% (Garden C: C1 and C4, 08/08/2019, 11:25 am). At noon, the temperature of type 2 (shrub-grass) and type 1 (imperious surface) was significantly higher than the type 3 (tree-grass) and type 4 (tree-shrub-grass), indicating that the tree cover was the core factor affecting temperature. The comparison of humidity showed that the humidity of type 3 and type 4 was obviously higher (%) than that of type 1 and type 2, indicating that tree cover can increase the humidity of the environment.

⁴¹ RH1, RH2, RH3, RH4 is the relative humidity of four coverage types: 1-Impervious surface; 2-Shrub-grass; 3-Tree-grass; 4-Tree-shrub-grass.

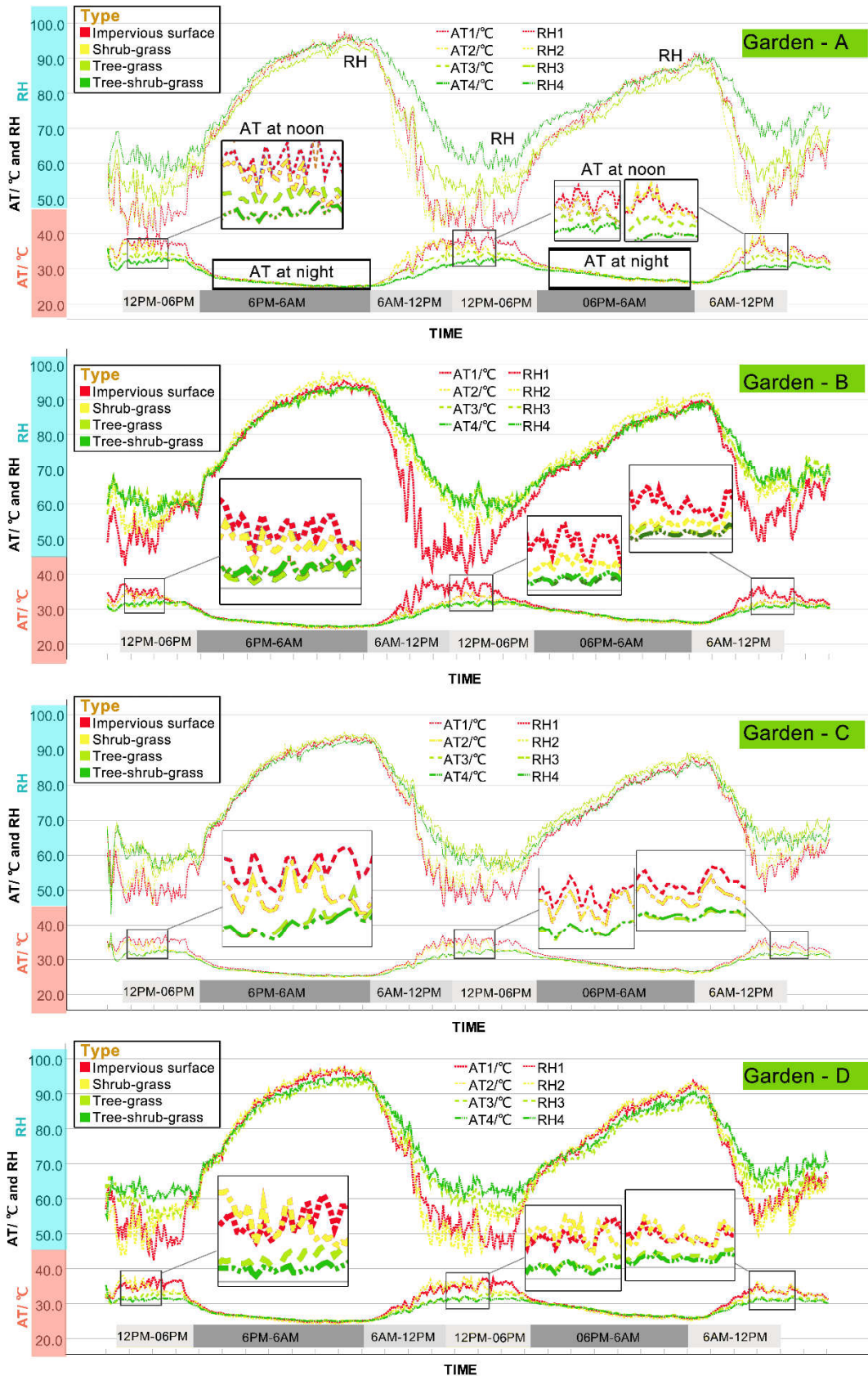


Figure 4.31: Air temperature (AT) and relative humidity (RH) changes of 16 points in four gardens (A; B; C; D) during the measurement period (7-9, August 2019).

4.3.3 Comparison of influencing factors on green space cooling and humidification

The vertical solar radiation period (the angle between the light and the surface is close to 90 degrees) was around noon (11:30 am-12:30 pm). Vegetation coverage, shadows and photosynthesis have the strongest influence on the surface. The average temperature of this time period as the temperature values of 16 observation points, and it can be sentenced that the analyzed **four factors** (photosynthetically active radiation (PAR), canopy density (CD), mean leaf angle (MLA), leaf area index (LAI)) **have effect on** air temperature and relative humidity.

Table 4.7 Pearson correlation coefficients of the characteristics of surface type on AT and RH

		PAR	CD	MLA	LAI
AT	Pearson Correlation	0.820**	-0.921**	0.813**	-0.763**
	Sig. (2-tailed)	0.000	0.000	0.000	0.001
RH	Pearson Correlation	-0.825**	0.905**	-0.796**	0.733**
	Sig. (2-tailed)	0.000	0.000	0.000	0.001

Correlation is significant at the 0.01 level (2-tailed).

First, **Pearson correlation** was used to analyze the influencing factors. The results showed that the correlation between air temperature (AT) and relative humidity (RH) and plant community characteristics is **very high** (both are greater than 0.7, $p < 0.001$). The highest correlation between AT and CD reached 0.921 (negative correlation) (**Table 4.7**). In short, there was a **close correlation between temperature, relative humidity, surface cover types and vegetation structural characteristics**. Therefore, it is necessary to make further study on the regression relationship between the characteristics of vegetation structure and the effect of cooling and humidification.

The results of linear regression analysis revealed that CD ($R^2_{AT}=0.848$, $R^2_{RH}=0.819$, **Figure 4.32a**) and LAI ($R^2_{AT}=0.538$, $R^2_{RH}=0.581$, **Figure 4.32b**) had a positive effect on cooling air temperature and increasing relative humidity, while average PAR and MLA had a negative effect on cooling AT and increasing RH (**Figure 4.32c; 4.32d**). The relative contribution order of surface coverage features to cooling AT and increasing relative humidity was bigger in case of CD than in case of LAI. In addition, it was discovered that other factors such as solar radiation and wind speed also affect cooling and humidification effects (B.-S. Lin, Lin 2010; Shashua-Bar et al. 2009). The regression results show that solar radiation has a positive significant effect on temperature increase and relative humidity decrease (**Table 4.7; Figure 4.32c**). However, due to the small range of changes in wind speed during the observation period (**Table 4.6**), its impact on temperature and relative humidity is small, thus, no separate wind related analysis was performed.

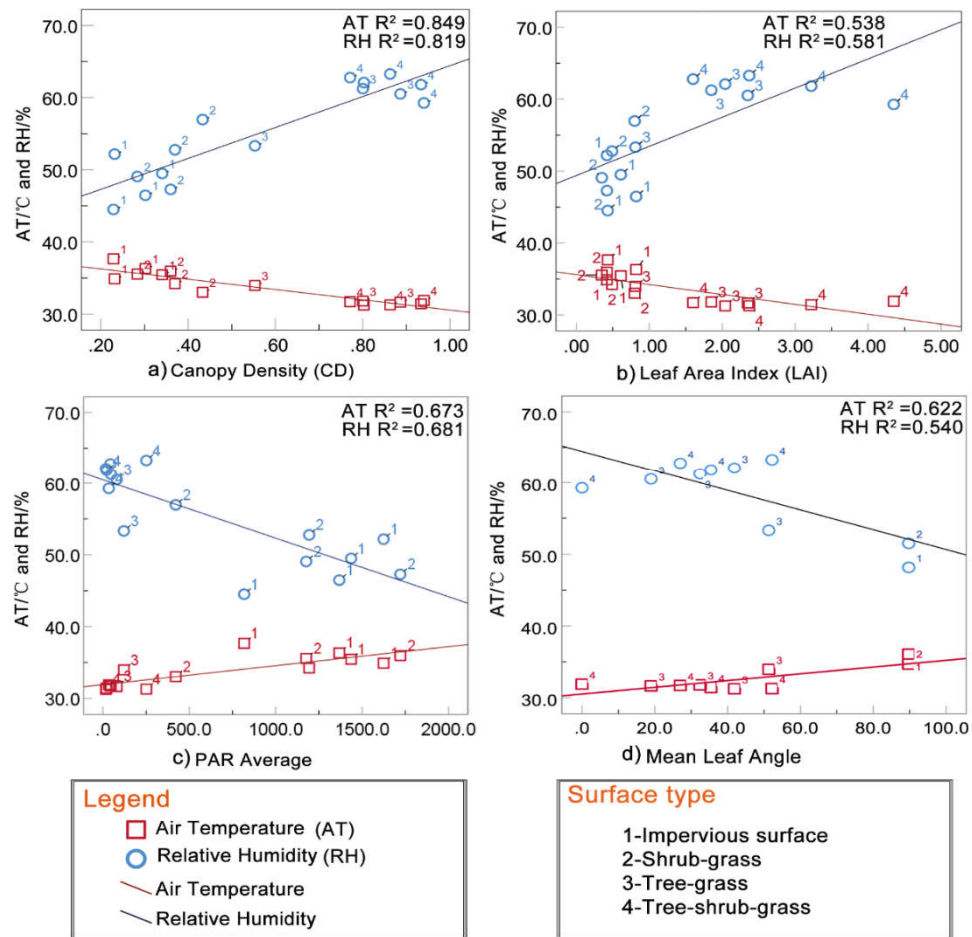


Figure 4.32: Linear regression analysis between canopy density (CD), leaf area index (LAI), photosynthetically active radiation (PAR), mean leaf angle (MLA) and air temperature (AT) and relative humidity (RH).

4.3.4 Discussion and further research proposals

In the following, the discussion based on results will be divided into three parts: 1) Influence of coverage types on thermal microclimate; 2) Influence of vegetation structure on microclimate; 3) Implications for Urban Planning and Landscape Design

4.3.4.1 Influence of coverage types on thermal microclimate

Previous studies on urban heat island on a large scale indicated that the heat islands intensity during the day changed differently from the heat islands at night, and the atmospheric UHI intensity at night was greater (Oke 1982; US EPA 2014a). However, on a small scale like in this study, **the temperature difference** between the vegetation space and the non-vegetation space was small at night, while the air temperature and relative humidity difference during the day were large. Thus, we can realize that small green spaces (SGSs) have faster heat conduction with surrounding than that of between urban and rural regions. The cooling effect of green space can be explained

essentially from the perspective of **heat balance** (Monteith, Unsworth 2013). **First of all**, the heat source comes from solar radiation. Infrared rays in sunlight can warm up the irradiated material, and the temperature of the material is mainly determined by the heat capacity of the material itself. Compared with the impervious surface, the **leaves of plants have higher heat capacity**. Therefore, under the same amount of radiation and time, the temperature of the area covered by the plant rises more slowly. The reason for the higher heat capacity of plants is photosynthesis. In this process, the **evaporation** of water from the earth will **evaporate the heat and reduce the temperature**. **Secondly**, in heat conduction, the heat energy (sensible heat flux) absorbed by the green space from the surrounding environment should be equal to the excess energy resistance (latent heat flux) generated by photosynthesis and transpiration, to balance the heat conduction. More green space means more energy dissipation, which leads to more heat energy conduction. Therefore, the types with **high vegetation cover density** and **larger plant leaf area density** have **higher energy resistance**, thereby reducing the Bowen ratio, and the cooling effect is also the most obvious.

The impervious surface is the **core area of the urban heat island**. In consistence with the large-scale research (Azhdari et al. 2018; Doick et al. 2014; Y. Li et al. 2012), among the different types of urban land use, the SUHI is mainly concentrated in the urban impervious areas, such as industrial areas, urban squares, roads, building roofs, and other gray infrastructure.

The **urban cold islands** (UCI) are mainly concentrated in urban green space such as urban forests, parks and water areas. The city is combined of impervious surface and vegetated surface similar to SGS. To some extent, the different coverage types of SGS reflect the different spatial distribution of the city and the elements of UHI phenomena are similar.

4.3.4.2 Influence of vegetation structure on microclimate

Concerning the characteristics of plant communities, this study showed that **with tree cover types (3-tree-grass, 4-tree-shrub-grass)** are the key factors affecting the **urban canopy heat island effect** and comfort. The same results are shown in previous studies (Jamei et al. 2016; Taleghani et al. 2015; Yan et al. 2018). The **cooling effect** is related to tree **shade**, building shading, and other shadows, which could reduce radiation and lower temperature (Andreou 2014; J. Chen et al. 2020; Erell et al. 2014; B.-S. Lin, Lin 2010). But compared with building shadows, **plants** not only provide shade, but also **increase humidity** (Armson et al. 2012; B.-S. Lin, Lin 2010). At the same time, photosynthesis can also produce oxygen, absorb harmful substances in the air and purify the environment. Other studies had also drawn relevant conclusions, in Zhengzhou city (China), large parks have a significant cooling effect, and the cooling effect is positively related to the vegetation coverage inside of the park (Li et al. 2019; Li, et al. 2020). In the urban parks of Taipei, the average PCI during the daytime in summer is only 0.81 °C but no consistent cooling effect was found in small parks (less than 3 hectares). The low cooling effect of these green spaces is probably related to high humidity levels and consequently, **low evapotranspiration** (Cao et al.

2010). In the study of parks in Lisbon (Portugal), the maximum cooling temperature of the city park reached 6.9 °C, and the cooling temperature was related to the shadow of the building and the surrounding shape (Oliveira et al. 2011). In an Algerian microclimate study, the vegetation can produce an average cooling effect of 2 to 3 °C. The calculation showed that the maximum cooling range at night can reach 10 °C (bencheikh, Rchid 2012). In Nagoya (Japan), it was found that the temperature difference between the studied green area and its surrounding was small, but this cooling effect was found to last for hundreds of meters or more (Hamada, Ohta 2010). In view of the above results, it is necessary to **conduct localization studies** for each urban environment in order to adapt and to maximize the benefits of green spaces based on the characteristics of each city.

In previous studies, the entire **vegetation coverage types** were different at different times and in different seasons, but they all had **significant cooling and humidifying effects throughout the year** (four seasons) (Hamada, Ohta 2010; Mathew et al. 2017). In case of human comfort, vegetation has the greatest cooling and humidification effect **in summer**. This further supports the conclusion that the higher the temperature, the stronger the cooling effect of vegetation (Shi et al. 2020). In this study, the maximum temperature difference between multi-layer vegetation communities and the impervious surface ranges from 5.2°C to 8.9°C, and the maximum relative humidity difference ranges from 14.4% to 28.5%.

I found that **multi-layer plant communities were most effective** in cooling and humidifying effects, but the plant community was diverse in structure and rich in variety. In addition, the leaf area of the multi-layer plant communities was larger than other coverage types. Vegetation communities (with tree coverage) can reflect more direct solar radiation than other vegetation communities (no-tree cover) (Yupeng Wang, Akbari 2016).

This study also proved that the cooling and humidifying effects of **shrubs and grass plant communities** were significantly lower than those of canopy-covered tree communities. This study identified four factors that affect temperature and relative humidity. The regression results on the factors that affect the cooling and humidifying effect showed that the four factors of CD, LAI, MLA and PAR had a significant effect on the cooling and relative humidity increase. Canopy Density (CD) was the most effective for cooling and humidification. In addition, under the same type of multi-layer plant community structure, the angle of the leaves also influences the cooling effect. Specifically, the **smaller the angle between the plant leaf and the horizontal plane, the more obvious the effect of cooling and humidification is**. These findings can provide a basis and reference for landscape architects. However, other elements (such as tree shape, evapotranspiration, plant age, etc.) need further study to understand the quantitative relationship of plant communities.

4.3.4.3 Implications for Urban Planning and Landscape Design

Under the urban homogenization hypothesis (Groffman et al. 2014; Lososová et al. 2012; Qian et al. 2016), urban design is becoming more and more homogenous. The ecological functions of plant communities are similar. They all have obvious cooling and humidifying effects on the urban microclimate. **The microclimate and heat island regulation function of SGS**; and their role in urban comfort cannot be ignored. SGS are more conducive to renovation and renewal than large green spaces to some extent. The results of this study may help future urban design and urban renewal. In summary, this study makes the following recommendations:

- It is recommended that urban planners increase the number and proportion of green spaces in the city and increase the tree canopy coverage in the overall urban planning process.
- In city planning, plant species design should be based on the local climatic conditions, increasing the multi-layered community structure of the plant, considering the characteristics of the leaf area index and the blade angle of plant.
- In a small-scale green space landscape design, conifers should be combined with broad-leaved trees, and the tree-shrub-grass compound should be designed to maximize the cooling and humidification effects of the microclimate.

4.3.5 Summary of cooling and humidification effects of different vegetation coverage types

In this study, the field observation and measurement method was used to study cooling and humidification effects of different vegetation coverage types in small green space (SGS). By selecting four green spaces in the university campus as sample plots, using meteorological data to analyze spatial and temporal characteristics of the SGSs, I compared the effects of four coverage types (1-impervious surface; 2-shrub-grass; 3-tree-grass; 4-tree-shrub-grass) on microclimate. At last, I analyzed the four impact factors (PAR, CD, MLA, LAI) of the SGSs among all 16 plots. The research results in this paper provide a scientific basis for characterizing the microclimate changes of green space. The conclusions of this are as follows:

- There are obvious differences in temperature between the four types in SGSs. The largest difference is concentrated in the noon period when solar radiation was strongest during the day, but the difference between the types at night is small. Specifically, the difference in temperature and humidity between the four types during the day was large, and the temperature is expressed as $AT1^{42} > AT2 > AT3 > AT4$. At noon, the difference reached the maximum, and the humidity order was the opposite $RH4 > RH3 > RH2 > RH1$. The four types at night show that the temperature and humidity values are relatively close.

⁴² Air Temperature 1 = is air temperature of type 1 (impervious surface), AT4 is air temperature of type 4 (tree-shrub-grass).

- The four coverage types of four gardens basically showed the same trend. Type 1 (impervious surface) has the highest temperature and the lowest relative humidity, while the type 4 (tree-shrub-grass) multi-layer vegetation structure has the lowest temperature and the highest humidity. This type has the highest temperature difference as well, that can reach 8.9 °C (Garden B, B1, and B4, 09/08/2019, 10:45 am.). The maximum relative humidity difference is 28.5% (Garden B, B1, and B4). Those results show that tree cover types are cooler and more humid than no tree-cover types, which reveals that tree cover is the core factor affecting the temperature.
- There is a close correlation between surface coverage types and plant community characteristics. Canopy density (CD) and leaf area index (LAI) have a positive effect on cooling and relative humidity, while photosynthetically active radiation (PAR) and mean leaf angle (MLA) have a negative effect on cooling and relative humidity.

The results can provide recommendations for green space management and future landscape design, which can alleviate urban heat island effects, enhance and improve the ecological benefits of urban green spaces.

4.4. Characterize the vertical and green spaces factors on SUHI

In this survey, I answered Research **Question 4: What is the relation between the vertical factors such as elevation, slope aspect, building height, building orientation, vegetation height and LST? How do these vertical parameters influence SUHI effect and what could do to mitigate UHI in design?**

To explore and investigate the questions, Budapest was taken as the study area (as Budapest owns a significant terrain in the urban area). On this basis, this survey was carried out by applying remote sensing data (**section 3.2.2.2; Table 3.2, Table 3.3**), field survey, and measurement (thermal camera). More specifically, the vertical data was extracted from the DEM and DSM using GIS analysis, besides the buildings' height from the particular products made by Copernicus institution and Lechner Institution. Tree height data extracted from the DSM map and tree layer was based on vegetation layer (Street tree layer; Forest type layer, Dominant Leaf Type, Small Woody Feature, Grassland in **Table 3.3**). Those data could achieve the analysis of the vertical factors on SUHI impacts. It included two main parts in terms of the research questions. Firstly, this survey analyzed the relationship between **vertical parameters** such as tree height, building height, elevation, slope aspect, and LST. Secondly, this survey analyzed the green space factors such as tree cover density, vegetation types (grass, small woody, tree leaf types), and their correlation to LST.

4.4.1 Elevation and slope aspect influence on LST.

Based on the SRTM⁴³ digital elevation data, I analyzed how the elevation and aspect influence the land surface temperature (**Figure 4.33a**). By comparing the average surface temperature (**Appendix 35**) of the two elevation classes (higher than 300 m asl⁴⁴ and lower than 120 m asl), it could be seen that the higher the altitude, the lower the surface temperature is. It could be concluded in the topographical division of Budapest that the surface temperature in the lowland was higher. The difference between the two elevation classes was 2.06 °C on average (**Figure 4.33b**) in winter, and this value reached 7.0°C on average in Summer (**Figure 4.33c**). The single image analysis showed that the lowest temperatures could be detected in the hills (below -4°C) while the highest was in the lowlands (sometimes above 10 °C). Those lowlands areas are mostly dense built-up areas, while the hill areas have mostly vegetation, this results not only indicated the “elevation” factors, but in fact revealed that low elevation, densely built-up areas are

⁴³ The Shuttle Radar Topography Mission (SRTM) was flown aboard the space shuttle Endeavour February 11-22, 2000. The National Aeronautics and Space Administration (NASA) and the National Geospatial-Intelligence Agency (NGA) participated in an international project to acquire radar data which were used to create the first near-global set of land elevations.

⁴⁴ Land surface elevation in metres above sea level (asl).

the urban heat islands in Budapest.

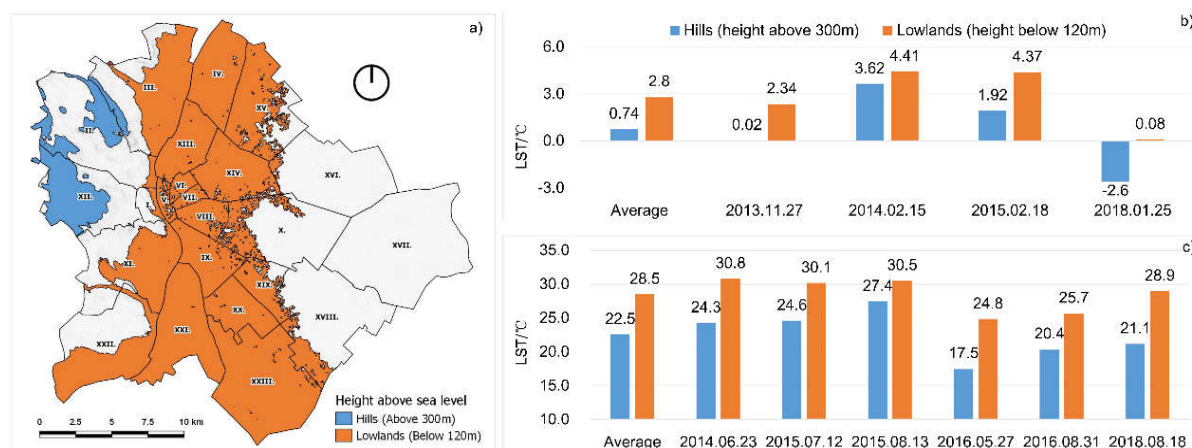


Figure 4.33: Comparison histogram mean land surface temperature (LST) of hills and lowlands comparison in Budapest: a) location; b) in winter; c) in summer.

In this part, I used the **average LST map**⁴⁵ (*Appendix 36*) to represent the Budapest surface temperature in order to improve the accuracy of the LST results. LST maps influenced by changes by seasonal harvest (e.g. agricultural land), changes in green infrastructure/elements over time (e.g. leaf changes in plants) in Budapest city area. The surface temperature is directly related to the sunlight, the absorption, and the heat storage capacity of the surface. Therefore, the slope orientation (exposure) will inevitably affect the distribution of surface temperature. Comparing the aspect data extracted from the SRTM digital elevation model can be seen in *Figure 4.34*. The temperature in the southern slope surface was higher than the northern slope both in summer and winter. From the mean value in *Figure 4.34 a and b*, winter (on average 2.74 °C) was more significant than **summer** (on average 0.87 °C), more specifically, southern slope surface is every case higher than any slope on the north side in winter. The high-resolution field survey with the thermal camera (section 3.2.2.2) made the phenomenon even more obvious as the extreme temperatures of different slope aspects and building orientations show this in more detail (*Figure 4.35 and 4.36*). Concluding the results of satellite image analysis and thermal image analysis, it could be stated that during the winter season, a special kind of heat island could have been determined (in Budapest study area) due to low sun angle. The vertical factor of slope aspect on SUHI can result in a special kind of heat island the "**vertical heat island**". The vertical elements are illuminated by the sun mostly from the side, so the heat island shows up on slopes, walls, facades significantly, which means that it may be detected and measured better from the field than from the air. Therefore it is also recommended to have field surveys with thermal camera

⁴⁵ Here I used several years' LST maps to calculate an average LST map to represent Budapest's temperature.

applications.

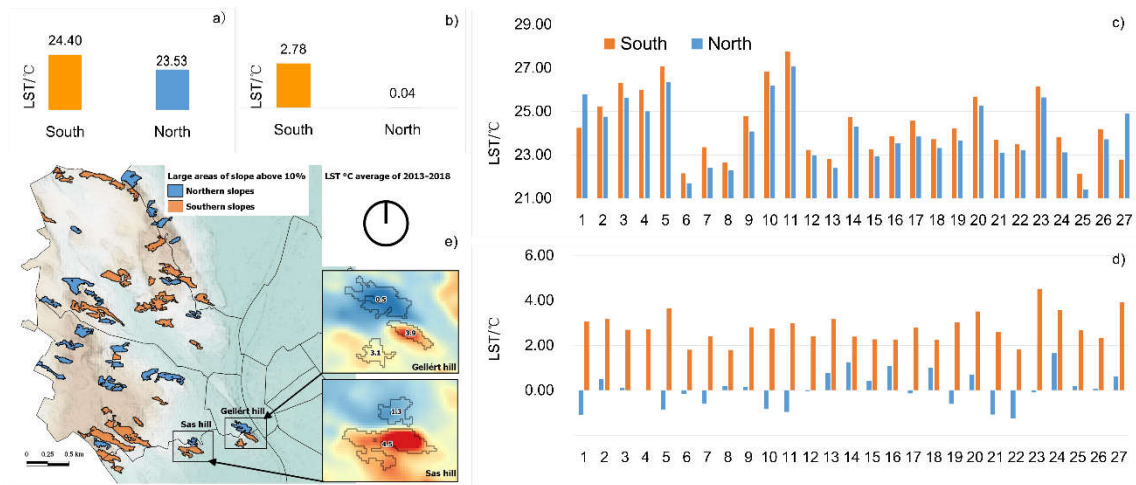


Figure 4.34: Comparison Land surface temperature (LST) between northern and southern slopes in summer and winter in Budapest: a) mean LST in summer; b) mean LST in winter; c) all plots in summer; d) all plots in winter; e) selected plots.

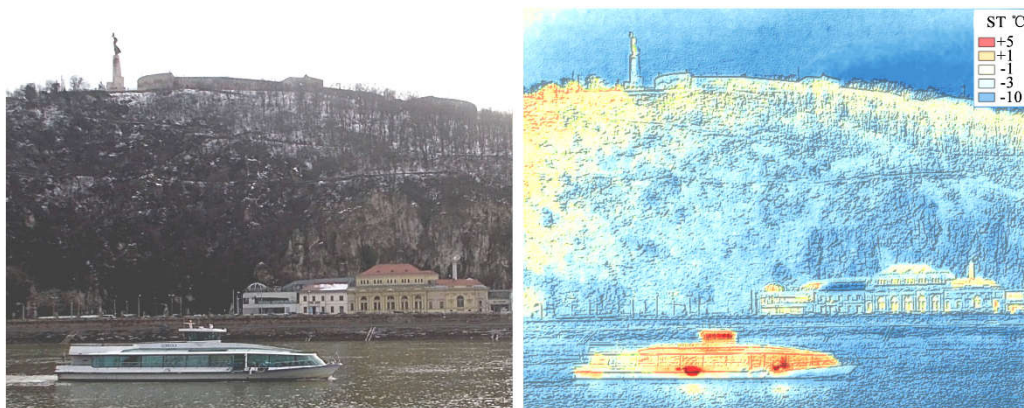


Figure 4.35: The northern slopes of Gellért hill were, in some cases, 10 °C colder than the southern slopes on high-resolution thermal camera image (taken at 14:20 on 13. 01. 2019).

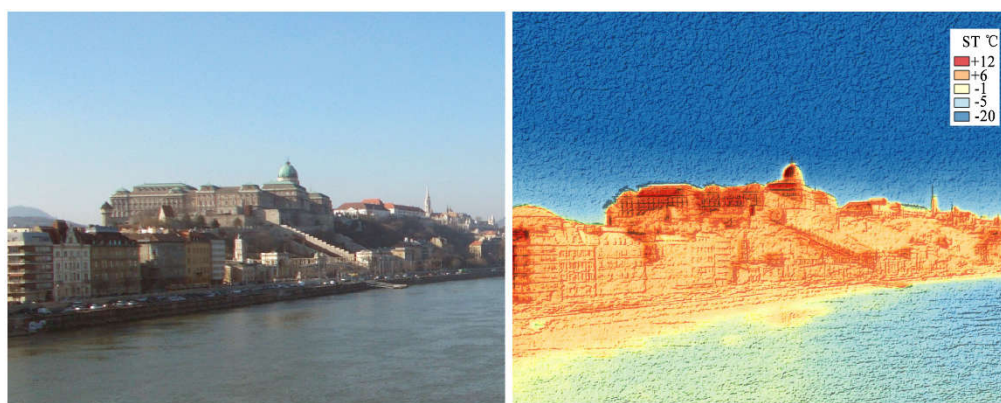


Figure 4.36: Surface temperature (ST) of southeast slopes in Buda Castle hill. The castle walls facing south have significantly higher values than the walls facing east (taken at 14:09 on 07. 02. 2019.).

The Buda Castle complex showed that the groups of buildings facing different directions could result in a temperature difference of 10 °C due to the actual horizontal sun angle.

4.4.2 Vegetation height and building height effect on LST

Based on the method presented in section 3.3.4, the building height data (**Figure 4.37, Appendix 37**) and vegetation height data (**Figure 4.38**) were generated from the products provided by Copernicus and Lechner Institution. The LST map was generated in the summertime of 2015 (**Figure 4.37**), which can maximally illustrate the difference in surface temperature. **Figure 4.37** shows that with the building height increasing, the land surface temperature of the building becomes higher, building height has an impact on surface temperature. For instance, when the building height from 0 to 5 meters to 20 to 30 meters, the median values of LST increased from 30.29 °C to 32.22 °C. However, with the increase of building height from 20 to 25 meters to 30 to 35 meters, the median values of LST appeared a decrease from 32.22°C to 31.14°C (**Appendix 38**), but the LST generally higher than the lower buildings. Subsequently, the figure shows an increase when buildings are getting taller.

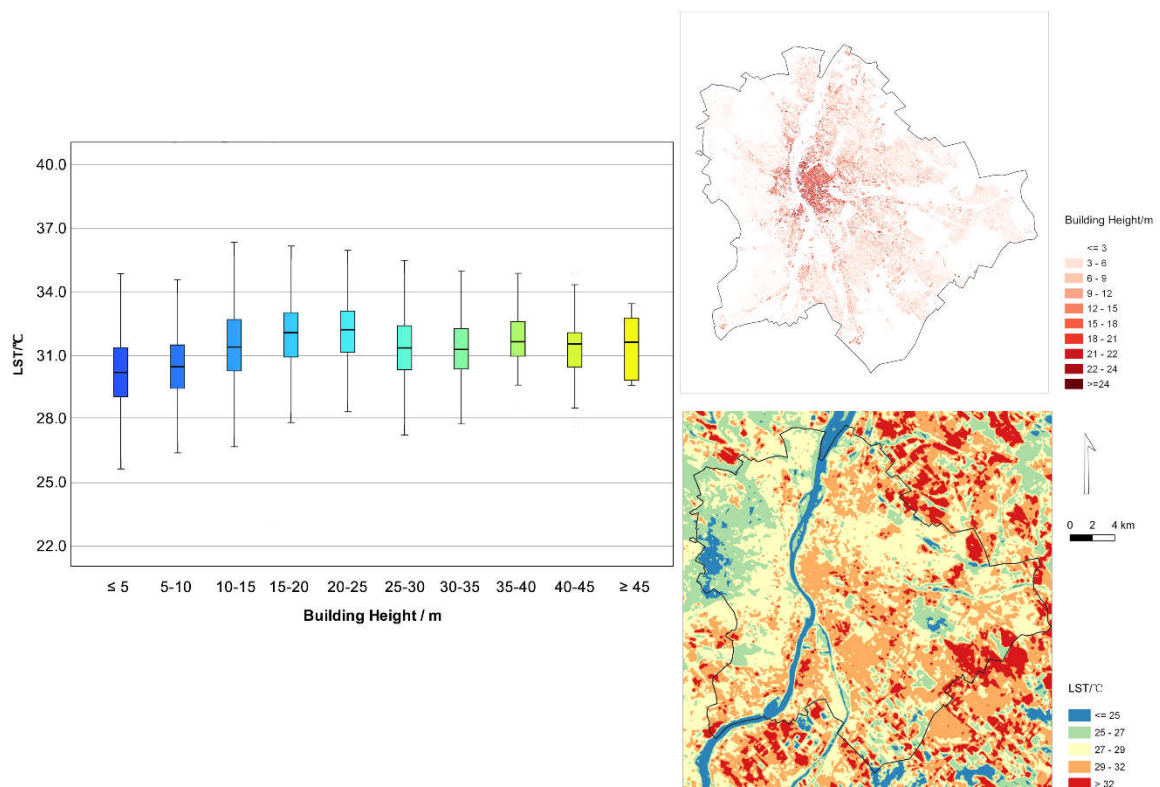


Figure 4.37: Box plots showing the relationships of building height category (m) with LST (range, minimum, maximum, median value in °C) in Budapest.

Compare with the building height factor, the vegetation height had a more significant correlation with LST. In general, the higher vegetation is cooler than the lower vegetation. More specifically, we can see the median values of LST decreased 3.77°C when the vegetation height increased from 0 to 2.5 meters to above 22.5 meters (**Figure 4.38, Appendix 39**). However, there was a slight difference in LST between the vegetation height from 0 to 2.5 meters to 7.5 to 10 meters, and the median values of LST of the four groups were 29.16°C, 29.32°C, 29.15°C, 28.71°C, respectively (**Appendix 39**). For every 2.5 m increase in vegetation height, the average temperature decreases by 0.45 °C.

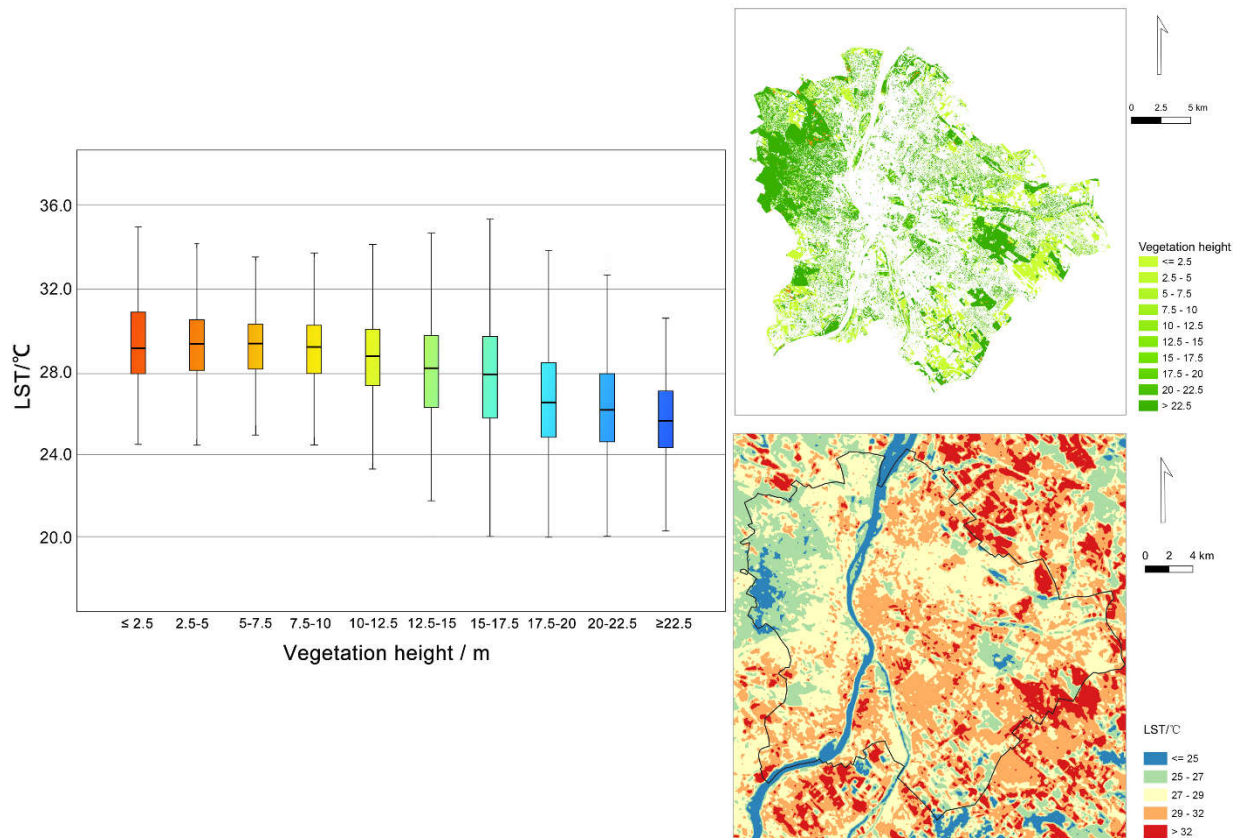


Figure 4.38: Box plots showing the relationships of vegetation height (m) with LST (range, minimum, maximum, median value in °C) in Budapest.

Accordingly, the height of vegetation and building has a significant correlation with LST from the analysis in **Figure 4.36 and 4.37** in Budapest. Higher vegetation groups are always cooler than lower vegetation groups in general, while taller buildings tend to perform higher LST than lower height buildings. It can be concluded that both vegetation height and building height correlate with the LST from the vertical level at the urban scale in Budapest.

In order to **eliminate the influence of impervious surface and neighbouring land cover type** and other factors on the results, I selected 10 sample plots (3023 pixels), which are in the center of an area with vegetation cover, **without the interference of other factors**, and only reflect the

relationship between the height of vegetation on surface temperature. From the *Figure 4.39*, we can see that the mean temperature (23.18°C) of high vegetation (≥ 16 m) is significantly lower than that of the mean temperature (27.59°C) of low vegetation (≤ 4 m). Thus we can conclude that vegetation height has a significant effect on surface temperature.

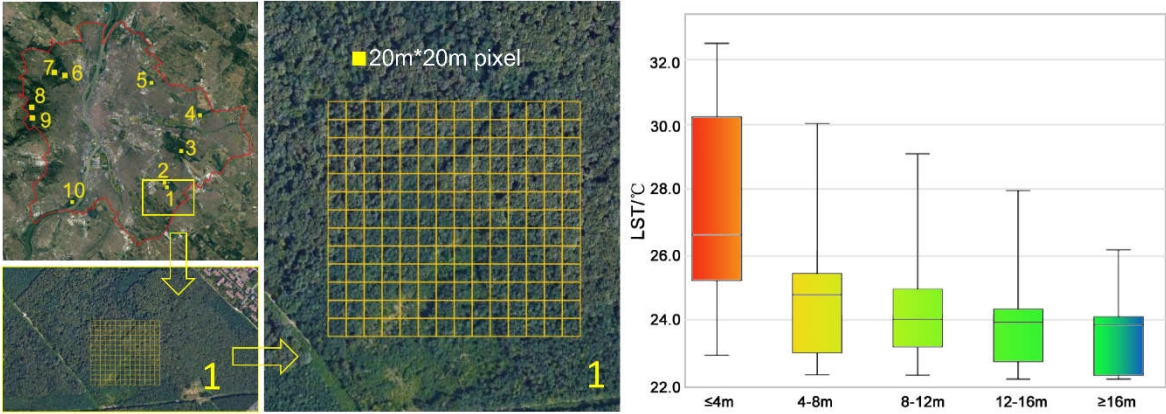


Figure 4.39: Box plots showing the relationships between vegetation height (m) and LST (°C) within only vegetation coverage area in selected 10 samples (Details of plot 1 is shown).

4.4.3 Green space factor’s effect on LST

Based on the method presented in section 3.3.4, coupled with the tree cover density (TCD) data (*Appendix 40*) was generated from the products provided by Copernicus. The LST map generated in the summertime of 2015 (*Figure 4.40*), the relationship between the TCD and LST were shown in *Figure 4.40*. It was found that the TCD had a significant correlation with the LST. The median values of LST decreased 5.85°C when the TCD percentage increased from group 0-10% to group 90-100% (*Appendix 41*). A high vegetation coverage rate generally reduced the LST.

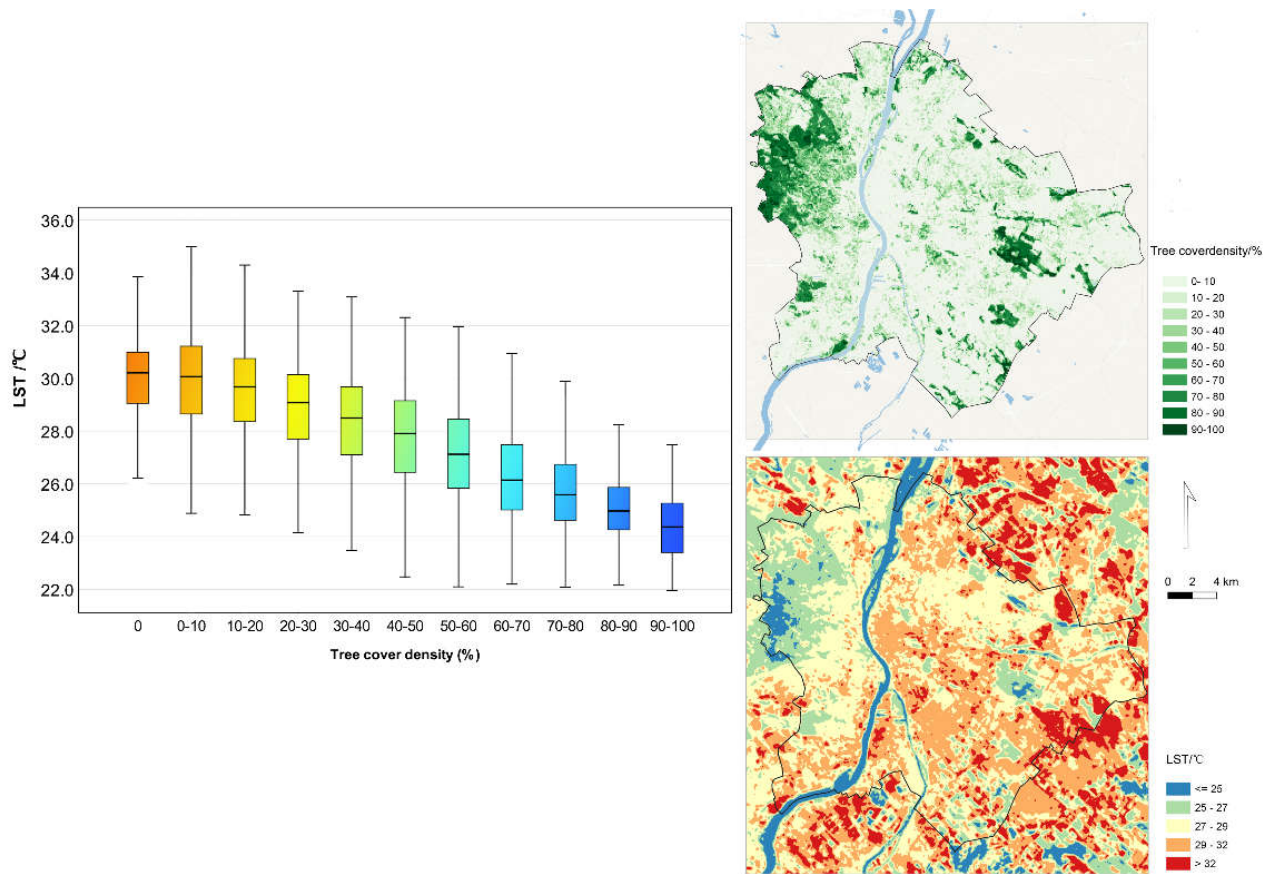


Figure 4.40: Box plots of the relationships of tree cover density (%) with LST (range, minimum, maximum, median value in °C) in Budapest.

In addition to the tree cover density, in this survey, the vegetation type and its correlation with LST were also investigated at an urban scale in Budapest. **Figure 4.41** shows that vegetation type had a significant correlation with the LST, with the vegetation coverage types (**Appendix 42, 43, 44**) shifting from grass⁴⁶, small woody⁴⁷, large woody⁴⁸, and forest⁴⁹, the LST became lower and lower, and the mean LST value is 29.35 °C, 29.33 °C, 28.38 °C, 26.31 °C (**Appendix 45**), respectively. The forest type (mostly broadleaved vegetation areas, average height is 8.83m⁵⁰) are cooler than woody feature areas (average height is 4.83m) and grassland. The average temperature

⁴⁶ This grassland includes all kinds of grasslands: managed grassland, semi-natural grassland and natural grassy vegetation. (Source: [Copernicus](#))

⁴⁷ Small Woody Features (SWFs) layer contains woody linear, and small patchy elements, but will not be differentiated into trees, hedges, bushes and scrub. (Source: [Copernicus](#))

⁴⁸ Large woody area : Woody features that are neither linear nor patchy SWA, but which are connected to linear or patchy SWA and isolated woody features that are not linear nor patchy SWA, but which present an area above 1500m² (linear features wider than 30m, and out-of-specifications patches). (Source: [Copernicus](#))

⁴⁹ The forest product allows to get as close as possible to the [FAO \(2000a\) forest definition](#). Forest includes natural forests and forest plantations. It refers to land with a tree canopy cover of more than 10 percent and area of more than 0.5 ha. Forests are determined both by the presence of trees and the absence of other predominant land uses. The trees should be able to reach a minimum height of 5 m. (Source: [Copernicus](#))

⁵⁰ The average height is extracted from DSM products which obtained in 2015, see section 3.2.2.1.

of broadleaved vegetation areas is about 3.04 °C lower than the average temperature of grassland.

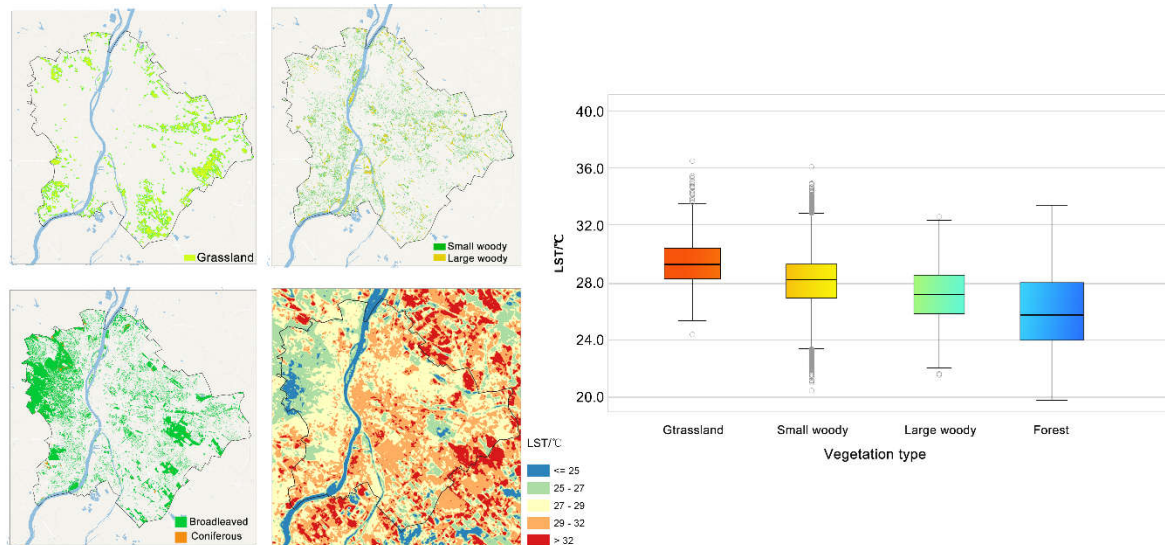


Figure 4.41: Box plots of the relationships of vegetation type with LST (°C) in Budapest.

In general, at an urban scale in Budapest, the vegetation type also plays a vital role in mitigating urban heat islands.

4.4.4. Discussions and further research proposals

In the following, the discussion based on results will be divided into two parts: 1) Vertical factors effect on SUHI; 2) Implications for Urban Planning and Landscape Design

4.4.4.1 Vertical factors effect on SUHI

This survey analyzed and investigated the vertical factors related to heat island research. Geographic factors are important factor that affect urban heat islands. In a broad sense, geographic variables include climate zone, southern/northern hemisphere, topography, altitude, elevation, etc. Within a city, it is mainly topographic and altitude factors (De Reu et al. 2013). In my dissertation I analyzed the elevation of Budapest, I compared the surface temperature of zones at different altitudes. The temperature in the high-elevation area is lower than that in the low-elevation area. This is mainly because the low-elevation flat area is the main built-up area of the city, which gathers high-density buildings and impermeable surface of a city, so the temperature is higher. High-elevation areas are generally not suitable for large-scale housing construction, and low-elevation areas are mainly covered by vegetation, which has a cooling effect, so high-elevation areas have lower temperatures. This is the essence of the influence of the vertical factor on the terrain on temperature. These results were consistent with the previous study in India (Khandelwal et al. 2018; Mathew et al. 2017). Besides, the influence of the slope aspect on temperature can be attributed to sunlight. In this study, winter season reduces the influence of vegetation on temperature to a certain extent. Taking the northern hemisphere as an example, the south-facing

slope receives sufficient sunlight, and the temperature is higher. The temperature on the northern slope is low due to insufficient sunlight. On the other hand, no matter the building's orientation or the hillside's orientation, it is time-sensitive changing with the sun's position.

The average LST map is a higher accuracy method to represent the surface temperature in a particular study area than using a single LST map, which calculates the average LST value from several LST maps. This average LST method minimizes the impacts of many factors such as: 1) land cover short-period change, such as the land cover changes by seasonal harvest in the agricultural land; 2) urban temporary land-use types such as renewal of abandoned land; 3) the changes in green infrastructure/elements over time, especially short-term leaf changes in plants, e.g. lawns, shrubs, fast-growing plants, etc. 4) meteorological conditions, such as clouds, wind, etc. Therefore, this average LST method could be applied in future study.

4.4.4.2 Implications for Urban Planning and Landscape Design

Based on the results, I give the following general guidance for further research and proposals for planning and design:

- 1) From urban climate point of view it is recommended to increase the vegetation height and decrease the building height in the newly built towns /districts.
- 2) It is recommended to increase the vegetation coverage rate and decrease the imperviousness surface in urban planning.
- 3) Urban heat island characteristics of winter and summer should be further compared in future research. Some elements show that the elements of summer's advantage are winter's disadvantage (For example, a high-density green spaces area in winter makes the environment cooler than a low-density area, increasing heating consumption.), and some elements of winter's advantage is summer's disadvantage This can be influenced by coloring, choice of built or plant material, shading by built structures or trees.
- 4) It is recommended to planners avoid the introduction of evergreen trees as shading elements near the southern side of buildings, as they provide a cooling effect in winter and block sunshine.

4.4.5 Summary of vertical factor effects

In this study, combination of field measurement and geospatial data had been applied to investigate the vertical factors on the urban heat island effect. Budapest was taken as a study area, and the vertical data was extracted from the DEM and DSM using GIS analysis. Besides the buildings' height, vegetation data such as tree cover density, Street tree layer; Forest type layer, Dominant Leaf Type, Small Woody Feature, Grassland were downloaded from the particular products made

by Copernicus institution.

The results showed that south-facing slopes and south-oriented buildings that absorbed long-time solar heat were warmer than north-facing slopes and buildings oriented to the north. Thanks to low sun angle, a special kind of heat island, the “**Vertical Heat Island**” (VHI) could be recognized. The landscape's vertical elements were lighted and warmed up by the sun mostly from the side, so the heat island shows up on hill-slopes, walls, and facades of huge hills and buildings. The high-height buildings group appeared a higher LST than the low-height buildings group in general. By applying the vegetation information data and its correlation with LST, it was found that **vegetation height had a significant negative impact on LST; the higher vegetation is cooler than, the lower vegetation.** It was found that vegetation types also had a significant effect on LST, with the vegetation coverage changing from grass, small woody, large woody, and forest, the LST became lower and lower.

Based on the above research results, it is recommended to modify the temperature by increasing vegetation height, increasing vegetation coverage density, increasing large-size vegetation while controlling the height of buildings. A better understanding of the impact of vertical variables on LST may lead to informed decisions within the city.

5. NEW SCIENTIFIC RESULTS

The results of the research are summarized in the following 9 theses:

Thesis 1: Identification of an efficient method for land surface temperature retrieval and mapping.

Based on the scientific literature and a large amount of image process practice, I identified two important land surface temperature (LST) methods: Image-based Method LST retrieval methods and average LST mapping, which could improve the accuracy and efficiency of UHI heat island research.

- a) I identified and tested five land surface temperature (LST) **retrieval methods**⁵¹ based on satellite image LST calculations. I found **Image-based Method** could be widely used and is suitable for satellite images **in case no atmospheric data available**. It is especially true for the early history of satellite imagery (1980-ies, 90-ies). However, the accuracy of the Image-based Method is lower than the method with atmospheric data correction.
- b) I identified the **average LST map** is a higher accuracy method to represent the surface temperature in a particular study area than using a single LST map, which calculates the average LST value from several LST maps. This average LST method minimizes the impacts of:
 - short-period land cover changes, such as the vegetation changes by seasonal harvest in the agricultural area.
 - temporary land-use types (e.g. floods, fire, organized events, construction sites).
 - changes in green infrastructure/elements over time, especially short-term leaf changes in green spaces or individual plants due to maintenance, e.g. lawns, shrubs, fast-growing plants, canopy cut, trimming, etc.
 - meteorological conditions, such as clouds, wind, etc.

⁵¹ Five retrieval algorithms: Plank function, Radiative Transfer Equation (RTE); Single Channel Algorithm (SCA); Mono-Window algorithm (MWA); Image-based Method (IBM).

Thesis 2: Determination of urban heat island's research trend currently.

Based on the literature review and scientific analysis from urban heat island publications, I identified the research trends of urban heat island studies currently.

Using the **bibliometric method**, I analyzed **7808 publications** from the Web of Science in urban heat island (UHI) studies from **1975 to 2020**. I defined the growth tendency in the number of UHI related publications and I summarized the general results (method trends, research direction) on urban heat island studies.

- a) **Urban heat island problems are increasing all over world.** The number of the research publications number was multiplied decade by decade. From 1990 to 2000 this number became **four times** bigger (from 65 to 257 publications); then from 2000 to 2010, the UHI researches increased **five times** more (from 257 to 1157), finally, from 2010 to 2020, the numbers **increased almost six times** more (1157 to 5985).
- b) **The main trend is the adaptation to the changing urban heat environment currently.** Research trends from the publications based on keywords: from 1975 to 2012 period; the main topic was vegetation and UHI; UHI model; temperature measurement; from 2013 to 2020; the main topics were: Urban heat island and its impacts, **adaptation and mitigation**.

Thesis 3: Determination of the relation between urban climate warming and urbanization process in Zhengzhou city

I identified the relationship between urban climate warming and the urbanization process. I have determined that urban growth (e.g.: built-up area density increase, impervious surface sprawl) significantly contributes to the urban heat compared to its rural surroundings by the analyzed long-term meteorological data.

Despite global warming makes the temperature increasing both in urban and rural areas, the **temperature rising** in the urban areas is more predominant due to the **urbanization process**. The urbanization process contributes to urban warming and the urban heat island effect. **China has a specific high speed of urbanization** growth even more intensive than other Western countries (in the US and the EU). From this perspective, I analyzed the dynamics of the urban and rural air temperature in Zhengzhou city over the **last 38 years (1981-2019)**. During the study period, urbanization made a significant warming rate of about **+0.67°C per decade** on average in the city. This **warming rate** is about **0.43°C per decade, higher** on average than the adjacent **rural area**. It is about **2.2 times bigger (+1.96°C)** than the average **global land temperature increase magnitude (+0.9°C)** in the last 40 years, indicating that **urbanization has a significant contribution to global warming**.

Thesis 4: Determination of optimizing methods for assessing surface urban heat islands and its characteristics of the city with high urbanization rate.

I have applied two methods to assess the surface urban heat island based on satellite images from 1989 to 2019. Based on the two Surface Urban Heat Island Intensity (SUHII) and Urban Heat Island Ratio Index (URI) method⁵², I identified surface urban heat island change characteristics in the rapidly urbanizing city of Zhengzhou. I have evaluated the impact of urban construction guided by ecological concept on the urban heat island effect, and I have found:

- a) **The increase of urban green infrastructure significantly reduces the urban heat island aggregation.** Especially the increase of green infrastructure in the central urban area can mitigate the heat island effect. The increase of blue and green infrastructure in the central urban area of Zhengzhou from 2009 to 2019 has reduced the average surface heat island intensity in summer by 1.3°C.
- b) **The green infrastructure development concept for urban development is crucial and successful from urban climate aspects.** It is due to the implementation of the ecological city construction plan from 2009 to 2019 in Zhengzhou: improving the structure of **green space network**, building **urban water system**, thus greatly increasing the coverage rate of **blue-green infrastructure** in the urban area, the urban heat island effect was mitigated.

⁵² Two methods:

1) Surface Urban Heat Island Intensity (SUHII), which is expressed by calculating the difference between the average surface temperature of built-up areas and non-built-up areas according to the land use classification. This method provides a way to assess the surface urban heat island and the evaluation and comparison of the surface urban heat island intensity.

2) Urban heat island Ratio Index (URI) is an indicator that shows the spatial ratio (%) of the highest temperature category. The index classifies land, based on surface temperature to 5 categories (driven by standard deviation). First the surface temperature is categorized based on standard deviation, then the territorial ratio of the highest-temperature zone is calculated. This method can be used to compare the surface heat island intensity of different time periods.

Thesis 5: Identification of cooling characteristics of park type.

I identified the relation between park types, Land Surface Temperature, and Park Cooling Intensity in Zhengzhou city, which can guide future urban park planning from the perspective of urban heat island mitigation.

Based on **five park types**⁵³ and **123 sample parks** investigation in the study area (Zhengzhou city). I have determined the relationship between **park types** and **park surface temperature** and **park cooling intensity** (PCI). Among the selected five park types (**urban park, theme park, street park, linear park, urban square**)⁵⁴, I identified that:

- a) **The theme park** has the lowest surface temperature, and **its average cooling intensity is the highest**. For instance, the average surface temperature of the theme park category is 2.14°C lower than the average temperature of Zhengzhou city. The cooling effect of this category is the strongest, as its average park cooling intensity reached 2.76 °C.
- b) **The urban square type** has the highest surface temperature.
- c) **The linear park** type has the lowest park cooling intensity⁵⁵(0.64°C).

According to my results, I recommend **considering park types** in dealing with urban heat island problems in the future, not only the construction of more parks and green spaces.

⁵³ Five park types: Urban park, theme park, street park, linear park, urban square, which based on 《Standard for Classification of Urban Green Space》CJdJ/T85-2017 in China.

⁵⁴ Urban park (e.g. City park, District park); Theme park (e.g. Botanical garden, Zoo); Street park (e.g. Pocket park, community park); Linear park (e.g. Riverside park, roadside park); Urban square (e.g. Parks with square).

⁵⁵ Zhengzhou's linear parks mostly located beside the channels and rivers.

Thesis 6: Identification of spectral index-based method to quantify the factors and assess park cooling effect.

I built a spectral index-based method to assess the relationship between park surface temperature and park coverage characteristics (vegetation cover, water surface, and impervious surface). The spectral indices can provide a comprehensive and fast character quantification of urban parks. This help to recognize the urban park plan and design parameters to modify the park surface temperature.

Based on the satellite images, I used three spectral indices: **Fractional Vegetation Cover (FVC)**, **Normalized Difference Water Index (NDWI)**, and **Normalized Difference Impervious Surface Index (NDISI)** to represent the park characteristics. With the analysis of 123 sample parks in Zhengzhou city. I have found that Fractional Vegetation Cover (FVC) and Normalized Difference Water Index (NDWI) **play a negative role** in park surface temperature, indicating that more **vegetation cover makes parks cooler**, and more water surface also **cools down the park**. On the contrary, the Normalized Difference Impervious Surface Index (NDISI) has a **positive effect** on park LST.

From the regression model between LST and NDISI, the coefficient of determination (R^2) reached 0.926, revealing that the impervious surfaces significantly impact park temperature in Zhengzhou. The **impervious surface is the main contributor** to the warm heat conditions of parks. In conclusion, **water and vegetation positively impact the park's cooling role** in Zhengzhou, while the impervious surface increases the park's warmth. Therefore, it is recommended to add more parks (green spaces) within a densely built up district with high impervious surface ratio, such as built-up areas (transport lines and stations, commercials, business districts, residential areas etc.).

Thesis 7: Determination of the park characteristics on mitigating urban heat island.

I determined the correlation between park characteristics and the park cooling effect, and I proved that those park metrics have significance in park design. This way I quantified the planning and design parameters of the urban park to regulate the surface temperature.

Based on the **satellite images** and the analysis of **123 sample parks** in Zhengzhou city, I have examined special **park characteristics** that impact the **park cooling effect**. I used **four park metrics (Size; Fractal dimension; Perimeter area ratio, Shape index⁵⁶)** to investigate the park cooling effect's **mechanism**. In case of increasing park (or green space) cooling effect, I have determined the following common strategies:

- a) **The park size and perimeter-area ratio play a more critical role than other patch metrics in parks.**
- b) **Large-size parks have a higher cooling effect.** I have found that parks with a size larger than 15 hectares have significant cooling intensity (average PCI 2.23 °C).
- c) **Based on the above results, large urban parks** should be planned.
- d) **Based on the above results,** following urban heat mitigation aspects, **fewer curving boundaries and fewer waving edges could be recommended** in urban and landscape design to reach stronger cooling effect.

Regarding the common features above, my results can give guidance to urban landscape planners and designers.

⁵⁶ Fractal Dimension Index reflects the extent of shape complexity across a range of spatial scales (Lei et al. 2012);

Perimeter-Area Ratio equals the ratio of the patch perimeter (m) to area (m²) (Lei et al. 2012);

Shape index provides a standardized measure of total edge or edge density that adjusts for the size of the landscape (Lei et al. 2012).

Thesis 8: Determination of vegetation structure factors on mitigating thermal effect.

Determination of the cooling and humidification effects of different coverage types in green spaces. I have determined the best vegetation structure type (tree-shrub-grass)⁵⁷ in terms of mitigating the thermal effect.

By selecting four green spaces in a university campus as sample plots, using **meteorological data** to analyze spatial and temporal characteristics of the green spaces, I have compared the effects of **four coverage types (impervious surface; shrub-grass; tree-grass; tree-shrub-grass)** on microclimate. I have analyzed the **four impact factors (Canopy Density, Leaf Area Index, Photosynthetically Active Radiation, Mean Leaf Angle)** of the green space.

I have determined the relationship between temperature and humidity and surface cover types of green space:

- a) **Multiple vegetation layers** (tree-shrub-grass) have higher cooling and humidification effect than the types with fewer layers (e.g. shrub-grass).
- b) **Tree** is the key factor that contributes to the cooling and humidification of the environment.
- c) **Trees with a dense canopy and more leaves are cooler and more humid.**
- d) **Trees with smaller leaf angles⁵⁸** contribute to **cooler and more humid** green space.

The results can guide green space management and future landscape design, The green space design applying multiple vegetation layers, can better regulate the urban heat environment, and improve human thermal comfort.

⁵⁷ Among four types of coverage: Impervious surface; Shrub-grass; Tree-grass; Tree-shrub-grass.

⁵⁸ Refers to the angle between the leaves and the horizontal direction, thus small leaf angle means near horizontal leaves.

Thesis 9: Determination of vertical vegetation factors on mitigating urban heat island.

I identified those vegetation height-related factors that influence surface urban heat island. The high vegetation area is cooler than low vegetation area, and forest type green areas are cooler than grass type area and woody type areas.

Based on my research, I have determined those vegetation height-related factors that could be used to modify urban heat island problems as below:

a) **The high vegetation is cooler than low vegetation.** I found that areas covered by higher vegetation (trees, woodlands, etc.), had lower temperature (26.31 °C) than areas covered by lower vegetation (e.g. shrublands, transitional vegetation (28.38 °C)) or areas with low vegetation (e.g. grassland (29.35 °C)) in the 10 sample areas (3023 points) of Budapest (2015). For every 2.5 m increase in vegetation height, the average temperature decreases by 0.45 °C.

b) **The broadleaved vegetation areas⁵⁹ (average height⁶⁰ is 8.83m) are cooler than woody feature⁶¹ areas (average height is 4.83m⁶²) and grassland.** The average temperature of **broadleaved vegetation areas** is about 3.04 °C lower than the average temperature of grassland.

The above factors could be considered from the perspective of urban heat mitigation.

⁵⁹ The forest product allows to get as close as possible to the [FAO \(2000a\) forest definition](#). Forest includes natural forests and forest plantations. It refers to land with a tree canopy cover of more than 10 percent and area of more than 0.5 ha. Forests are determined both by the presence of trees and the absence of other predominant land uses. The trees should be able to reach a minimum height of 5 m. (Source: [Copernicus](#))

⁶⁰ The average height was extracted from DSM products of Budapest which obtained in 2015 by using the forest type layer from [Copernicus](#).

⁶¹ Woody area are exclusively covered by ligneous vegetation (woody plants) and comprise linear hedges and tree rows along field boundaries, riparian and roadside vegetation, as well as scattered patches of trees and scrubs, but will not be differentiated into trees, hedges, bushes and scrub.

⁶² The average height was extracted from DSM products of Budapest which obtained in 2015 by using the forest type layer from [Copernicus](#).

6. CONCLUSION AND USABILITY OF RESULTS

6.1 Summary of the dissertation

This dissertation seeks answers to questions about the characteristics of urban heat islands and mitigation measures:

First, by reviewing the historical development of urban heat island literature, deepen the understanding of the existing problems and challenges in the existing urban heat island effect research practice. Based on literature research and method practice, I aimed to find a suitable method for studying the urban heat island effect. I prepared for a comprehensive assessment of heat island effect and subsequent research in two pilot cities (Zhengzhou, Budapest).

According to my research goals and research questions, my dissertation could be divided into **four main scales**. The research was separated from large to small scale, **from urban scale, local scale, and finally to micro-scale and additionally considers vertical factors**:

- 1) I analyzed the characteristics of the heat island in the urban scale to determine the **characteristics of the urban heat island and the cooling factors**;
- 2) I studied the cooling effect of green space with urban parks as the object, analyze the **influencing factors** and characteristics of the **park cooling effect**;
- 3) I took the small green space as an example, analyze the effect of the internal **vegetation structure** of the green space on **temperature and humidity**.
- 4) Finally, I checked the effect of specific **vertical factors of heat island**. The dissertation studies the heat island from the **horizontally** (surface temperature, etc.) and conducts a supplementary study of the heat island from the **vertical direction** (vegetation height, elevation, etc.).

The **first pillar** of this dissertation was to **identify the urban heat island problems** in the rapidly urbanized city of Zhengzhou in China. The research involved **methods to quantify** the characteristics of urban heat island, It was carried out using map analysis, diagrams, different historical and spatial data to **analyze and summarize the spatio-temporal changes and characteristics** of urban heat island.

- 1) On the **temporal scale**, the **meteorological data of 38 years (1981-2019) long-term observation** is selected to analyze the characteristics of heat island changes over time.
- 2) Regarding the **spatial distribution of heat islands**, **16 images** were selected from 128 satellite images to illustrate and analyze the spatial distribution characteristics of urban heat islands.
- 3) Simultaneously I combined long-term (1981-2019) **urban indicators** (urbanization rate, population density, GDP, etc.) to analyze other influencing factors of urban heat islands. A **comprehensive analysis and evaluation** of urban heat island on the **spatio-temporal scale** are

carried out, and the characteristics of urban heat island are summarized. The reasons and mechanisms of the generation and evolution of heat island are determined.

The **second pillar** investigated the **cooling effect of urban parks**. A total of **123 sample parks** were selected from **5 types** of parks. I analyzed two aspects:

- 1) The **park internal characteristics** (vegetation, water surface, and impervious surface) influence on park temperature;
- 2) The influence of **park characteristics (category, location, surrounding land type, size, shape index, structure, etc.)** influence on **cooling effect**.

The analysis showed that parks with high vegetation and water surface coverage index have lower temperatures; high impervious surface indexes have lower cooling effects. The **larger the park's size, the higher the cooling effect**. Additionally the cooling effect of **complex-shaped parks with long boundary** is smaller than that of **compact parks (with short boundary)**. Parks in **high-density construction areas** have the **highest cooling effect**.

The **third pillar** studied the micro-scale mechanism of vegetation cooling and humidification effects. I selected **four coverage types** (impervious surface; shrub-grass; tree-grass; tree-shrub-grass) for a total of **16 measurement plots**, and introduced **four vegetation indices** (Canopy Density, Leaf Area Index, Photosynthetically Active Radiation, Mean Leaf Angle) to assess the **impact** of vegetation coverage types based on vegetation structure **on the temperature and humidity**. The analysis shows that **tree cover is the key factor** that affects vegetation cooling and humidification regarding the **four coverage types**. On this basis, the **more vegetation layers** we have, the **higher the cooling effect is**. Simultaneously, high canopy density, high leaf area index, and low vegetation **leaf angle** make the environment cooler and more humid. The research on the micro-scale has important practical significance for landscape design, especially plant design.

The **last pillar** I analyzed the characteristics of the urban heat island from a **vertical** perspective. Budapest was the study area by analyzing **elevation maps, vegetation height maps, vegetation coverage type maps (grassland, woody, forest), building height maps**, and surface temperature data. I analyzed and **determined factors in the vertical direction** (elevation position, building orientation, vegetation height, building height, vegetation cover type) on temperature. The results show that the temperature in **high-elevation areas** is **lower** than that of **low-elevation areas**. The **higher the vegetation height, the lower the temperature**. The higher the building height, the higher the temperature. Meanwhile, it can **adjust vegetation height, building height, and building orientation to mitigate the heat island**. The **vegetation cover type** can be **rationally applied** to mitigate the heat as well.

In addition to the scientific results, the research also put forward some suggestions to implement a more **ecological urban planning method**, rationally **arrange the urban structure**, build a **blue-green network of the city**, build a **park system**, and reasonable **vegetation coverage**

characteristics in the future green space design. It is recommended for planners to consider the impact of vegetation height and type on the environment. This paper's results are expected to stimulate further research and to contribute to the establishment of livable and sustainable cities in the future.

6.2 Implications for urban and landscape planning

Chapter 5 determined the scientific results related to the UHI characteristics and its impact factors. The results proved that using different methods (urban planning, urban landscape design, park planning and design, architectural design, plant design, and geographic design, etc.) at different scales can mitigate urban heat island effect.

The relationship between land surface temperature (LST) and urban landscape indicators is of great significance for urban planning and land use management and the mitigation of urban heat island. The previous study and my study all show the positive effect of vegetation and other types of green infrastructure on reducing the temperature in the city areas. At the city scale, the landscape metrics, such as the distribution of land surface coverage types and the impervious surface, contributes the highest temperature to urban heat island according to the study. Although we need residential land, transportation land, buildings, and other impervious surface areas for the urban system, we still can mitigate the LST by increasing the service of green space system in the high-density city center. We can use this to develop a vision to influence urban landscape planning and inform about the know how to make the urban environment more comfortable and healthy for residents. Urban green infrastructure has been used as a mitigating strategy to lower the land surface temperatures in cities all over the world.

Based on my study, regarding the urban heat island mitigation strategy, the planner and designer can follow the **recommendations**:

- Regulate the urban planning model, implement more **sustainable urban planning and renewal concepts**, increase the proportion and coverage of urban green space;
- Plan a complete water system network, more reasonable layout of the urban water system network system; based on the **blue-green infrastructure system effect** (*Appendix 46*) to mitigate urban heat island effect.
- Increase the **number and ratio of green spaces** in the city and increase the **tree canopy coverage** in the overall urban planning process.
- Construct **water surface** (e.g. lakes, fountains, channels, reservoirs) and **forest connected** with or integrated with green spaces in urban planning.
- Develop **low-density built-up areas** with a **high rate of green spaces**.
- Increase the **vegetation coverage rate and decrease the impervious surface density** to mitigate the urban heat environment in the newly built towns /districts.

- Increase the number of **theme park types** in the city, increase the **park size** and the **number of compact parks** in a new town/district planning.
- In city planning, **plant species** selection should be based on the local climatic conditions, increasing the multi-layered type of the plant, considering the characteristics of the **leaf area index** and the **leaf angle** of the plant.
- In green space landscape design, conifers should be combined with **broad-leaved trees**, and the tree-shrub-grass compound should be more often applied in design to maximize the cooling and humidification effects of the microclimate.
- Increase **vegetation height, with planting more trees** in the newly built towns /districts regarding mitigating the urban heat island effect. From the aspect of urban heat island effect mitigation, the grasslands are less useful, even if grass is beneficial from social aspects.
- Avoid the introduction of **evergreen trees** as shading elements near the southern side of buildings (in the northern hemisphere), as they provide a cooling effect in winter and block sunshine.
- Urban heat island characteristics of **winter and summer** should be both considered in the future. Some elements show that the summer's advantage is winter's disadvantage. This can be influenced by coloring, choice of built or plant material, shading by built structures (for example: pergola, green wall, green facade) or trees.
- For future heat island research, the research methods in this paper, such as **average LST**, surface temperature inversion methods, and **indicators** for assessing heat island characteristics can provide references for researchers to better assess and analyze heat island characteristics for cities in a comprehensive way.
- In the future **urban management**, for mitigating and adapting to urban heat island, urban management should establish monitoring system and regulations, and consider various strategies comprehensively, and a more intelligent urban development strategy is necessary.
- In future heat island **research direction**, the characteristics of heat islands should be evaluated in **multiple dimensions**, for example, not only the **horizontal but also the vertical** heat islands should be considered.

REFERENCES

1. ADELIA, A. S., YUAN, C., LIU, L., SHAN, R. Q. (2019): Effects of urban morphology on anthropogenic heat dispersion in tropical high-density residential areas. In: *Energy and Buildings*, 186 368–383 pp.
2. AKBARI, H. (2005): *Energy Saving Potentials and Air Quality Benefits of Urban Heat Island Mitigation*. (No. LBNL-58285) Ernest Orlando Lawrence Berkeley National Laboratory, Berkeley, CA (US) <https://www.osti.gov/biblio/860475>.
3. ALEXANDER, P. J., FEALY, R., MILLS, G. M. (2016): Simulating the impact of urban development pathways on the local climate: A scenario-based analysis in the greater Dublin region, Ireland. In: *Landscape and Urban Planning*, 152 72–89 pp.
4. ALONSO, M. S., FIDALGO, M. R., LABAJO, J. L. (2007): The urban heat island in Salamanca (Spain) and its relationship to meteorological parameters. In: *Climate Research*, 34 (1) 39–46 pp.
5. ALONSO, J. M., CASTIELLO, C., MENCAR, C. (2018): A Bibliometric Analysis of the Explainable Artificial Intelligence Research Field. In: J. Medina, M. Ojeda-Aciego, J. L. Verdegay, D. A. Pelta, I. P. Cabrera, B. Bouchon-Meunier, & R. R. Yager (Eds.), *Information Processing and Management of Uncertainty in Knowledge-Based Systems. Theory and Foundations*. Cham: Springer International Publishing. 3–15 pp.
6. ANDREOU, E. (2014): The effect of urban layout, street geometry and orientation on shading conditions in urban canyons in the Mediterranean. In: *Renewable Energy*, 63 587–596 pp.
7. ANTONIADIS, D., KATSOULAS, N., KITTAS, C. (2018): Simulation of schoolyard’s microclimate and human thermal comfort under Mediterranean climate conditions: effects of trees and green structures. In: *International Journal of Biometeorology*, 62 (11) 2025–2036 pp.
8. ANTONINI, E., VODOLA, V., GASPARI, J., DE GIGLIO, M. (2020): Outdoor Wellbeing and Quality of Life: A Scientific Literature Review on Thermal Comfort. In: *Energies*, 13 (8) 2079 pp.
9. ARMSON, D., STRINGER, P., ENNOS, A. R. (2012): The effect of tree shade and grass on surface and globe temperatures in an urban area. In: *Urban Forestry & Urban Greening*, 11 (3) 245–255 pp.
10. ARNFIELD, A. J. (2003): Two decades of urban climate research: a review of turbulence, exchanges of energy and water, and the urban heat island. In: *International Journal of Climatology*, 23 (1) 1–26 pp.
11. AZHDARI, A., SOLTANI, A., ALIDADI, M. (2018): Urban morphology and landscape structure effect on land surface temperature: Evidence from Shiraz, a semi-arid city. In: *Sustainable Cities and Society*, 41 853–864 pp. 853–864 pp.
12. BALÁZS, B., UNGER, J., GÁL, T., SÜMEGHY, Z., GEIGER, J., SZEGEDI, S. (2009): Simulation of the mean urban heat island using 2D surface parameters: empirical modelling, verification and extension. In: *Meteorological Applications*, 16 (3) 275–287 pp.
13. BARSİ, J. A., SCHOTT, J. R., PALLUCONI, F. D., HELDER, D. L., HOOK, S. J., MARKHAM, B. L., CHANDER, G., O’DONNELL, E. M. (2003): Landsat TM and ETM+ thermal band calibration. In: *Canadian Journal of Remote Sensing*, 29 (2) 141–153 pp.
14. BARSİ, J. A., BARKER, J. L., SCHOTT, J. R. (2003): An Atmospheric Correction Parameter Calculator for a single thermal band earth-sensing instrument. In: *IGARSS 2003. 2003 IEEE International Geoscience and Remote Sensing Symposium. Proceedings (IEEE Cat. No.03CH37477)*. Vol. 5. 3014–3016 pp.
15. BARTESAGHI KOC, C., OSMOND, P., PETERS, A. (2018): Evaluating the cooling effects of green infrastructure: A systematic review of methods, indicators and data sources. In: *Solar Energy*, 166 486–508 pp.

16. BECK, H. E., ZIMMERMANN, N. E., MCVICAR, T. R., VERGOPOLAN, N., BERG, A., WOOD, E. F. (2018): Present and future Köppen-Geiger climate classification maps at 1-km resolution. In: *Scientific Data*, 5 (1) 180214 pp.
17. BECKER, F., LI, Z.-L. (1990): Towards a local split window method over land surfaces. In: *International Journal of Remote Sensing*, 11 (3) 369–393 pp.
18. BENCHEIKH, H., RCHID, A. (2012): The Effects of Green Spaces (Palme Trees) on the Microclimate in Arides Zones, Case Study: Ghardaia, Algeria. In: *Energy Procedia*, 18 10–20 pp.
19. BHATTACHARYA, B. K., MALLICK, K., PADMANABHAN, N., PATEL, N. K., PARIHAR, J. S. (2009): Retrieval of land surface albedo and temperature using data from the Indian geostationary satellite: a case study for the winter months. In: *International Journal of Remote Sensing*, 30 (12) 3239–3257 pp.
20. BODRI, L., CERMAK, V., KRESL, M. (2005): Trends in precipitation variability: Prague (the czech republic). In: *CLIMATIC CHANGE*, 72 (1–2) 151–170 pp.
21. BOKAIE, M., ZARKESH, M. K., ARASTEH, P. D., HOSSEINI, A. (2016): Assessment of Urban Heat Island based on the relationship between land surface temperature and Land Use/ Land Cover in Tehran. In: *Sustainable Cities and Society*, 23 94–104 pp.
22. BORNSTEIN, R. D. (1968): Observations of the Urban Heat Island Effect in New York City. In: *Journal of Applied Meteorology*, 7 (4) 575–582 pp.
23. BOTTEMA, M. (1997): Urban roughness modelling in relation to pollutant dispersion. In: *Atmospheric Environment*, 31 (18) 3059–3075 pp.
24. BOWEN, I. S. (1926): The Ratio of Heat Losses by Conduction and by Evaporation from any Water Surface. In: *Physical Review*, 27 (6) 779–787 pp.
25. BOWLER, D. E., BUYUNG-ALI, L., KNIGHT, T. M., PULLIN, A. S. (2010): Urban greening to cool towns and cities: A systematic review of the empirical evidence. In: *Landscape and Urban Planning*, 97 (3) 147–155 pp.
26. Budapest - History, Language, Population, Climate, & Facts. In: (n.d.) <https://www.britannica.com/place/Budapest>. Accessed: 2020. 11. 23.
27. CAO, X., ONISHI, A., CHEN, J., IMURA, H. (2010): Quantifying the cool island intensity of urban parks using ASTER and IKONOS data. In: *Landscape and Urban Planning*, 96 (4) 224–231 pp.
28. CARLSON, T. N., RIPLEY, D. A. (1997): On the relation between NDVI, fractional vegetation cover, and leaf area index. In: *Remote Sensing of Environment*, 62 (3) 241–252 pp.
29. CASILLO, R. (1992): Lewis Mumford and the Organicist Concept in Social Thought. In: *Journal of the History of Ideas*, 53 (1) 91–116 pp.
30. CHAN, F. K. S., GRIFFITHS, J. A., HIGGITT, D., XU, S., ZHU, F., TANG, Y.-T., XU, Y., THORNE, C. R. (2018): “Sponge City” in China—A breakthrough of planning and flood risk management in the urban context. In: *Land Use Policy*, 76 772–778 pp.
31. CHANG, C.-R., LI, M.-H., CHANG, S.-D. (2007): A preliminary study on the local cool-island intensity of Taipei city parks. In: *Landscape and Urban Planning*, 80 (4) 386–395 pp.
32. CHAOLIN, G., LIYA, W., COOK, I. (2012): Progress in research on Chinese urbanization. In: *Frontiers of Architectural Research*, 1 (2) 101–149 pp.
33. CHAPMAN, S., WATSON, J. E. M., SALAZAR, A., THATCHER, M., MCALPINE, C. A. (2017): The impact of urbanization and climate change on urban temperatures: a systematic review. In: *Landscape Ecology*, 32 (10) 1921–1935 pp.
34. CHATTERJEE, S., KHAN, A., DINDA, A., MITHUN, S., KHATUN, R., AKBARI, H., KUSAKA, H., MITRA,

- C., BHATTI, S. S., DOAN, Q. V., WANG, Y. (2019): Simulating micro-scale thermal interactions in different building environments for mitigating urban heat islands. In: *Science of The Total Environment*, 663 610–631 pp.
35. CHEN, F., YANG, S., SU, Z., HE, B. (2015): A new single-channel method for estimating land surface temperature based on the image inherent information: The HJ-1B case. In: *ISPRS Journal of Photogrammetry and Remote Sensing*, 101 80–88 pp.
 36. CHEN, J., JIN, S., DU, P. (2020): Roles of horizontal and vertical tree canopy structure in mitigating daytime and nighttime urban heat island effects. In: *International Journal of Applied Earth Observation and Geoinformation*, 89 102060 pp.
 37. CHEN, X., SU, Y., LI, D., HUANG, G., CHEN, W., CHEN, S. (2012): Study on the cooling effects of urban parks on surrounding environments using Landsat TM data: a case study in Guangzhou, southern China. In: *International Journal of Remote Sensing*, 33 (18) 5889–5914 pp.
 38. CHEN, X.-L., ZHAO, H.-M., LI, P.-X., YIN, Z.-Y. (2006): Remote sensing image-based analysis of the relationship between urban heat island and land use/cover changes. In: *Remote Sensing of Environment*, 104 (2) 133–146 pp.
 39. CHEN, Y. (2011): Derivation of the functional relations between fractal dimension of and shape indices of urban form. In: *Computers, Environment and Urban Systems*, 35 (6) 442–451 pp.
 40. CHOW, W. T. L., ROTH, M. (2006): Temporal dynamics of the urban heat island of Singapore. In: *International Journal of Climatology*, 26 (15) 2243–2260 pp. 2243–2260 pp.
 41. CHRISTOFF, P. (2008): The Bali roadmap: Climate change, COP 13 and beyond. In: *Environmental Politics*, 17 (3) 466–472 pp.
 42. COHEN, P., POTCHTER, O., MATZARAKIS, A. (2012): Daily and seasonal climatic conditions of green urban open spaces in the Mediterranean climate and their impact on human comfort. In: *Building and Environment*, 51 285–295 pp.
 43. COHEN, S., PALATCHI, Y., PALATCHI, D. P., SHASHUA-BAR, L., LUKYANOV, V., YAAKOV, Y., MATZARAKIS, A., TANNY, J., POTCHTER, O. (2020): Mean radiant temperature in urban canyons from solar calculations, climate and surface properties – Theory, validation and ‘Mr.T’ software. In: *Building and Environment*, 178 106927 pp.
 44. COLL, C., CASELLES, V., SOBRINO, J. A., VALOR, E. (1994): On the atmospheric dependence of the split-window equation for land surface temperature. In: *International Journal of Remote Sensing*, 15 (1) 105–122 pp.
 45. DE REU, J., BOURGEOIS, J., BATS, M., ZWERTVAEGHER, A., GELORINI, V., DE SMEDT, P., CHU, W., ANTROP, M., DE MAEYER, P., FINKE, P., VAN MEIRVENNE, M., VERNIERS, J., CROMBÉ, P. (2013): Application of the topographic position index to heterogeneous landscapes. In: *Geomorphology*, 186 39–49 pp.
 46. DEILAMI, K., KAMRUZZAMAN, Md., LIU, Y. (2018): Urban heat island effect: A systematic review of spatio-temporal factors, data, methods, and mitigation measures. In: *International Journal of Applied Earth Observation and Geoinformation*, 67 30–42 pp.
 47. DEMANUELE, C., MAVROGIANNI, A., DAVIES, M., KOLOKOTRONI, M., RAJAPAKSHA, I. (2011): Using localised weather files to assess overheating in naturally ventilated offices within London’s urban heat island: In: *Building Services Engineering Research and Technology*. 33 (4) 351–369 pp.
 48. DENG, Y., FAN, F., CHEN, R. (2012): Extraction and Analysis of Impervious Surfaces Based on a Spectral Un-Mixing Method Using Pearl River Delta of China Landsat TM/ETM+ Imagery from 1998 to 2008. In: *Sensors*, 12 (2) 1846–1862 pp.
 49. DEPARTMENT OF THE INTERIOR, U.S. GEOLOGICAL SURVEY (2019): *Landsat 7 (L7) Data Users Handbook*. 151 pp.

50. DOICK, K. J., PEACE, A., HUTCHINGS, T. R. (2014): The role of one large greenspace in mitigating London's nocturnal urban heat island. In: *Science of The Total Environment*, 493 662–671 pp.
51. DOUGHERTY, J. (1981): BROADACRE CITY: FRANK LLOYD WRIGHT'S UTOPIA. In: *The Centennial Review*, 25 (3) 239–256 pp.
52. DU, H., CAI, W., XU, Y., WANG, Z., WANG, Y., CAI, Y. (2017): Quantifying the cool island effects of urban green spaces using remote sensing Data. In: *Urban Forestry & Urban Greening*, 27 24–31 pp.
53. DU, H., SONG, X., JIANG, H., KAN, Z., WANG, Z., CAI, Y. (2016): Research on the cooling island effects of water body: A case study of Shanghai, China. In: *Ecological Indicators*, 67 31–38 pp.
54. VAN ECK, N. J., WALTMAN, L. (2007): Bibliometric mapping of the computational intelligence field. In: *International Journal of Uncertainty, Fuzziness and Knowledge-Based Systems*, 15 (05) 625–645 pp.
55. ELIASSON, I. (1996): Intra-urban nocturnal temperature differences: a multivariate approach. In: *Climate Research*, 7 21–30 pp.
56. ERELL, E., PEARLMUTTER, D., BONEH, D., KUTIEL, P. B. (2014): Effect of high-albedo materials on pedestrian heat stress in urban street canyons. In: *Urban Climate*, 10 367–386 pp.
57. ESTOQUE, R. C., MURAYAMA, Y., MYINT, S. W. (2017): Effects of landscape composition and pattern on land surface temperature: An urban heat island study in the megacities of Southeast Asia. In: *Science of The Total Environment*, 577 349–359 pp.
58. FALAGAS, M. E., PITSOUNI, E. I., MALIETZIS, G. A., PAPPAS, G. (2008): Comparison of PubMed, Scopus, Web of Science, and Google Scholar: strengths and weaknesses. In: *FASEB Journal: Official Publication of the Federation of American Societies for Experimental Biology*, 22 (2) 338–342 pp.
59. FALLMANN, J., FORKEL, R., EMEIS, S. (2016): Secondary effects of urban heat island mitigation measures on air quality. In: *Atmospheric Environment*, 125 199–211 pp.
60. FAN, H., YU, Z., YANG, G., LIU, T. Y., LIU, T. Y., HUNG, C. H., VEJRE, H. (2019): How to cool hot-humid (Asian) cities with urban trees? An optimal landscape size perspective. In: *Agricultural and Forest Meteorology*, 265 338–348 pp.
61. FITTING, P. (2002): Urban Planning/Utopian Dreaming: Le Corbusier's Chandigarh Today. In: *Utopian Studies*, 13 (1) 69–93 pp.
62. FU, Y., LI, J., WENG, Q., ZHENG, Q., LI, L., DAI, S., GUO, B. (2019): Characterizing the spatial pattern of annual urban growth by using time series Landsat imagery. In: *Science of The Total Environment*, 666 274–284 pp.
63. FUNG, W. Y., LAM, K. S., NICHOL, J., WONG, M. S. (2009): Derivation of Nighttime Urban Air Temperatures Using a Satellite Thermal Image. In: *Journal of Applied Meteorology and Climatology*, 48 (4) 863–872 pp.
64. GAFFIN, S. R., ROSENZWEIG, C., KHANBILVARDI, R., PARSHALL, L., MAHANI, S., GLICKMAN, H., GOLDBERG, R., BLAKE, R., SLOSBERG, R. B., HILLEL, D. (2008): Variations in New York city's urban heat island strength over time and space. In: *Theoretical and Applied Climatology*, 94 (1) 1–11 pp.
65. GAGO, E. J., ROLDAN, J., PACHECO-TORRES, R., ORDÓÑEZ, J. (2013): The city and urban heat islands: A review of strategies to mitigate adverse effects. In: *Renewable and Sustainable Energy Reviews*, 25 749–758 pp.
66. GÁL, T., LINDBERG, F., UNGER, J. (2009): Computing continuous sky view factors using 3D urban raster and vector databases: comparison and application to urban climate. In: *Theoretical and Applied Climatology*, 95 (1–2) 111–123 pp.
67. GALAGODA, R. U., JAYASINGHE, G. Y., HALWATURA, R. U., RUPASINGHE, H. T. (2018): The impact of urban green infrastructure as a sustainable approach towards tropical micro-climatic changes and human thermal

- comfort. In: *Urban Forestry & Urban Greening*, 34 1–9 pp.
68. GAO, B. (1996): NDWI—A normalized difference water index for remote sensing of vegetation liquid water from space. In: *Remote Sensing of Environment*, 58 (3) 257–266 pp.
 69. GARTLAND, L. (2008): *Heat islands: understanding and mitigating heat in urban areas*. London ; Sterling, VA: Earthscan. 192 p.
 70. GIANNINI, M. B., BELFIORE, O. R., PARENTE, C., SANTAMARIA, R. (2015): Land Surface Temperature from Landsat 5 TM images: comparison of different methods using airborne thermal data. In: *Journal of Engineering Science and Technology Review*, 8 (3) 83–90 pp. 83–90 pp.
 71. GIRIDHARAN, R., KOLOKOTRONI, M. (2009): Urban heat island characteristics in London during winter. In: *Solar Energy*, 83 (9) 1668–1682 pp.
 72. GOLDEN, J. S. (2004): The Built Environment Induced Urban Heat Island Effect in Rapidly Urbanizing Arid Regions – A Sustainable Urban Engineering Complexity. In: *Environmental Sciences*, 1 (4) 321–349 pp.
 73. GÖNDÖCS, J., BREUER, H., PONGRÁCZ, R., BARTHOLY, J. (2017): Urban heat island mesoscale modelling study for the Budapest agglomeration area using the WRF model. In: *Urban Climate*, 21 66–86 pp.
 74. GRIEND, A. A. V. D., OWE, M. (1993): On the relationship between thermal emissivity and the normalized difference vegetation index for natural surfaces. In: *International Journal of Remote Sensing*, 14 (6) 1119–1131 pp.
 75. GRIMMOND, C. S. B., OKE, T. R. (1999): Heat Storage in Urban Areas: Local-Scale Observations and Evaluation of a Simple Model. In: *Journal of Applied Meteorology*, 38 (7) 922–940 pp.
 76. GRIMMOND, C. S. B., OKE, T. R. (2002): Turbulent Heat Fluxes in Urban Areas: Observations and a Local-Scale Urban Meteorological Parameterization Scheme (LUMPS). In: *Journal of Applied Meteorology*, 41 (7) 792–810 pp.
 77. GROFFMAN, P. M., CAVENDER-BARES, J., BETTEZ, N. D., GROVE, J. M., HALL, S. J., HEFFERNAN, J. B., HOBBIE, S. E., LARSON, K. L., MORSE, J. L., NEILL, C., NELSON, K., O’NEIL-DUNNE, J., OGDEN, L., PATAKI, D. E., POLSKY, C., CHOWDHURY, R. R., STEELE, M. K. (2014): Ecological homogenization of urban USA. In: *Frontiers in Ecology and the Environment*, 12 (1) 74–81 pp.
 78. GULYÁS, Á., UNGER, J., MATZARAKIS, A. (2006): Assessment of the microclimatic and human comfort conditions in a complex urban environment: Modelling and measurements. In: *Building and Environment*, 41 (12) 1713–1722 pp.
 79. GUNAWARDENA, K. R., WELLS, M. J., KERSHAW, T. (2017): Utilising green and bluespace to mitigate urban heat island intensity. In: *Science of The Total Environment*, 584–585 1040–1055 pp.
 80. HAGGETT, P., CLIFF, A. D., & FREY, A. (1977). *Locational analysis in human geography* (Vol. 2, pp. 259-605). London: Arnold.
 81. HAMADA, S., OHTA, T. (2010): Seasonal variations in the cooling effect of urban green areas on surrounding urban areas. In: *Urban Forestry & Urban Greening*, 9 (1) 15–24 pp.
 82. HAMADA, S., TANAKA, T., OHTA, T. (2013): Impacts of land use and topography on the cooling effect of green areas on surrounding urban areas. In: *Urban Forestry & Urban Greening*, 12 (4) 426–434 pp.
 83. HÄMMERLE, M., GÁL, T., UNGER, J., MATZARAKIS, A. (2011): Comparison of models calculating the sky view factor used for urban climate investigations. In: *Theoretical and Applied Climatology*, 105 (3–4) 521–527 pp.
 84. HANSEN, J., RUEDY, R., SATO, M., LO, K. (2010): Global Surface Temperature Change. In: *Reviews of Geophysics*, 48 (4) pp.

85. HART, M. A., SAILOR, D. J. (2009): Quantifying the influence of land-use and surface characteristics on spatial variability in the urban heat island. In: *Theoretical and Applied Climatology*, 95 (3) 397–406 pp.
86. HIEN, W. N., JUSUF, S. K., SAMSUDIN, R., ELIZA, A., IGNATIUS, M. (2011): A Climatic Responsive Urban Planning Model for High Density City: Singapore’s Commercial District. In: *International Journal of Sustainable Building Technology and Urban Development*, 2 (4) 323–330 pp.
87. HONG, J.-W., HONG, J., KWON, E. E., YOON, D. K. (2019): Temporal dynamics of urban heat island correlated with the socio-economic development over the past half-century in Seoul, Korea. In: *Environmental Pollution*, 254 112934 pp.
88. HOWARD, L. (1818): *The Climate of London: Deduced from Meteorological Observations, Made at Different Places in the Neighbourhood of the Metropolis*. W. Phillips, sold also by J. and A. Arch. 376 p.
89. HRISKO, J., RAMAMURTHY, P., MELECIO-VÁZQUEZ, D., GONZALEZ, J. E. (2021): Spatiotemporal Variability of Heat Storage in Major U.S. Cities—A Satellite-Based Analysis. In: *Remote Sensing*, 13 (1) 59 pp.
90. HUANG, Q., GUO, H., XI, X., LI, X., DU, X., YANG, H. (2012): Improved method of Land Surface Emissivity retrieval from Landsat TM/ETM+ data. In: *2012 IEEE International Geoscience and Remote Sensing Symposium*. 4206–4208 pp.
91. HÜTT, C., KOPPE, W., MIAO, Y., BARETH, G. (2016): Best Accuracy Land Use/Land Cover (LULC) Classification to Derive Crop Types Using Multitemporal, Multisensor, and Multi-Polarization SAR Satellite Images. In: *Remote Sensing*, 8 (8) 684 pp.
92. ISAYA NDOSSI, M., AVDAN, U. (2016): Application of Open Source Coding Technologies in the Production of Land Surface Temperature (LST) Maps from Landsat: A PyQGIS Plugin. In: *Remote Sensing*, 8 (5) 413 pp.
93. JAMEI, E., RAJAGOPALAN, P., SEYEDMAHMOUDIAN, M., JAMEI, Y. (2016): Review on the impact of urban geometry and pedestrian level greening on outdoor thermal comfort. In: *Renewable and Sustainable Energy Reviews*, 54 1002–1017 pp.
94. JANSSON, C., JANSSON, P.-E., GUSTAFSSON, D. (2007): Near surface climate in an urban vegetated park and its surroundings. In: *Theoretical and Applied Climatology*, 89 (3) 185–193 pp.
95. JENDRITZKY, G., NÜBLER, W. (1981): A model analysing the urban thermal environment in physiologically significant terms. In: *Archives for Meteorology, Geophysics, and Bioclimatology, Series B*, 29 (4) 313–326 pp.
96. JENERETTE, G. D., HARLAN, S. L., BRAZEL, A., JONES, N., LARSEN, L., STEFANOV, W. L. (2007): Regional relationships between surface temperature, vegetation, and human settlement in a rapidly urbanizing ecosystem. In: *Landscape Ecology*, 22 (3) 353–365 pp.
97. JIANG, J., TIAN, G. (2010): Analysis of the impact of Land use/Land cover change on Land Surface Temperature with Remote Sensing. In: *Procedia Environmental Sciences*, 2 571–575 pp.
98. JIANG, Z., HUETE, A. R., CHEN, J., CHEN, Y., LI, J., YAN, G., ZHANG, X. (2006): Analysis of NDVI and scaled difference vegetation index retrievals of vegetation fraction. In: *Remote Sensing of Environment*, 101 (3) 366–378 pp.
99. JIMENEZ-MUNOZ, J. C., CRISTOBAL, J., SOBRINO, J. A., SORIA, G., NINYEROLA, M., PONS, X. (2009): Revision of the Single-Channel Algorithm for Land Surface Temperature Retrieval From Landsat Thermal-Infrared Data. In: *IEEE Transactions on Geoscience and Remote Sensing*, 47 (1) 339–349 pp.
100. JIMÉNEZ - MUÑOZ, J. C., SOBRINO, J. A. (2003): A generalized single-channel method for retrieving land surface temperature from remote sensing data. In: *Journal of Geophysical Research: Atmospheres*, 108 (D22) pp.
101. JIMÉNEZ - MUÑOZ, J. C., SOBRINO, J. A. (2004): Correction to “A generalized single-channel method for retrieving land surface temperature from remote sensing data” by Juan C. Jiménez-Muñoz and José A. Sobrino. In: *Journal of Geophysical Research: Atmospheres*, 109 (D8) pp.

102. JIMÉNEZ-MUÑOZ, J. C., SOBRINO, J. A., SKOKOVIĆ, D., MATTAR, C., CRISTÓBAL, J. (2014): Land Surface Temperature Retrieval Methods From Landsat-8 Thermal Infrared Sensor Data. In: *IEEE Geoscience and Remote Sensing Letters*, 11 (10) 1840–1843 pp.
103. JIMENEZ-MUNOZ, Juan C., SOBRINO, J. A. (2010): A Single-Channel Algorithm for Land-Surface Temperature Retrieval From ASTER Data. In: *IEEE Geoscience and Remote Sensing Letters*, 7 (1) 176–179 pp.
104. KANDA, M., MORIIZUMI, T. (2009): Momentum and Heat Transfer over Urban-like Surfaces. In: *Boundary-Layer Meteorology*, 131 (3) 385–401 pp.
105. KARILA, K., MATIKAINEN, L., LITKEY, P., HYYPPÄ, J., PUTTONEN, E. (2019): The effect of seasonal variation on automated land cover mapping from multispectral airborne laser scanning data. In: *International Journal of Remote Sensing*, 40 (9) 3289–3307 pp.
106. KARL, T. R., DIAZ, H. F., KUKLA, G. (1988): Urbanization: Its Detection and Effect in the United States Climate Record. In: *Journal of Climate*, 1 (11) 1099–1123 pp.
107. KATO, Soushi, YAMAGUCHI, Y. (2007): Estimation of storage heat flux in an urban area using ASTER data. In: *Remote Sensing of Environment*, 110 (1) 1–17 pp.
108. KATO, Shinsuke, HIYAMA, K. (EDS.) (2012): *Ventilating cities: air-flow criteria for healthy and comfortable urban living*. Dordrecht ; New York: Springer. 197 p.
109. KATSOULAS, N., ANTONIADIS, D., TSIROGIANNIS, I. L., LABRAKI, E., BARTZANAS, T., KITTAS, C. (2017): Microclimatic effects of planted hydroponic structures in urban environment: measurements and simulations. In: *International Journal of Biometeorology*, 61 (5) 943–956 pp.
110. KAWASHIMA, S. (1990): Effect of vegetation on surface temperature in urban and suburban areas in winter. In: *Energy and Buildings*, 15 (3–4) 465–469 pp.
111. KHANDELWAL, S., GOYAL, R., KAUL, N., MATHEW, A. (2018): Assessment of land surface temperature variation due to change in elevation of area surrounding Jaipur, India. In: *The Egyptian Journal of Remote Sensing and Space Science*, 21 (1) 87–94 pp.
112. KIKON, N., SINGH, P., SINGH, S. K., VYAS, A. (2016): Assessment of urban heat islands (UHI) of Noida City, India using multi-temporal satellite data. In: *Sustainable Cities and Society*, 22 19–28 pp.
113. KIM, Y.-H., BAIK, J.-J. (2005): Spatial and Temporal Structure of the Urban Heat Island in Seoul. In: *Journal of Applied Meteorology and Climatology*, 44 (5) 591–605 pp.
114. KLYSIK, K., FORTUNIAK, K. (1999): Temporal and spatial characteristics of the urban heat island of Łódź, Poland. In: *Atmospheric Environment*, 33 (24) 3885–3895 pp.
115. KOLOKOTRONI, M., GIRIDHARAN, R. (2008): Urban heat island intensity in London: An investigation of the impact of physical characteristics on changes in outdoor air temperature during summer. In: *Solar Energy*, 82 (11) 986–998 pp.
116. KONG, F., YIN, H., WANG, C., CAVAN, G., JAMES, P. (2014): A satellite image-based analysis of factors contributing to the green-space cool island intensity on a city scale. In: *Urban Forestry & Urban Greening*, 13 (4) 846–853 pp.
117. KOTTHAUS, S., GRIMMOND, C. S. B. (2014): Energy exchange in a dense urban environment – Part I: Temporal variability of long-term observations in central London. In: *Urban Climate*, 10 261–280 pp.
118. LANDSBERG, H. E. (1981): *The urban climate*. New York: Academic Press. 275 p.
119. LEE, H., MAYER, H. (2016): Validation of the mean radiant temperature simulated by the RayMan software in urban environments. In: *International Journal of Biometeorology*, 60 (11) 1775–1785 pp.

120. LEE, P. S.-H., PARK, J. (2020): An Effect of Urban Forest on Urban Thermal Environment in Seoul, South Korea, Based on Landsat Imagery Analysis. In: *Forests*, 11 (6) 630 pp.
121. LEE, S.-H., BAIK, J.-J. (2010): Statistical and dynamical characteristics of the urban heat island intensity in Seoul. In: *Theoretical and Applied Climatology*, 100 (1) 227–237 pp.
122. LEE, T.-W., LEE, J. Y., WANG, Z.-H. (2012): Scaling of the urban heat island intensity using time-dependent energy balance. In: *Urban Climate*, 2 16–24 pp.
123. LEITAO, A. B., MILLER, J., AHERN, J., MCGARIGAL, K. (2012): *Measuring Landscapes: A Planner's Handbook*. Island Press. 277 p.
124. LI, B., SHI, X., WANG, H., QIN, M. (2020): Analysis of the relationship between urban landscape patterns and thermal environment: a case study of Zhengzhou City, China. In: *Environmental Monitoring and Assessment*, 192 (8) 540 pp.
125. LI, HUAWEI, WANG, G., JOMBACH, S. (2020): Characteristics of Winter Urban Heat Island in Budapest at Local and Micro Scale. In: *Journal of Environmental Geography*, 13 (3–4) 34–43 pp.
126. LI, HUAWEI, WANG, G., TIAN, G., JOMBACH, S. (2019a): Mapping and Assessment of the Urban Heat Island in Zhengzhou City. In: *Proceedings of the Fábos Conference on Landscape and Greenway Planning*, 6 (1) pp.
127. LI, HUAWEI, WANG, G., TIAN, G., JOMBACH, S. (2020): Mapping and Analyzing the Park Cooling Effect on Urban Heat Island in an Expanding City: A Case Study in Zhengzhou City, China. In: *Land*, 9 (2) 57 pp.
128. LI, HUIDONG, ZHOU, Y., WANG, X., ZHOU, X., ZHANG, H., SODOUDI, S. (2019): Quantifying urban heat island intensity and its physical mechanism using WRF/UCM. In: *Science of The Total Environment*, 650 3110–3119 pp.
129. LI, J., WANG, X., WANG, X., MA, W., ZHANG, H. (2009): Remote sensing evaluation of urban heat island and its spatial pattern of the Shanghai metropolitan area, China. In: *Ecological Complexity*, 6 (4) 413–420 pp.
130. LI, Y., ZHANG, H., KAINZ, W. (2012): Monitoring patterns of urban heat islands of the fast-growing Shanghai metropolis, China: Using time-series of Landsat TM/ETM+ data. In: *International Journal of Applied Earth Observation and Geoinformation*, 19 127–138 pp.
131. LIN, B.-S., LIN, Y.-J. (2010): Cooling Effect of Shade Trees with Different Characteristics in a Subtropical Urban Park. In: *HortScience*, 45 (1) 83–86 pp.
132. LIN, W., YU, T., CHANG, X., WU, W., ZHANG, Y. (2015): Calculating cooling extents of green parks using remote sensing: Method and test. In: *Landscape and Urban Planning*, 134 66–75 pp.
133. LINDBERG, F., GRIMMOND, C. S. B., GABEY, A., HUANG, B., KENT, C. W., SUN, T., THEEUWES, N. E., JÄRVI, L., WARD, H. C., CAPEL-TIMMS, I., CHANG, Y., JONSSON, P., KRAVE, N., LIU, D., MEYER, D., OLOFSON, K. F. G., TAN, J., WÄSTBERG, D., XUE, L., ZHANG, Z. (2018): Urban Multi-scale Environmental Predictor (UMEP): An integrated tool for city-based climate services. In: *Environmental Modelling & Software*, 99 70–87 pp.
134. LINDÉN, J., FONTI, P., ESPER, J. (2016): Temporal variations in microclimate cooling induced by urban trees in Mainz, Germany. In: *Urban Forestry & Urban Greening*, 20 198–209 pp.
135. LITVAK, E., MANAGO, K. F., HOGUE, T. S., PATAKI, D. E. (2017): Evapotranspiration of urban landscapes in Los Angeles, California at the municipal scale. In: *Water Resources Research*, 53 (5) 4236–4252 pp.
136. LIU, H., WENG, Q. (2008): Seasonal variations in the relationship between landscape pattern and land surface temperature in Indianapolis, USA. In: *Environmental Monitoring and Assessment*, 144 (1–3) 199–219 pp.
137. LOSOSOVÁ, Z., CHYTRÝ, M., TICHÝ, L., DANIHELKA, J., FAJMON, K., HÁJEK, O., KINTROVÁ, K.,

- LÁNÍKOVÁ, D., OTÝPKOVÁ, Z., ŘEHOŘEK, V. (2012): Biotic homogenization of Central European urban floras depends on residence time of alien species and habitat types. In: *Biological Conservation*, 145 (1) 179–184 pp.
138. MAO, J., YANG, J. H., AFSHARI, A., NORFORD, L. K. (2017): Global sensitivity analysis of an urban microclimate system under uncertainty: Design and case study. In: *Building and Environment*, 124 153–170 pp.
139. MAO, K., QIN, Z., SHI, J., GONG, P. (2005): A practical split - window algorithm for retrieving land - surface temperature from MODIS data. In: *International Journal of Remote Sensing*, 26 (15) 3181–3204 pp.
140. MASTERTON, J. M., RICHARDSON, F. A. (1979): Humidex: a method of quantifying human discomfort due to excessive heat and humidity. Environment Canada, Atmospheric Environment. 45 pp.
141. MATHEW, A., KHANDELWAL, S., KAUL, N. (2017): Investigating spatial and seasonal variations of urban heat island effect over Jaipur city and its relationship with vegetation, urbanization and elevation parameters. In: *Sustainable Cities and Society*, 35 157–177 pp.
142. MEMON, R. A., LEUNG, D. Y. C. (2010): Impacts of environmental factors on urban heating. In: *Journal of Environmental Sciences*, 22 (12) 1903–1909 pp. 1903–1909 pp.
143. MIAO S., CHEN F., LEMONE M. A., TEWARI M., LI Q., WANG Y. (2009): An Observational and Modeling Study of Characteristics of Urban Heat Island and Boundary Layer Structures in Beijing. In: *Journal of Applied Meteorology and Climatology*, 48 (3) 484–501 pp.
144. MIDDEL, A., BRAZEL, A. J., GOBER, P., MYINT, S. W., CHANG, H., DUH, J.-D. (2012): Land cover, climate, and the summer surface energy balance in Phoenix, AZ, and Portland, OR. In: *International Journal of Climatology*, 32 (13) 2020–2032 pp.
145. MIN, M., ZHAO, H., MIAO, C. (2018): Spatio-Temporal Evolution Analysis of the Urban Heat Island: A Case Study of Zhengzhou City, China. In: *Sustainability*, 10 (6) 1992 pp.
146. MIRZAEI, P. A. (2015): Recent challenges in modeling of urban heat island. In: *Sustainable Cities and Society*, 19 200–206 pp.
147. MIRZAEI, P. A., HAGHIGHAT, F. (2010): Approaches to study Urban Heat Island – Abilities and limitations. In: *Building and Environment*, 45 (10) 2192–2201 pp.
148. MOHAJERANI, A., BAKARIC, J., JEFFREY-BAILEY, T. (2017): The urban heat island effect, its causes, and mitigation, with reference to the thermal properties of asphalt concrete. In: *Journal of Environmental Management*, 197 522–538 pp.
149. MOHAMED, A. A., ODINDI, J., MUTANGA, O. (2017): Land surface temperature and emissivity estimation for Urban Heat Island assessment using medium- and low-resolution space-borne sensors: A review. In: *Geocarto International*, 32 (4) 455–470 pp.
150. MONGEON, P., PAUL-HUS, A. (2016): The journal coverage of Web of Science and Scopus: a comparative analysis. In: *Scientometrics*, 106 (1) 213–228 pp.
151. MONTEITH, J. L., UNSWORTH, M. H. (2013): Principles of environmental physics: plants, animals, and the atmosphere. Amsterdam ; Boston: Elsevier/Academic Press. 401 p.
152. MORRIS, C. J. G., SIMMONDS, I., PLUMMER, N. (2001): Quantification of the Influences of Wind and Cloud on the Nocturnal Urban Heat Island of a Large City. In: *Journal of Applied Meteorology and Climatology*, 40 (2) 169–182 pp.
153. MU, B., MAYER, A. L., HE, R., TIAN, G. (2016): Land use dynamics and policy implications in Central China: A case study of Zhengzhou. In: *Cities*, 58 39–49 pp.
154. NDOSSI, M. I., AVDAN, U. (2016): Inversion of Land Surface Temperature (LST) Using Terra ASTER Data:

- A Comparison of Three Algorithms. In: *Remote Sensing*, 8 (12) 993 pp.
155. NG, E., CHEN, L., WANG, Y., YUAN, C. (2012): A study on the cooling effects of greening in a high-density city: An experience from Hong Kong. In: *Building and Environment*, 47 256–271 pp.
 156. NG, E., YUAN, C., CHEN, L., REN, C., FUNG, J. C. H. (2011): Improving the wind environment in high-density cities by understanding urban morphology and surface roughness: A study in Hong Kong. In: *Landscape and Urban Planning*, 101 (1) 59–74 pp.
 157. NICHOL, J. (2005): Remote Sensing of Urban Heat Islands by Day and Night. In: *Photogrammetric Engineering & Remote Sensing*, 71 (5) 613–621 pp.
 158. NORMAN, J. M., JARVIS, P. G. (1974): Photosynthesis in Sitka Spruce (*Picea sitchensis* (Bong.) Carr.). III. Measurements of Canopy Structure and Interception of Radiation. In: *Journal of Applied Ecology*, 11 (1) 375–398 pp.
 159. NUNEZ, M., OKE, T. R. (1977): The Energy Balance of an Urban Canyon. In: *Journal of Applied Meteorology and Climatology*, 16 (1) 11–19 pp.
 160. OFFERLE, B., GRIMMOND, C. S. B., FORTUNIAK, K., KŁYSIK, K., OKE, T. R. (2006): Temporal variations in heat fluxes over a central European city centre. In: *Theoretical and Applied Climatology*, 84 (1) 103–115 pp.
 161. OKE, T. R. (1973): City size and the urban heat island. In: *Atmospheric Environment* (1967), 7 (8) 769–779 pp.
 162. OKE, T. R. (1982): The energetic basis of the urban heat island. In: *Quarterly Journal of the Royal Meteorological Society*, 108 (455) 1–24 pp.
 163. OKE, T. R. (1988): Street design and urban canopy layer climate. In: *Energy and Buildings*, 11 (1) 103–113 pp.
 164. OKE, T. R. (2009): Chandler, T.J. 1965: The climate of London. London: Hutchinson, 292 pp. In: *Progress in Physical Geography: Earth and Environment*, 33 (3) 437–442 pp.
 165. OKE, T. R., CLEUGH, H. A. (1987): Urban heat storage derived as energy balance residuals. In: *Boundary-Layer Meteorology*, 39 (3) 233–245 pp.
 166. OKE, T. R., EAST, C. (1971): The urban boundary layer in Montreal. In: *Boundary-Layer Meteorology*, 1 (4) 411–437 pp.
 167. OKE, T. R., FUGGLE, R. F. (1972): Comparison of urban/rural counter and net radiation at night. In: *Boundary-Layer Meteorology*, 2 (3) 290–308 pp.
 168. OKE, T. R., ZEUNER, G., JAUREGUI, E. (1992): The surface energy balance in Mexico City. In: *Atmospheric Environment. Part B. Urban Atmosphere*, 26 (4) 433–444 pp.
 169. OLIVEIRA, S., ANDRADE, H., VAZ, T. (2011): The cooling effect of green spaces as a contribution to the mitigation of urban heat: A case study in Lisbon. In: *Building and Environment*, 46 (11) 2186–2194 pp.
 170. OOKA, R., SATO, T., HARAYAMA, K., MURAKAMI, S., KAWAMOTO, Y. (2011): Thermal Energy Balance Analysis of the Tokyo Metropolitan Area Using a Mesoscale Meteorological Model Incorporating an Urban Canopy Model. In: *Boundary-Layer Meteorology*, 138 (1) 77–97 pp.
 171. OTSU, N. (1979): A Threshold Selection Method from Gray-Level Histograms. In: *IEEE Transactions on Systems, Man, and Cybernetics*, 9 (1) 62–66 pp.
 172. PARK, J., KIM, J.-H., LEE, D. K., PARK, C. Y., JEONG, S. G. (2017): The influence of small green space type and structure at the street level on urban heat island mitigation. In: *Urban Forestry & Urban Greening*, 21 203–212 pp.
 173. PLA, F., LATORRE-CARMONA, P., MYINT, S. W., CAETANO, M., KIEU, H. V. (2017): Characterizing the relationship between land use land cover change and land surface temperature. In: *ISPRS Journal of Photogrammetry and Remote Sensing*, 124 119–132 pp.
 174. PLANCK, M. (2013): The theory of heat radiation. Courier Corporation

175. PRICE, J. C. (1983): Estimating surface temperatures from satellite thermal infrared data—A simple formulation for the atmospheric effect. In: *Remote Sensing of Environment*, 13 (4) 353–361 pp.
176. PRICE, J. C. (1984): Land surface temperature measurements from the split window channels of the NOAA 7 Advanced Very High Resolution Radiometer. In: *Journal of Geophysical Research: Atmospheres*, 89 (D5) 7231–7237 pp.
177. QIAN, S., QI, M., HUANG, L., ZHAO, L., LIN, D., YANG, Y. (2016): Biotic homogenization of China's urban greening: A meta-analysis on woody species. In: *Urban Forestry & Urban Greening*, 18 25–33 pp.
178. QIN, Z., KARNIELI, A., BERLINER, P. (2001): A mono-window algorithm for retrieving land surface temperature from Landsat TM data and its application to the Israel-Egypt border region. In: *International Journal of Remote Sensing*, 22 (18) 3719–3746 pp.
179. RASUL, A., BALZTER, H., SMITH, C., REMEDIOS, J., ADAMU, B., SOBRINO, J., SRIVANIT, M., WENG, Q. (2017): A Review on Remote Sensing of Urban Heat and Cool Islands. In: *Land*, 6 (2) 38 pp.
180. REICHLER, D. E. (2020): Chapter 11 - Anthropogenic alterations to the global carbon cycle and climate change. In: D. E. Reichler (Ed.), *The Global Carbon Cycle and Climate Change*. Elsevier. 209–251 pp.
181. REN G., ZHOU Y., CHU Z., ZHOU J., ZHANG A., GUO J., LIU X. (2008): Urbanization Effects on Observed Surface Air Temperature Trends in North China. In: *Journal of Climate*, 21 (6) 1333–1348 pp.
182. RIZWAN, A. M., DENNIS, L. Y. C., LIU, C. (2008): A review on the generation, determination and mitigation of Urban Heat Island. In: *Journal of Environmental Sciences*, 20 (1) 120–128 pp.
183. ROBERTS, S. M., OKE, T. R., GRIMMOND, C. S. B., VOOGT, J. A. (2006): Comparison of Four Methods to Estimate Urban Heat Storage. In: *Journal of Applied Meteorology and Climatology*, 45 (12) 1766–1781 pp.
184. RODLER, A., LEDUC, T. (2019): Local climate zone approach on local and micro scales: Dividing the urban open space. In: *Urban Climate*, 28 100457 pp.
185. ROMERO RODRÍGUEZ, L., SÁNCHEZ RAMOS, J., SÁNCHEZ DE LA FLOR, F. J., ÁLVAREZ DOMÍNGUEZ, S. (2020): Analyzing the urban heat Island: Comprehensive methodology for data gathering and optimal design of mobile transects. In: *Sustainable Cities and Society*, 55 102027 pp.
186. SAILOR, D. J., LU, L. (2004): A top-down methodology for developing diurnal and seasonal anthropogenic heating profiles for urban areas. In: *Atmospheric Environment*, 38 (17) 2737–2748 pp.
187. SALVATI, A., PALME, M., CHIESA, G., KOLOKOTRONI, M. (2020): Built form, urban climate and building energy modelling: case-studies in Rome and Antofagasta. In: *Journal of Building Performance Simulation*, 13 (2) 209–225 pp.
188. SANGIORGIO, V., FIORITO, F., SANTAMOURIS, M. (2020): Development of a holistic urban heat island evaluation methodology. In: *Scientific Reports*, 10 (1) 17913 pp.
189. SANTAMOURIS, M., CARTALIS, C., SYNNEFA, A., KOLOKOTSA, D. (2015): On the impact of urban heat island and global warming on the power demand and electricity consumption of buildings—A review. In: *Energy and Buildings*, 98 119–124 pp.
190. SEKERTEKIN, A. (2019): Validation of Physical Radiative Transfer Equation-Based Land Surface Temperature Using Landsat 8 Satellite Imagery and SURFRAD in-situ Measurements. In: *Journal of Atmospheric and Solar-Terrestrial Physics*, 196 105161 pp.
191. SEKERTEKIN, A., BONAFONI, S. (2020): Land Surface Temperature Retrieval from Landsat 5, 7, and 8 over Rural Areas: Assessment of Different Retrieval Algorithms and Emissivity Models and Toolbox Implementation. In: *Remote Sensing*, 12 (2) 294 pp.
192. SEZGIN, M., SANKUR, B. (2004): Survey over image thresholding techniques and quantitative performance evaluation. In: *Journal of Electronic Imaging*, 13 (1) 146–165 pp.

193. SHARMIN, T., STEEMERS, K., HUMPHREYS, M. (2019): Outdoor thermal comfort and summer PET range: A field study in tropical city Dhaka. In: *Energy and Buildings*, 198 149–159 pp.
194. SHASHUA-BAR, L., PEARLMUTTER, D., ERELL, E. (2009): The cooling efficiency of urban landscape strategies in a hot dry climate. In: *Landscape and Urban Planning*, 92 (3) 179–186 pp.
195. SHEN, H., HUANG, L., ZHANG, L., WU, P., ZENG, C. (2016): Long-term and fine-scale satellite monitoring of the urban heat island effect by the fusion of multi-temporal and multi-sensor remote sensed data: A 26-year case study of the city of Wuhan in China. In: *Remote Sensing of Environment*, 172 109–125 pp.
196. SHI, D., SONG, J., HUANG, J., ZHUANG, C., GUO, R., GAO, Y. (2020): Synergistic cooling effects (SCEs) of urban green-blue spaces on local thermal environment: A case study in Chongqing, China. In: *Sustainable Cities and Society*, 55 102065 pp.
197. SHIRANI-BIDABADI, N., NASRABADI, T., FARYADI, S., LARIJANI, A., SHADMAN ROODPOSHTI, M. (2019): Evaluating the spatial distribution and the intensity of urban heat island using remote sensing, case study of Isfahan city in Iran. In: *Sustainable Cities and Society*, 45 686–692 pp.
198. SINHA, S., PANDEY, P. C., SHARMA, L. K., NATHAWAT, M. S., KUMAR, P., KANGA, S. (2014): Remote Estimation of Land Surface Temperature for Different LULC Features of a Moist Deciduous Tropical Forest Region. In: Prashant K. Srivastava, S. Mukherjee, M. Gupta, & T. Islam (Eds.), *Remote Sensing Applications in Environmental Research*. Cham: Springer International Publishing. 57–68 pp.
199. SIU, L. W., HART, M. A. (2013): Quantifying urban heat island intensity in Hong Kong SAR, China. In: *Environmental Monitoring and Assessment*, 185 (5) 4383–4398 pp.
200. SKELHORN, C., LINDLEY, S., LEVERMORE, G. (2014): The impact of vegetation types on air and surface temperatures in a temperate city: A fine scale assessment in Manchester, UK. In: *Landscape and Urban Planning*, 121 129–140 pp.
201. SKOULIKA, F., SANTAMOURIS, M., KOLOKOTSA, D., BOEMI, N. (2014): On the thermal characteristics and the mitigation potential of a medium size urban park in Athens, Greece. In: *Landscape and Urban Planning*, 123 73–86 pp.
202. SOBRINO, J. A., LI, Z.-L., STOLL, M. P., BECKER, F. (1996): Multi-channel and multi-angle algorithms for estimating sea and land surface temperature with ATSR data. In: *International Journal of Remote Sensing*, 17 (11) 2089–2114 pp.
203. SOBRINO, J. A., RAISSOUNI, N., LI, Z.-L. (2001): A Comparative Study of Land Surface Emissivity Retrieval from NOAA Data. In: *Remote Sensing of Environment*, 75 (2) 256–266 pp.
204. SOBRINO, José A., JIMÉNEZ-MUÑOZ, J. C. (2014): Minimum configuration of thermal infrared bands for land surface temperature and emissivity estimation in the context of potential future missions. In: *Remote Sensing of Environment*, 148 158–167 pp.
205. SPRONKEN-SMITH, R. A., OKE, T. R. (1998): The thermal regime of urban parks in two cities with different summer climates. In: *International Journal of Remote Sensing*, 19 (11) 2085–2104 pp.
206. SRIVASTAVA, P. K., MAJUMDAR, T. J., BHATTACHARYA, A. K. (2009): Surface temperature estimation in Singhbhum Shear Zone of India using Landsat-7 ETM+ thermal infrared data. In: *Advances in Space Research*, 43 (10) 1563–1574 pp.
207. STATHOPOULOU, M., CARTALIS, C. (2007): Use of Satellite Remote Sensing in Support of Urban Heat Island Studies. In: *Advances in Building Energy Research*, 1 (1) 203–212 pp.
208. STEENEVELD, G. J., KOOPMANS, S., HEUSINKVELD, B. G., THEEUWES, N. E. (2014): Refreshing the role of open water surfaces on mitigating the maximum urban heat island effect. In: *Landscape and Urban Planning*, 121 92–96 pp.

209. STEVAN, S., JANOS, U., TAMAS, G., DRAGAN, M., ZLATICA, P. (2013): Urban heat island research of novi sad (serbia): A review. In: *GEOGRAPHICA PANNONICA*, 17 (1) 32–36 pp.
210. SUN, Z., WANG, C., GUO, H., SHANG, R. (2017): A Modified Normalized Difference Impervious Surface Index (MNDISI) for Automatic Urban Mapping from Landsat Imagery. In: *Remote Sensing*, 9 (9) 942 pp.
211. SUSSKIND, J., ROSENFELD, J., REUTER, D., CHAHINE, M. T. (1984): Remote sensing of weather and climate parameters from HIRS2/MSU on TIROS-N. In: *Journal of Geophysical Research: Atmospheres*, 89 (D3) 4677–4697 pp.
212. TAHA, H. (1997): Urban climates and heat islands: albedo, evapotranspiration, and anthropogenic heat. In: *Energy and Buildings*, 25 (2) 99–103 pp.
213. TALEGHANI, M., KLEEREKOPER, L., TENPIERIK, M., VAN DEN DOBBELSTEEN, A. (2015): Outdoor thermal comfort within five different urban forms in the Netherlands. In: *Building and Environment*, 83 65–78 pp.
214. TERRAY, L., CASSOU, C. (2000): Modes of low-frequency climate variability and their relationships with land precipitation and surface temperature: application to the Northern Hemisphere winter climate. In: *Stochastic Environmental Research and Risk Assessment*, 14 (4) 0339–0369 pp.
215. THANI, S. K. S. O., MOHAMAD, N. H. N., ABDULLAH, S. M. S. (2013): The Influence of Urban Landscape Morphology on the Temperature Distribution of Hot-Humid Urban Centre. In: *Procedia - Social and Behavioral Sciences*, 85 356–367 pp.
216. THORSSON, S., LINDBERG, F., ELIASSON, I., HOLMER, B. (2007): Different methods for estimating the mean radiant temperature in an outdoor urban setting. In: *International Journal of Climatology*, 27 (14) 1983–1993 pp.
217. TIAN, L., LI, Y., LU, J., WANG, J. (2021): Review on Urban Heat Island in China: Methods, Its Impact on Buildings Energy Demand and Mitigation Strategies. In: *Sustainability*, 13 (2) 762 pp.
218. TIZOT, J.-Y. (2018): Ebenezer Howard’s Garden City Idea and the Ideology of Industrialism. In: *Cahiers Victoriens et Édouardiens*, (87 Printemps).
219. TOMLINSON, C. J., CHAPMAN, L., THORNES, J. E., BAKER, C. (2011a): Remote sensing land surface temperature for meteorology and climatology: a review. In: *Meteorological Applications*, 18 (3) 296–306 pp.
220. TOMLINSON, C. J., CHAPMAN, L., THORNES, J. E., BAKER, C. J. (2011b): Including the urban heat island in spatial heat health risk assessment strategies: a case study for Birmingham, UK. In: *International Journal of Health Geographics*, 10 (1) 42 pp.
221. TOWNSHEND, J. R. G., JUSTICE, C. O., SKOLE, D., MALINGREAU, J.-P., CIHLAR, J., TEILLET, P., SADOWSKI, F., RUTTENBERG, S. (1994): The 1 km resolution global data set: needs of the International Geosphere Biosphere Programme†. In: *International Journal of Remote Sensing*, 15 (17) 3417–3441 pp.
222. TSOU, J., ZHUANG, J., LI, Y., ZHANG, Y. (2017): Urban Heat Island Assessment Using the Landsat 8 Data: A Case Study in Shenzhen and Hong Kong. In: *Urban Science*, 1 (1) 10 pp.
223. TZAVALI, A., PARAVANTIS, J. P., MIHALAKAKOU, G. (2015): Urban heat island intensity: A literature review. In: *Fresenius Environmental Bulletin*, 24 (12) 21 pp.
224. UNGER, J (1999): Urban-rural air humidity differences in Szeged, Hungary. In: *INTERNATIONAL JOURNAL OF CLIMATOLOGY*, 19 (13) 1509–1515 pp.
225. UNGER, J., SÜMEGHY, Z., GULYÁS, Á., BOTTYÁN, Z., MUCSI, L. (2001): Land-use and meteorological aspects of the urban heat island. In: *Meteorological Applications*, 8 (2) 189–194 pp.
226. UNGER, JÁNOS (2004): Intra-urban relationship between surface geometry and urban heat island: review and new approach. In: *CLIMATE RESEARCH*, 27 253–264 pp.

227. UNGER, JANOS (2008): Connection between urban heat island and sky view factor approximated by a software tool on a 3D urban database. In: *International Journal of Environment and Pollution*. 36.59-80 pp.
228. UNGER, JÁNOS, BOTTYÁN, Z., SÜMEGHY, Z., GULYÁS, Á. (2000): Urban heat island development affected by urban surface factors. In: *Időjárás / Quarterly Journal of The Hungarian Meteorological Service*, 104 253–268 pp.
229. UNGER, JÁNOS, SKARBIT, N., GÁL, T. (2018): Absolute moisture content in mid-latitude urban canopy layer: Part 2: results from Szeged, Hungary. In: *Acta Climatologica et Chorologica*, 51–52 (1) 47–56 pp.
230. UNGER, JÁNOS, SÜMEGHY, Z., SZEGEDI, S., KISS, A., GÉCZI, R. (2010): Comparison and generalisation of spatial patterns of the urban heat island based on normalized values. In: *Physics and Chemistry of the Earth, Parts A/B/C*, 35 (1) 107–114 pp.
231. UNGER, JÁNOS, SÜMEGHY, Z., ZOBOKI, J. (2001): Temperature cross-section features in an urban area. In: *Atmospheric Research*, 58 (2) 117–127 pp.
232. UNITED NATIONS (2020): *World Population Prospects 2019 - Volume II: Demographic Profiles*. UN
233. UNITED NATIONS, DEPARTMENT OF ECONOMIC AND SOCIAL AFFAIRS, POPULATION DIVISION (2019): *World urbanization prospects: the 2018 revision*.
234. UPMANIS, H., ELIASSON, I., LINDQVIST, S. (1998): The influence of green areas on nocturnal temperatures in a high latitude city (Göteborg, Sweden). In: *International Journal of Climatology*, 18 (6) 681–700 pp.
235. USGS (2019): *Landsat 8 (L8) Data Users Handbook*. 114 pp.
236. US EPA, O. (2014a, February 28): Heat Island Effect. In: [Collections and Lists] <https://www.epa.gov/heat-islands>.
237. US EPA, O. (2014b, June 17): Learn About Heat Islands. In: [Overviews and Factsheets] <https://www.epa.gov/heat-islands/learn-about-heat-islands>.
238. VALOR, E., CASELLES, V. (1996): Mapping land surface emissivity from NDVI: Application to European, African, and South American areas. In: *Remote Sensing of Environment*, 57 (3) 167–184 pp.
239. VANDERBILT, V. C. (1985): Measuring plant canopy structure. In: *Remote Sensing of Environment*, 18 (3) 281–294 pp.
240. VERBAI, Z., LAKATOS, A., KALMAR, F. (2014): Prediction of energy demand for heating of residential buildings using variable degree day. In: *ENERGY*, 76 780–787 pp.
241. VOOGT, J. A., OKE, T. R. (2003): Thermal remote sensing of urban climates. In: *Remote Sensing of Environment*, 86 (3) 370–384 pp.
242. WALTMAN, L., VAN ECK, N. J., NOYONS, E. C. M. (2010): A unified approach to mapping and clustering of bibliometric networks. In: *Journal of Informetrics*, 4 (4) 629–635 pp.
243. WAN, Z., DOZIER, J. (1996): A generalized split-window algorithm for retrieving land-surface temperature from space. In: *IEEE Transactions on Geoscience and Remote Sensing*, 34 (4) 892–905 pp.
244. WANG, F., QIN, Z., SONG, C., TU, L., KARNIELI, A., ZHAO, S. (2015): An Improved Mono-Window Algorithm for Land Surface Temperature Retrieval from Landsat 8 Thermal Infrared Sensor Data. In: *Remote Sensing*, 7 (4) 4268–4289 pp.
245. WANG, G., LI, H., YANG, Y., JOMBACH, S., TIAN, G. (2019): "City in the park," Greenway Network Concept of High-Density Cities: Adaptation of Singapore Park Connector Network in Chinese Cities. In: *Proceedings of the Fábos Conference on Landscape and Greenway Planning*, 6 (1) pp.
246. WANG, Yafei, BAKKER, F., DE GROOT, R., WÖRTCHE, H. (2015): Effects of urban green infrastructure (UGI) on local outdoor microclimate during the growing season. In: *Environmental Monitoring and Assessment*, 187 (12) pp.

247. WEATHER - met.hu. In: (website): <https://www.met.hu/en/idojaras/>. Accessed: 2020. 5. 10.
248. WENG, Q., LARSON, R. C. (2005): Satellite Remote Sensing of Urban Heat Islands: Current Practice and Prospects. In: R. R. Jensen, J. D. Gatrell, & D. D. McLean (Eds.), *Geo-Spatial Technologies in Urban Environments*. Berlin, Heidelberg: Springer. 91–111 pp.
249. WENG, Q. (2003): Fractal Analysis of Satellite-Detected Urban Heat Island Effect. In: *Photogrammetric Engineering & Remote Sensing*, 69 (5) 555–566 pp.
250. WENG, Q. (2009): Thermal infrared remote sensing for urban climate and environmental studies: Methods, applications, and trends. In: *ISPRS Journal of Photogrammetry and Remote Sensing*, 64 (4) 335–344 pp.
251. WENG, Q., LU, D., SCHUBRING, J. (2004): Estimation of land surface temperature–vegetation abundance relationship for urban heat island studies. In: *Remote Sensing of Environment*, 89 (4) 467–483 pp.
252. WOODCOCK, C. E., STRAHLER, A. H. (1987): The factor of scale in remote sensing. In: *Remote Sensing of Environment*, 21 (3) 311–332 pp.
253. WU, Z., KONG, F., WANG, Y., SUN, R., CHEN, L. (2016): The Impact of Greenspace on Thermal Comfort in a Residential Quarter of Beijing, China. In: *International Journal of Environmental Research and Public Health*, 13 (12) 1217 pp.
254. WU, Z., REN, Y. (2019): A bibliometric review of past trends and future prospects in urban heat island research from 1990 to 2017. In: *Environmental Reviews*, 27 (2) 241–251 pp.
255. XIONG, Y., HUANG, S., CHEN, F., YE, H., WANG, C., ZHU, C. (2012): The Impacts of Rapid Urbanization on the Thermal Environment: A Remote Sensing Study of Guangzhou, South China. In: *Remote Sensing*, 4 (7) 2033–2056 pp.
256. XU, H. (2006): Modification of normalised difference water index (NDWI) to enhance open water features in remotely sensed imagery. In: *International Journal of Remote Sensing*, 27 (14) 3025–3033 pp.
257. XU, H. (2010): Analysis of Impervious Surface and its Impact on Urban Heat Environment using the Normalized Difference Impervious Surface Index (NDISI). In: *Photogrammetric Engineering & Remote Sensing*, 76 (5) 557–565 pp.
258. YAHIA, M. W., JOHANSSON, E., THORSSON, S., LINDBERG, F., RASMUSSEN, M. I. (2018): Effect of urban design on microclimate and thermal comfort outdoors in warm-humid Dar es Salaam, Tanzania. In: *International Journal of Biometeorology*, 62 (3) 373–385 pp.
259. YAN, H., WU, F., DONG, L. (2018): Influence of a large urban park on the local urban thermal environment. In: *Science of The Total Environment*, 622–623 882–891 pp.
260. YANG, G., YU, Z., JØRGENSEN, G., VEJRE, H. (2020): How can urban blue-green space be planned for climate adaption in high-latitude cities? A seasonal perspective. In: *Sustainable Cities and Society*, 53 101932 pp.
261. YANG, H., XI, C., ZHAO, X., MAO, P., WANG, Z., SHI, Y., HE, T., LI, Z. (2020): Measuring the Urban Land Surface Temperature Variations Under Zhengzhou City Expansion Using Landsat-Like Data. In: *Remote Sensing*, 12 (5) 801 pp.
262. YILMAZ, S., MUTLU, E., YILMAZ, H. (2018): Alternative scenarios for ecological urbanizations using ENVI-met model. In: *Environmental Science and Pollution Research*, 25 (26) 26307–26321 pp.
263. YIN, X., ZHANG, Q. (2014): Analysis between AMSR-E swath brightness temperature and snow cover area in winter time over Sierra Nevada, Western U.S. In: T. J. Jackson, J. M. Chen, P. Gong, & S. Liang (Eds.) *Presented at the SPIE Asia-Pacific Remote Sensing*. Beijing, China. 92604K pp.
264. YU, X., GUO, X., WU, Z. (2014): Land Surface Temperature Retrieval from Landsat 8 TIRS—Comparison between Radiative Transfer Equation-Based Method, Split Window Algorithm and Single Channel Method. In:

- Remote Sensing, 6 (10) 9829–9852 pp.
265. YUAN, F., BAUER, M. E. (2007): Comparison of impervious surface area and normalized difference vegetation index as indicators of surface urban heat island effects in Landsat imagery. In: Remote Sensing of Environment, 106 (3) 375–386 pp.
 266. ZARDO, L., GENELETTI, D., PÉREZ-SOBA, M., VAN EUPEN, M. (2017): Estimating the cooling capacity of green infrastructures to support urban planning. In: Ecosystem Services, 26 225–235 pp.
 267. ZHANG, H., QI, Z., YE, X., CAI, Y., MA, W., CHEN, M. (2013): Analysis of land use/land cover change, population shift, and their effects on spatiotemporal patterns of urban heat islands in metropolitan Shanghai, China. In: Applied Geography, 44 121–133 pp.
 268. ZHANG, JINGUANG, YU, Z., ZHAO, B., SUN, R., VEJRE, H. (2020): Links between green space and public health: A bibliometric review of global research trends and future prospects from 1901 to 2019. In: Environmental Research Letters
 269. ZHANG, JINQU, WANG, Y., LI, Y. (2006): A C++ program for retrieving land surface temperature from the data of Landsat TM/ETM+ band6. In: Computers & Geosciences, 32 (10) 1796–1805 pp.
 270. ZHANG, Z. M., LEE, B. J. (2009): Chapter 3 Theory of Thermal Radiation and Radiative Properties. In: Z. M. Zhang, B. K. Tsai, & G. Machin (Eds.), Experimental Methods in the Physical Sciences. Academic Press. Vol. 42. 73–132 pp.
 271. ZHANG, Z., LV, Y., PAN, H. (2013): Cooling and humidifying effect of plant communities in subtropical urban parks. In: Urban Forestry & Urban Greening, 12 (3) 323–329 pp.
 272. ZHAO, H., ZHANG, H., MIAO, C., YE, X., MIN, M. (2018): Linking Heat Source–Sink Landscape Patterns with Analysis of Urban Heat Islands: Study on the Fast-Growing Zhengzhou City in Central China. In: Remote Sensing, 10 (8)1268 pp.
 273. ZHAOLIANG, L., BOHUI, T., WU, H., REN, H., YAN, G., WAN, Z., TRIGO, I. F., SOBRINO, J. A. (2013): Satellite-derived land surface temperature: Current status and perspectives. In: Remote Sensing of Environment, 131 14–37 pp.

LIST OF FIGURES

Figure 1.1: Structure of the dissertation

Figure 2.1: Day and night Surface temperature and Air temperature changes in different area (*modified EPA 2008*)

Figure 2.2: Comparison of evapotranspiration between urban areas and natural ground cover areas (modified from EPA, 2008)

Figure 2.3: Concept of heat balance of urban surface layer

Figure 2.4: Depiction of the urban surface energy balance components in a typical urban control volume.

Figure 2.5: Three scales to distinguish urban area and atmosphere for climatic study

Figure 2.6: The workflow of the bibliometrics methods and the keywords used in searching UHI scientific publications in WOS database.

Figure 2.7: Scientific productions during 1975-2020 from Web of Science (WoS).

Figure 2.8: Types and percentage of the publications from 1975-2020 from WOS database

Figure 2.9: Keywords word cloud from the UHI publications from 1975-2020.

Figure 3.1: Location of the study area Zhengzhou in Henan province, Henan province in China.

Figure 3.2: Topographic elevation analysis map of Zhengzhou city

Figure 3.3: Monthly average weather data summary based on the Zhengzhou national weather station (No.570830, Elevation 110m).

Figure 3.4: The location and green spaces of Budapest

Figure 3.5: The annual mean temperature of Budapest from 1901-2020

Figure 3.6: Location of surface stations in Zhengzhou city and its surrounding rural observatories: a) urban area; b) Rural station:Xinzheng; (modified from ©2019 Google earth maps)

Figure 3.7: The real image and the thermal image showing the Budapest city center's surface temperature measured by the Seek Pro heat camera from Gellért hill (at 12:50 on 28. 12. 2018).

Figure 3.8: Location of study area and the 16 measurement sites, four coverage types of each garden in HAU campus

Figure 3.9: 16 measurement points in garden A, B, C, D; Plant canopy imager and weather station used in measurement.

Figure 3.10: The 123 sample parks in Zhengzhou

Figure 3.11: The research framework of park cooling effect survey

Figure 3.12: Summary of workflow and method components in the research framework

Figure 4.1: The annual average temperature of three weather stations (urban station: Zhengzhou; rural station: Xinzheng) from 1981 to 2019.

Figure 4.2: Annual and seasonal mean of atmospheric UHI intensity (UHII) in Zhengzhou over the past decades

(1981-2019)

Figure 4.3: Mean of atmospheric UHI intensity (UHII) of each year at different daytime and nighttime hours in Zhengzhou over the past years (1981-2019).

Figure 4.4: Four hourly mean of atmospheric UHI intensity (UHII) of four seasons in Zhengzhou over the past years (1981-2019).

Figure 4.5: Regression analysis between the urban compactness ratio (UCR) and time (left), linear regression between UCR and UHII (right) from 1981-2019.

Figure 4.6: Maps of LULC (land use land cover) classification of Zhengzhou central city on Jun. 2, 1989; Aug.27, 2000; Aug.12, 2009; Jul.7, 2019.

Figure 4.7: Changes of LULC based on the five classes from the 1989-2019 of Zhengzhou central urban.

Figure 4.8: Maps of LST pattern based on the LSTi classes approach of Zhengzhou central city on Jun. 2, 1989; Aug.27, 2000; Aug.12, 2009; Jul.7, 2019.

Figure 4.9: Mean LST degree of eight zones based on the spatial cardinal direction of Zhengzhou central urban, the angle of each zone is 45 degree, and all the temperature range is from 27 °C- 32 °C, each grid is 1 °C.

Figure 4.10: The LST change based on E-W and S-N profile on Jun. 2, 1989; Aug.27, 2000; Aug.12, 2009; Jul.7, 2019, respectively.

Figure 4.11: Comparison of mean LST of three rings based on the distance from the urban center, the three rings were detected by the city main road of Zhengzhou central urban. The four dates are on Jun. 2, 1989; Aug.27, 2000; Aug.12, 2009; Jul.7, 2019, respectively.

Figure 4.12: LST class distribution in different seasons from 1989 to 2019 of Zhengzhou central urban.

Figure 4.13: Surface UHII (left) and URI (right) values of the selected dates from 1989-2019 of Zhengzhou

Figure 4.14: NDVI maps of Zhengzhou central city on Jun. 2, 1989; Aug.27, 2000; Aug.12, 2009; Jul.7, 2019

Figure 4.15: Linear regression between NDVI and LST on Jun. 2, 1989; Aug.27, 2000; Aug.12, 2009; Jul.7, 2019, respectively.

Figure 4.16: Linear regression analysis between NDISI (left), MNDWI (right) and LST from the random point samples (exclude the outliers and values of NDISI <0).

Figure 4.17: The land surface temperature (LST) of shadow and non-shadow 10 plot in Zhengzhou city.

Figure 4.18: Comparison of LST between new town areas and old town areas of Zhengzhou in 2019. Old town: a). South station of Zhengzhou; b). Zhengzhou railway station. New town samples: c). CBD; d). Longzihu zone.

Figure 4.19: a) LST map of Zhengzhou city in 07/07/2019; b) Distribution of 123 parks samples; c) Five park type examples: 1-urban park; 2-theme park; 3-street park; 4-linear park; 5-urban square

Figure 4.20: Regression analysis among mean park LST and, a) FVC, b) NDWI, c) NDISI.

Figure 4.21: Regression analysis among mean park LST and park characteristics: a) Size; b) Frac_Dim; c) Paratio; d) Shape_Idx; e) Three park examples.

Figure 4.22: Regression analysis of park PCI and a) mean FVC; b) mean NDWI; c) mean NDISI.

Figure 4.23: Regression analysis among PCI and mean park characteristics: a)Size; b) Frac_Dim; c) Paratio; d) Shape_Index;

Figure 4.24: Regression analysis between the PCI and the impact factor of park surrounding area (500m buffer).

Figure 4.25: Analysis between PCI and location factor and park types (all 123 samples). a)PCI and park location in three city rings; b) PCI and five park types: 1-urban park; 2-theme park; 3-street park; 4-linear park; 5-urban square.

Figure 4.26: Buffer zones near the Zoo and the land surface cover condition detail in the first 3 buffers: a) Urban road; b) Gym, c) Buildings and road

Figure 4.27: Regression analysis between PCI and different buffer size.

Figure 4.28: Parks LST changes with buffer distance grows

Figure 4.29: Comparison of PCI with different fractal dimensions (Frac_Dim) and perimeter area ratios (Paratio). Typical park shapes with higher Frac_Dim and Paratio values (a, b, e, f,) and typical shapes with lower Frac_Dim and Paratio values (c, d, g, h)

Figure 4.30: The wind direction of each days in August 7-9, 2019

Figure 4.31: Air temperature (AT) and relative humidity (RH) changes of 16 points in four gardens (A; B; C; D) during the measurement period (7-9, August 2019). Coverage types: Red- Impervious surface; Yellow-Shrub-grass; Light green-Tree-grass; Dark green-Tree-shrub-grass.

Figure 4.32: Linear regression analysis between canopy density (CD), leaf area index (LAI), photosynthetically active radiation (PAR), mean leaf angle (MLA) and air temperature (AT) and relative humidity (RH).

Figure 4.33: Comparison histogram mean land surface temperature (LST) of hills and lowlands comparison in Budapest: a) location; b) in winter; c) in summer.

Figure 4.34: Comparison Land surface temperature (LST) between northern and southern slopes in summer and winter in Budapest: a) mean LST in summer; b) mean LST in winter; c) all plots in summer; d) all plots in winter; e) selected plots.

Figure 4.35: The northern slopes of Gellért hill were, in some cases, 10 °C colder than the southern slopes on high-resolution thermal camera image (taken at 14:20 on 13. 01. 2019.).

Figure 4.36: Surface temperature (ST) of southeast slopes in Buda Castle hill. The castle walls facing south have significantly higher values than the walls facing east (taken at 14:09 on 07. 02. 2019.).

Figure 4-37: Box plots showing the relationships of building height category (m) with LST (range, minimum, maximum, median value in °C) in Budapest.

Figure 4.38: Box plots showing the relationships of vegetation height (m) with LST (range, minimum, maximum, median value in °C) in Budapest.

Figure 4.39: Box plots showing the relationships between vegetation height (m) and LST (°C) within only vegetation coverage area in selected 10 samples (Details of plot 1 is shown).

Figure 4.40: Box plots of the relationships of tree cover density (%) with LST (range, minimum, maximum, median value in °C) in Budapest.

Figure 4.41: Box plots of the relationships of vegetation type with LST (°C) in Budapest.

LIST OF TABLES

Table 2.1: General characteristics difference between Surface and Atmospheric Urban Heat Islands (UHI) modified from (EPA, 2014)

Table 2.2: Algorithm based on the NDVI image.

Table 2.3: Summary of the main LST retrieval methods

Table 2.4: A summary of main factors in related to UHI trends. Sources: modified from (Arnfield 2003)

Table 2.5: Summary of reviews of UHI publications from 1997

Table 3.1: Geospatial database used in this research of Zhengzhou

Table 3.2: Landsat images used to estimate land surface temperature

Table 3.3: High resolution layers used in this research from Copernicus

Table 3.4: Temperature classification by using mean standard deviation method.

Table 3.5: Spectral indexes of Landsat image used in study.

Table 3.6: Statistics and details of 123 sample parks by types

Table 3.7: Park metrics

Table 4.1: Pearson correlation analysis between the socio-economic development indicators and UHII

Table 4.2: Correlation analysis between the UHII and socio-economic driving factors in Zhengzhou

Table 4.3: Mean LST (°C) of the three rings form 1989 of Zhengzhou central urban

Table 4.4: Statistical parameters in the total urban area and the green space samples

Table 4.5: Statistics of LST and average park cooling intensity (PCI) in different park types

Table 4.6: The meteorological data statistics from the study period

Table 4.7: Pearson correlation coefficients of the characteristics of surface type on AT and RH

ACKNOWLEDGEMENT

First of all, I wish to sincerely acknowledge my supervisor, Dr. Sandor Jombach, for his academic supervision, professional guidance, not only on research but also on personal development. I feel grateful to him for encouraging me to grow as a researcher with the thinking aptitude.

I am grateful to my tutor in China, Prof. Guohang Tian from Henan Agriculture University, for his support and guidance during my studies in Hungary, his constant help regarding measurement equipment and funding.

I would like to thank the department head Dr. László Kollányi, Dr. Ágnes Sallay, Dr. Krisztina Filep-Kovács, Dr. István Valánszki, Dr. Szilvácsku Miklós Zsolt, Dr. Edina Klára Dancsokné Fóris, Paloma Gonzalez de Linares, Guifang Wang, Ernest Amoako-Atta from Dept. of Landscape Planning and Regional Development, thanks for all of your kind assistance.

I would also thank the Doctoral School of Landscape Architecture and Landscape Ecology, Prof. Dr. László Bozó, Prof. Dr. Kinga Mezősné Szilágyi, Prof. Dr. Ágnes Sallay, Prof. Dr. Albert Fekete, and other members from the doctoral school, Mrs. Fanny Szondy. Thanks for all your assistance and kind guidance throughout my Ph.D. study.

Concerning the research measurement campaign, I express my warm thanks to Prof. Ruizhen He, Prof. Yakai Lei, my colleague from the Department of Landscape architecture and Art, for providing constant technical support for the fieldwork. Special appreciation to Yuchen Guo, YangYang, Yongge Hu, Yongqiang Wang for assisting with 2019's summer measurement and the following measurement,

Thanks to the dean Prof. Dr. Albert Fekete, I gratefully acknowledge the Faculty of Landscape Architecture and Urbanism's support. Thanks for the funding support for my publications and international conference, personal help, and guidance.

Thanks also go to my friends and colleagues, Dr. Dóra Csizmadia, Dr. Zelenák Fruzsina, Zita Szabó, Sarah Ben Salem, Paloma Gonzalez de Linaresfor, for helping me to adjust to studying in Budapest.

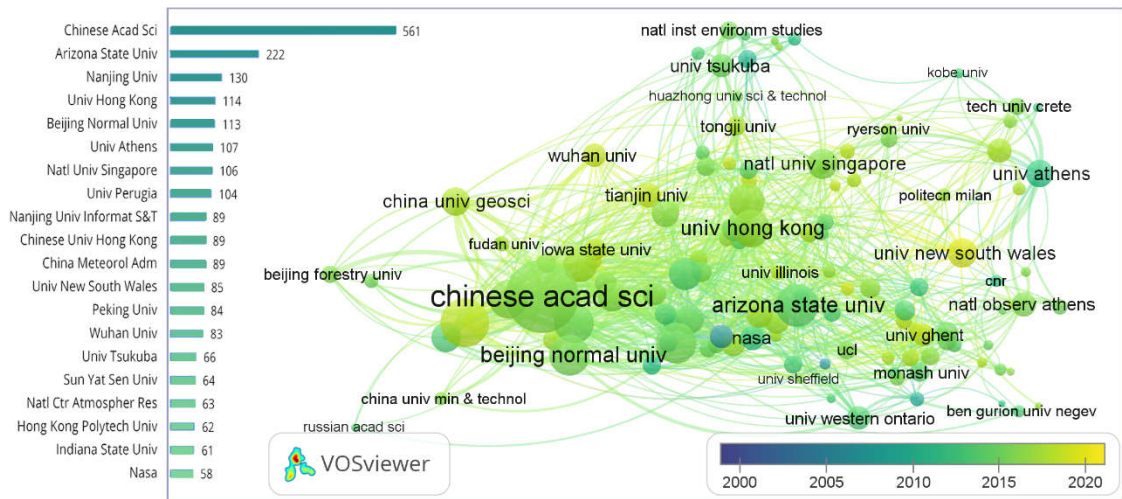
I am deeply grateful to my family for all their love, support, and encouragement. I gratitude to my parents, who raised me and deeply love me in all these years, and my two big sisters who encouraged me to pursue a scholar's career. Finally, but most importantly, my deepest affection goes to my wife and my lovely son, who has always been at my side and accompanied me across the study period.

Finally, I would like to express my gratitude to everyone that helped me throughout my Ph.D. studies in Hungary.

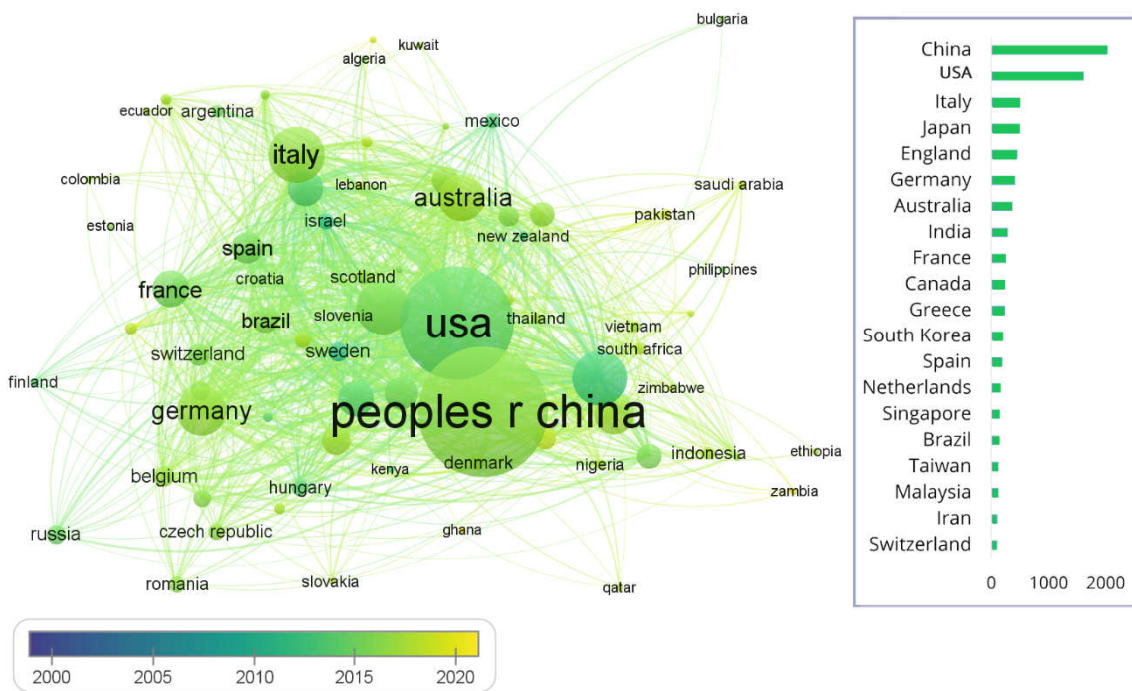
APPENDIX

Appendix 1: The 20 most frequently occurrences keywords ranked in descending order over three decades

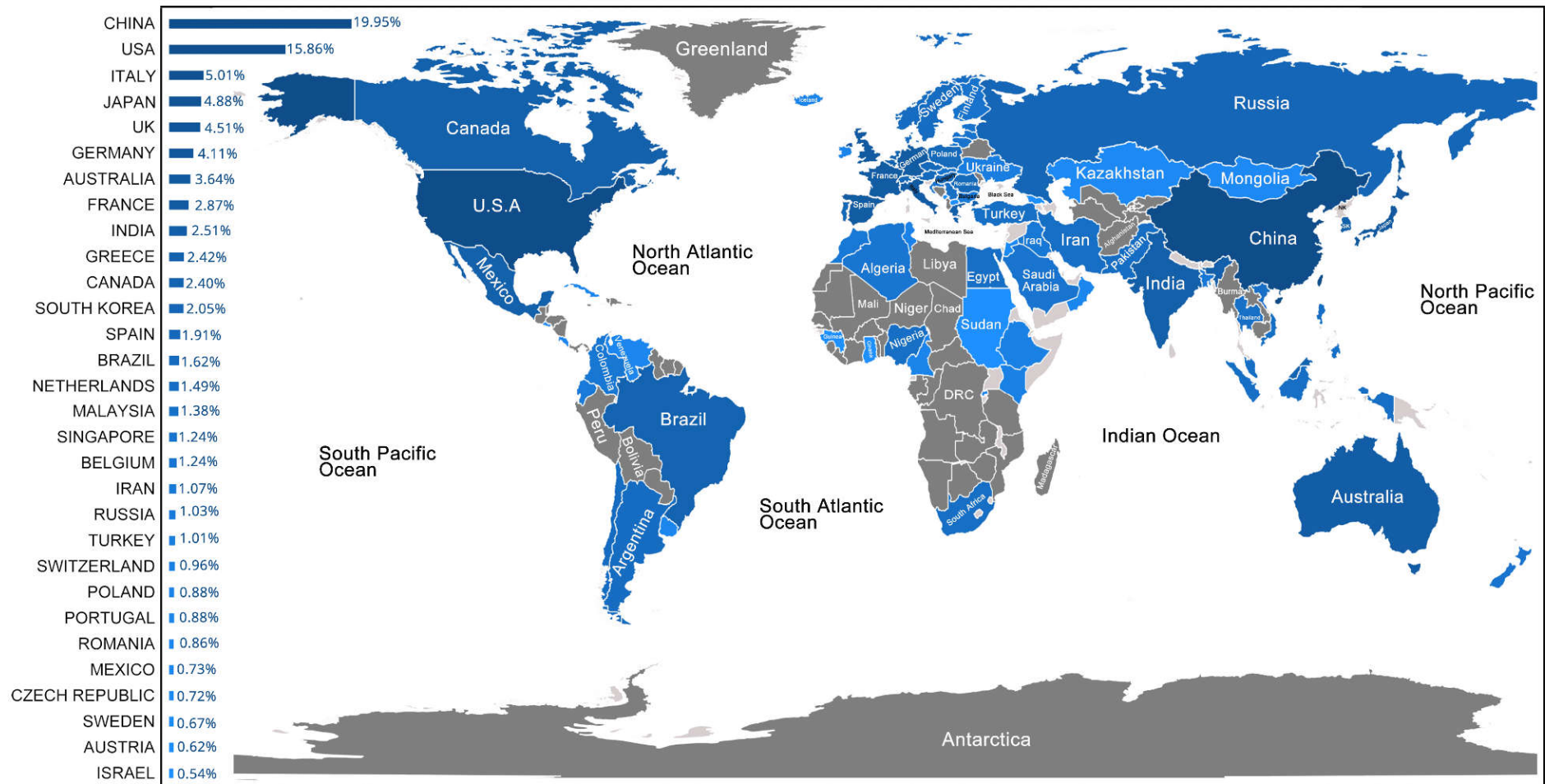
1990-1999		2000-2009		2010-2020	
Words	Times	Words	Times	Words	Times
heat-island	22	heat-island	158	heat-island	1422
model	17	urban heat-island	106	urban heat-island	1201
urban heat-island	17	model	97	impact	1179
temperature	16	temperature	90	climate	893
urban	11	climate	88	temperature	872
canyon	8	city	83	city	778
canyon geometry	8	simulation	70	model	601
trends	8	areas	56	urbanization	584
boundary-layer	7	boundary-layer	54	climate-change	546
planetary boundary-layer	7	impact	54	vegetation	522
simulation	7	vegetation	44	cities	501
area	6	land-use	43	energy	453
avhrr data	6	cities	41	impacts	433
satellite	6	urbanization	37	land-surface temperature	407
surface	6	parameterization	34	performance	397
city	5	surface	34	simulation	397
energy-balance	5	surface-temperature	34	mitigation	377
evapotranspiration	5	energy	33	air-temperature	348
radiation	5	impacts	32	cover	282
surface-temperature	5	cover	31	environment	279



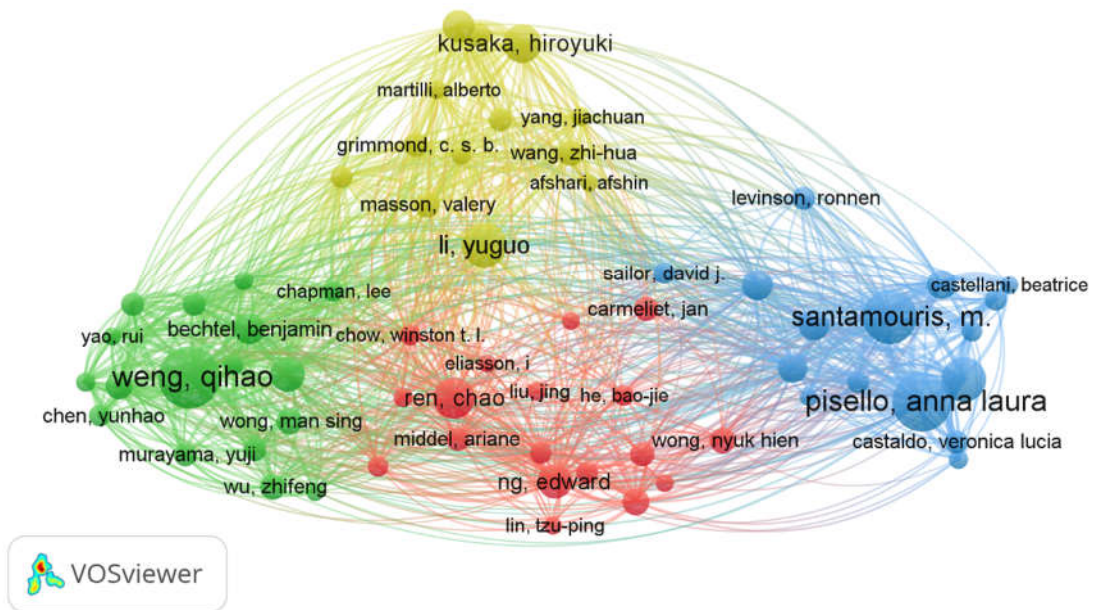
Appendix 2: The top institutions of UHI publications based on the bibliometric analysis from 1975-2020 on Web of Science.



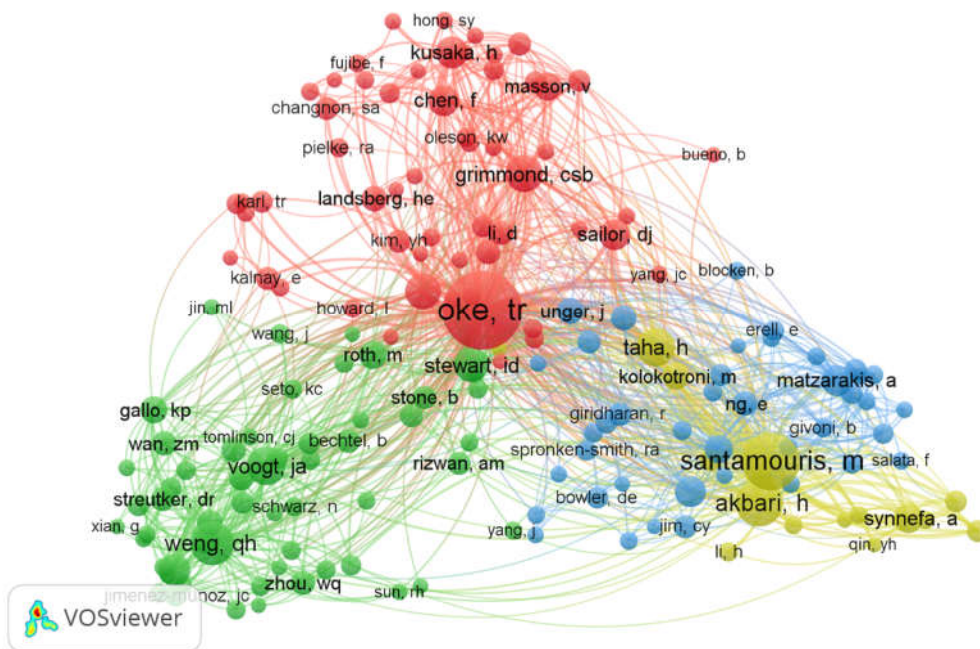
Appendix 3: The top countries of UHI publications based on the bibliometric analysis from 1975-2020 on Web of Science.



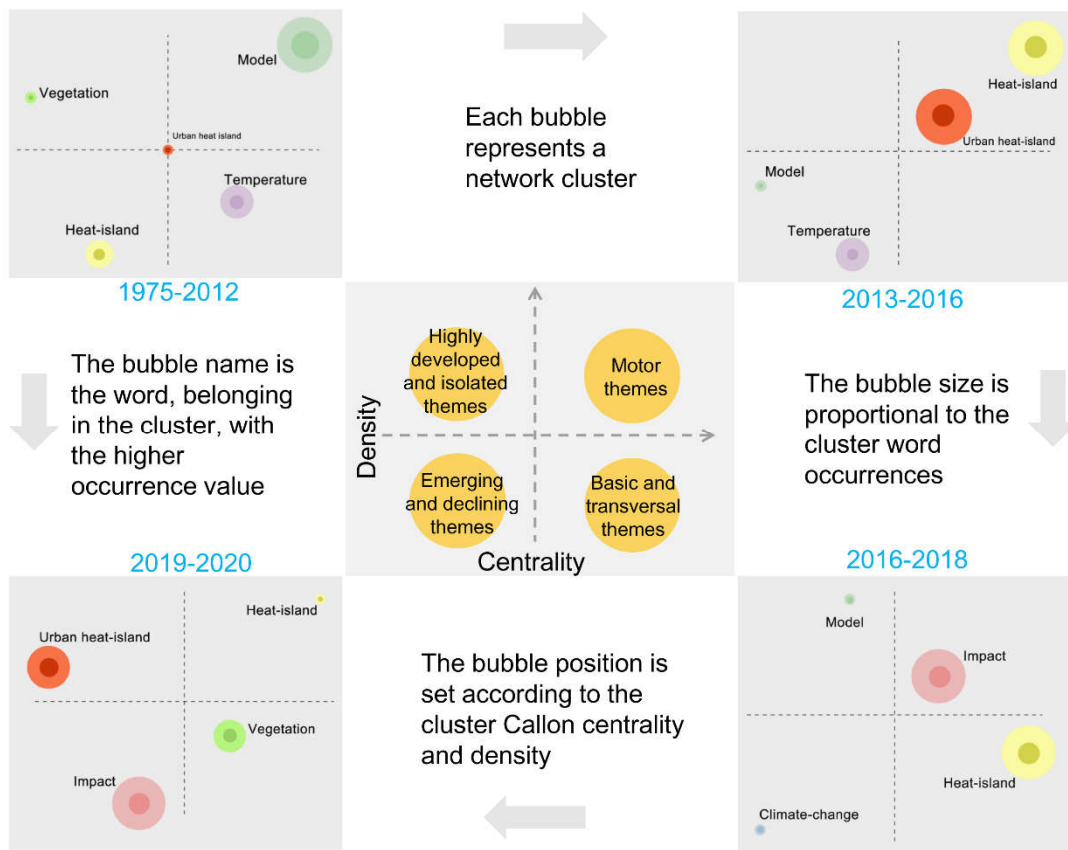
Appendix 4: The top countries of UHI publications map based on the bibliometric analysis from 1975-2020 on Web of Science.



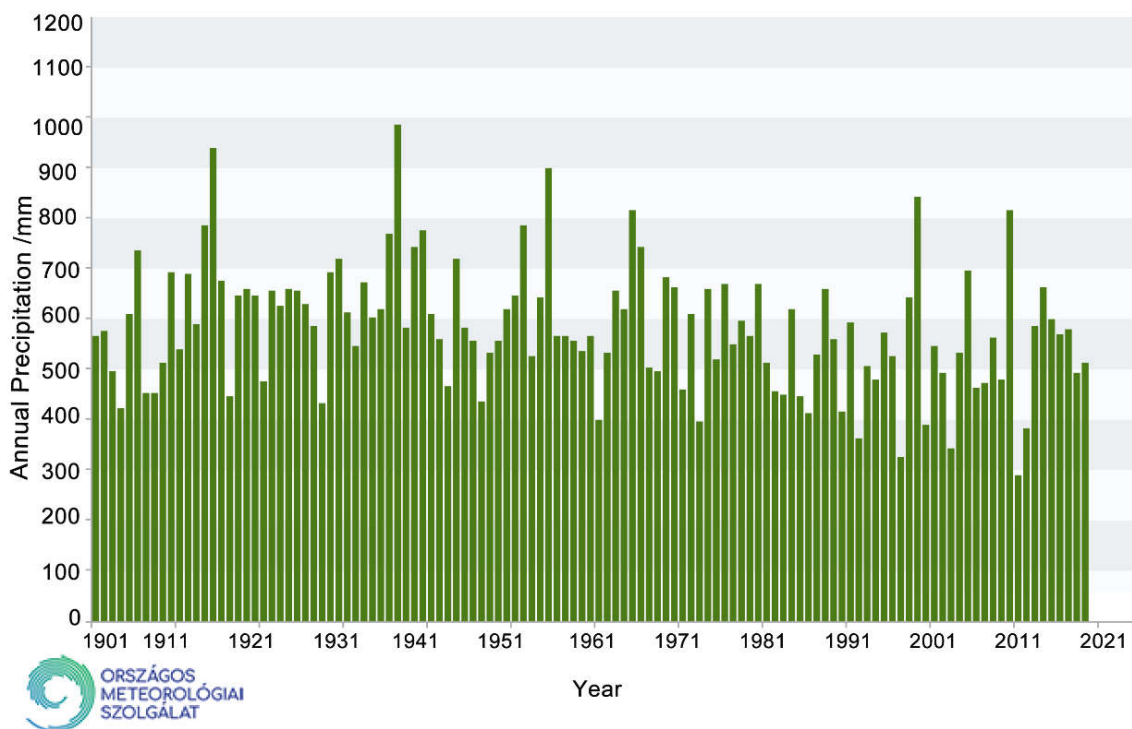
Appendix 5: The top authors of UHI publications based on the bibliometric analysis from 1975-2020 on Web of Science.



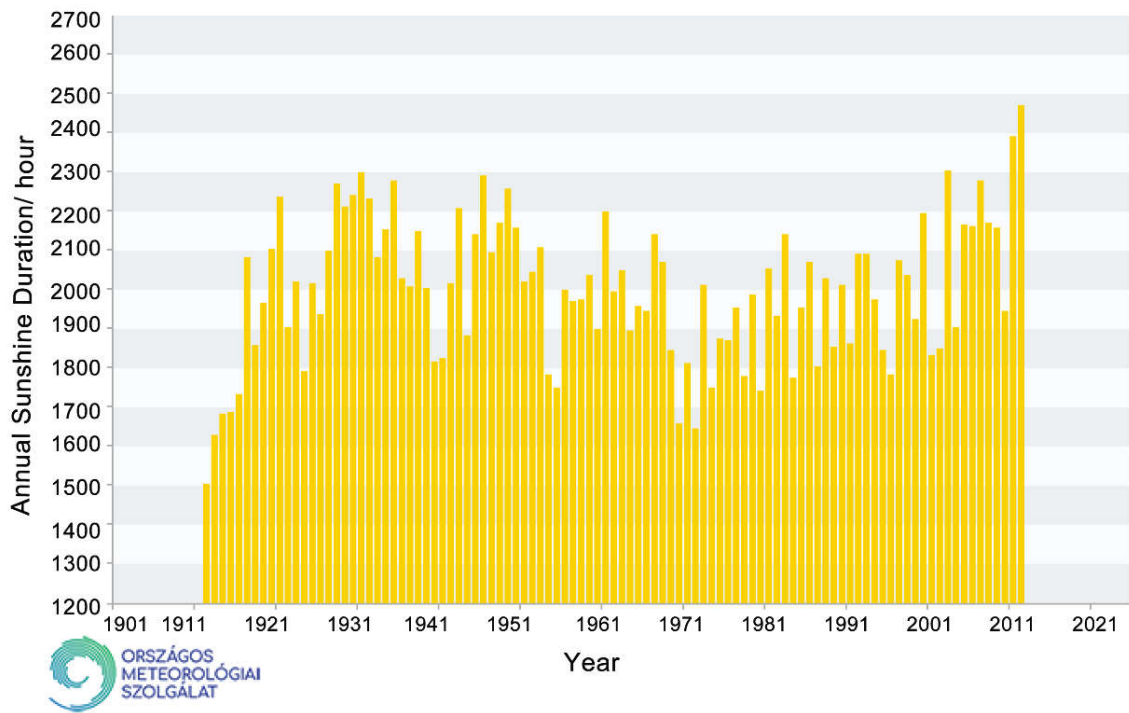
Appendix 6: The top cited authors of UHI publications based on the bibliometric analysis from 1975-2020 on Web of Science.



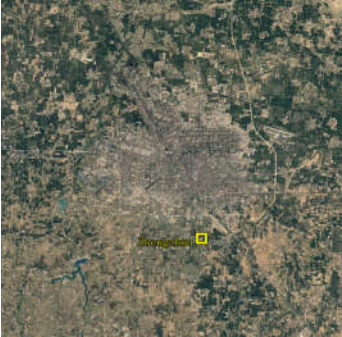
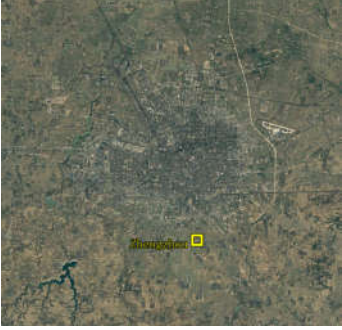
Appendix 9: Research trends of UHI based on the bibliometric analysis in four periods from 1975-2020 on Web of Science.

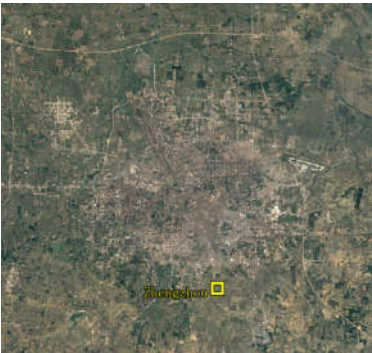
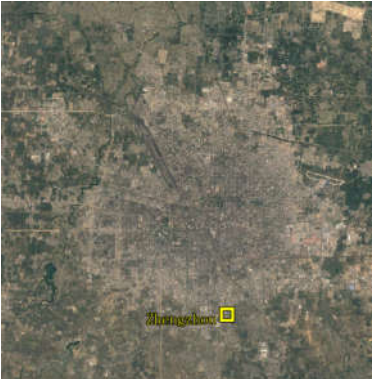
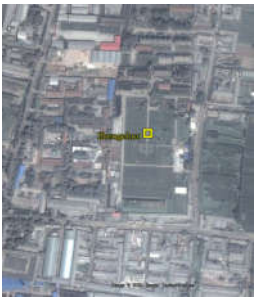
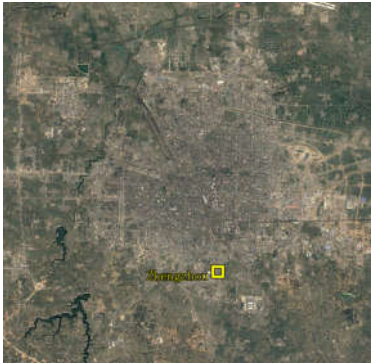

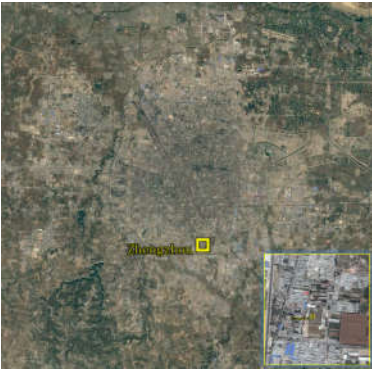



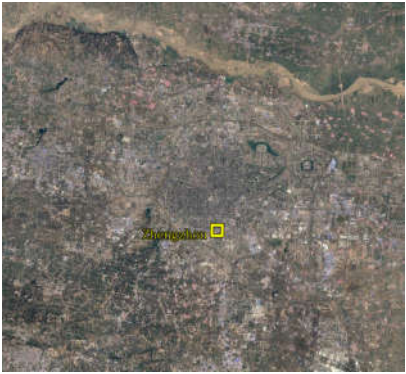

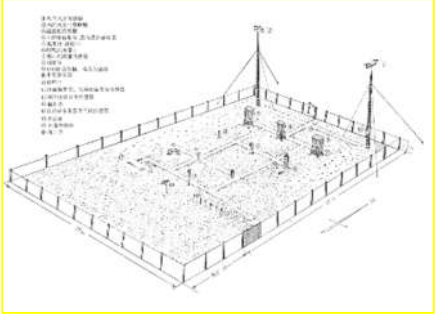




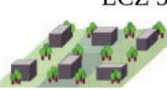
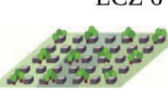




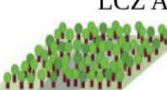

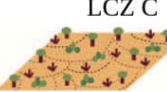

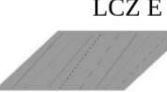
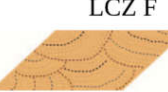
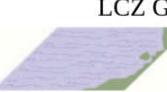




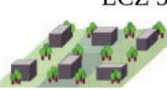
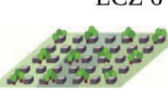




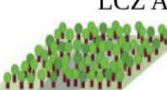

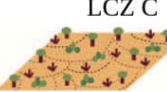

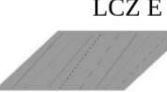
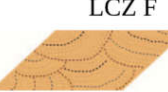
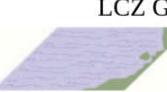




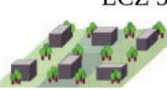
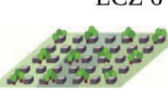




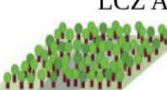

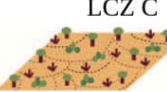

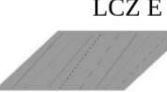
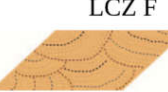
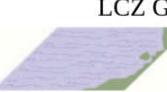
Appendix 10: The annual precipitation (mm) of Budapest from 1901-2020. Sources from the OMSZ, met.hu

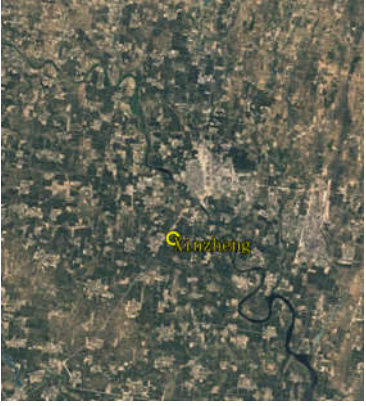
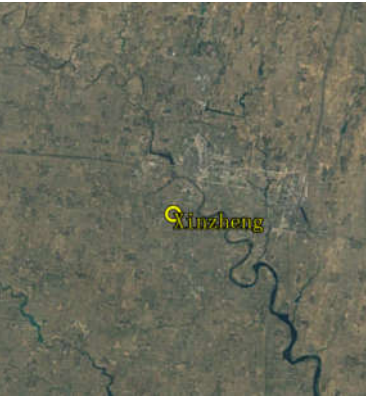
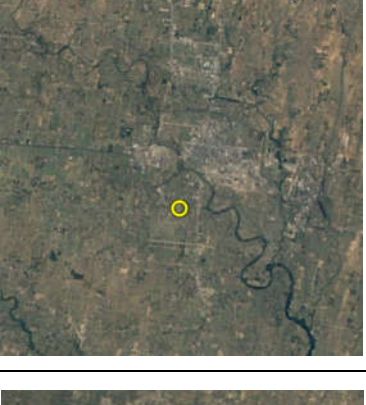
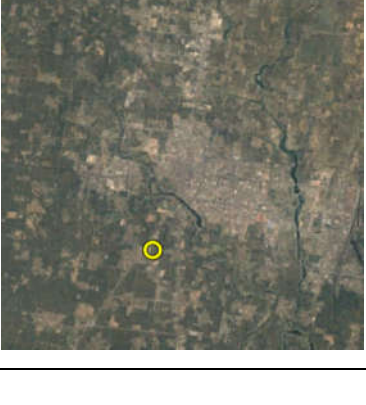


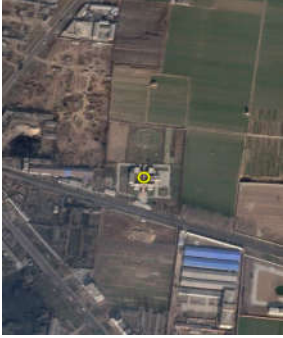

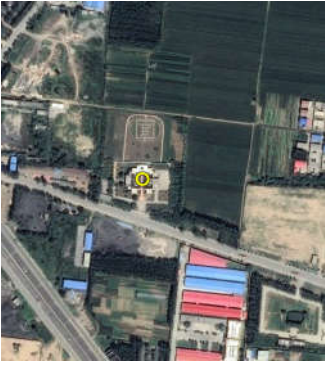
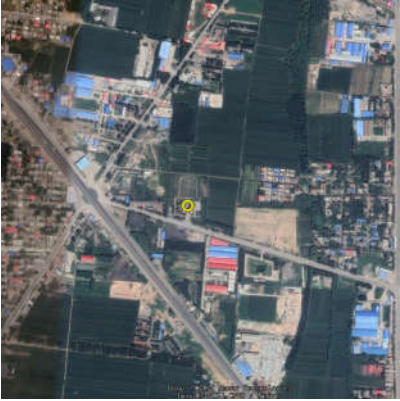


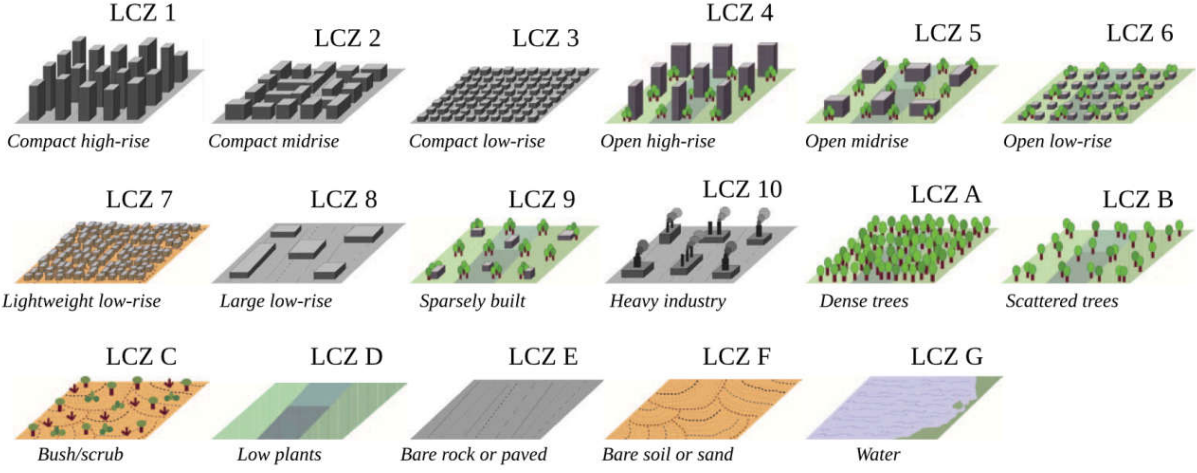
Appendix 11: The annual sunshine duration (hour) of Budapest from 1901-2020. Sources from the OMSZ, met.hu

Appendix 12 Zhengzhou national weather station LCZ		
Year	LCZ type	Aerial images
1988	LCZ D-Agriculture land	
1991	LCZ D-Agriculture land	

<p>1995</p>	<p>LCZ D-Agriculture land</p>	
<p>2001</p>	<p>LCZ D-Agriculture land</p>	
<p>2005</p>	<p>LCZ-6 Open low-rise</p> 	
<p>2007</p>	<p>LCZ-4 Open mid-rise</p> 	

2019	<p>LCZ- 1 Open high-rise</p> 																			
National Standard Station model	<p>Aerial map</p> 	 <p>Reference model from 《 Specifications for surface meteorological observation 》 QX / T 61-2007 National Standard</p>																		
<p>Local climate zone types (Stewart & Oke 2012)</p> <table border="0"> <tr> <td data-bbox="220 1025 419 1182"> <p>LCZ 1</p>  <p>Compact high-rise</p> </td> <td data-bbox="419 1025 619 1182"> <p>LCZ 2</p>  <p>Compact mid-rise</p> </td> <td data-bbox="619 1025 818 1182"> <p>LCZ 3</p>  <p>Compact low-rise</p> </td> <td data-bbox="818 1025 1018 1182"> <p>LCZ 4</p>  <p>Open high-rise</p> </td> <td data-bbox="1018 1025 1217 1182"> <p>LCZ 5</p>  <p>Open mid-rise</p> </td> <td data-bbox="1217 1025 1417 1182"> <p>LCZ 6</p>  <p>Open low-rise</p> </td> </tr> <tr> <td data-bbox="220 1182 419 1339"> <p>LCZ 7</p>  <p>Lightweight low-rise</p> </td> <td data-bbox="419 1182 619 1339"> <p>LCZ 8</p>  <p>Large low-rise</p> </td> <td data-bbox="619 1182 818 1339"> <p>LCZ 9</p>  <p>Sparsely built</p> </td> <td data-bbox="818 1182 1018 1339"> <p>LCZ 10</p>  <p>Heavy industry</p> </td> <td data-bbox="1018 1182 1217 1339"> <p>LCZ A</p>  <p>Dense trees</p> </td> <td data-bbox="1217 1182 1417 1339"> <p>LCZ B</p>  <p>Scattered trees</p> </td> </tr> <tr> <td data-bbox="220 1339 419 1496"> <p>LCZ C</p>  <p>Bush/scrub</p> </td> <td data-bbox="419 1339 619 1496"> <p>LCZ D</p>  <p>Low plants</p> </td> <td data-bbox="619 1339 818 1496"> <p>LCZ E</p>  <p>Bare rock or paved</p> </td> <td data-bbox="818 1339 1018 1496"> <p>LCZ F</p>  <p>Bare soil or sand</p> </td> <td data-bbox="1018 1339 1217 1496"> <p>LCZ G</p>  <p>Water</p> </td> <td></td> </tr> </table>			<p>LCZ 1</p>  <p>Compact high-rise</p>	<p>LCZ 2</p>  <p>Compact mid-rise</p>	<p>LCZ 3</p>  <p>Compact low-rise</p>	<p>LCZ 4</p>  <p>Open high-rise</p>	<p>LCZ 5</p>  <p>Open mid-rise</p>	<p>LCZ 6</p>  <p>Open low-rise</p>	<p>LCZ 7</p>  <p>Lightweight low-rise</p>	<p>LCZ 8</p>  <p>Large low-rise</p>	<p>LCZ 9</p>  <p>Sparsely built</p>	<p>LCZ 10</p>  <p>Heavy industry</p>	<p>LCZ A</p>  <p>Dense trees</p>	<p>LCZ B</p>  <p>Scattered trees</p>	<p>LCZ C</p>  <p>Bush/scrub</p>	<p>LCZ D</p>  <p>Low plants</p>	<p>LCZ E</p>  <p>Bare rock or paved</p>	<p>LCZ F</p>  <p>Bare soil or sand</p>	<p>LCZ G</p>  <p>Water</p>	
<p>LCZ 1</p>  <p>Compact high-rise</p>	<p>LCZ 2</p>  <p>Compact mid-rise</p>	<p>LCZ 3</p>  <p>Compact low-rise</p>	<p>LCZ 4</p>  <p>Open high-rise</p>	<p>LCZ 5</p>  <p>Open mid-rise</p>	<p>LCZ 6</p>  <p>Open low-rise</p>															
<p>LCZ 7</p>  <p>Lightweight low-rise</p>	<p>LCZ 8</p>  <p>Large low-rise</p>	<p>LCZ 9</p>  <p>Sparsely built</p>	<p>LCZ 10</p>  <p>Heavy industry</p>	<p>LCZ A</p>  <p>Dense trees</p>	<p>LCZ B</p>  <p>Scattered trees</p>															
<p>LCZ C</p>  <p>Bush/scrub</p>	<p>LCZ D</p>  <p>Low plants</p>	<p>LCZ E</p>  <p>Bare rock or paved</p>	<p>LCZ F</p>  <p>Bare soil or sand</p>	<p>LCZ G</p>  <p>Water</p>																




Appendix 13 Xinzheng national weather station LCZ		
Year	LCZ type	Aerial images
1988	LCZ D-Agriculture land	
1991	LCZ D-Agriculture land	
1995	LCZ D-Agriculture land	
2001	LCZ D-Agriculture land	






2009	<p>LCZ D-Agriculture land</p> 	
2013	<p>LCZ-9 Sparsely built</p> 	
2019	<p>LCZ- 4 Open low-rise</p> 	
 <p>Local climate zone types (Stewart & Oke 2012)</p>		

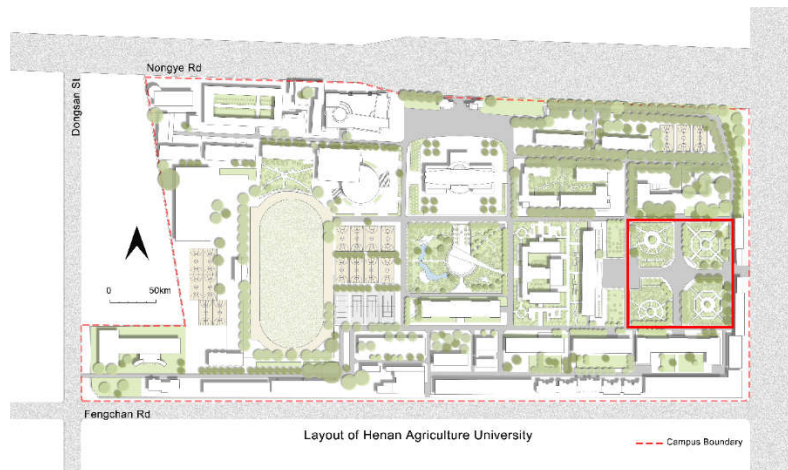
Appendix 14: Multi-spectral Landsat images used to estimate land surface temperature and land use/land cover

Date	Season	Satellite types	Path	Row
02/02/1989	Winter	Landsat 5 TM	124	36
14/03/1989	Spring	Landsat 5 TM	123	36
02/06/1989	Summer	Landsat 5 TM	124	36
24/10/1989	Autumn	Landsat 5 TM	124	36
05/04/2000	Spring	Landsat 5 TM	124	36
16/06/2000	Summer	Landsat 5 TM	124	36
27/08/2000		Landsat 7 ETM+	124	36
06/10/2000	Autumn	Landsat 5 TM	123	36
25/12/2000	Winter	Landsat 5 TM	124	36
06/04/2009	Spring	Landsat 5 TM	124	36
12/08/2009	Summer	Landsat 5 TM	124	36
15/10/2009	Autumn	Landsat 5 TM	124	36
18/12/2009	Winter	Landsat 5 TM	124	36
31/01/2019	Winter	Landsat 8 OLI-TIRS	123	36
18/04/2019	Spring	Landsat 8 OLI-TIRS	124	36
07/07/2019	Summer	Landsat 8 OLI-TIRS	124	36
27/10/2019	Autumn	Landsat 8 OLI-TIRS	124	36

Appendix 15: Instruments and tools used in survey measurement

Instrument	Model	No.	Function	Photo
iButton	DS1923 (Dallas Semiconductor, USA)	16	Digital Hygrometer Measures Humidity with 8-Bit (0.6%RH) or 12-Bit (0.04%RH) Resolution Temperature Accuracy Better Than $\pm 0.5^{\circ}\text{C}$ from -10°C to $+65^{\circ}\text{C}$ with Software Correction Measures Temperature with 8-Bit (0.5°C) or 11-Bit (0.0625°C) Resolution Operating Range: -20°C to $+85^{\circ}\text{C}$; 0 to 100% RH	
Weather station	RR-9150 (BJYL Co, China)	4	Air temperature(AT); Relative Humidity (RH); Wind Direction (WD); Wind Speed (WS); Radiation Area (RA). Five index.	
Plant Canopy Imager	CI-110 (CID Bio-Science, USA)	1	The CI-110 Plant Canopy Analyzer is a unique tool that integrates two common methods of plant canopy analysis into one instrument. A self-leveling, wide-angled lens allows the user to capture hemispherical photographs for the analysis of leaf area index (LAI) and gap fraction analysis, while the photosynthetically active radiation (PAR) sensors in the arm of the instrument give the user alternative options for LAI calculation as well as additional information about radiation levels and sunflecks.	

Tripod	Regular tools	8	Tripod is used to fix Ibutton temperature and humidity recorder	
Radiation shield	Home-made cup	16	The louver box is to reduce the influence of the environment such as solar radiation and strong wind on the measurement results during the measurement	
Camera	SONY-NEX7 (SONY, JP)	1	Obtain photos of survey plots	
Portable weather meter	REED LM-8000 (REED, USA)	3	The temperature measurement range is -100.0 ~ 1300.0 °C, and the accuracy is ± 1%. The relative humidity measurement range is 10% ~ 95%, and the accuracy is ± 4% (temperature 0 ~ 50.0 °C). The wind speed is 0.4 ~ 30m/s, and the accuracy is ± 3% (temperature 0 ~ 50 °C).	
GPS, Clip board, Tape measure.	Regular			

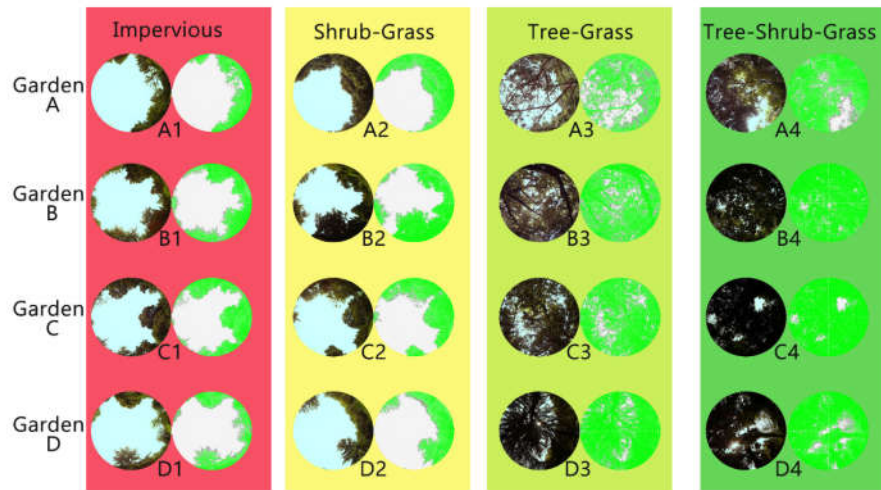


Appendix 16: The layout of Henan Agricultural University (HAU) and the study plot (red rectangle).

Appendix 17. The statistics of each site

No.	Types	Latitude	Longitude	
Garden-A	A1	Impervious surface	34.78642	113.6592
	A2	Shrub-grass	34.78647	113.6591
	A3	Tree-grass	34.78647	113.6592
	A4	Tree-shrub-grass	34.7865	113.6594
Garden-B	B1	Impervious surface	34.7864	113.6597
	B2	Shrub-grass	34.78638	113.6598
	B3	Tree-grass	34.78644	113.6597
	B4	Tree-shrub-grass	34.78626	113.6598
Garden-C	C1	Impervious surface	34.78577	113.6599
	C2	Shrub-grass	34.78574	113.66
	C3	Tree-grass	34.78596	113.6598
	C4	Tree-shrub-grass	34.78584	113.6599
Garden-D	D1	Impervious surface	34.78582	113.6592
	D2	Shrub-grass	34.78578	113.6594
	D3	Tree-grass	34.78575	113.6592
	D4	Tree-shrub-grass	34.78597	113.6592

The four selected campus green spaces are the experimental bases for the teaching of landscape architecture. Each garden has open spaces and different vegetation coverage types. The four gardens are mainly composed of evergreen plants (such as *Cedrus deodara*, *Ligustrum compactum*, *Buxus mollicula*, etc.), deciduous plants (*Platanus orientalis* Linn., *Cinnamomum camphora*; *Bischofia javanica*, *Salix babylonica*, *Styphnolobium japonicum*, *Magnolia denudata*, etc.), shrub (*Fatsia japonica*; *Lagerstroemia indica*, etc.) and grass (*Ophiopogon japonicus*; *Shamrock*.etc.) with high vegetation coverage.



Appendix 18: Fish eye images and leaf area images of each point in four gardens measured by the Plant canopy imager (four coverage types

Appendix 19: The statistics of each site

	No.	Types	La.	Lo.	PAR ($\mu\text{mol}/\text{m}^2\text{s}$)	CD (%)	LAI	MLA($^{\circ}\text{C}$)
G-A	A1	IS	34.78642	113.6592	817	22.9	0.43	89.8
	A2	C	34.78647	113.6591	1721	36.0	0.42	89.8
	A3	T-G	34.78647	113.6592	121	55.3	0.81	51.3
	A4	T-S-G	34.7865	113.6594	42.73	77.1	1.6	27.1
G-B	B1	IS	34.7864	113.6597	1367.6	30.2	0.82	89.74
	B2	S-G	34.78638	113.6598	421.29	43.3	0.8	89.74
	B3	T-G	34.78644	113.6597	17.14	80.3	2.04	41.86
	B4	T-S-G	34.78626	113.6598	20.8	93.4	3.22	35.43
G-C	C1	IS	34.78577	113.6599	1436.3	34.1	0.61	89.74
	C2	S-G	34.78574	113.66	1193.44	37.0	0.49	89.74
	C3	T-G	34.78596	113.6598	46.65	80.0	1.85	32.43
	C4	T-S-G	34.78584	113.6599	33.71	94.0	4.35	10.22
G-D	D1	IS	34.78582	113.6592	1623.88	23.2	0.42	89.74
	D2	S-G	34.78578	113.6594	1176.27	28.4	0.35	89.74
	D3	T-G	34.78575	113.6592	79.91	88.6	2.35	18.97
	D4	T-S-G	34.78597	113.6592	251.26	86.3	2.37	52.20

G-A (Garden-A); G-B (Garden-B); G-C (Garden-C); G-D (Garden-D); IS (impervious surface); S-G (Shrub-grass), T-G (Tree-grass), T-S-G (Tree-shrub-grass); La.(Latitude), Lo.(Longitude); PAR(Photosynthetically active radiation); CD (canopy density); LAI (Leaf area index); MLA(Mean leaf angle).

Appendix 20: Statistic of annual data of urban development in Zhengzhou city from 1981-2019

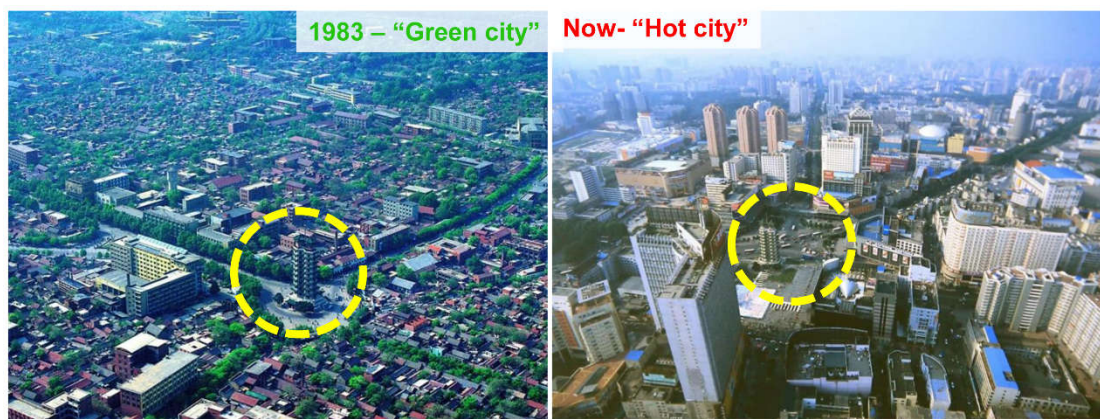
Data source: Zhengzhou Bureau of Statistics Department

Year	Built-up/km²	Citizens/M	Urbanization rate /%	Population density/km²	GDP/CNY
1981	65	4.58	35	616	31.1
1982	66	4.67	35.8	628	33.3
1983	67.8	4.74	36.7	637	37.5
1984	69.3	4.8	37.6	645	43.3
1985	70.2	4.85	38.4	652	49.7
1986	80.5	4.91	39.3	660	53.4
1987	94.2	5.00	40.1	672	66.3
1988	102	5.10	41	686	81.5
1989	110.9	5.21	41.9	700	97.8
1990	112	5.57	42.7	749	116.4
1991	117.2	5.65	43.9	759	138.7
1992	93.1	5.70	45.2	767	167.4
1993	99.5	5.81	46.4	781	218.4
1994	101.9	5.88	47.7	791	287.9
1995	108.3	6.00	48.9	806	386.4
1996	112.8	6.07	50.1	816	498.2
1997	116.2	6.14	51.4	826	566
1998	119.8	6.22	52.6	836	610
1999	124.5	6.31	53.9	848	632.9
2000	133.2	6.65	55.1	894	728.4
2001	142.4	6.77	55.5	909	815.8
2002	156.4	6.87	56	924	913.9
2003	212.4	6.97	57	937	1074.1
2004	243.3	7.08	57.9	951	1335.2
2005	262	7.16	59.2	962	1660.6
2006	282	7.24	60.2	973	2007.8
2007	302	7.35	61.3	988	2486.7
2008	328.7	7.43	62.3	999	3012.9
2009	336.7	7.52	63.4	1010	3305.9
2010	342.7	8.66	63.6	1163	4029.3
2011	354.7	8.85	64.8	1189	4954.1
2012	373	9.03	66.3	1213	5517.1

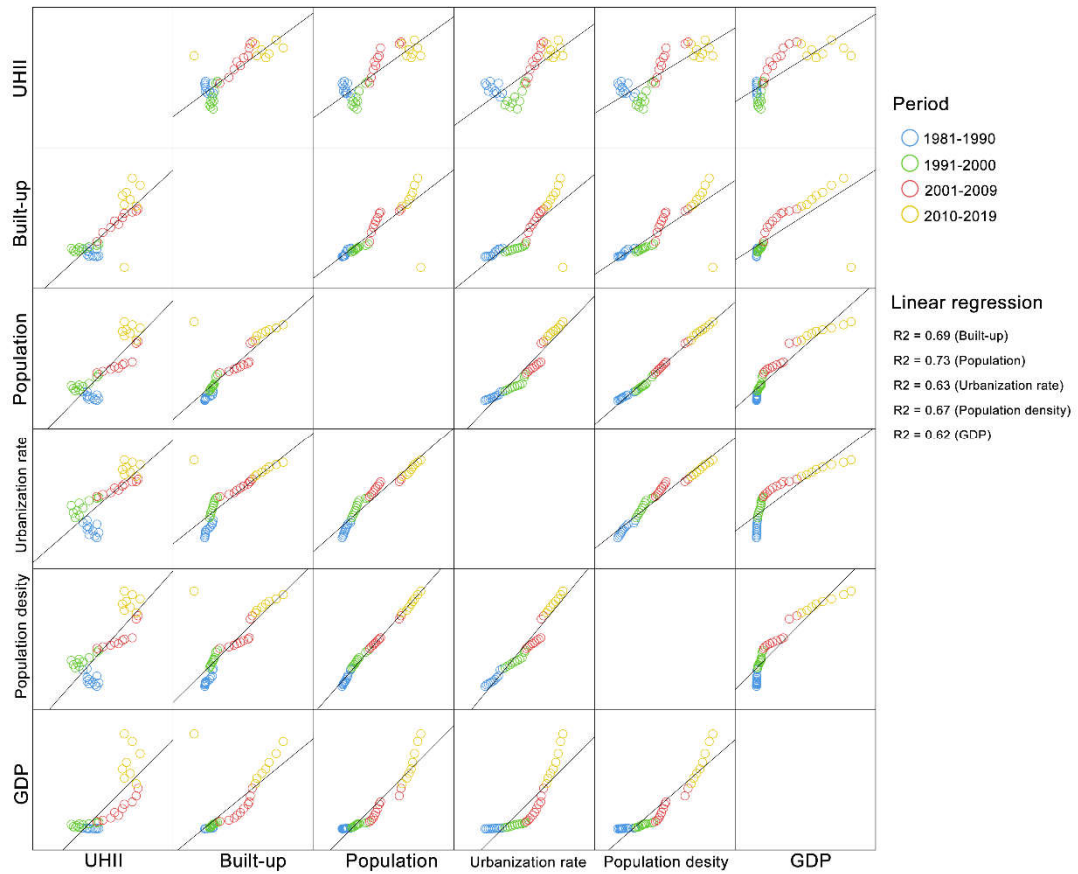
2013	382.7	9.19	67.1	1234	6197.4
2014	412.7	9.37	68.3	1259	6777
2015	437.6	9.56	69.7	1285	7311.5
2016	456.6	9.72	71	1306	8114
2017	500.8	9.88	72.2	1327	9193.8
2018	543.9	10.13	73.4	1361	10670.1
2019	0	10.35	74.6	1390	11589.7

Appendix 21: Thermal sensation classes for human beings in Central Europe (with an internal heat production of 80 W and a heat transfer resistance of the clothing of 0.9 clo (clothing value)) modified after Matzarakis and Mayer (1996).

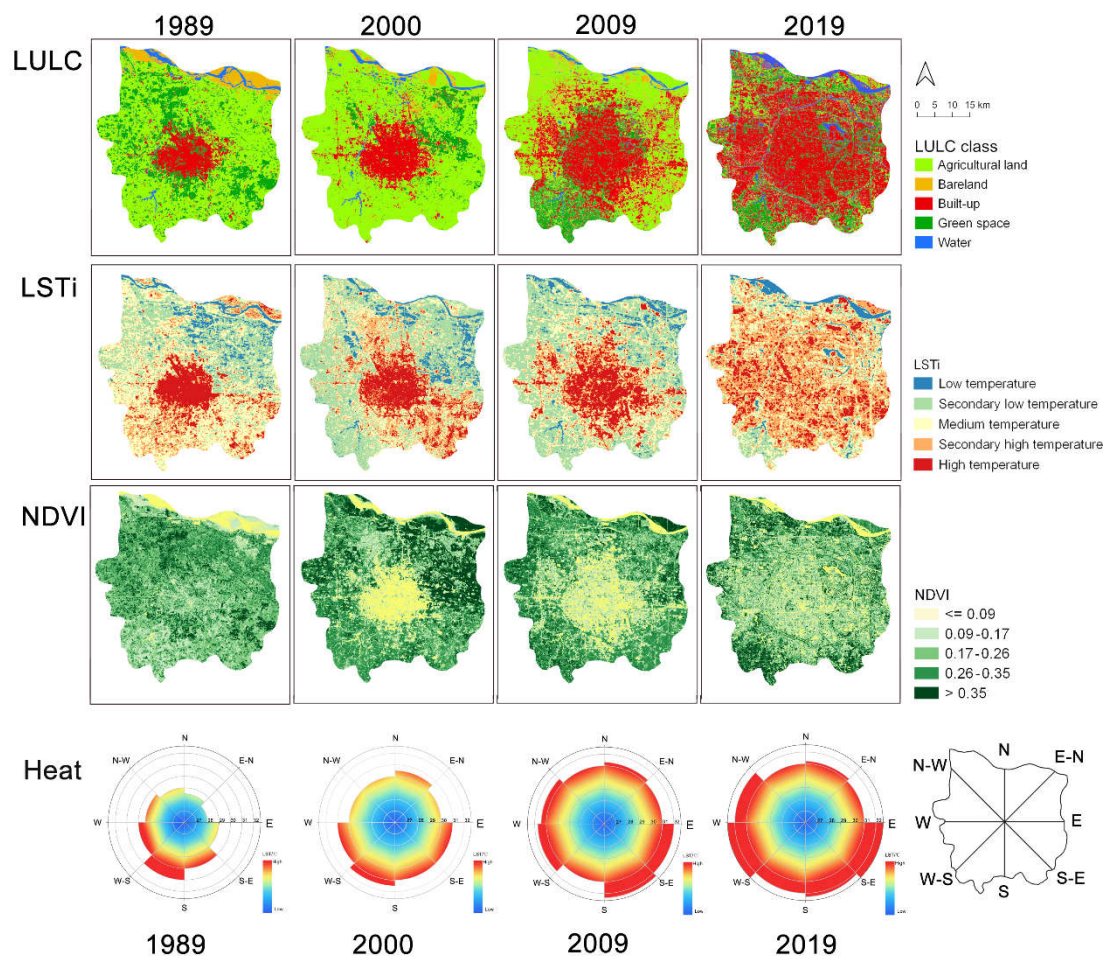
PET (°C)	Thermal Perception	Grade of physical stress
> 41	Very hot	Extreme heat stress
35 - 41	Hot	Strong heat stress
29 - 35	Warm	Moderate heat stress
23 - 29	Slightly warm	Slight heat stress
18 - 23	Comfortable	No thermal stress
13 - 18	Slightly cool	Slight cold stress
8 - 13	Cool	Moderate cold stress
4 - 8	Cold	Strong cold stress
≤ 4	Very cold	Extreme cold stress



Appendix 22: Zhengzhou’s dramatic urbanization process comparison, in 1983(left) and 2019 (right), the yellow circle area is the landmark of Zhengzhou named “Erqi” tower, its surrounding built-up area density changed significantly due to the urbanization.



Appendix 23: The linear regression between the UHII and year-end data: Built-up area, Population, Urbanization rate, Population density, GDP.



Appendix 24: Integrated maps of LULC, LSTi, NDVI, heat extension of eight zones of Zhengzhou city on Jun. 2, 1989; Aug.27, 2000; Aug.12, 2009; Jul.7, 2019 .

Appendix 25: Mean, Standard Deviation (SD), and ranges in value of LST/°C of four seasons in Zhengzhou central city from 1989-2019.

Year	Season	Mean/°C	SD/°C	Min/°C	Max/°C	Ranges
1989	Spring	16.97	2.77	-1.30	25.41	26.71
	Summer	30.56	2.78	21.38	39.31	17.93
	Autumn	21.17	2.40	12.84	27.94	15.11
	Winter	3.54	1.60	-1.84	10.44	12.29
2000	Spring	28.71	2.95	11.79	41.02	29.24
	Summer	35.01	2.06	26.82	46.54	19.72
	Autumn	21.40	1.12	9.47	29.19	19.72
	Winter	3.42	0.84	-11.56	12.36	23.92
2009	Spring	24.07	2.88	9.47	34.48	25.00
	Summer	31.90	2.76	21.95	46.33	24.38
	Autumn	22.77	2.20	8.49	34.08	25.58
	Winter	2.43	0.88	-6.29	8.02	14.32
2019	Spring	26.81	2.10	14.73	35.58	20.85
	Summer	32.18	2.33	20.11	46.10	25.99
	Autumn	18.26	1.83	-5.84	31.63	37.46
	Winter	4.95	0.93	-13.78	15.56	29.33

Appendix 26: Statistics of the LST (°C) by different LULC types of four seasons of Zhengzhou central city in 1989

1989	14/03/1989(Spring day)					02/06/1989(Summer day)				
LULC	Mean	SD	Min	Max	Range	Mean	SD	Min	Max	Range
AL	17.00	2.15	-1.30	23.69	24.99	31.11	2.61	24.40	38.16	13.76
BL	13.02	3.61	0.84	23.26	22.42	28.42	3.39	22.68	37.39	14.71
BU	18.18	1.81	-1.30	25.41	26.71	31.50	2.10	23.97	39.31	15.34
GS	17.20	2.08	1.89	24.12	22.23	30.10	1.77	24.40	36.61	12.21
WS	9.88	2.24	6.50	19.73	13.23	23.60	1.92	21.38	34.26	12.88

1989	24/10/1989 (Autumn day)					02/02/1989(Winter day)				
LULC	Mean	SD	Min	Max	Range	Mean	SD	Min	Max	Range
AL	21.98	2.17	13.78	27.53	13.74	3.79	1.41	-1.30	8.49	9.79
BL	19.87	2.72	12.84	25.83	13.00	1.15	1.86	-1.84	7.50	9.35
BU	20.73	1.26	15.18	27.94	12.76	3.59	1.14	-1.30	10.44	11.75
GS	19.81	1.57	16.11	26.26	10.15	3.09	1.22	-0.76	8.00	8.76
WS	16.05	1.88	12.84	24.55	11.71	0.44	1.23	-1.84	6.50	8.35

Range means the temperature difference between the maximum temperature (Max) and minimum temperature (Min) in a particular LULC type. SD stands for standard deviation of the mean temperature. Agricultural land (AL); Bare Land (BL); Built-up Land (BU); Green Spaces (GS); Water Surface (WS). Same abbreviation to the Appendix 25, 26, 27 behind.

Appendix 27: Statistics of the LST (°C) by different LULC types of four seasons in Zhengzhou in 2000

2000	05/04/2000 (Spring day)					27/08/2000 (Summer day)				
LULC	Mean	SD	Min	Max	Range	Mean	SD	Min	Max	Range
AL	28.69	2.71	18.54	40.10	21.57	34.70	1.59	29.75	43.51	13.76
BL	28.10	3.73	11.79	38.23	26.44	35.04	2.09	26.82	45.68	18.86
BU	30.46	2.01	17.99	41.02	23.04	37.65	2.03	29.27	46.54	17.27
GS	27.71	2.85	22.30	39.17	16.87	33.55	1.31	30.74	42.65	11.91
WS	22.55	3.27	17.99	38.70	20.71	32.39	1.18	30.23	45.25	15.02

2000	06/10/2000 (Autumn day)					15/12/2000 (Winter day)				
LULC	Mean	SD	Min	Max	Range	Mean	SD	Min	Max	Range
AL	21.50	1.05	9.47	25.83	16.36	3.48	0.80	-11.56	11.89	23.45
BL	21.30	1.09	12.84	29.19	16.36	3.00	0.96	-7.44	8.00	15.44
BU	21.93	0.96	13.31	28.78	15.47	3.70	0.75	-4.60	12.36	16.96
GS	20.31	0.69	12.84	24.12	11.28	2.82	0.80	-0.23	6.00	6.23
WS	19.34	0.91	13.31	27.10	13.79	3.05	0.95	-0.23	7.01	7.23

Appendix 28: Statistics of the LST (°C) by different LULC types of four seasons in Zhengzhou in 2009

2009	06/04/2009 (Spring day)					12/08/2009 (Summer day)				
Class	Mean	SD	Min	Max	Range	Mean	SD	Min	Max	Range
AL	23.81	2.88	9.47	33.68	24.20	30.19	1.41	25.85	40.33	14.48
BL	24.90	3.17	9.47	33.28	23.80	32.41	1.98	26.26	45.22	18.96
BU	24.23	1.86	10.44	34.48	24.03	34.46	2.42	21.95	46.33	24.38
GS	25.40	1.88	14.72	31.25	16.53	31.17	1.97	26.26	41.92	15.66
WS	15.22	4.68	9.47	31.66	22.19	27.88	1.93	25.40	43.73	18.33
2009	15/10/2009 (Autumn day)					18/12/2009 (Winter day)				
Class	Mean	SD	Min	Max	Range	Mean	SD	Min	Max	Range
AL	23.33	2.45	16.56	33.28	16.71	2.73	0.81	-5.71	7.51	13.22
BL	22.65	1.87	11.89	31.66	19.77	2.44	0.80	-6.30	6.47	12.77
BU	22.46	1.74	8.49	34.08	25.58	1.94	0.79	-5.71	8.03	13.73
GS	22.36	1.46	17.48	30.02	12.54	2.61	0.72	-1.67	7.51	9.18
WS	18.25	1.49	16.56	29.61	13.04	3.20	1.24	-0.55	6.99	7.54

Appendix 29: Statistics of the LST (°C) by different LULC types of four seasons in Zhengzhou in 2019

2019	18/04/2019 (Spring day)					07/07/2019 (Summer day)				
Class	Mean	SD	Min	Max	Range	Mean	SD	Min	Max	Range
AL	27.26	1.77	16.95	31.43	14.48	31.95	1.63	25.08	39.53	14.44
BL	27.91	1.06	18.27	32.62	14.35	33.94	1.20	24.67	39.74	15.07
BU	27.16	1.41	15.31	35.58	20.27	33.06	1.75	20.11	46.10	25.99
GS	26.62	1.40	16.34	31.65	15.31	30.70	1.65	24.26	39.85	15.59
WS	22.69	4.55	14.73	32.66	17.93	28.31	3.78	23.13	39.52	16.39
2019	27/10/2019 (Autumn day)					31/01/2019 (Winter day)				
Class	Mean	SD	Min	Max	Range	Mean	SD	Min	Max	Range
AL	18.52	1.88	-1.58	23.92	25.49	5.40	0.67	-1.33	8.45	9.78
BL	19.40	1.49	2.49	31.40	28.91	5.29	0.78	-1.14	15.26	16.40
BU	18.46	1.61	-2.61	31.63	34.24	4.80	1.02	-13.78	15.56	29.33
GS	18.02	1.44	-2.39	25.05	27.44	5.11	0.70	0.78	10.03	9.25
WS	16.09	2.93	-5.84	28.11	33.95	4.77	0.78	0.61	12.37	11.76

Appendix 30: The representation of NDVI range

Values	Represent types
-1 to 0	Water bodies
-0.1 to 0.1	Barren rocks, sand, or snow
0.2 to 0.5	Shrubs and grasslands or senescing crops
0.6 to 1.0	Dense vegetation or tropical rainforest

Appendix 31: Mean, Standard Deviation (SD), and differences in value of LST/°C green space samples in Zhengzhou central city in 2019

Name	Land use	Area (km ²)	Mean	S D	Min	Max	Range
Renmin Park	City park	0.30	30.13	0.80	28.86	32.32	3.46
Ruyihu Park	District park	0.36	29.58	0.63	28.69	32.02	3.33
Jiangang reservoir	Wetland	19.41	28.77	1.43	25.67	33.66	7.98
Zhengzhou Zoo	Special Park	0.20	29.79	0.89	28.12	32.43	4.31
Xiongerhe Park	Park	1.02	29.57	0.85	28.09	32.69	4.60
Nursery	Nursery	1.84	28.43	1.04	26.59	31.09	4.50
Zijingshan Park	City park	0.16	30.43	0.86	28.92	32.21	3.29
Dragon lake park	New CBD	8.29	29.67	0.89	25.00	34.52	9.52
Yellow river area	Forest	6.40	29.53	0.66	27.62	31.60	3.99
Average			29.54	0.89	27.51	32.50	5.00

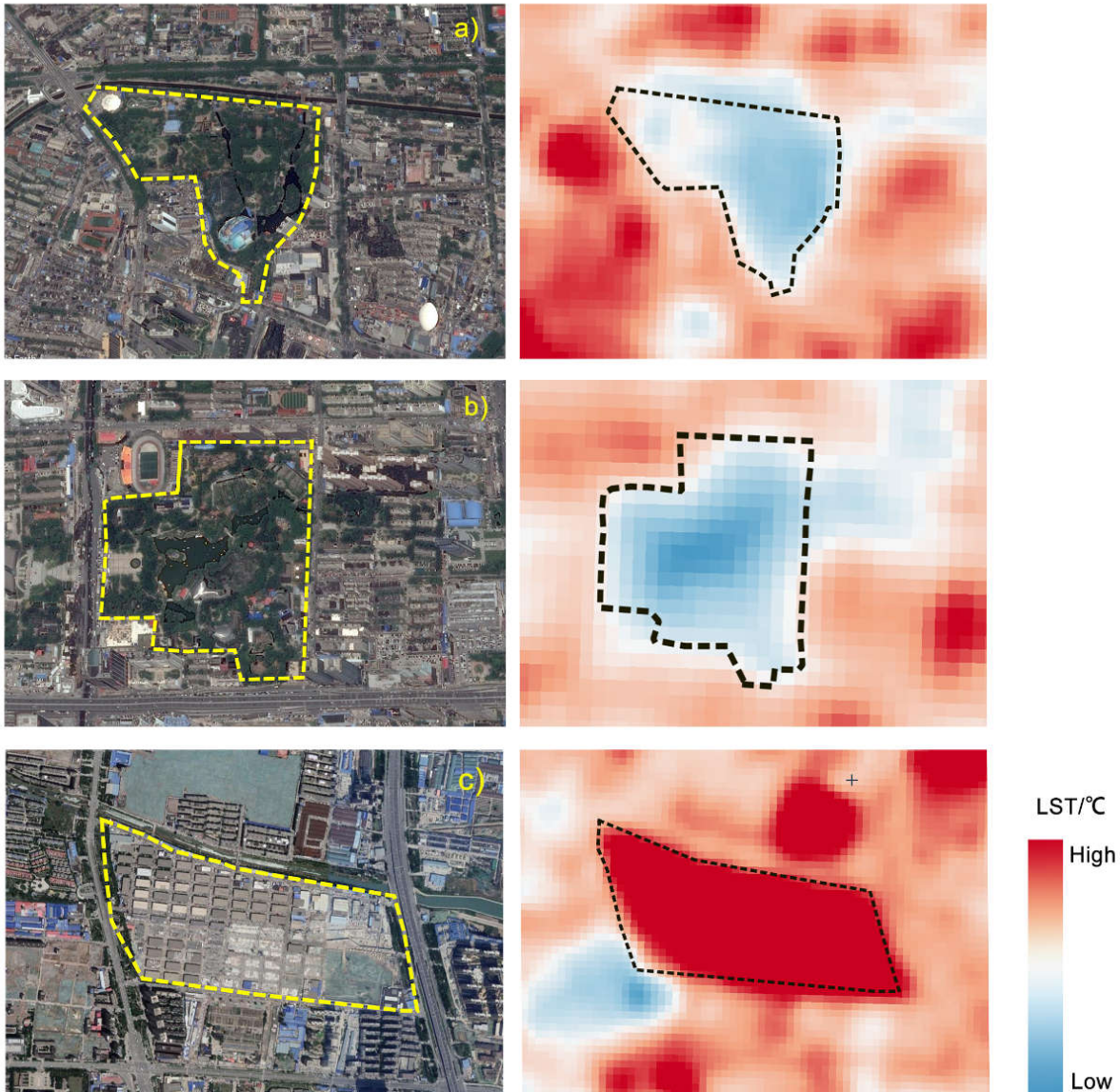


Appendix 32: Renmin Park (Right) and Zijingshan Park (Left) in Zhengzhou central city

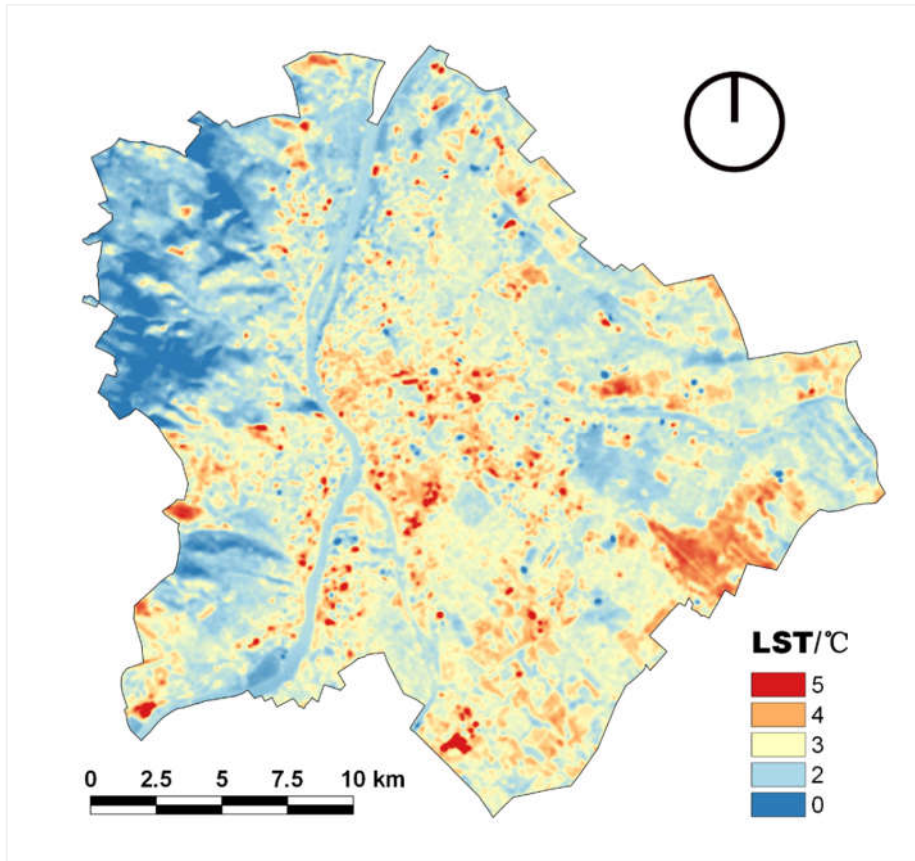
Appendix 33. Ten sample plots for shadow analysis in Zhengzhou urban

Plot	Google Satellite Images	Plot	Google Satellite Images
A		F	
B		G	
C		H	
D		I	
E		J	

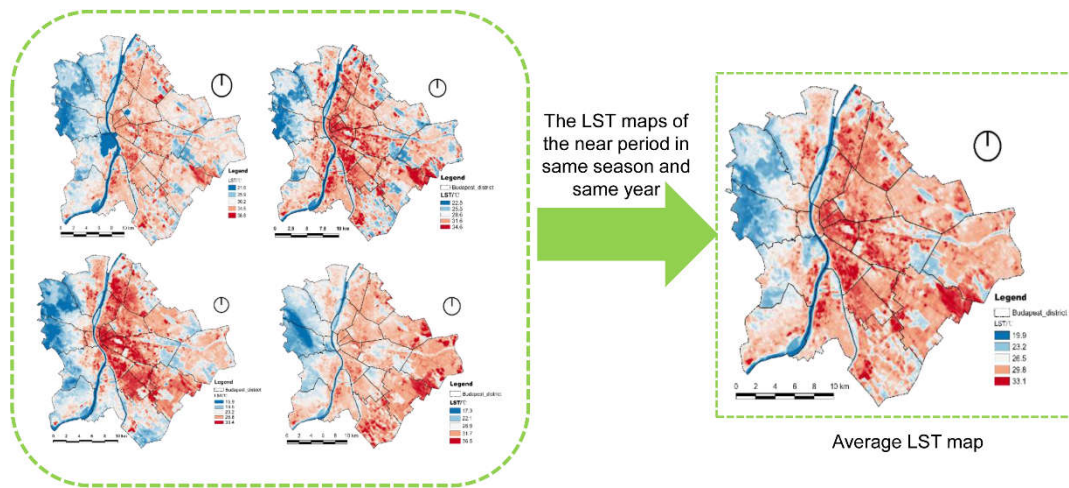
The 10 sample plots were all selected along the road and divided into shadow and non-shadow areas. Due to the resolution of 30 m, the length of the set square was greater than 100 and the width was greater than 30 m.



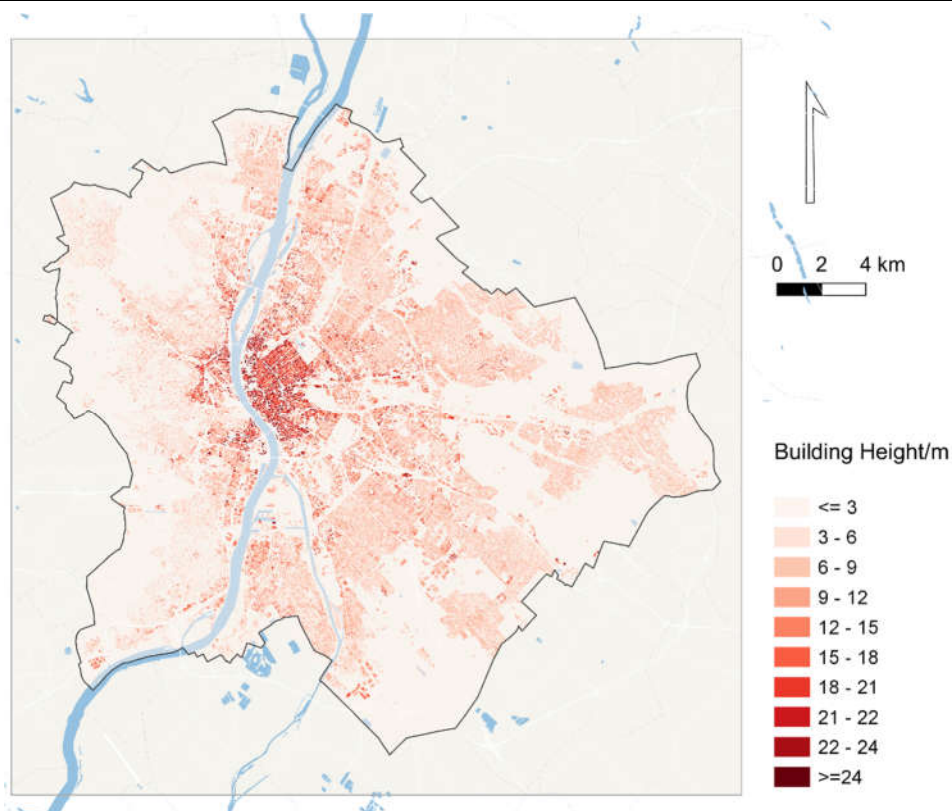
Appendix 34: Google satellite map and LST of Remin Park(a), Zhengzhou Zoo(b), and hot spot sample (c) in Zhengzhou central city. The LST map date is Jun. 07, 2019.



Appendix 35: The average winter land surface temperature (LST) map (2013-2018) in Budapest



Appendix 36. The Average LST calculation process flow



Appendix 37. Distribution of Building height classes in Budapest (2012)

Description of Building height (BH) map:

A 10m high resolution raster layer containing height information is generated for core urban areas of capitals of the EEA39 as part of the Urban atlas. Height information is based on IRS-P5 stereo images and derived datasets like the digital surface model, the digital terrain model and the normalized DSM.

This product is generated based on IRS-P5 stereo images acquired as close as possible to the defined reference year. Based on these stereo images a digital surface model is generated. Afterwards a digital terrain model is derived from the DSM with different filter algorithms and the assistance of Urban Atlas 2012 datasets. The calculation of the normalized DSM is done by a simple subtraction of the DTM from the DSM. The final product is then clipped based on UA 2012 building blocks and fully quality controlled.

Resource:

<https://land.copernicus.eu/local/urban-atlas/building-height-2012>

Pan-European High Resolution Layers (HRL) provide information on specific land cover characteristics, and are complementary land cover / land use mapping such as in the CORINE land cover (CLC) datasets. The HRLs are produced from satellite imagery through a combination of automatic processing and interactive rule based classification. Five themes have been identified so far, corresponding with the main themes from CLC, i.e. the level of sealed soil (imperviousness), tree cover density and forest type, grasslands, wetness and water, and small woody features. All of these five products are continuing existing products, some with longer time series existing (Imperviousness and tree-cover/forest), and three products that have only one previous reference year (2015) (grassland, the water & wetness products and Small Woody Features). All products are mapping the features under consideration for the whole of the EEA-39 area. They are produced in a combined centralized and decentralized approach, involving service industry through market mechanisms and participating countries through grant agreements. DSM of Budapest was bought from the commercial company which provides the surface information.

Appendix 38. Building height (m) range and land surface temperature (°C) distribution

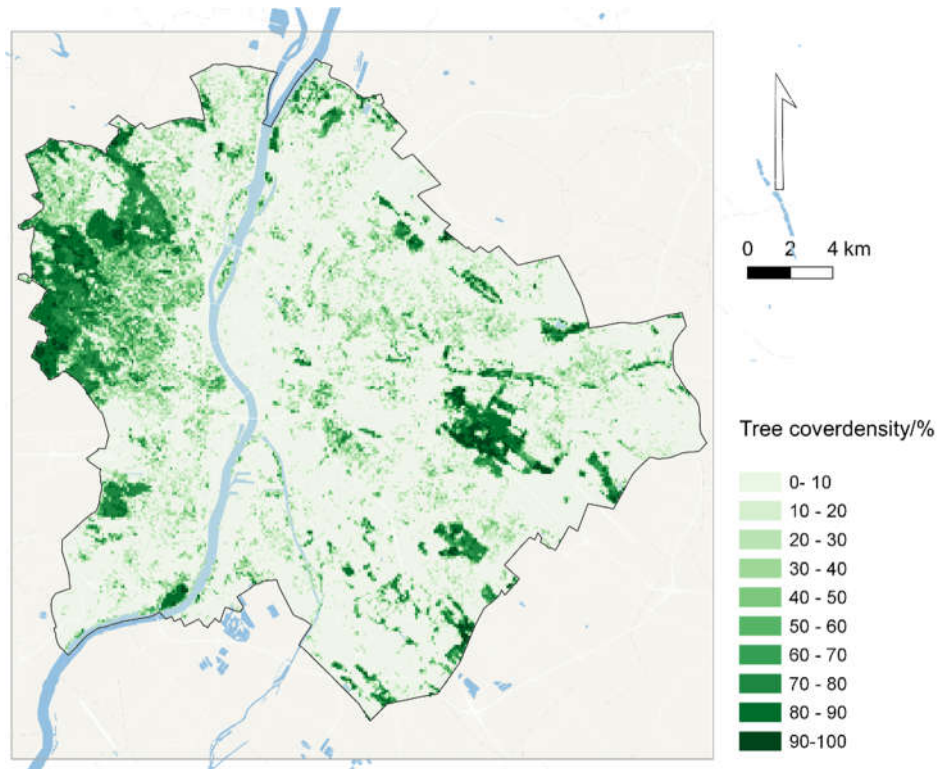
Range	Max	Min	Median	Mean	St.
≤5	43.041	24.72	30.84	30.96	1.58
5-10	43.03	23.08	30.29	30.31	1.88
10-15	42.32	22.92	30.75	30.86	1.86
15-20	41.60	23.06	31.58	31.60	1.80
20-25	39.29	23.31	32.14	31.99	1.54
25-30	38.28	23.81	32.22	32.07	1.44
30-35	36.78	26.51	31.48	31.43	1.48
35-40	35.48	27.09	31.14	31.01	1.44
40-45	35.34	27.91	31.53	31.50	1.40
≥45	34.91	27.16	32.34	31.61	1.47

Five number summary (“minimum” (Min), first quartile (Q1), median, third quartile (Q3), and “maximum” (Max)).

Appendix 39. Vegetation height (m) range and land surface temperature (°C) distribution

Range	Max	Min	Median	Mean	St.
≤2.5	35.68	21.51	29.16	28.98	2.02
2.5-5.0	36.00	22.30	29.32	29.14	1.62
5.0-7.5	35.76	20.14	29.15	28.98	1.73
7.5-10.0	35.62	21.89	28.71	28.56	1.97
10.0-12.5	35.83	20.21	28.13	27.99	2.23
12.5-15.0	35.29	20.00	27.84	27.74	2.42
15.0-17.5	34.59	19.96	26.48	26.66	2.40
17.5-20.0	33.49	20.00	26.12	26.32	2.43
20.0-22.5	32.65	19.89	25.54	25.66	2.27
≥22.5	30.61	19.97	25.39	25.46	2.36

Five number summary (“minimum” (Min), first quartile (Q1), median, third quartile (Q3), and “maximum” (Max)).



Appendix 40. Distribution of tree cover density in Budapest

Description of Small Woody Features (SWFs) map:

Semi-automatic classification of pre-processed multitemporal High Resolution (HR) satellite image data (Sentinel-2, Landsat 8) with reference year 2015 (+/- 1 year), using supervised and unsupervised elements, leading to scene-based initial land cover classifications. Performing of a time series analysis to extract tree cover. Subsequently, interactive manual corrections of the derived tree cover mask have been performed and integrated to a seamless mosaic. Thereafter a monotemporal, regression-based thematic classification of Tree Cover Density values has been performed on HR_IMAGE_2015, Landsat 8 and Sentinel-2 data using the HRL Forest reference products for calibration and validation. Tree cover density providing level of tree cover density in a range from 0-100%. In its original (20m) resolution it consists of two products: 1) a dominant leaf type product that has an MMU of 0.5 ha, as well as a 10% tree cover density threshold applied, For the final 100m product trees under agricultural use and urban context from the support layer are removed. The high resolution forest change products comprise a simple tree cover density change product for 2012-2015 (% increase or decrease of real tree cover density changes).

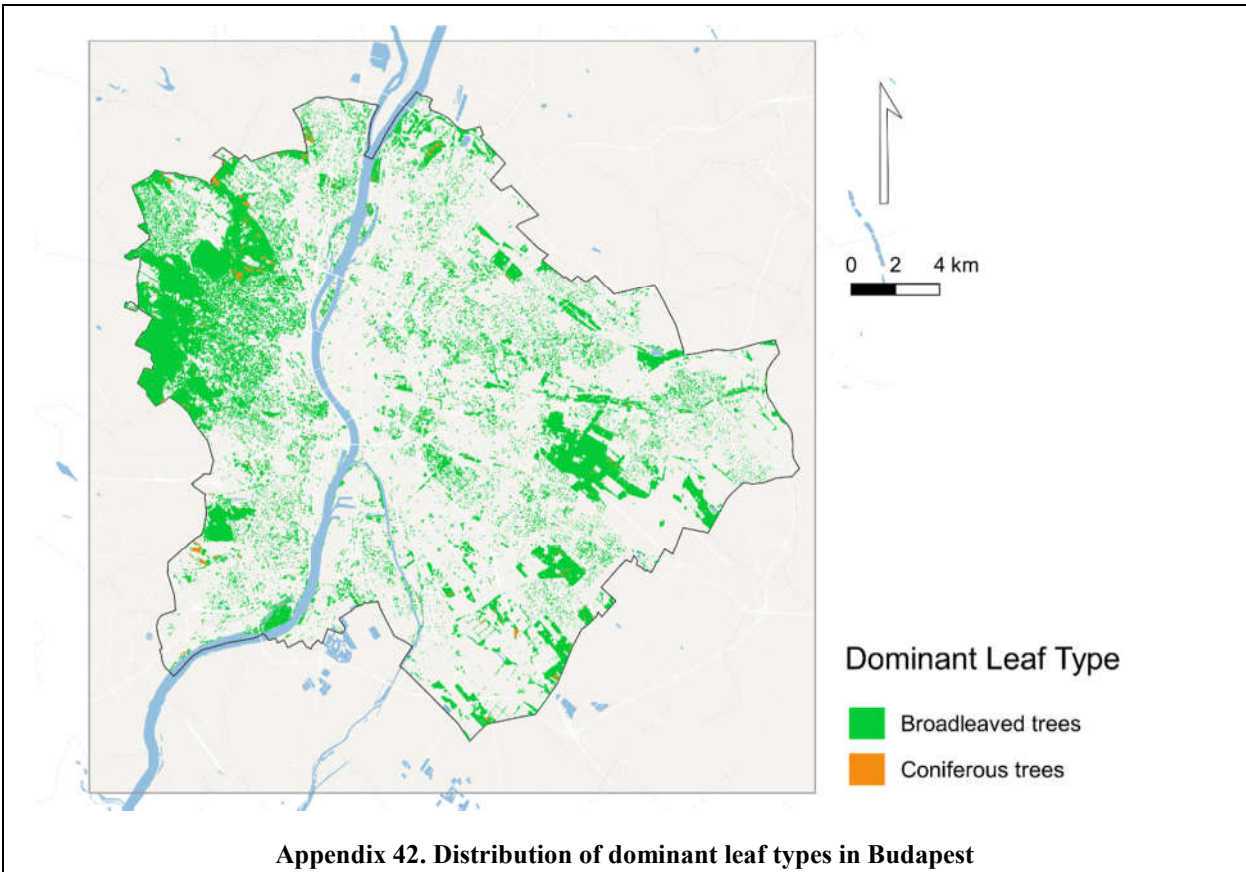
Resource:

<https://land.copernicus.eu/pan-european/high-resolution-layers/forests/tree-cover-density/status-maps/2015?tab=metadata>

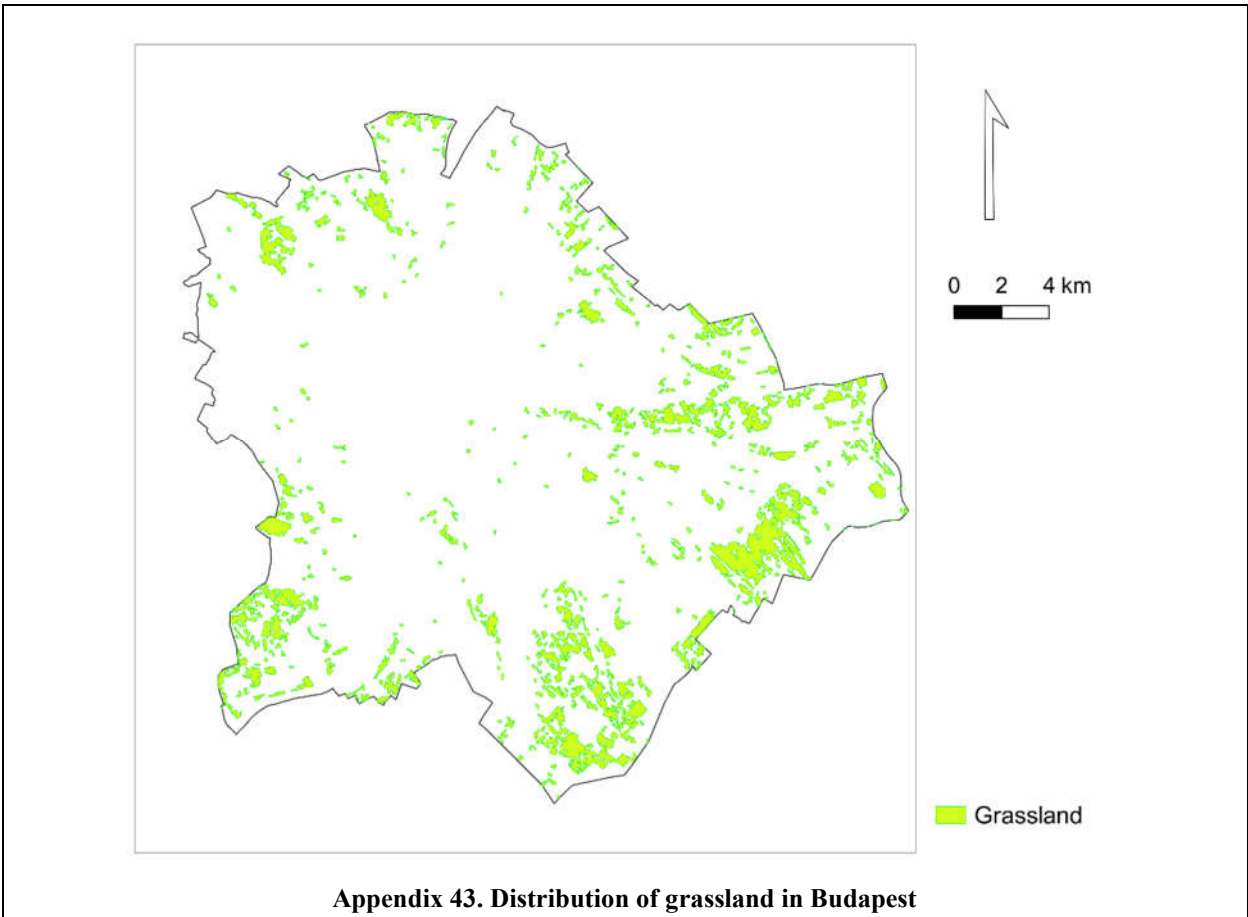
Appendix 41. Tree cover density(%) range and land surface temperature (°C) distribution

Range	Max	Min	Median	Mean	St
0-10	37.42	20.87	30.05	29.83	2.08
10-20	36.68	21.09	29.67	29.46	1.89
20-30	34.37	20.2	29.07	28.85	1.84
30-40	33.07	20.95	28.49	28.3	1.81
40-50	33.29	21.56	27.9	27.79	1.83
50-60	34.98	22.09	27.11	27.12	1.79
60-70	34.02	22.19	26.13	26.28	1.71
70-80	30.64	20.23	25.58	25.71	1.54
80-90	28.57	22.15	24.96	25.07	1.23
90-100	28.73	21.94	24.35	24.4	1.38

Five number summary (“minimum” (Min), first quartile (Q1), median, third quartile (Q3), and “maximum” (Max)).

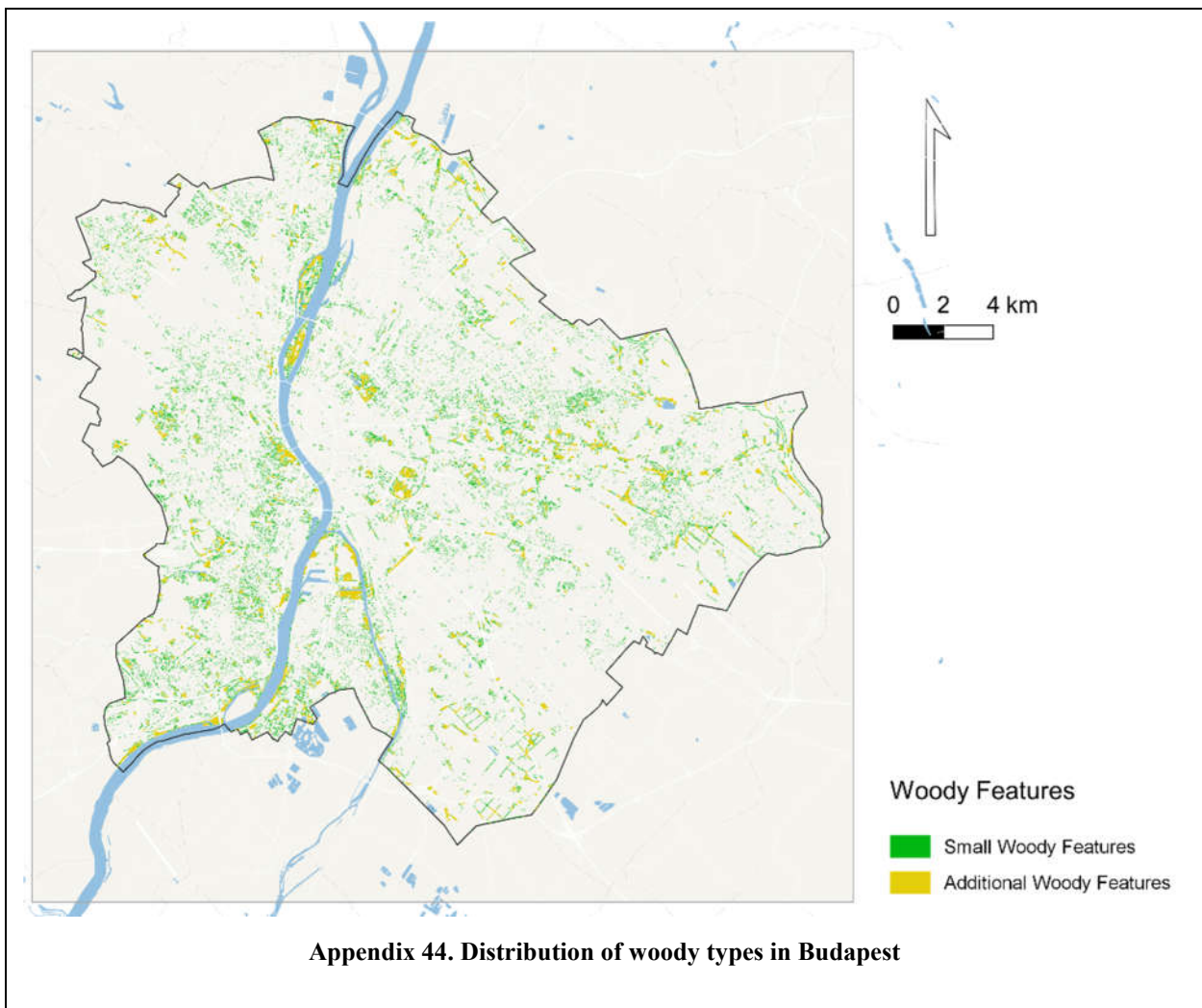


<p>Description of dominant leaf types (DLT) map:</p> <p>The high resolution forest product consists of three types of (status) products and additional change products. The status products are available for the 2012 and 2015 reference years: 1. Tree cover density providing level of tree cover density in a range from 0-100% 2. Dominant leaf type providing information on the dominant leaf type: broadleaved or coniferous 3. A Forest type product. The forest type product allows to get as close as possible to the FAO forest definition. In its original (20m) resolution it consists of two products: 1) a dominant leaf type product that has a MMU of 0.5 ha, as well as a 10% tree cover density threshold applied, and 2) a support layer that maps, based on the dominant leaf type product, trees under agricultural use and in urban context (derived from CLC and high resolution imperviousness 2009 data). For the final 100m product trees under agricultural use and urban context from the support layer are removed. The high resolution forest change products comprise a simple tree cover density change product for 2012-2015 (% increase or decrease of real tree cover density changes).</p>
<p>Resource:</p> <p>https://land.copernicus.eu/pan-european/high-resolution-layers/forests/dominant-leaf-type/status-maps/2015?tab=metadata</p>



Appendix 43. Distribution of grassland in Budapest

<p>Description of grassland (GRA) map:</p>
<p>The main high resolution grassland product is the Grassland layer, a grassland/non-grassland mask for the EEA39 area. This grassy and non-woody vegetation baseline product includes all kinds of grasslands: managed grassland, semi-natural grassland and natural grassy vegetation. It is a binary status layer mapping grassland and all non-grassland areas in 20m and (aggregated) 100m pixel size. Thematic accuracy: The thematic accuracy assessment will be made on the primary layer, the grassland mask. The target will be set at 85 % to be achieved within each biogeographic region. A quantitative approach will be used based on a set of stratified random point samples compared to external datasets (e.g. GoogleEarth, national orthophotos or national grassland datasets). Achieved overall accuracy: 96.66%. Geometric accuracy (positioning accuracy): Less than half a pixel. According to orthorectified satellite image base delivered by ESA.</p>
<p>Resource:</p>
<p>https://land.copernicus.eu/pan-european/high-resolution-layers/grassland/status-maps/2015?tab=metadata</p>



Description of Small Woody Features (SWFs) map:

The Small Woody Features (SWFs) layer contains woody linear, and small patchy elements, but will not be differentiated into trees, hedges, bushes and scrub. The spatial pattern shall be limited to linear structures and isolated patches (patchy structures) on the basis of geometric characteristics. Additional Woody Features (AWFs) are also included in this product. They consist of woody structures that do not fulfil the SWF geometric specifications but which are connected to valid SWFs structures. The Minimum Mapping Unit (MMU) for small patches of trees is 200 m² while the Maximum Mapping Unit (MaxMU) is defined by 5000 m². The Minimum Mapping Length (MML) of linear elements is 50 m. There is also an other distinction between this two structures: width (30 m maximum for linear instead of 30 m minimum for patchy). Additional Woody Features (code = 3) consist of woody structures that do not fulfil the SWF geometric specifications but which are connected to valid SWFs structures, as well as patchy structures too large to be considered as valid SWF. No data (code = 254). Out of Large Region limits (code = 255).

Resource:

<https://land.copernicus.eu/pan-european/high-resolution-layers/small-woody-features/small-woody-features-2015?tab=metadata>

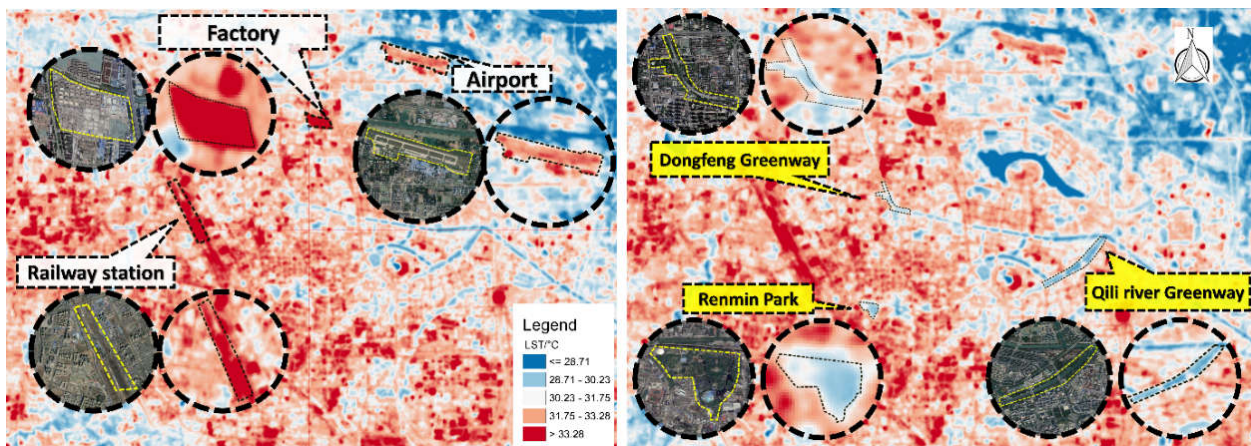
Appendix 45. Vegetation type and land surface temperature (°C) distribution in Budapest

Type	Max	Min	Median	Mean	St
Grassland	36.45	24.30	29.20	29.35	1.78
Small woody	37.35	21.68	29.44	29.33	1.75
Large woody	33.83	22.75	28.39	28.38	1.82
Forest	34.35	20.01	25.32	26.31	2.56

Five number summary (“minimum” (Min), first quartile (Q1), median, third quartile (Q3), and “maximum” (Max)).

Small woody area (SWA) are exclusively covered by ligneous vegetation (woody plants) and comprise linear hedges and tree rows along field boundaries, riparian and roadside vegetation, as well as scattered patches of trees and scrubs. SWA are mapped in the following categories:

- **Linear:** represent landscape features such as hedgerows or tree alignments that are defined by a compactness criterion less or equal to 0.75, up to 30m width and at least 50m length. They are only distinguished as separate attributes in the vector layer.
- **Patchy:** represent areas of isolated and scattered patches of trees or scrubs defined by a compactness criterion greater than 0.75, at least 10m width and with an area greater than 200m² and less than 5,000m². They are only distinguished as separate attributes in the vector layer.
- **Large woody area :** Woody features that are neither linear nor patchy SWA, but which are connected to linear or patchy SWA and isolated woody features that are not linear nor patchy SWA, but which present an area above 1500m² (linear features wider than 30m, and out-of-specifications patches).



Appendix 46. Critical situations and proposals in Zhengzhou to mitigate UHI